

# **Investigation into the immune prompting mechanisms of calreticulin for targeted cancer cell death and immunotherapy.**

**Submitted by Trefa Mohammed Abdullah to the University of Exeter as a thesis for the degree of Doctor of Philosophy in Medical Studies, October 2019.**

This thesis is available for Library use on the understanding that it is copyright material and that no quotation from the thesis may be published without proper acknowledgement.

I certify that all material in this thesis which is not my own work has been identified and that no material has previously been submitted and approved for the award of a degree by this or any other University.

Signature: .....

Trefa Mohammed Abdullah Norman

## Abstract

Ovarian cancer is the leading cause of death from gynaecological malignancies. Late diagnosis following metastasis combined with frequent relapse after initial treatment, has led to a 5-year survival rate <50%. Thus, new and improved therapeutic strategies are urgently required.

One possible novel therapy involves engaging the adaptive immune system in a process of immunogenic cell death (ICD). Apoptotic tumour cell death is usually immunologically silent because cells are cleared by phagocytes without the involvement of adaptive immunity. However, in ICD apoptotic cells have immunogenic properties and immune responses against cancer cell specific antigens or altered self-antigens can occur. Cells undergoing ICD also have surface expression of damage-associated molecular pattern molecules (DAMPs) which facilitate recognition and engulfment e.g. by dendritic cells, and subsequent activation of a cancer cell specific T lymphocyte response. A select group of cancer therapies induce ICD in addition to their known cytotoxic effects e.g. the anthracycline doxorubicin and radiotherapy.

The endoplasmic reticulum (ER) chaperone protein calreticulin (CRT) is a key DAMP. CRT translocation from the ER to the cell surface during ICD induced by cytotoxic agents that induce ER stress promotes cancer cell immunogenicity. Thus, strategies to enhance ovarian cancer cell surface CRT may offer therapeutic options for patients. Therefore, the aims of this project were (a) to obtain a purified preparation of CRT (b) to determine the conditions that give rise to enhanced surface levels of CRT in ovarian cancer cells; specifically externalisation of endogenous CRT or cellular binding of exogenously added CRT and (c) to determine if ovarian cancer cells with enhanced surface CRT induce dendritic cell activation and subsequent T lymphocyte responses. Doxorubicin and the known ER stressor thapsigargin stimulated apoptosis in ovarian cancer cells. This was accompanied by enhanced binding of exogenous CRT, enhanced externalisation of endogenous CRT, increased cell expression of CRT and increased secretion of the protein. All of these actions were significantly inhibited by the ER stress inhibitor tauroursodeoxycholic acid, confirming the involvement of ER stress. Ovarian cancer cells with enhanced surface CRT induced maturation and activation of dendritic cells and subsequent activation i.e. proliferation, of cytotoxic T-lymphocytes, hence stimulating an anticancer immune response.

## **Publication and abstracts arising from this thesis.**

### **Publications**

1. UM Pandya, C Egbuta, TM Abdullah Norman, CE Chiang, VR Wiersma, RG Panchal, E Bremer, P Eggleton, L Gold. (2019). The Biophysical Interaction of the Danger-Associated Molecular Pattern (DAMP) Calreticulin with the Pattern-Associated Molecular Pattern (PAMP) Lipopolysaccharide. *Int J Mol Sci*, 20;408.
2. VR Wiersma, M Michalak, TM Abdullah, E Bremer & P Eggleton. (2015) Mechanisms of translocation of ER chaperones to the cell surface and immunomodulatory roles in cancer and autoimmunity. *Frontiers in Oncology* 5;1-14.

### **In preparation:**

TM Abdullah, JL Whatmore, E Bremer, R Slibinskas, M Michalak. P Eggleton.

Release and binding of calreticulin from ovarian cancer cells under various states of ER stress.

### **Conference attended**

Oral presentation at Endoplasmic reticulum in health and disease: the 12th International Calreticulin Workshop, Delphi, Greece (*J Cell Mol Med*, 21, 3141-3149).

**Title:** Investigation into the mechanisms of calreticulin binding and release from targeted cancer cells: implications for immunotherapy

<b>Table of contents</b>	<b>Pages</b>
Acknowledgement .....	12
List of Figures.....	13
List of Tables .....	19
Abbreviations .....	20
<b>Chapter 1: Introduction.....</b>	<b>23</b>
<b>1.1 Ovarian cancer .....</b>	<b>23</b>
1.1.1 Epidemiology .....	23
1.1.2 Risk factors.....	23
1.1.3 Overview of ovarian cancer types.....	24
1.1.4 Staging of ovarian cancer.....	25
1.1.5 Chemotherapy in EOC .....	27
<b>1.2 An overview of the immune system .....</b>	<b>28</b>
1.2.1 Innate immune system.....	28
1.2.2 Complement 1q.....	30
1.2.3 Adaptive immunity.....	31
1.2.4 Antibody – mediated immunity (humoral).....	32
1.2.5 Cell - mediated immunity.....	32
1.2.6 Antigen presenting cells APCs .....	33
1.2.6.1 Macrophages.....	34
1.2.6.2 Dendritic cells .....	34
1.2.7 MHC-1.....	35
1.2.8 T- Cells .....	36
<b>1.3 The immune system and cancer .....</b>	<b>37</b>
<b>1.4 Cancer immunotherapy .....</b>	<b>39</b>
<b>1.5 Immunogenic cell death (ICD) in cancer cells .....</b>	<b>40</b>
1.5.1 ER stress-driven immunogenic cancer cell death.....	42
1.5.2 The role of intracellular chaperones as DAMPs .....	43

<b>1.6 Apoptosis and necrosis</b> .....	44
1.6.1 The extrinsic apoptotic pathway.....	45
1.6.2 The intrinsic pathway.....	46
1.6.3 Morphological changes in apoptosis.....	47
1.6.4 Necrosis.....	47
1.6.5 Assessment of cell death.....	49
1.6.6 Assessment of apoptosis using annexin V.....	49
1.6.7 Apoptosis in cancer .....	51
<b>1.7 Calreticulin</b> .....	52
1.7.1 Calreticulin expression in cancers.....	52
1.7.2 Structure and function of CRT.....	54
1.7.3 Calreticulin in the ER.....	55
1.7.4 CRT and the innate immune system.....	55
1.7.5 CRT in adaptive immunity.....	56
1.7.6 Role of CRT surface exposure during ICD in cancer treatment.....	57
1.7.7 CRT as a therapeutic agent.....	60
<b>1.8 ER stress inducers</b> .....	60
1.8.1 Doxorubicin.....	61
1.8.2 Thapsigargin.....	62
1.8.3 Tauroursodeoxycholate (TUDCA) reduces ER stress.....	63
<b>1.9 Overview of research presented and aims of this study</b> .....	64
<b>Chapter 2: Materials and general methods</b> .....	66
<b>2.1 Suppliers and sources of experimental materials</b> .....	66
<b>2.2 Buffers and Solutions</b> .....	68

<b>2.3 Cell culture</b> .....	70
<b>2.3.1 Cell culture conditions</b> .....	70
<b>2.3.2 THP-1 cell (human monocytic cell line)</b> .....	70
<b>2.3.3 HCMEC/D3 human cerebral microvascular endothelial cells</b> .....	71
<b>2.3.4 Freezing cells</b> .....	71
<b>2.3.5 Thawing cells</b> .....	71
<b>2.3.6 Seeding cells into 6 well plates</b> .....	71
<b>2.4 Flow cytometry</b> .....	74
<b>2.4.1 Gating for live cells</b> .....	74
<b>2.4.2 Compensation</b> .....	76
<b>2.4.3 Flow cytometry to assess cell apoptosis and necrosis</b> .....	78
<b>2.5 ELISAs</b> .....	80
<b>2.5.1 CRT ELISA</b> .....	80
<b>2.5.2 ELISA for IL-12/IL-23p40</b> .....	82
<b>2.6 Determination of protein concentration</b> .....	83
<b>2.7 SDS-PAGE (sodium dodecyl sulfate polyacrylamide gel electrophoresis) and western blotting</b> .....	85
<b>2.7.1 SDS PAGE to determine protein molecular weight under   reducing conditions Western blotting for CRT</b> .....	85
<b>2.7.2 Western blotting for CRT</b> .....	85
<b>Chapter 3: Purification of calreticulin and preparation of monomeric CR</b> .....	87
<b>3.1 Introduction</b> .....	87
<b>3.2 Aims of this chapter</b> .....	89

<b>3.3 Methods</b> .....	91
<b>3.3.1</b> Source of CRT.....	91
<b>3.3.2</b> Ion exchange chromatography (Mono Q).....	91
<b>3.3.3</b> MonoQ column cleaning and equilibration.....	93
<b>3.3.4</b> Mono-Q sample application.....	93
<b>3.3.5</b> SDS PAGE to determine MW of eluted proteins under reducing conditions.....	94
<b>3.3.6</b> Gel Filtration of recombinant CRT.....	94
<b>3.3.7</b> Treatment of E -Coli expressed CRT monomeric protein fractions (from Mono Q) with polymyxin B(PMB).....	95
<b>3.4 Results</b> .....	96
<b>3.4.1</b> CRT elutes in two separate peaks using anion chromatography.....	96
<b>3.4.2</b> SDS PAGE to determine MW under reducing conditions.....	98
<b>3.4.3</b> Gel filtration of recombinant CRT.....	98
<b>3.5 Discussion</b> .....	101
<b>3.6 Conclusion</b> .....	102
<b>Chapter 4: An investigation into the conditions required for ovarian cancer cell surface association with either endogenous or exogenous CRT calreticulin</b> .....	103
<b>Chapter 4a. Examination of the conditions required for binding of exogenous calreticulin to ovarian cancer cells</b> .....	103
<b>4a.1.</b> Introduction.....	103
<b>4a.2.</b> Aim.....	105
<b>4a.3.</b> Methods.....	105

4a.3.1	Conjugation of CRT or HSA with FITC.....	105
4a.3.2	Culture of cancer cells.....	107
4a.3.3	Exogenous CRT binding to ovarian cancer cells assessed by flow cytometry.....	107
4a.3.4	Staining for cell morphology .....	107
4a.3.5	immunofluorescent cell staining.....	107
4a.3.6	Treatment of cancer cells.....	110
4a.3.7	Assessment of surface bound CRT on cells undergoing apoptosis and necrosis.....	111
4a.3.8	Immunocytochemistry.....	111
4a.3.9	Data analysis.....	113
4a.4.	Results.....	113
4a.4.1	Binding of CRT to cancer cells under non-stress conditions.....	113
4a.4.2	CRT-FITC binds to the surface of cancer cells as assessed by flow cytometry.....	113
4a.4.3	CRT-FITC binds to the surface of cancer cells as assessed by immunofluorescence microscopy .....	118
4a.4.4	Binding of CRT to cancer cells under stress and ER stress conditions.....	118
4a.4.5	Treatment of both OVCAR3 and SKOV3 cells with thapsigargin and doxorubicin treatment alone, and combined, increases CRT binding to dying cells.....	129
4a.4.6	Inhibition of ER stress reduced binding of exogenous CRT in doxorubicin and thapsigargin treated cells.....	132
<b>Chapter 4b. Examination of the conditions required for surface exposure of translocated endogenous calreticulin in ovarian cancer cells .....</b>		<b>140</b>
4b.1	<b>Introduction .....</b>	<b>140</b>
4b.2	<b>Aim.....</b>	<b>141</b>
4b.3	<b>Methods.....</b>	<b>141</b>



<b>4b.3.1</b>	Treatment of cancer cells with doxorubicin.....	141
<b>4b.3.2</b>	Treatment of cancer cells with thapsigargin.....	141
<b>4b.3.3</b>	Treatment of cancer cells with TUDCA.....	142
<b>4b.3.4</b>	Immunocytochemistry.....	142
<b>4b.3.5</b>	HCMEC/D3.....	142
<b>4b.3.6</b>	CRT ELISA.....	142
<b>4b.3.7</b>	Preparation of cell lysates for western blotting.....	142
<b>4b.3.8</b>	Western blotting.....	143
<b>4b.3.9</b>	Assessment of apoptosis and necrosis.....	143
<b>4b.4</b>	<b>Results</b> .....	144
<b>4b.4.1</b>	Doxorubicin treatment of cancer cells increased release of endogenous CRT.....	144
<b>4b.4.2</b>	The effect of doxorubicin on cell death and CRT externalisation on non- cancer cells.....	146
<b>4b.4.3</b>	Treatment of both OVcar3 and SKOV3 cells with thapsigargin and doxorubicin alone and in combination increases surface exposure of endogenous CRT.....	147
<b>4b.4.4</b>	Inhibition of ER stress by TUDCA reduced externalization of CRT from doxorubicin treated ovarian cancer cells.....	154
<b>4b.4.5</b>	Effect of ER-stressors and inhibitors on CRT expression and release from OVcar3 cells.....	160
<b>4.1</b>	<b>Discussion</b> .....	162
<b>4.2</b>	<b>Conclusion</b> .....	167
 <b>Chapter 5: Investigation into whether exogenous CRT or cancer cells expressing surface CRT can induce maturation of DCs and subsequent activation of T- cells</b> .....		
<b>5.1</b>	<b>Introduction</b> .....	168

<b>5.2 Aims</b> .....	172
<b>5.3 Methods</b> .....	173
<b>5.3.1 Cell culture</b> .....	173
<b>5.3.2 Isolation of human blood mononuclear cells (Protocol 1)</b> .....	173
<b>5.3.3 Generation of mDCs from monocytes (Protocol 2)</b> .....	175
<b>5.3.4 Co-culture of imDCs with doxorubicin (DX) pre-treated OVcar3 cells or purified CRT (see Figure5.2)</b> .....	176
<b>5.3.5 ELISA protocol</b> .....	178
<b>5.3.6 Isolation of human T lymphocytes</b> .....	178
<b>5.3.7 Examination of T-cell activation by mDCs (see Figure 5.3)</b> .....	179
<b>5.3.8 Treatment of T cells with human T-activator CD3/CD28 Dynabeads</b> .....	180
<b>5.3.9 Activation of human T cells with CD3/CD28 T-activator Dynabeads</b> .....	182
<b>5.3.10 Flow cytometry</b> .....	183
<b>5.3.11 Statistical analysis</b> .....	184
<b>5.4 Results</b> .....	184
<b>5.4.1 Generation of imDCs from the human monocytic THP-1 cell line</b> .....	184
<b>5.4.2 Phenotypic maturation of imDCs derived from THP-1 monocytes to mDCs by LPS</b> .....	188
<b>5.4.3 The effect of CRT on maturation of THP-1 derived imDCs</b> .....	188
<b>5.4.4 Monocyte isolation</b> .....	193
<b>5.4.5 Generation of imDCs from isolated peripheral monocytes</b> .....	193
<b>5.4.6 Generation of mDCs from imDCs derived from peripheral blood monocytes</b> .....	197
<b>5.4.7 CRT promotes monocyte derived imDC maturation</b> .....	197
<b>5.4.8 DCs derived from peripheral blood monocytes exhibit a dendritic morphology</b> .....	202
<b>5.4.9 Activation of DC maturation by ovarian cancer cells (OVcar3) treated with doxorubicin to induce surface expression of CRT</b> .....	202
<b>5.4.10 Doxorubicin-treated ovarian cancer cells (OVcar3) induce DC maturation</b> .....	204
<b>5.4.11 Maturation of dendritic cells derived from peripheral monocytes is associated with</b>	

increased secretion of IL12/IL23.....	212
<b>5.4.12</b> Maturation of dendritic cells derived from THP-1 cells is also associated with increased secretion of IL12/IL23.....	215
<b>5.4.13</b> The effect of mDCs on T-cell proliferation.....	218
<b>5.4.14</b> Activation of human T cells by Human T-Activator CD3/CD28 Dynabeads®.....	220
<b>5.4.15</b> Activation of human T cells by mDCs induced to mature by various treatments (see Figure 5.30).....	220
<b>5.5 Discussion</b> .....	225
<b>5.6 Conclusions</b> .....	233
<b>Chapter 6: Final discussion</b> .....	234
<b>Chapter 7: Critique of the experimental approaches used in this thesis</b> .....	241
<b>7.1 Chapter 3. Purification of calreticulin and preparation of monomeric     CRT</b> .....	241
<b>7.2 Chapter 4a. Examination of the conditions required for binding of     exogenous calreticulin to EOC cells</b> .....	242
<b>7.3 Chapter 4b. Examination of the conditions required for surface exposure of     translocated endogenous calreticulin in ovarian cancer cells</b> .....	251
<b>7.4 Chapter 5. Investigation into whether exogenous CRT or cancer cells     expressing surface CRT can induce maturation of DCs and subsequent     activation of T-cells.</b> .....	253
<b>References</b> .....	258

## **Acknowledgements**

I am extremely grateful to my supervisor Dr Jacqueline Whatmore for her unending encouragement, support and continuing to mind me and help me along with my project. She willingly lent me her time, resources and expertise without which the completion of this thesis would not have been possible.

Special thanks to my supervisor Dr Paul Eggleton for his support and encouragement during this project. At many stages in this research project, I benefited from his advice. His positive outlook and confidence in my research inspired me and gave me confidence. His careful editing contributed enormously to the production of this thesis. A big thank you to my supervisors Dr Edwin Bremer and professor Marek Michalak for all the support and encouragement they gave me.

I would also like to thank Dr Chris Scotton for his help and advice at the start of the project. He provided very helpful and encouraging feedback.

A massive thank you to The Higher Committee for Education Development in Iraq (HCED) for funding in this research.

I want to sincerely thank my three angels for giving me the space and time—out to write my thesis and of course I must thank my best friend and my husband, Ahmed for a terrific support and great source of encouragement. Thanks also to my parents and siblings- from the bottom of my heart.

Thanks also go to my colleagues all my IBCS colleagues, who expressed an interest in the project and for your kindness and support.

## List of figures

<b>Figure Description</b>	<b>pages</b>
<b>1.1</b> Overview of the origin of tumours within the ovary.....	25
<b>1.2</b> Outline of adaptive immunity .....	33
<b>1.3</b> A diagram showing the MHC -1 complex on the cell membrane.....	36
<b>1.4</b> A diagrammatic image showing the main morphological stages of apoptosis.....	48
<b>1.5</b> Schematic representation of the detection of the apoptotic process using fluorescently labelled PI and annexin V to detect changes.....	50
<b>1.6</b> A model of CRT and its domain organisation.....	54
<b>1.7</b> Disruption of the “don’t eat me” signal by CRT.....	58
<b>1.8</b> Immunogenic cell death and DAMPS.....	59
<b>2.1</b> Counting of cells on a haemocytometer.....	72
<b>2.2</b> This graph displays two measurement parameters.....	75
<b>2.3</b> EpCAM-cy5 fluorescence did not overlap with FITC and PE staining.....	77
<b>2.4</b> Representative plot of cell viability of ovarian cancer cells assessed by flow cytometry.....	79
<b>2.5</b> CRT ELISA standard curve.....	81
<b>2.6</b> BCA assay standard curve.....	84
<b>3.1</b> A schematic diagram of calreticulin.....	89
<b>3.2</b> Summary of CRT purification steps.....	90
<b>3.3</b> Mono Q chromatographic analysis of human rCRT from E coli and Pichia pastoris.....	97
<b>3.4</b> Only CRT is detected by SDS PAGE in Mono Q fractions of chromatographed E Coli CRT.....	99
<b>3.5</b> Size exclusion chromatography of (A) Pichia expressed and (B) E. coli expressed human calreticulin.....	100
<b>4a.1</b> An example of the experimental set up of the CRT binding (in this case to OVcar3 cells).....	109

<b>4a.2</b>	Workflow figure showing cells treated with labelled proteins and analysed by fluorescence microscopy.....	109
<b>4a.3</b>	Experimental design of the studies examining CRT binding to cancer cells pre-treated with thapsigargin or doxorubicin (DX).....	110
<b>4a.4</b>	Gating of Ovcar3 cancer cells treated with thapsigargin .....	112
<b>4a.5</b>	Sample FPLC traces showing of FITC-conjugation to CRT and HSA .....	114
<b>4a.6</b>	Morphological characteristics of the cancer cell lines studies.....	114
<b>4a.7</b>	Demonstration of FITC-CRT, FITC-HSA and FITC-IgG binding to OVcar3 cancer cells by flow cytometry.....	116
<b>4a.8</b>	FITC-CRT binds to four cancer cell lines at all concentrations tested.....	117
<b>4a.9</b>	FITC-CRT and FITC-HSA bind to the surface of cancer cells as assessed by fluorescence microscopy.....	119
<b>4a.10</b>	Dose response effect of doxorubicin on cancer cell survival.....	120
<b>4a.11</b>	Doxorubicin treatment of OVcar3 ovarian cancer cells induces cell apoptosis (early and late) and necrosis as quantified by flow cytometry using Annexin V and PI.....	121
<b>4a.12</b>	The percentage of living and dying cancer cells pre and post doxorubicin treatment.....	122
<b>4a.13</b>	Degree of FITC-CRT binding to A2780 ovarian cancer cells before and after treatment with doxorubicin.....	125
<b>4a.14</b>	Mean fluorescence intensity (MFI) of FITC-CRT binding to living and dying cells pre and post treatment with doxorubicin.....	126
<b>4a.15</b>	Doxorubicin treatment of OVcar3 ovarian cancer cells enhances CRT binding.....	128
<b>4a.16</b>	Representative flow cytometry histograms showing that exogenous FITC-CRT binding to SKOV3 ovarian cancer cells is increased under stress conditions using the ER-stressors doxorubicin and thapsigargin.....	130
<b>4a.17</b>	Doxorubicin and thapsigargin can induce cell death in ovarian cancer cells and exogenous CRT preferentially binds to cancer cells undergoing apoptosis after treatment with thapsigargin and doxorubicin.....	131
<b>4a.18</b>	TUDCA does not induce cell death, and protects against doxorubicin and thapsigargin induced toxicity, in ovarian cancer cells.....	135

<b>4a.19</b> TUDCA promoted a decrease in exogenous CRT binding to doxorubicin (DX) treated ovarian cancer cells.....	136
<b>4a.20</b> Treatment with TUDCA reduced the exogenous FITC-CRT binding to ovarian cancer cells when compared with cells treated with doxorubicin and thapsigargin.....	138
<b>4a.21</b> TUDCA reduces binding of exogenous CRT to doxorubicin (DX) treated Ovc3 ovarian cancer cells as assessed by immunofluorescent staining.....	139
<b>4b.1</b> Doxorubicin treatment increases surface expression of endogenous CRT on non-permeabilised SKOV3 cancer cells.....	145
<b>4b.2</b> Doxorubicin dose-dependently induces apoptosis and necrosis in OVcar3 ovarian cancer cells, but not HCMEC/D3 human endothelial cells.....	149
<b>4b.3</b> The ER stressors doxorubicin and thapsigargin alone and in combination induce CRT exposure in SKov3 and OVcar3 ovarian cancer cells.....	151
<b>4b.4</b> Surface expression of endogenous CRT is significantly increased in ovarian cancer cells in varying stages of apoptosis and necrosis in cells treated with doxorubicin and/or thapsigargin.....	152
<b>4b.5</b> Surface exposure of CRT from cancer cells is induced by doxorubicin and thapsigargin individually and enhanced by treatment with both together.....	153
<b>4b.6</b> TUDCA reduces cell death and externalisation of endogenous CRT in doxorubicin or thapsigargin treated OVcar3.....	156
<b>4b.7</b> TUDCA reduces cell death and externalisation of endogenous CRT in doxorubicin or thapsigargin treated SKov3.....	158
<b>4b.8</b> TUDCA reduced the amount of endogenous CRT externalised on the cell surface of OVcar3 ovarian cancer cells treated with the ER stressor thapsigargin.....	159
<b>4b.9</b> Effect of Doxorubicin and thapsigargin on secretion and expression of CRT in OVcar3 cells.....	161
<b>5.1</b> Schematic representation of the major signals involved in activating T-cell responses.....	170
<b>5.2</b> Schematic describing the experimental design of treatments potentially inducing DC maturation.....	177

<b>5.3</b>	Schematic describing the experimental design of T-cell isolation and activation/proliferation as assessed by CFSE staining.....	181
<b>5.4</b>	Diagram indicating the mechanism by which T cell expansion activated using anti-CD3/anti-CD28 coated Dynabeads mimics T-cell activation in vivo by antigen presenting cells.....	182
<b>5.5</b>	Morphology of THP-1 cells at 0 day.....	185
<b>5.6</b>	THP-1 cells can be induced to express markers of imDCs.....	187
<b>5.7</b>	DC maturation status examined using flow cytometry analysis of surface markers.....	189
<b>5.8</b>	CRT induced maturation of THP-1 derived imDCs to mDCs.....	190
<b>5.9</b>	CRT induced expression of mDC markers in THP-1 derived imDCs.....	192
<b>5.10</b>	Isolation procedure for purification of monocytes from peripheral human blood.....	194
<b>5.11</b>	Characterisation of enriched monocyte population.....	184
<b>5.12</b>	Peripheral monocytes can be differentiated into imDCs.....	196
<b>5.13</b>	imDCs derived from peripheral blood monocytes can be differentiated into mDC by LPS.....	198
<b>5.14</b>	Exogenous CRT can induce maturation of imDCs derived from peripheral monocytes.....	199
<b>5.15</b>	CRT induced expression of mDC markers in peripheral blood monocyte derived imDCs.....	201
<b>5.16</b>	The morphology of isolated peripheral blood monocytes changes during differentiation to imDCs and maturation to mDCs.....	203
<b>5.17</b>	EpCAM is expressed on ovarian cancer cells, but DC markers are not.....	205
<b>5.18</b>	Ovcar3 cells express high surface levels of EpCAM and low levels of DC markers.....	206
<b>5.19</b>	mDCs do not express EpCAM.....	207
<b>5.20</b>	Co-incubation of doxorubicin treated OVcar3 cells with peripheral blood derived imDCs induced DC maturation.....	208
<b>5.21</b>	Co-incubation of doxorubicin treated OVcar3 cells with peripheral monocyte derived imDCs induced DC maturation.....	209
<b>5.22</b>	Co-incubation of doxorubicin treated OVcar3 cells with THP-1 derived imDCs induced DC maturation.....	210



<b>5.23</b>	Co-incubation of doxorubicin treated OVcar3 cells with THP-1 derived imDCs induced DC maturation.....	211
<b>5.24</b>	Peripheral blood monocyte derived DC maturation by CRT is associated with secretion of the cytokines IL12 and IL23.....	213
<b>5.25</b>	Co-incubation of doxorubicin treated OVcar3 cells and peripheral monocyte-derived imDCs induces secretion of IL12/IL23.....	214
<b>5.26</b>	THP-1 derived DC maturation is only associated with secretion of the cytokines IL12 and IL23 when induced by high concentrations of CRT.....	216
<b>5.27</b>	OVcar3 cells pre-treated with high concentrations of doxorubicin induce secretion of IL12/IL23 from THP-1 derived DCs during DC maturation.....	217
<b>5.28</b>	Flow cytometry analysis of a typical CD8 T-cell purification using negative selection magnetic bead technology.....	219
<b>5.29</b>	T lymphocyte proliferation induced by human T-activator anti-CD3/CD28 Dynabeads™ and assessed by CFSE fluorescence.....	221
<b>5.30</b>	Schematic showing the experimental plan of studies carried out to examine whether DCs induced to mature by various treatments could subsequently stimulate T cell proliferation.....	222
<b>5.31</b>	DCs induced to mature by either exogenous or cancer cell surface bound CRT subsequently induce T-cell activation as assessed by proliferation.....	224
<b>5.32</b>	Schematic representation of the experimental procedures used in this chapter.....	227
<b>6.1</b>	Flowchart representing the key finding of this study.....	237
<b>6.2</b>	Possible use of EpCAM / CRT bi-specific antibody fragments that directly target CRT to tumour cells.....	239
<b>6.3</b>	Possible future <i>in vivo</i> strategies to test whether enhancing surface levels of CRT could be an anti-cancer therapeutic strategy ...	240
<b>7.1</b>	Free FITC does not bind to the surface of OVcar3 ovarian cancer cells .....	243
<b>7.2</b>	Demonstration of FITC-CRT, FITC-HSA and FITC-IgG binding to OVcar3 cancer cells by flow cytometry.....	245
<b>7.3</b>	Exogenous FITC-CRT binds to four cancer cell lines at all concentrations tested.....	246

<b>7.4</b>	Doxorubicin induces externalisation of phosphatidylserine in A2780 ovarian cancer cells as assessed by annexin V binding.....	248
<b>7.5</b>	No non-specific binding of secondary antibody is observed in cells treated with vehicle in place of primary antibody prior to staining with results in Cy5 secondary antibody .....	252
<b>7.6</b>	Mature DCs induce significantly more T-cell proliferation than imDCs .....	254
<b>7.7</b>	OVcar3 ovarian cancer cells pre-treated with high concentrations of doxorubicin induce secretion of IL12/IL23 from THP-1 derived imDCs during DC maturation .....	256

## List of tables

Table	Description	Page
1.1	International Federation of Gynaecology and Obstetrics (FIGO) nomenclature staging system for ovarian cancer.....	26
1.2	A table displaying the principle white blood cell types.....	30
1.3	Expression of level CRT in different cancers.....	53
1.4	Characteristics of clinically relevant ER stressors.....	63
3.1	Preparation of MonoQ buffer A, pH 8.....	92
3.2	Preparation of MonoQ buffer B, pH 8.....	92
4a.1	Dose-dependent effects of doxorubicin in tumour cells.....	123
4a.2	Mean fluorescent intensity (MFI) of FITC-CRT binding to OVcar3, SKOV3, A2870 and FaDu tumour cells pre- and post- doxorubicin treatment.....	127
4b.1	Doxorubicin induces apoptosis and necrosis in OVcar3 ovarian cancer cells, but not HCMEC/D3 human endothelial cells.....	150
5.1	Major cell surface markers on mature DCs.....	169
5.2	Details of the antibodies and the isotype controls used characterisation of imDCs & mDCs.....	184

## Abbreviations

Apaf-1	Apoptotic protease activating factor 1
APCs	Antigen presenting cells
ATP	Adenosine triphosphate
B- Cell	B- lymphocytes
BCA	Bicinchoninic acid
BSA	Bovine serum albumin
C1q	Complement 1q
CD	Cluster of differentiation
CFSE	Carboxyfluorescein succinimidyl ester
CRT	Calreticulin
CTLs	Cytotoxic T lymphocytes
CV	Column volume
DAMP	Damage-associated molecular pattern
Dapi	4', 6-Diamidine-2'-phenylindole dihydrochloride
DCs	Dendritic cells
DISC	Death-inducing signalling complex
DMSO	Dimethyl sulfoxide
DPBS	Dulbecco's Phosphate Buffered Saline
DTT	Dithiothreitol
DX	Doxorubicin
E-coli	Escherichia coli
EDTA	Ethylenediaminetetraacetic acid
ELISA	Enzyme-linked immunosorbent assay
EOC	Epithelial ovarian cancer
EpCAM	Epithelial cell adhesion molecule
ER	Endoplasmic reticulum
ERAD	ER-associated protein degradation
FBS	Foetal bovine serum
FDA	U.S. Food and Drug Administration
FIGO	International Federation of Gynaecology and Obstetrics

FITC	Fluorescein isothiocyanate
FPLC	Fast Protein Liquid Chromatography
FSC	Forward scatter
GM-CSF	Granulocyte-macrophage colony-stimulating factor
HCl	Hydrogen chloride
HCMEC/D3	Human cerebral microvascular endothelial cell line
HLA	Human leukocyte antigen
HMGB1	High mobility group box 1 protein
HSA	Human serum albumin
IAP	Inhibitors of apoptosis proteins
ICD	Immunogenic cell death
ICF	Guava Instrument Cleaning Fluid
IFN- $\gamma$	Interferon- gamma
IgG	Immunoglobulin G
IL	Interleukins
imDCs	Immature dendritic cells
KDa	Kilo Daltons
LAK	Lymphokine-activated killer cells
Lith-CRT	Lithuania calreticulin
LPS	lipopolysaccharide
MAGE	Melanoma-associated antigen 1
mDC	Mature dendritic cells
MHCs	Major histocompatibility complexes
MW	Molecular weight
NaCl	Sodium chloride
NaOH	Sodium hydroxide
NK	Natural killer
PAMPs	Pathogen- associated molecular patterns
PBMCs	Peripheral blood mononuclear cells
PBS	Phosphate Buffered Saline
PI	Propidium iodide
PMB	Polymyxin B
PRRs	Pattern recognition receptors

PS	Phosphatidylserine
rCRT	Recombinant calreticulin
ROS	Reactive oxygen species
SDS PAGE.	Sodium dodecyl sulfate polyacrylamide gel electrophoresis
SERCA	Sarcoplasmic reticulum/ER Ca <sup>+2</sup> ATPase
SIRP- $\alpha$	Signal regulatory protein $\alpha$
SSC	Side scatter
T cells	T- lymphocytes
TBS	Tris buffered saline
TCR	T-cell receptor
TG	Thapsigargin
TLR	Toll-like receptor
TNF	Tumour necrosis factor
TRAIL	TNF-related apoptosis inducing ligand
TSP-1	Thrombospondin-1
TUDCA	Tauroursodeoxycholate
UPR	Unfolded protein response
USA	United States of America
WB	Western blot
$\alpha$	Alpha
$\beta$	Beta
$\Delta$	Delta

## **Chapter 1 Introduction**

### **1.1 Ovarian cancer**

Ovarian cancer is one of the most deadly forms of cancer (Siegel et al., 2016). Due to the difficulty of early detection, in approximately 80 percent of ovarian cancer cases, it is discovered after widespread dissemination throughout the abdomen and other areas of the body. Thus ovarian cancer is known as a silent killer with a poor prognosis (Coosemans et al., 2016). When diagnosed in the advanced stages, standard therapies are surgery, chemotherapy and radiation, and initially, although patients respond to these conventional therapies, within 5 years of diagnosis, there is often disease recurrence and death due to drug-resistant disease (Drakes and Stiff, 2016). A very brief overview of current theories describing the stages of ovarian will be discussed later in this chapter.

#### **1.1.1 Epidemiology**

Epithelial ovarian cancer (Binju et al., 2018) is the fifth most common cancer among women and the leading cause of death from gynaecological cancer in the UK. Each year more than 6,500 women are diagnosed with ovarian cancer in the UK and about 4,400 women die of the disease (Doufekas and Olaitan, 2014). Latest figures show that ovarian cancer accounts for 4% of all new cancer cases in females in the UK (@CR\_UK, 2016). Survival following a diagnosis of ovarian cancer has improved in England overall since the mid-1980s, from 57% to 73% for one-year survival and from 33% to 44% for five-year survival. However, there has been little or no improvement in both one- and five-year survival rates for the oldest women over the last 20 years (Nordin, 2012).

#### **1.1.2 Risk factors**

Although the mortality of ovarian cancer is high, its aetiology is not fully understood (Horne, 2018). However, certain factors associated with this cancer have been identified (Brinton et al., 2013). The majority of ovarian cancers are sporadic with only 5% - 10% familial. A history of infertility, low parity, long time from menarche to

menopause, the use of hormone replacement therapy and family history of breast and ovarian cancer seem to be associated with an elevated risk of ovarian cancer (Berek, 2003). There also appears to be an association between prior history of pelvic inflammatory disease, polycystic ovary syndrome and endometriosis, and an increased risk of ovarian cancer (Lin et al., 2011). Conversely, higher parity and the use of oral contraceptives have consistently been shown to decrease the risk of ovarian cancer (Trevino et al., 2012). In particular, the risk is significantly decreased with increased duration of oral contraceptive use; with persistent protection up to 25 years after the last dose (Brynhildsen, 2014). Interestingly, the majority of studies indicate that there is a 16 – 22% reduction in the risk of EOC with each pregnancy (Schock et al., 2014), suggesting that fewer ovulations protect against ovarian cancer. More recently, this incessant ovulation theory has been questioned by a study where women took progesterone-only oral contraceptives. This does not stop ovulation but proved to be as effective at reducing ovarian cancer risk as ovulation-inhibiting contraceptive pills (Brohet et al., 2007). Additionally, nulligravid women who have not been pregnant because of infertility are at 40% higher risk of developing ovarian cancer than nulligravid women who did not attempt to become pregnant (Diergaarde and Kurta, 2014).

### **1.1.3 Overview of ovarian cancer types**

Invasive EOCs constitute approximately 90% of all cases of ovarian malignancies whereas non-epithelial types are less common; with sex cord-stromal tumours making up 6% of all ovarian malignancies, germ cell tumours (3%) and all others only 1% collectively (see Figure 1.1) (Boussios et al., 2018). EOCs are divided into five histological subtypes: serous, mucinous, endometrioid, clear cell, and transitional, and of these, epithelial serous carcinomas represent the majority of all primary ovarian carcinomas. Of the EOCs approximately 80% are serous, 10% mucinous and 10% endometrioid cancers, with the other types making up only a very small % of the total (Holschneider and Berek, 2000).



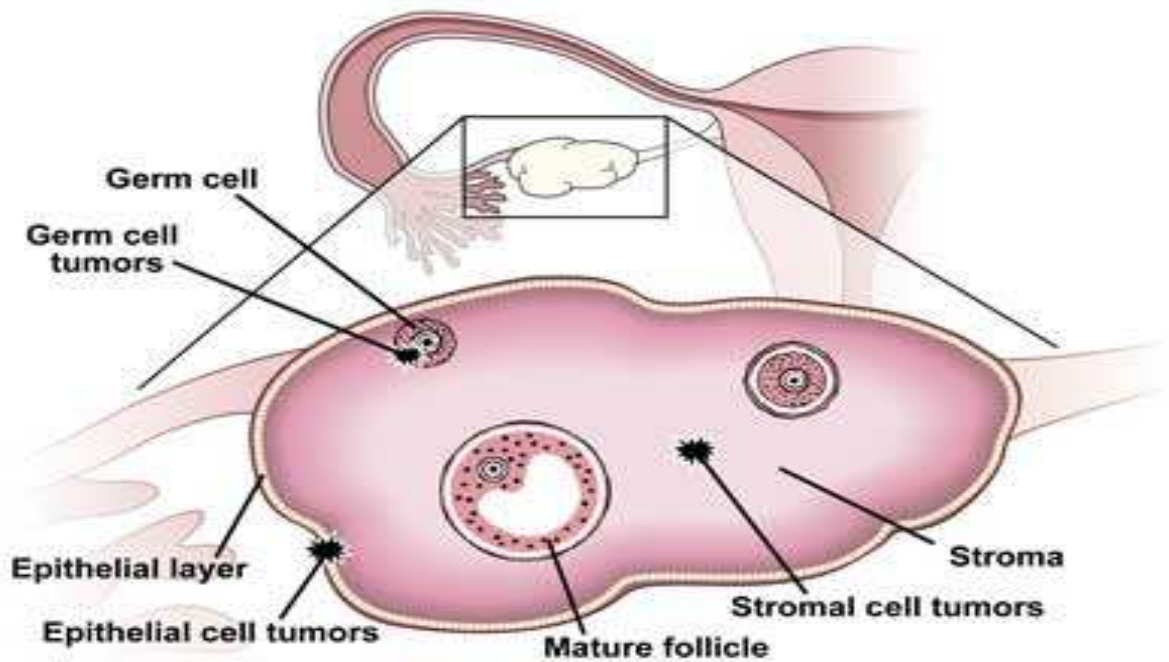


**Figure 1.1 Overview of the anatomy of the ovary and the histological origin of ovarian tumours.** Most ovarian tumours (approximately 90%) derive from the epithelial layer surrounding the ovary, although tumours can also arise from the germ (egg) cells or sex cord/stromal cells (mesenchyme). (Alicia Algeciras-Schimmich, 2013).

#### 1.1.4 Staging of ovarian cancer

There is no single universally accepted system for grading ovarian cancers. Over the years most of the staging systems for gynaecological cancers (with the exception of cervical cancer) have moved from a clinical basis to one of a surgical pathological nature. The rationale behind this decision arises in the necessity to evaluate the ovarian cancer patient during an initial surgery and the staging is then based on localisation and pathological features of a tumour. Further treatment and possible outcomes depend on the success of the initial operation and therefore a clear and fast staging system had to be created. For ovarian cancer, the International Federation of Gynaecology and Obstetrics (FIGO) proposed a staging that is widely used and is described in Table 1.1. The FIGO system is a surgical system, which does not incorporate the grade of a tumour (Pereira et al., 2015).

<b>Stage I - Growth limited to the ovaries</b>
<b>Ia</b> Growth limited to one ovary; no ascites containing malignant cells present; no tumour on the external surface; capsules intact.
<b>Ib</b> Growth limited to both ovaries; no ascites containing malignant cells, present; no tumour on the external surfaces; capsules intact
<b>Ic</b> Tumour either Stage Ia or Ib, but with: capsule ruptured, or ascites present containing malignant cells, or positive peritoneal washings
<b>Stage II - Growth involving one or both ovaries with pelvic extension</b>
<b>IIa</b> Extension and/or metastases to the uterus and/or fallopian tubes
<b>IIb</b> Extension to other pelvic tissues
<b>IIc</b> Tumour either Stage IIa or IIb, but with: capsule(s) ruptured, or ascites present containing malignant cells, positive peritoneal washings
<b>Stage III - Tumour involving one or both ovaries with histologically confirmed peritoneal implants outside the pelvis and/or positive retroperitoneal or inguinal nodes. Superficial liver metastases equals stage III. Tumour is limited to the true pelvis, but with histologically proven malignant extension to small bowel or omentum.</b>
<b>IIIb</b> Tumour of one or both ovaries with histologically confirmed implants, peritoneal metastasis of abdominal peritoneal surfaces, none exceeding 2 cm in diameter; nodes are negative.
<b>IIIc</b> Peritoneal metastasis beyond the pelvis >2 cm in diameter and/or positive retroperitoneal or inguinal nodes.
<b>Stage IV - Growth involving one or both ovaries with distant metastases*.</b> Parenchymal liver metastasis equals Stage IV. * If pleural effusion is present, there must be positive cytology to define a case as Stage IV.

**Table 1.1. International Federation of Gynaecology and Obstetrics (FIGO) nomenclature staging system for ovarian cancer (FIGO 2013).**

### **1.1.5. Chemotherapy in EOC**

Chemotherapy in treating newly diagnosed advanced EOC (Brohet et al., 2007, Harries and Gore, 2002) has been a standard of care for patients (Wright et al., 2016). However, there are abundant areas of controversy in treating this disease, including the role of cytoreductive surgery, the optimum drug combination regimen, the importance of dose intensity in chemotherapy, the effectiveness of intraperitoneal therapy, the benefit of abdomen irradiation, and the status of immunotherapy and hormones (Hacker, 1989).

Over the decades, chemotherapy for ovarian cancer has evolved and currently involves a combination of intravenous platinum and taxane chemotherapy (Cristea et al., 2010). The chemotherapy drugs used to treat ovarian cancer typically combine a platinum-based drug such as carboplatin (Paraplatin) or cisplatin, with a taxane such as paclitaxel (Taxol) or docetaxel (Taxotere). The number of treatment days varies with the drug given (Binju et al., 2018). The most effective treatment for the advanced disease involves reducing the tumour burden through surgery followed by chemotherapy.

Two different techniques are used to treat ovarian cancer. One technique, intravenous platinum/taxane therapy, was effective for ovarian cancer (Cristea et al., 2010). An alternative option is administration of chemotherapy via the intraperitoneal route (Armstrong et al., 2006). This enhances drug delivery at the peritoneal surface and may improve outcomes by eliminating residual disease more efficiently than intravenous administration of chemotherapy (Wright et al., 2016). Interestingly, some studies have reported that treatment via the intraperitoneal route gave a significant survival advantage compared with intravenous chemotherapy platinum and taxane (Ozols et al., 2006, Eoh et al., 2017). Additionally, it has been shown that the effect of intraperitoneal chemotherapy extends beyond treatment years (Eoh et al., 2017). However, the main disadvantage to intraperitoneal chemotherapy is that the side effects can be severe and lead to treatment change to intravenous chemotherapy. These issues of poor survival and chemotherapy regimens that reduce patient quality of life highlight the urgent need to find improved therapeutic strategies for patients with EOC. One alternative chemotherapeutic route might be the development of immunotherapy i.e. treatment that stimulates the body's own immune system to fight the cancer.

## 1.2. An overview of the immune system

The immune system utilises a series of defence mechanisms that help protect cells of the body from pathogens (West et al., 2006). In order for the immune system to be effective it must be able to distinguish between cells of the body and foreign agents that can bring harm. Thus, cells have unique molecules on the cell membrane and the immune system can recognise these biomolecules to identify 'self' cells. Classically, the immune system and its defence mechanisms are divided into non-specific (innate) immunity and specific (acquired) immunity (Vivier et al., 2011). The innate and acquired immune systems utilise a range of physical and cellular components that play a vital role in immune surveillance and immune defence. Therefore, the use of the immune system to eradicate cancer is a potential approach for curing cancer (Wang and Wang, 2012).

### 1.2.1 Innate immune system

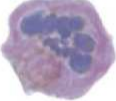


The innate immune system consists of non-specific defence mechanisms that not only act to prevent infection but also act immediately following infection, and is a primary line of defence against pathogens. Non-specific defence does not depend on the presence of specific antigens, that is, the innate immune system attacks all pathogens independently of presented antigens (Chaplin, 2010). The innate immune system functions not only to prevent physical movement of pathogens into the body but also to prevent their spread throughout the body if they do enter. Thus, the innate immune system consists of physical barriers such as skin, non specific defence mechanisms such as stomach acid, mucous or tears and general immune responses such as inflammation and non-specific cellular components

- **Physical defenses** There are several anatomical structures that act as physical barriers to pathogens (Amjadi et al., 2014).
  1. **Skin:** Skin consists of several layers that create a first line of defence against the movement of pathogens. Additionally, skin contains glands that secrete a fatty acid and this creates a layer in which bacteria cannot grow and survive (Belkaid and Hand, 2014).
  2. **Tears and saliva:** Saliva in the mouth and tears in the eyes contain lysozyme which helps break down the cell wall of bacteria (McDermott, 2013).
  3. **Mucous and cilia:** Air passages in the body including the nasal cavity, trachea

and bronchi have specialised cells called goblet cells which secrete a mucus which traps pathogens. Cilia can also be present and move pathogens to the outside or to the stomach (Bustamante-Marin and Ostrowski, 2017).

4. **Acidity of stomach acid:** Parietal cells release HCl, which creates a high acidity environment that kills most pathogens that enter the stomach via food or via mucus (Sahoo et al., 2017).
- **Inflammatory defenses:** Following entry of a pathogen into tissue the innate immune system initiates the process of inflammation. In this process, blood flow is increased to the infected area, enhancing delivery of key white blood cells (leukocytes) – neutrophils, eosinophils, basophils and macrophages (Nicholson, 2016).
  - **Non-specific cellular components:**
    1. Neutrophils: These cells are recruited to the infected area and engulf pathogens and harmful agents through release of cytotoxic granules and initiation of the oxidative burst. Each neutrophil is capable of killing 20 bacteria before dying (Selders et al., 2017) (Table 1.2).
    2. Basophils: Basophils release histamine, which causes dilation of blood vessels in the infected area, causing redness. The capillaries in the infected area also become more leaky, which causes oedema (Poerber and Sessa, 2014).
    3. Eosinophils: These cells are specialised to fight certain parasites e.g. the eosinophil is a defence against helminth parasites (Klionski and Nutman, 2004).
    4. Macrophages: Macrophages are phagocytic cells that can engulf hundreds of bacteria before dying (Nix et al., 2007). They also release cytokines that recruit additional immune cells.
    5. Mast cells: These are a type of leukocyte normally present in the connective tissue. After infection they release histamine and cytokines which cause vasodilation and enhanced vascular permeability, resulting in increased blood flow and white cell trafficking to infected area (Krystel-Whittemore et al., 2015).
    6. Natural killer (NK) cells: These are non-specific white blood cells. Although these are not involved in the inflammation response directly, they do kill infected cells and cancer cells in a non-specific way (Vivier et al., 2008).

The innate immune system is not educated, nor is it selective; no memory immune cells exist within the innate immune system (Boraschi and Italiani, 2018).

White blood cell	Functions
<b>Neutrophils</b> 	Early responder, phagocytosis and local killing
<b>Lymphocytes</b> 	Adaptive immunity, sub-divided into T-cells and B-cells
<b>Monocytes</b> 	Early responder, phagocytosis and antigen presentation. Mature as <b>macrophages</b> in the tissue.
<b>Basophils and eosinophils</b>	Granulocytes, rare in the circulation
	Bind IgE, defence against parasites, allergy

**Table 1.2: A table displaying the principle white blood cell types.** Non – granulocytes are lymphocytes and monocytes, these do not have granules. In contrast, granulocytes are granulated cells like neutrophils, basophils and eosinophils (Nicholson, 2016).

### 1.2.2 Complement 1q.

The complement system enhances the ability of antibodies and phagocytic cells to clear microbes and damaged cells and plays an essential role in both innate and adaptive immunity. The complement system refers to a large group of proteins circulating in the blood and tissue fluids that opsonize pathogens and cells and induce inflammatory responses to cause cell destruction and fight infection by three main mechanisms. Firstly, binding of activated complement proteins to pathogens, leading to opsonization and clearance by phagocytes e.g. macrophages and neutrophils, with corresponding complement receptors (classical pathway). Secondly, chemoattraction to recruit more phagocytes to the site of complement activation (alternative pathway). Thirdly, some complement components actually damage bacterial membranes (lytic pathway).

The classical pathway involves complement components C1, C2 and C4 and is triggered by antibody-antigen complexes binding to C1. Activation of these proteins can then create a cascade of events that ultimately destroys that antigen or pathogenic agent. The complement component C1 has three subcomponents, C1q, C1s and C1r. When activated, the constant region of certain antibodies ( IgM and IgG) can bind to the C1q molecule of the C1 complex. This, in turn, activates C1r and C1s and the pathway forms a C3 convertase which splits the complement component C3 into two fragments. The C3a can activate mast cells, causing the release of vasoactive mediators such as histamine. The C3b component can attach to microbial pathogens, resulting in opsonisation and lysis. Opsonisation by the C1 system is driven by receptor molecules on macrophages or neutrophils interacting with complement components on the cell e.g. C1qRp (CD93) or calreticulin (Ghebrehiwet and Peerschke, 2004).

The complement system also plays a key role in cell homeostasis by contributing to the lysis of cells undergoing apoptosis (Trouw et al., 2008). Specifically, extracellular plasma membrane changes occurring during apoptosis allow cells to bind complement molecules such as C1q. For instance, the ER chaperone protein calreticulin (CRT), which is externalised during apoptosis, has been shown to interact with C1q and to function as a recognition molecule on the apoptotic cell surface (by mediating recognition of phosphatidylserine, a key cellular marker of apoptosis) (Gold et al., 2010). It is now accepted that some cells and parasites develop mechanisms to avoid surveillance by the complement system e.g. by expressing molecules that interfere with the host complement system (Shao et al., 2019).

### **1.2.3. Adaptive immunity**

When infection begins, the innate immune system immediately uses non-specific mechanisms (e.g. inflammation) to destroy invading pathogens. The adaptive immune system is then activated (Figure 1.2). Adaptive immunity is educated in that it can “learn” and it has memory and can recall prior exposure to foreign antigens. It is specific and it has a selective, not general action. Several days may be needed to

activate the specific defence mechanisms of the adaptive immune system. Adaptive immunity can be subdivided into antibody-mediated (humoral) immunity and cell-mediated immunity (Bonilla and Oettgen, 2010).

#### **1.2.4. Antibody – mediated immunity (humoral)**

Humoral immunity involves leukocytes called B- lymphocytes. B- Lymphocytes are produced and mature in the bone marrow and are usually found in the lymph nodes. During the innate immune response, macrophages engulf and destroy pathogens. However, they process the pathogenic antigens and display them on their cell membrane. The B- lymphocytes express B- cell receptor on their membrane that can bind to these macrophage-bound antigens (Healey et al., 2005). Once the B- lymphocyte binds to a specific antigen, it interacts with T helper cells that initiate further differentiation. The B- lymphocyte then undergoes many cycles of mitosis to produce plasma cells and memory cells. Plasma cells produce antibodies specific to the original antigen exposed to the B- lymphocyte. Memory cells retain a copy of that antibody in case of reinfection. Antibodies are immunoglobulins that only recognise specific antigens.

#### **1.2.5. Cell - mediated immunity**

This involves leukocytes called T- lymphocytes (T cells). They are produced in the bone marrow but mature in the thymus. Helper T-cells release interleukins (Zhu et al., 2010) and interferons, which contribute to B- lymphocyte maturation into plasma cells and B memory cells. T- Lymphocytes express the membrane T-cell receptor. These cells can bind to antigen complexes and, with the help of helper T- cells, differentiate into T- cytotoxic cells (killer T-cells). These cytotoxic T- cells migrate to the infected area and bind a specific antigen. Once bound, they produce a protein (perforin) that can perforate and kill the pathogens. In addition T- lymphocytes can form memory cells, as well as suppresser cells, regulating the immune response (Hersperger et al., 2010).



### 1.2.6. Antigen presenting cells APCs

Antigen presenting cells (APCs) are cells that process and present antigen peptides on their cell surface complexed with major histocompatibility complexes (MHCs). The antigens can then be recognised by T- lymphocytes. Antigen presenting cells include macrophages, dendritic cells (DCs) and B- lymphocytes.

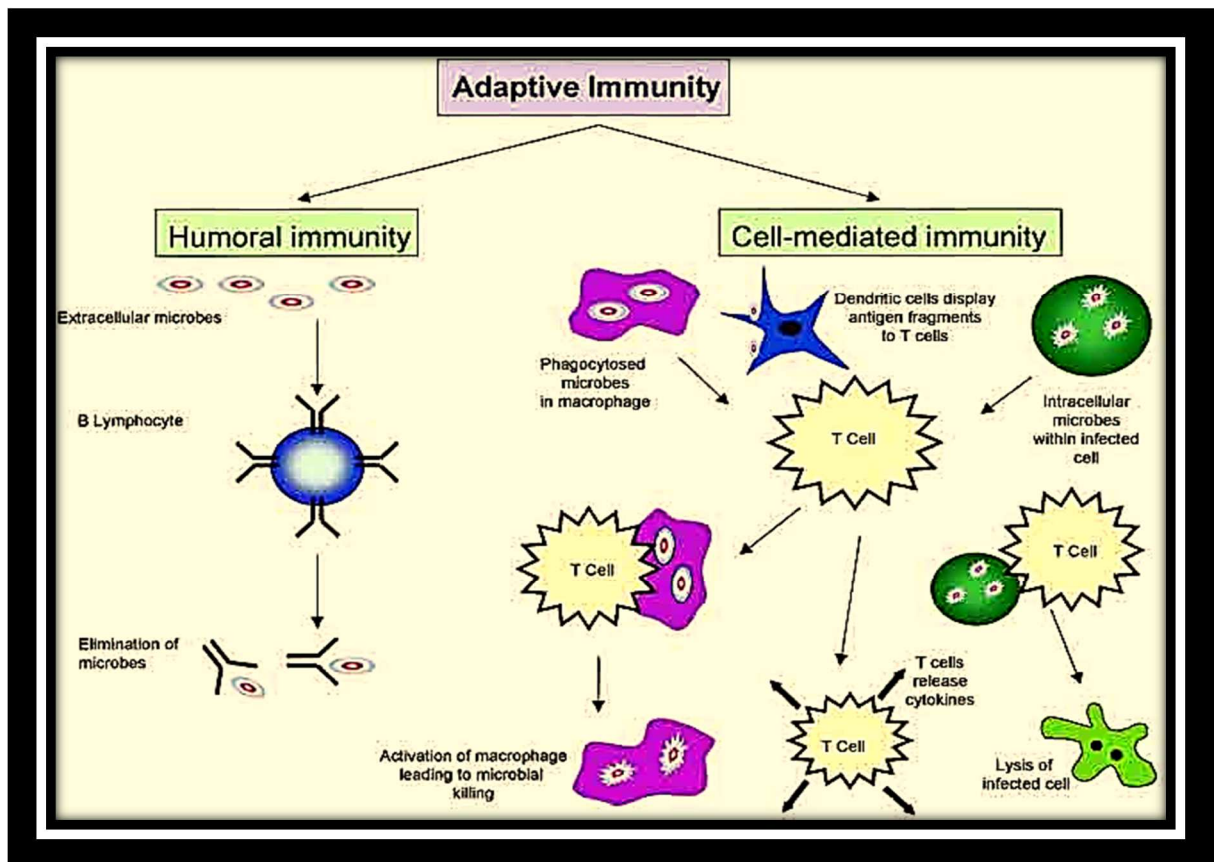


**Figure 1.2. Outline of adaptive immunity.** This includes humoral and cell-mediated immunity. B-lymphocytes release antibodies and are effective against many types of pathogens. T-lymphocytes are part of cell-mediated immunity and play an important role to activate macrophages to engulf foreign bodies and produce chemical factors to destroy pathogens (Rabb, 2002).

### **1.2.6.1. Macrophages**

Macrophages have multiple immune functions including detection and phagocytosis of pathogens, antigen presentation to T cells and cytokine production. Macrophages are derived from circulating monocytes which themselves have negligible immune activity (Kiertscher and Roth, 1996). They circulate in the blood, enter the tissue, and differentiate to mature macrophages following tissue damage or infection. Macrophages engulf pathogens and apoptotic cells, digest them inside vacuoles and present the pathogenic molecules on the MHC-class II found on their membrane (Berges et al., 2005).

### **1.2.6.2. Dendritic cells**

DCs are specialised antigen presenting cells found in the tissues, skin, lung and gastrointestinal tract. They essentially function as a bridge between innate immunity and adaptive immunity (Shortman and Naik, 2007). DCs are produced in the bone marrow and they migrate into the peripheral tissues from the blood stream where they initially remain in their immature state (Hansen and Andersen, 2017). Immature DCs express various pattern recognition receptors (PRRs). During infection, immature DCs recognise common features of many pathogens through these receptors and are thus able to bind to, and phagocytose, the pathogens. In this process, they capture and process antigens and display them on their MHC class II membrane proteins and become mature DCs. This maturation is accompanied by upregulation of co-stimulatory molecules such as CD40, CD80 and CD86 and increased secretion of inflammatory cytokines and chemokines (Savina and Amigorena, 2007) which are able to active naïve T-cells. The maturing DCs migrate to the lymph nodes or spleen and interact with T- lymphocytes – either killer T- cells (CD8+) or helper T-cells (CD4+).

### 1.2.7. MHC-1

The ability of the immune system to recognise its own cells and distinguish those cells from foreign pathogens depends on a group of protein markers found on the cell membrane called the major histocompatibility complex I (MHC-I) (<https://www.ncbi.nlm.nih.gov/books/NBK27156/>, 2001). These protein complexes are found on the surface of most nucleated cells. This is in contrast to the MHC-II complexes mentioned above which are found on APCs. The MHC-1 complex is formed of four peptide domains alpha 1, alpha 2, alpha 3 and beta 2 (Figure 1.3), with the alpha 3 subunit connected to the cell membrane. MHC molecules interact with peptide fragments derived from pathogens and display them on the cell surface, allowing leukocytes to differentiate healthy host cells from infected cells (Wieczorek et al., 2017). Healthy cells bind a self-antigen onto the MHC-1 complex allowing leukocyte recognition as a healthy cell and preventing immune destruction. In contrast in infected cells e.g. a virus, the cells display a non-self-antigen on MHC-I. Leukocytes can recognise these foreign antigens, bind to them and initiate a defensive mechanism that can destroy the infected cells (Alberts, 2002).

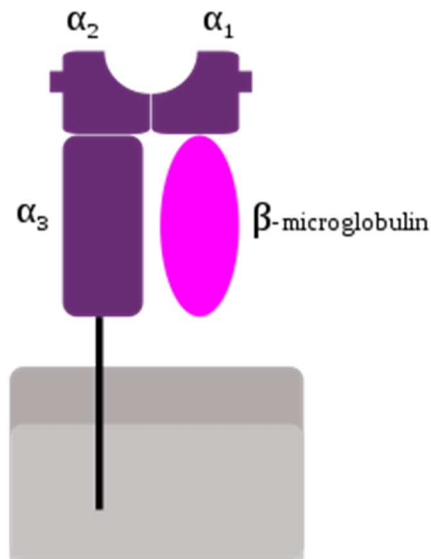


**Figure 1.3. A schematic diagram showing the MHC -1 complex on the cell membrane** (©kisspng.com, 2019). MHC-I is composed of two peptide chains, the alpha chain and beta 2 microglobulin with the former folded into three external domains; alpha 1, 2 and 3. The alpha chain has a transmembrane domain and a short stretch of hydrophilic amino acids which forms the cytoplasmic tail. The alpha chain 3 domain is invariant and contains the binding site for the T- cell co- receptor CD8. Beta microglobulin-2 binds non-covalently to the alpha chain and is essential for its correct folding.

### 1.2.8. T- cells

T-cells are very important in cell mediated immunity and they are distinguished from B-cells and natural killer cells through their surface expression of the T- cell receptor. T cells are categorised into two types, T- helper and T- cytotoxic cells (Vantourout and Hayday, 2013). T cells, via their T-cell receptor, identify antigenic peptides bound to MHC-I and -II molecules on the surface of host APCs. Initially, naive T-cells are triggered by identification of specific antigen/MHC complexes expressed by DCs which also present additional potent costimulatory signals for T-cell activation and proliferation. The ability of DCs to process and express antigens is essential to

produce T-cell mediated immunity, with activated T-cells damaging antigen-positive host cells, e.g., infected cells or tumour cells. Cancer cells can be targets for previously activated T-cells through the processing and presentation of relevant peptides (Houghton and Guevara-Patino, 2004).

### **1.3 The immune system and cancer**

It is now accepted that the cells of the immune system constantly monitor the body to identify and destroy cancer cells by a process of cancer immune-surveillance (Dunn et al., 2002). Indeed patients who are immunosuppressed have a higher rate of malignancy (Engels et al., 2011). This immune-surveillance can be particularly effective in the early stages of tumour development because the mutations that lead to the formation of a cancer cell can cause cell death or senescence and these damaged cells can be recognised and destroyed. NK cells can detect associated molecules on damaged cancer cells and DC cells activate cytotoxic T-cells which can sense tumour associated antigen via the T-cell receptor and other co-receptors (Vivier et al., 2012). Once activated, NK cells and cytotoxic T- cells release perforin and granzymes, which damage the surface of tumour cells causing death by apoptosis. Helper T-cells support these responses, acting with DCs to activate cytotoxic T-cells, producing cytokines such as interferon gamma and recruiting more NK cells (Topham and Hewitt, 2009)

Once tumours become more established immune recognition becomes more difficult because many of the tumour antigens that could be recognised by T- cells are self-related and are thus similar to normal cells (Truscott et al., 2008). There are however, several potential mechanisms for cancer cells to be recognised. For instance, there are a few antigens that are specifically expressed on cancer cells e.g. HER2 (30% of breast cancers are HER2/neu-positive, (Wilson et al., 2002) and RAIDD, Rb p107, Rb p130, SRF, and Tyk2 (Song et al., 2008). Additionally, alpha v beta 3/5 integrin has been reported to be expressed on glioblastoma and tumour vasculature of the brain (Przystal et al., 2019). Another feature of some cancer cells that could enable them to be recognised by the host immune system is via their modified surface characteristics.

For instance, changes in the lipid asymmetry of their plasma membrane which differs from normal cells e.g. cancer cells present phosphatidylserine (PS) in the outer leaflet of the plasma membrane which could be recognised by macrophages (Fadeel and Xue, 2009). Additionally, cytotoxic T- cells can detect the modified surface of cancer cells (Maher and Davies, 2004).

Over the past 20 years, studies have shown that the generation of cancer-specific immunity requires three steps. Firstly, if the tumour cells are recognised as non-self by APC then the tumour antigens are processed and presented in interaction with human leukocyte antigen (HLA) molecules and MHC molecules to T- cells. The T – cells can recognise the tumour antigens, but it has been reported that their capacity to recognise these antigens is not very strong (James, 2016). Recognition is enhanced by a second mechanism i.e. T- cell CD28 binding to CD80 or CD86 on the APCs (DCs or macrophages). For optimal -cell activation, both signals 1 and 2 are required (Mak, 2006). There are additional multiple agonist and antagonistic pairs of receptor – ligands that then interact to regulate T- cells to secrete cytokines i.e. step 3.

Cancer cells have developed various mechanisms to evade immune-surveillance e.g. by minimising expression of MHC molecules (and thus tumour antigens) on the surface of tumour cells compared to normal cells (Garrido et al., 2012). Additionally, cancer cells can have reduced expression of receptors and surface molecules that activate NK cells, release soluble ligands that compete for NK cell receptors and secrete soluble factors such as macrophage migration-inhibitory factor that create an immune-suppressant environment for NK activity reviewed by (Greppi et al., 2019)

Tumour-associated DCs are largely disturbed in their functional activity and so participate in decreased cancer immunity. During normal antigen processing DCs transport tumour antigens to lymph nodes, mature and present the antigens for activation of T lymphocytes as previously described. However, it has been reported that when DC maturation occurs within tumours, it is often not adequate to induce effective immunity, particularly in tumours which actively suppress immunity (Shortman and Naik, 2007). Using a novel technique to identify cancer antigens recognized by T cells, (Peng et al., 2008) suggested that tumour cell secreted galectin 3 may inhibit T-cell immune responses, promoting tumour growth in *vitro* and in *vivo* and providing a new mechanism for tumour immune tolerance. They used a mouse

tumour model and showed that high doses of galectin-3 inhibited tumour-reactive T cells and promoted tumour growth in mice receiving tumour-reactive CD8+ T cells. Other tumours have high levels of myeloid-derived suppressor cells in the tumour microenvironment which block T- cell function, reducing activation of the immune system and leading to poor immune responses (Wang and Wang, 2007). By-passing these suppressive pathways or directly activating relevant immune cells e.g. NK or DCs could potentially induce a therapeutic T cell response.

#### **1.4. Cancer immunotherapy**

Cancer immunotherapy requires the activation and development of cancer-specific T cells, which kill cancer cells by detection of their presented antigen targets. In recent years immunotherapy has revealed a great potential to eradicate cancer. Cancer immunotherapy includes active immunisation as well as nonspecific immune stimulation. Some of these strategies have achieved results in cancer clinical trials. For instance, the U.S. Food and Drug Administration (FDA) approved immunotherapy for the treatment of prostate cancer and metastatic melanoma with the vaccines/drugs sipuleucel-T (Provenge® (Kantoff et al., 2010) and ipilimumab (Yervoy®). Sipuleucel-T, is a personalised immunotherapy involving the reinfusion of patient DCs that have been modified to recognize prostatic acid phosphatase.

Successful immunotherapy in cancer relies mainly on the determination of specific cancer antigens for the generation of potent cancer vaccines and antigen-specific T cells. MAGE (melanoma-associated antigen 1) was one of the first human cancer antigens identified; using *in vitro* stimulated cancer-specific T cells from melanoma (Chaux et al., 1999). MAGE antigens are expressed on the surface of many human tumours but not on normal cells and this prompted clinical interest. However, although there have been several clinical trials the combined clinical data suggest that the methodologies used to date have not had any clinical benefit to cancer sufferers (reviewed by (Zajac et al., 2017). An increasing number of cancer antigens have now been identified in different tumour types, with about 403 cancer antigenic peptides in the peptide database (Vigneron et al., 2013). These include TRP1, TRP2, NY-ESO-1, EBNA-1, PSGR and SATB1 (Wang et al., 2014).

IL-2 has been shown to have antitumor activity in murine and human tumours and it was ultimately approved for use in patients with metastatic cancer who were administered with autologous lymphokine-activated killer cells (LAK) and recombinant lymphoid interleukin (IL)-2. Administration of  $1.8 - 18.4 \times 10^6$  autologous LAK cells and up to 90 doses of IL-2 regressed cancer by up to 50 % in 11 of 25 patients and reduced the formation of tumours in one patient with metastatic melanoma, an effect that was maintained for 10 months after therapy (Rosenberg et al., 1985).

Another potential strategy to advance cancer immunotherapy is the use of engineered nanoparticles to passively or actively target the tumour milieu and induce an immune response against cancer cells. For instance immunomodulation molecules such as receptors, tumour-associated antigens, ligands and antibodies could be encapsulated within nanoparticles or absorbed on the surface of nano-carriers. This would allow targeted cancer immunotherapy, activating different types of immune cells such as macrophages, dendritic cells, T- cells and could ultimately lead to tumour killing. This could be achieved by generation of long term memory responses, increased infiltration and activation of antigen presenting cells in the tumour milieu and secretion of pro-inflammatory cytokines which in turn activate T- cell cytotoxic of killing tumour cells (Singh and Bhaskar, 2014, Saleh and Shojaosadati, 2016).

### **1.5. Immunogenic cell death (ICD) in cancer cells**

Conventional therapeutic approaches for cancer are mostly aimed at eradicating cancer cells by cytostatic and cytotoxic effects. The classical anticancer agents, including anthracyclines, antimetabolites, and platinum drugs, were mainly developed based on their ability to kill preferentially neoplastic cells (Eccles and Welch, 2007). Cells can die by two main mechanisms – apoptosis which is programmed cell death and is considered to be immunologically silent and necrosis in which cell destruction facilitates an immune response (Sachet et al., 2017).

However, recent studies e.g. (Montico et al., 2018) have reported that cancer cells respond to some chemotherapeutic agents such doxorubicin and oxaliplatin to undergo immunogenic apoptosis. This means that the dying cells are engulfed by



professional APCs which in turn present tumour-associated antigens, leading to T cell activation and proliferation and eventually eradication of the tumour cells by an adaptive immune response. For instance, *in vitro* treatment of cancer cells with the anthracycline doxorubicin was able to elicit an effective anti-tumour vaccination response that suppressed the growth of inoculated colon carcinoma (Vandenberk et al., 2015). It is now accepted that these and other therapies such as radiotherapy and photodynamic therapies can trigger this type of cell death termed immunogenic cell death (ICD) which facilitates recognition and elimination of tumour cells and primes an anticancer immune response (Garg et al., 2010).

Recent findings have shown that immunogenic cancer cell death triggered by certain anticancer treatments might actually reset the immune system towards the activation of a long-lasting protective anti-tumour response (Wang et al., 2018). Indeed, the evidence suggests that the clinical success of conventional chemotherapy may not only be due to tumour cell toxicity, but also results from enhanced immune-surveillance, which has been largely neglected in the past preclinical and clinical research (Wang et al., 2018). It has been reported that unlike normal apoptosis, which does not induce immunogenic responses the immunogenic apoptosis of cancer cells can induce an effective antitumor immune response through activation of DCs and consequent activation of specific T cell responses (Spisek and Dhodapkar, 2007).

Recent studies suggest that conventional chemotherapeutics inducing ICD are capable of modulating tumour infiltrating lymphocytes, leading to a better prognosis for cancer patients. For example, in response to anthracyclines or oxaliplatin treatment, breast and colorectal cancer patients have increased numbers of modulating tumour infiltrating lymphocytes, associated with favourable therapeutic response (Wang et al., 2018). A combination of ICD-inducing conventional chemotherapy with immunotherapy (anti-tumour immune response) is a promising approach for improving the clinical outcomes of cancer patients (Schreiber et al., 2011).

The key to ICD induction for most of the agents mentioned is the sustained induction of endoplasmic reticulum (ER) stress (Tesniere et al., 2008). Amongst other

responses, this is thought to lead to production of reactive oxygen species (ROS), which have been reported to activate intracellular signalling pathways that govern ICD (Garg et al., 2010).

In response to ICD-inducing chemotherapeutics, tumour cells expose CRT on the cell surface prior to death (Obeid et al., 2007), and release other damage-associated molecular pattern (DAMP) molecules such as adenosine triphosphate (ATP) during apoptosis, or high mobility group box 1 protein (HMGB1) upon secondary necrosis (Dumitriu et al., 2005). These DAMPs stimulate the recruitment of DCs into the tumour bed, the uptake and processing of tumour cell antigens by DCs, and the optimal antigen presentation to T-cells, specifically cytotoxic T lymphocytes (CTLs) triggered by mature DCs and T-cells in an IL-1 $\beta$ - and IL-17-dependent manner (Krysko et al., 2012). Primed CTLs then elicit a direct cytotoxic response to kill remaining tumour cells through the generation of interferon (IFN)- $\gamma$  from the T-cytotoxic cells and perforin-1 (Tau et al., 2001). Therefore, the hallmarks of ICD include CRT plasma-membrane translocation, extracellular ATP and/or HMGB1 release, and stimulation of type I IFN responses.

The ICD hypothesis suggests that the tumour cell can also become more susceptible to ICD as a consequence of chemotherapy through additional mechanisms (Kroemer et al., 2013). For instance, several experimental models suggest that these therapies actually elicit a multistep process in dying cancer cells. This includes the release of “find-me” signals that attract phagocytes or DCs, exposure of “eat-me” signals (such as PS and CRT) on the surface of apoptotic cells and release of DAMPs that facilitate recognition by phagocytes or DCs. An additional factor that is involved in the success of the immunogenic chemotherapy may result from the activation of caspases to cleave and release apoptotic cell associated antigenic fragments, thus facilitating their processing and cross-presentation by DCs (“digest-me” signals) (Rawson et al., 2007)

### **1.5.1. ER stress-driven immunogenic cancer cell death**

Many of the agents inducing ICD target the ER. The ER is a major site of protein synthesis and transport, intracellular protein folding, lipid and steroid synthesis, carbohydrate metabolism and calcium storage (Araki and Nagata, 2011). Newly synthesised secretory proteins are first translocated into the lumen of the ER, where

they are folded and assembled before being delivered to intra- and extracellular destinations according to their function. This process is mediated by chaperone proteins resident in the ER lumen which prevent accumulation of misfolded or unfolded products in the cell. Unfolded proteins are recognised and targeted to the proteasome in a process called ER-associated protein degradation or ERAD which involves retro-translocation across the ER membrane to the cytosol. Malfunctioning of ERAD machinery or accumulation of defective proteins in the ER is associated with various human conditions ranging from neurodegenerative disorders, hypoxia, glucose deprivation, oxidative stress, and cancer (Hetz et al., 2013). High levels of ER stress e.g. caused by overexpression of proteins entering the secretory pathway, may eventually lead to cell death or release of intracellular proteins including the chaperones. Indeed it has been reported that a sign of increased malignancy may be the overexpression of chaperones, with CRT in particular, being over-expressed in numerous tumour tissues, possibly to cope with increased ER stress due to protein production errors. In tumour or malignancy, changed vascularization in the blood network into the tissue can lead to hypoxia and oxidative stress, causing reduced amino acid delivery, possibly altering the protein synthesis necessary for normal cell growth. This could ultimately lead to ER stress and an unfolded protein response in tumour cells (Wiersma et al., 2015). While increased chaperone expression could simply be a biomarker of increased ER stress due to malignancy, some studies have suggested that chaperones are also engaged directly in the spread of tumours by promoting cell proliferation (Chen et al., 2009).

### **1.5.2. The role of intracellular chaperones as DAMPs**

Many intracellular host and “self” proteins that are not normally presented to the immune system act as DAMPs or “alarmins” upon their release from (dying) cells. One of the most prominent is the HMGB1 DNA binding protein. HMGB1 normally resides in the nucleus of cells, loosely bound to chromatin, but is released into the extracellular space during necrosis. This is in contrast to apoptosis, where the interaction between HMGB1 and chromatin is strengthened, thus preventing the release of HMGB1 (Wiersma et al., 2015). A second major DAMP is the chaperone CRT which is thought to be crucial for the immunogenicity of dying cancer cells (Henson and Hume, 2006).

CRT is exposed on the surface of cells undergoing ER stress and as a DAMP it enhances cell immunogenicity, allowing cells to be recognised by immature DCs which then triggers DC maturation and T-cell responses (Palucka et al., 2011).

It has been shown that treatment with anthracycline antibiotics such as doxorubicin, which commonly induce ER stress, leads to externalisation of CRT (Obeid et al., 2007). Functionally, this chaperone has been reported to bind to various receptors on immune cells, such as CD91 and certain scavenger receptors (Kroemer et al., 2013). Pre-apoptotic CRT surface exposure seems to be an important mediator of ICD immunogenicity, by acting as a potent pre-apoptotic 'eat me' signal that assists in phagocytic uptake of a dying cancer cell (Park and Kim, 2017). Moreover, CRT has been shown to enhance DC maturation and MHC I-based antigen presentation, particularly to CD8+ cytotoxic T lymphocytes (CTL) (Obeid et al., 2007).

It may be possible to exploit the potential physiology of CRT to enhance the immune ability to detect cancer cells by using strategies that increase cell surface exposure of CRT to make cancer cells more "visible".

## **1.6. Apoptosis and necrosis**

Apoptosis is a pathway of cell death induced by a tightly regulated intracellular program (Kerr et al., 1972). The cell effectively commits suicide and this eventually results in the clearance of the dying cell from the tissue in a process referred to as programmed cell death. Briefly, apoptosis results from activation of certain enzymes which cause the destruction of DNA and cytoplasmic proteins with the cell membrane remaining intact (Elmore, 2007). Apoptosis occurs in physiological and pathological conditions. For example, during embryogenesis apoptosis occurs throughout the implantation and organogenesis stages of development as cells that are no longer needed die via apoptosis in a programmed manner (Boehm, 2006). Additionally, destruction of hormone dependent tissue such as during menopause and weaning, loss of cells in proliferating cell populations and removal of self-reactive lymphocytes all occur via apoptosis.

Pathological apoptosis is cell death that occurs under various injurious stimuli, mainly

radiation and cytotoxic drugs which damage DNA and the cell cannot repair this (Hassan et al., 2014). When tumour cells are regressing due to some treatments, many cells die via apoptosis (Agostini et al., 2011). Misfolded protein accumulation can lead to the build-up of these proteins inducing the apoptotic pathway (Rao and Bredesen, 2004). Apoptosis can also be seen in a cell which is infected with virus. In this case the cytotoxic T-cell kills the virus-infected cell by apoptosis (Kaminsky and Zhivotovsky, 2010).

Apoptosis can broadly be divided into three steps-initiation, execution and phagocytosis. Initiation may be initiated by two different mechanisms depending on whether the initiating signal comes from inside or outside the cell i.e. the extrinsic or death receptor pathway and the intrinsic or mitochondrial pathway (Wong, 2011). However, there is now evidence that the two pathways are linked and that molecules in one pathway can affect the other (Igney and Krammer, 2002). The execution phase involves activation of caspases, followed by the execution pathway which is basically nuclear breakdown by endonuclease activation and breakdown of the cytoskeleton (Elmore, 2007). This cleavage results in cells showing morphological features of apoptosis (Saraste and Pulkki, 2000).

### **1.6.1. The extrinsic apoptotic pathway**

The extrinsic pathway involves single molecules originating outside the cell that stimulate apoptosis. Healthy cells contain integral membrane proteins (death receptors) that can bind complementary molecules called death activators (Wajant, 2002). This binding process stimulates the internal pathway that activates caspase-8 (Fulda and Debatin, 2006), initiating a cascade that leads to the destruction of the cell. The extrinsic pathway is divided into paths based on the signalling molecules and receptors involved. The first pathway is via the extracellular molecule tumour necrosis factor (TNF) alpha, a cell signalling cytokine produced by activated macrophages, natural killer cells and CD4 positive cells (Putchá et al., 2002). A second pathway is via Fas, a transmembrane protein receptor on the cell membrane (Li et al., 2002). In this pathway the Fas- ligand protein, an extracellular signalling molecule belonging to TNF family, and expressed on cytotoxic T-cells and NK cells, binds to the Fas receptor ultimately leading to formation of a death-inducing signalling complex (DISC) and activation of caspase-8 (Burikhanov et al., 2009).

### **1.6.2. The intrinsic pathway**

The intrinsic pathway is known as mitochondrial apoptosis because of the origin of this pathway within the cytosol. Healthy cells have a protein called Bcl-2 on their mitochondrial membrane, which normally inhibits apoptosis. When the cell is damaged, it stimulates the cytosolic protein Bax to move onto the outer membrane of mitochondria and associate with the Bcl-2 protein on the outer membrane of mitochondria, suppressing its normal anti-apoptotic function. During apoptosis, Bax punctures holes in the outer membrane of mitochondria, leading to leakage of cytochrome C from the inner membrane of mitochondria to the cytoplasm (Radogna et al., 2007). Cytochrome C then attaches to Apaf-1 (apoptotic protease activating factor 1) causing the aggregation of a protein complex called the apoptosome in the cytoplasm which binds to, and activates, the caspase 9 complex. The caspase 9 proteins cleave and break down DNA and other internal structures within the cells, eventually leading to cell death (Inoue et al., 2009).

This process is commonly blocked in tumour cells, and restoring the intrinsic apoptotic pathway after it is been activated may promote cell death (Saelens et al., 2004). It appears that certain other caspases are necessary for apoptosis. For instance, mouse embryonic fibroblasts with a deficiency in caspases 3 and 7 and 9 and treated with thapsigargin to induce ER stress-induced apoptosis, tunicamycin, the calcium ionophore A23187, or brefeldin A failed to display apoptosis. This suggests that caspases 3 and 9 have an important role in the intrinsic pathway in apoptosis (Masud et al., 2007). As mentioned previously, apoptosis is considered to be an immunologically silent process.

### **1.6.3. Morphological changes in apoptosis**

Morphological features of apoptotic cell death that concern both the nucleus and the cytoplasm are remarkably similar across cell types and species (Saraste and Pulkki, 2000). The first notable feature in the morphology of apoptosis is cell shrinking as a result of the cytoplasm becoming denser. The second feature is chromatin condensation in the nucleus and nuclear fragmentation (Wlodkowic et al., 2011), termed pyknosis. The nucleus becomes dark as the DNA becomes condensed and eventually the cells form membrane blebs, although the membrane is still intact. The cell eventually fragments into individual apoptotic bodies which can be engulfed by phagocytes (Brauchle et al., 2014) (Figure 1.4).

### **1.6.4. Necrosis**

Cells can also die by the process of necrosis. Necrosis is a pathological process of irreversible cell injury which is caused when a cell is exposed to extreme conditions that are very different from the normal living conditions, leading to damage to the internal cellular environment and tissue damage (Galluzzi et al., 2018). The basic ability of the cell to maintain homeostasis when exposed to these conditions is lost, leading to complete discord in the cellular function and eventually death. A key difference between apoptosis and necrosis is a loss of the integrity of the cell membrane which leads to swollen cell contents as well as the disintegration of the body of the cell (Proskuryakov and Gabai, 2010). The intracellular components leak out and elicit an inflammatory response. There are several agents which have reported to trigger necrosis such as hypoxia, physical damage, chemical damage, bacteria and immunological agents (Adigun and Bhimji, 2018). Two common characteristic features of cell injury and necrosis are denaturation of proteins and cell degradation, with changes happening with nuclear material, cellular structure and function. Cell damage causes lysosome rupture with release of destructive enzymes which leads to proteolysis and ingestion of cellular components (Proskuryakov et al., 2003). This initiates more morphological changes. The necrotic cells attract inflammatory cells such as neutrophils and macrophages, which migrate to the injured area and release destructive enzymes to further digest and ultimately phagocytose the dying cell (Rock and Kono, 2008). Thus, unlike apoptosis, necrosis does elicit an immunogenic response.

## Apoptosis (Programmed Cell Death)

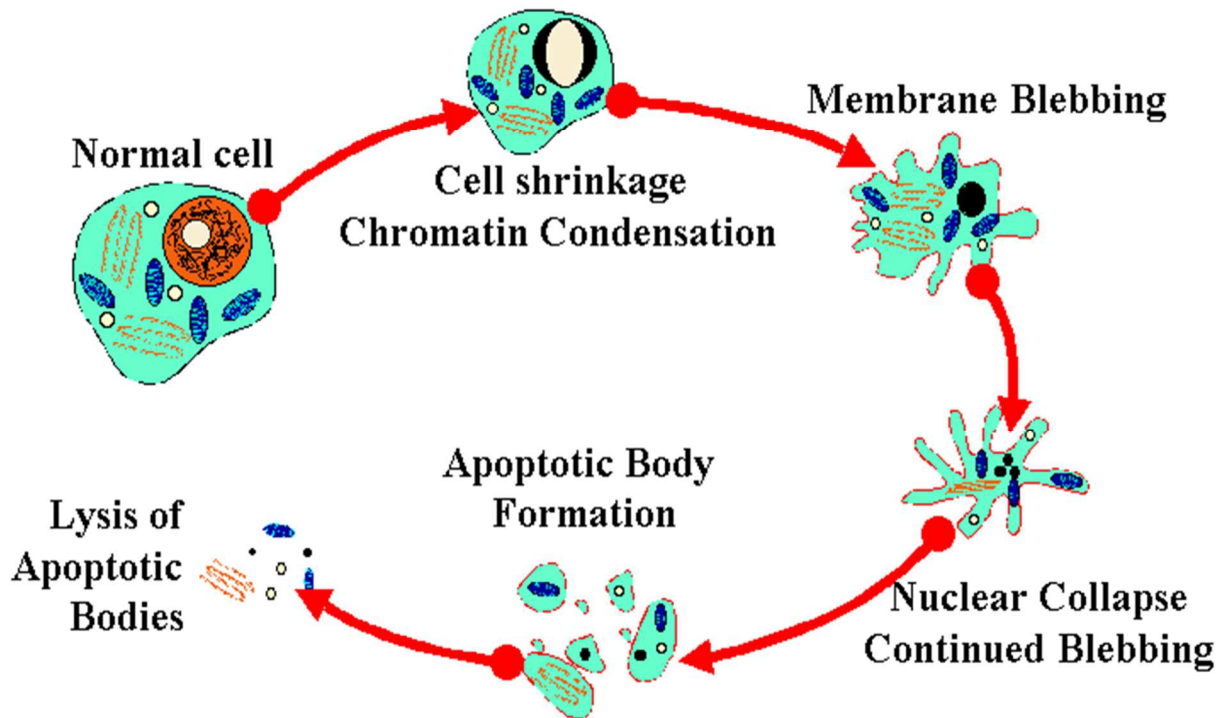


**Figure 1.4.** A diagrammatic image showing the main morphological stages of **apoptosis**. Cells undergoing apoptosis go through several stages that are characterised by distinct changes in cell morphology. There is initial chromatin condensation, nuclear collapse and cell shrinkage. The DNA then condenses more tightly and the cells break apart with the formation of nuclear blebs and cell membrane fragments. These form apoptotic bodies, the DNA is broken down by DNase and the apoptotic bodies and cell fragments are eventually engulfed by phagocytic cells. (<http://www.biology.lifeeasy.org/742/what-is-programmed-cell-death-pcd>)



### **1.6.5. Assessment of cell death**

For many cell based studies it is important to be able to quantify both total levels of cell death and type of cell death i.e. apoptosis or necrosis.

Assessment of total cell death can be achieved using staining to distinguish membrane integrity. Specifically fluorescent or coloured dyes which can penetrate cells with a compromised cell membrane to stain nucleic acids, but don't cross the membrane of live cells, can be used to quantify dead cells in a population (Coleman et al., 2001). Fluorescent cell stains are available with a variety of excitation and emission spectra, allowing cell viability to be assessed in combination with many fluorophores. One of the most common dyes is propidium iodide (PI) (Wallberg et al., 2016) which simply enters the cell when membrane integrity is lost, staining the nucleus (Atale et al., 2014).

### **1.6.6. Assessment of apoptosis using annexin V**

Annexin V staining is the most widely used technique to detect apoptosis in the cell. It is a  $\text{Ca}^{2+}$  dependent phospholipid-binding protein with a high affinity for PS. normally, cells have the phospholipid PS presented on the inner leaflet of the cell membrane. When cells enter the apoptotic pathway then the cell membrane is changed and the PS flips from the cytosolic portion to the outer section of the cell membrane. Fluorescence-conjugated annexin V can be used to detect and quantify this externalised PS (Schutte et al., 1998, Demchenko, 2013).

Fluorescent annexin V and PI (with different fluorophores) (Figure 1.5) can be used together to distinguish between cells undergoing apoptosis and dead cells. If cells are mixed with fluorescence conjugated annexin V and PI there is no fluorescent in viable cells because PS is presented inside the cell and annexin V cannot bind and PI cannot enter the cells. Once these cells start entering apoptosis, the PS is flipped out and annexin V can bind to give a fluorescence signal (van Genderen et al., 2008), but the membrane is still intact so the PI cannot enter. In dead cells with advanced apoptosis PI enters and binds to DNA and annexin V is also bound so the cells have dual staining. It is possible to analyse the cells by flow cytometry to detect the fluorescence. In a population undergoing cell death four major cell populations can be detected (a) annexin V negative and PI negative = healthy cells (b) annexin V

positive and PI negative = cells undergoing apoptosis with an intact plasma membrane (c) double positive for annexin V and PI = late apoptosis where membrane integrity is lost (d) in necrosis PI can stain the nucleus, but PS is not exposed (Cornelissen et al., 2002) (Sawai and Domae, 2011).

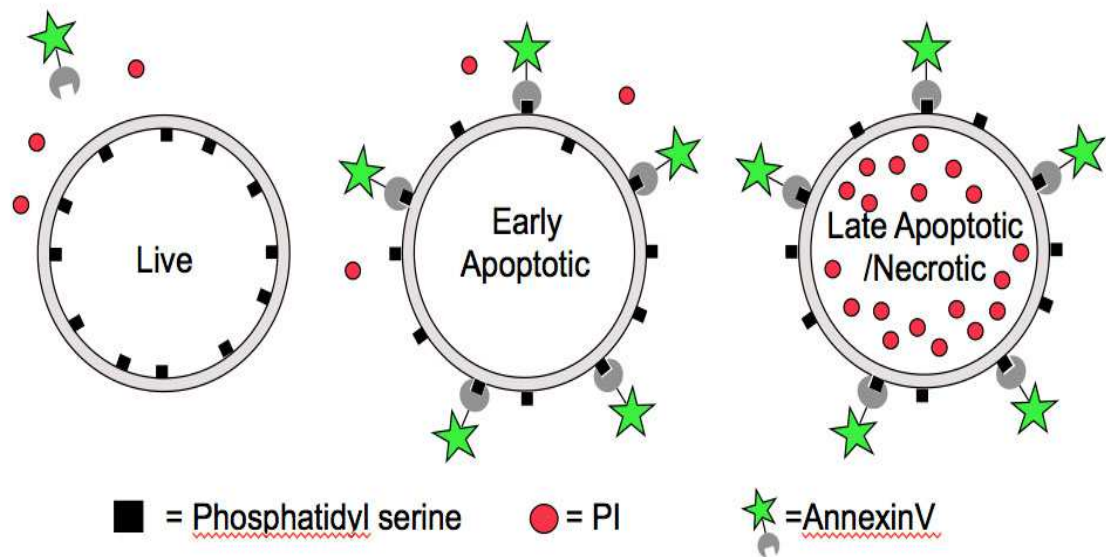


**Figure 1.5. Schematic representation of the detection of the apoptotic process using fluorescently labelled PI and annexin V to detect changes.** Annexin V is a protein that has the ability to bind to PS. It cannot bind to PS when it is in the inner plasma membrane leaflet, but during apoptosis, PS flips from inside the cell to the outer cell surface and annexin V can bind it. To allow visual detection annexin V is bound to a green fluorescent dye. PI is used to detect cell death. Since it cannot penetrate through intact cell membranes, it can only stain cells with disrupted membranes or dead cells where the membrane is completely damaged, allowing PI to penetrate. In the necrotic condition PS is not flipped out to the outer leaflet but PI can stain the cell. (<https://www.lifesci.dundee.ac.uk/>, 2017).

### 1.6.7. Apoptosis in cancer

Apoptosis is one of the mechanisms by which an organism limits the growth and replication of cells. If apoptosis did not occur, there would be no way to control cell growth and tissue homeostasis would be lost. In fact, this is a key mechanism in cancer growth where genetic alterations or environmental factors in the cancer cell lead to increased cellular proliferation and growth, and loss of apoptosis i.e. there is too much cell growth, and too little cell death in malignant tissue. In some malignant cells, there is resistance to apoptosis due to overexpression of anti-apoptotic proteins, for example survivin is an anti-apoptotic protein found in many cancers. Increased expression of survivin has been found in myeloid leukaemic cells and it was found to block cytokine stimulated apoptotic pathways and caspase-3 activation (Carter et al., 2001).

Bcl-2, while generally anti-apoptotic has also been implicated in loss of control in cancer if dysregulated simultaneously with other key molecules e.g. oncogenes. This has been observed in leukaemias where alterations in the balance of pro-apoptotic and anti-apoptotic proteins results in uncontrolled growth of malignant cells (Pandey et al., 2016). Conversely, deactivation mutations of pro-apoptotic molecules such as Bax is seen in some gastrointestinal tumours (Gao and Wang, 2009) and leukaemias (Moazami-Goudarzi et al., 2016). Activation of transcription factors can also lead to apoptotic resistance. This occurs when nuclear factor Kappa B (NF- $\kappa$ B) or transcription factors are overexpressed in tumours which leads to increased transcription of anti-apoptotic members of the inhibitors of apoptosis proteins (IAP) and Bcl-2 families (Hoesel and Schmid, 2013)

As a result some anti-cancer agents have been developed which target anti-apoptotic molecules, for instance short segments of DNA complementary to RNA of Bcl-2 or antisense oligonucleotides have been designed to reduce translation of anti-apoptotic proteins (BCL-2, BCL-XL, BCL-W, MCL-1, BFL-1/A1) (Kirkin et al., 2004). Additionally, Bortezomib is a 26S proteasome inhibitor that is thought to prevent degradation of anti-apoptotic proteins and is used in the treatment of multiple myeloma (Shahshahan et al., 2011).

## **1.7. Calreticulin**

As previously described CRT is an intracellular protein that can be translocated to the external surface of the cell during ICD. CRT is a highly conserved ER chaperone protein that also displays extracellular multifunctional properties in various cellular processes (Wiersma et al., 2015). It was first identified as a Ca<sup>2+</sup>-binding protein in 1974 (Ostwald and MacLennan, 1974). Later, the gene coding for this protein was cloned and the product was named “calreticulin”, reflecting its ability to bind calcium and its primary localization to the ER (Smith and Koch, 1989). Accumulated evidence indicates that CRT impacts on the development of different cancers and the effect of CRT on tumour formation and progression may depend on cell type and clinical stages.

### **1.7.1. Calreticulin expression in cancers**

The correlation between CRT expression levels and tumorigenesis has been extensively studied in various cancers and most reports have indicated that CRT is aberrantly overexpressed in tumour tissues compared with normal tissues (Zamanian et al., 2013), summarised in Table 1.3. Studies have shown correlation between CRT expression levels and clinical stages and lymph node metastasis in gastric cancer (Chen et al., 2009) and breast cancer (Lwin et al., 2010). In addition, patients with higher CRT levels had a lower survival rate in pancreatic cancer and oesophageal squamous cell carcinoma (Du et al., 2007). Other studies also detected high expression levels of CRT in oral cancer (Chiang et al., 2013), breast ductal carcinoma (Song et al., 2012), prostate cancer (Alaiya et al., 2000) and vaginal carcinoma (Hellman et al., 2004). Furthermore, CRT levels not only increased in bladder cancer tissues, but urinary CRT has been shown to be a biomarker for bladder urothelial cancer detection (Kageyama et al., 2004). These results suggest that increased CRT expression might play an important role during development of cancer. However, the effect of CRT on tumour formation and development may depend on different tumour types and clinical stages.

<b>Cancer</b>	<b>CRT levels*</b>	<b>Clinical outcomes</b>
<b>Oral</b>	Increased	_____
<b>oesophagus</b>	Increased	↓survival (Chen et al.)
<b>Breast</b>	Increased	↑Metastasis, ↑ invasion
<b>Pancreas</b>	Increased	↑Lymph node metastasis
<b>Gastric</b>	Increased	↑Lymph node metastasis , ↑invasion
<b>Colon</b>	Increased	_____
<b>Bladder</b>	Increased	↑Urinary CRT , ↑histological grade , ↑pathological T stage
<b>Prostate</b>	Increased	_____
<b>Vagina</b>	Increased	_____
<b>#Ovarian</b>	Increased	Better response to chemotherapy
<b>#Neuroblastoma</b>	Increased	↑Differentiated, ↑survival

**Table 1.3: Expression of level CRT in different cancers (Lu et al., 2015).**

↑: increased; ↓: decreased.

\*CRT levels in tumour tissue except ovarian carcinoma in effusion fluids.

#higher levels of CRT seem to correlate with good prognosis for the diseases.

### 1.7.2. Structure and function of CRT

CRT is a ubiquitous  $\text{Ca}^{2+}$ -binding protein, found in a wide range of species and in all nucleated cell types, and has a variety of important biological functions. These include protein folding in newly-synthesized proteins (Gelebart et al., 2005) and maintaining  $\text{Ca}^{2+}$  homeostasis in the ER lumen. Both functions are critical for many cellular processes and, when impaired, may lead to pathology (Arruda and Hotamisligil, 2015) e.g. CRT mutations have been found in patients suffering from myeloperoxidase deficiency (Theocharides et al., 2016).

The biophysical analysis of CRT indicates it has three structural and functional domains. Nine exons encode the N-domain (including the N-terminal signal sequence), the proline-rich P-domain, and the C domain of CRT respectively (Figure 1.6). The protein contains an N-terminal amino acid signal sequence and a C-terminal KDEL (Lys-Asp-Glu-Leu) ER retrieval signal. CRT possesses 3 cysteine residues and a single disulfide bridge in the N domain (Michalak et al., 1999). The N and C segments form an N-C globular head domain, while the proline-rich domain forms an elongated hair-pinned loop structure (Fig. 1.6).

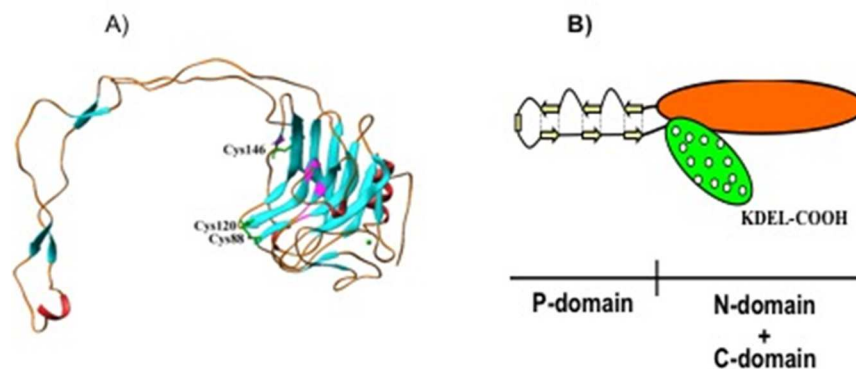


**Figure 1.6. A model of CRT and its domain organisation.** (A) The x-ray crystallography structure of CRT. (B) Domain structure of CRT which comprises of an N-C domain of approximately 290 amino acids in length, together with a P domain of approximately 110 amino acids ((taken from (Young et al., 2006)).

### **1.7.3. Calreticulin in the ER**

Calreticulin has many cellular functions both, intracellular and extracellular. In addition to its intracellular roles in  $\text{Ca}^{2+}$  homeostasis and glycoprotein folding in the ER, extracellular CRT has been identified on the cell surface of apoptotic and necrotic cells and is involved in wound healing. CRT is an essential protein for life, for instance, studies have also revealed that CRT deficient mice embryos die from heart failure at day 14 due to the loss of the normal role of CRT as a calcium buffer in the ER (Mesaeli et al., 1999).

Intracellularly, native proteins synthesized in ribosomes on the rough ER translocate into the ER lumen where some, via interaction with CRT, are identified as “misfolded” and directed to the ERAD pathway (Benham, 2012). Thus, together with other chaperones, CRT effectively marks misfolded proteins and ensures that only correctly folded proteins exit the ER. Additionally, as an ER chaperone, calreticulin is important for the normal trafficking of many cell surface proteins (Wiersma et al., 2015). CRT binds transiently to most glycoproteins that pass through the ER, slowing the folding rate but increasing folding efficiency; largely by preventing aggregation. It also promotes correct disulfide bond formation in bound substrates by recruitment of ERp57 chaperone. CRT therefore participates in quality control, monitoring glycoprotein folding status and retaining folding intermediates of terminally misfolded glycoproteins in the ER. It may also participate in targeting misfolded proteins for degradation (Ferris et al., 2014)

### **1.7.4. CRT and the innate immune system**

Early studies showed that calreticulin was found on the surface of many mammalian cells (Arosa et al., 1999). CRT is translocated from within cells by unknown mechanisms under stress conditions such as treatment of cells with anthracyclines, oxaliplatin, ultraviolet C and  $\gamma$ -radiation (Tarr et al., 2010b). It has an important function at the cell surface by mediating phagocytosis of apoptotic or dying tumour cells. CRT was first found to function on phagocytic cells as a receptor for complement I of the classical pathway (Vandivier et al., 2002). Extracellular CRT is not simply the result of

unregulated exposure of ER contents during cell death, but a pre-apoptotic event that appears to be highly regulated. Cancer chemotherapy such as anthracyclines induce CRT exposure in cancer cells within one hour, preceding the apoptosis-associated PS exposure. This CRT translocation is important for the immunogenicity of dying tumour cells, which is key to the success of chemotherapy (Obeid et al., 2007).

Surface bound CRT has been reported serve as an “eat me” signal on the surface of apoptotic cells and to have several binding partners that may positively impact on innate immunity, most notably complement C1q (Osman et al., 2017, Stuart et al., 1997) Through these binding partners CRT can enhance the innate immunity responses, especially phagocyte removal of cells. CRT was initially characterized as a receptor for the C1q binding to apoptotic cells where CRT binding to apoptotic cells coated with C1q enhanced the phagocyte-mediated removal of cells by macrophages (Ogden et al., 2001). Extracellular CRT binds to C1q on the surface of apoptotic cells and acts as a bridging molecule by binding to CD91 on macrophages (also called LDL-receptor related protein) allowing macrophages to engulf the C1q opsonised cells (Gardai et al., 2005, Verneret et al., 2014).

It is believed that CRT also acts as an 'eat-me' signalling molecule by blocking the ability of the cellular CD47 ('don't-eat-me' signal) to bind to its ligand on the macrophage i.e. signal regulatory protein  $\alpha$  (SIRP- $\alpha$ ) (Chao et al., 2010). SIRP- $\alpha$  is a heavily glycosylated transmembrane protein on the engulfing cell which facilitates uptake of target cells. Disruption of this CD47-SIRP- $\alpha$  axis can be important in cancer. Indeed, in apoptotic breast cancer cells, CD47 was altered and/or lost and no longer activated SIRP $\alpha$  on macrophages or DCs, preventing clearance (Lv et al., 2015). Thus, in the presence of CRT an apoptotic cell “don't eat me” signal could instead be recognised as “eat me”; signalling cells for removal (Chao et al., 2010) (see Figure 1.6).

### **1.7.5. CRT in adaptive immunity**

CRT also has multiple functions in adaptive immunity. Intracellularly, CRT can promote folding and assembly of glycoproteins including major histocompatibility complex (MHC) class I molecules. CRT also directs foreign antigens into the MHC



class I antigen presentation pathway which is called cross-presentation (Raghavan, 2010). MHC I presentation of these antigenic peptides at the cell surface plays a vital role in distinguishing healthy cells from infected cells and mediates interactions between immune cells. CRT also stabilises this MHC-1 complex (Peaper and Cresswell, 2008).

#### **1.7.6. Role of CRT surface exposure during ICD in cancer treatment**

As mentioned previously the immunogenic characteristics of ICD are mediated mainly by molecules called DAMPs, most of which are recognised by pattern recognition motifs called Toll-like receptor (TLR) system on macrophages and DC (Piccinini and Midwood, 2010). Some DAMPs are actively released by cells undergoing ICD (e.g. CRT and ATP) whereas others are released passively (e.g. HMGB1). Recent studies have shown that these three DAMPs play a crucial role in anti-cancer therapy by interacting with the immune system (Figure 1.7) (Krysko et al., 2012). In addition, the ER releases other ER chaperones which would normally not be considered to be immunogenic, but many reports have now highlighted their role as DAMPs in the extracellular space such as BiP, and gp96. However, some studies have suggested that CRT has the major role in ICD (Wiersma et al., 2015). Importantly, in cancer treatment, anthracyclines triggered the translocation of CRT to the cell surface of apoptotic tumour cells, which is dependent on the induction of an ER-stress response (Garg et al., 2012, Martins et al., 2011).

CRT expressed on the cell surface of dying cancer cells then clears the dead cells by enhancing maturation of DCs. This is accompanied by release of intracellular DAMP molecules such as ATP and HMGB1 from late apoptotic cells which further enhance DC maturation and subsequent clonal expansion of cytotoxic CD<sup>8+</sup> T-cells (Apetoh et al., 2007) (Figure 1.8). ICD has been discussed in a preclinical setting for an ever-expanding set of cytotoxic therapies, including many chemotherapeutics, radiation therapy, and photodynamic therapy. Interestingly, treatment of cancer cells with a recombinant form of the TNF-related apoptosis inducing ligand (TRAIL) -a death receptor ligand was reported to induce CRT cell surface exposure and ICD (Panaretakis et al., 2009).

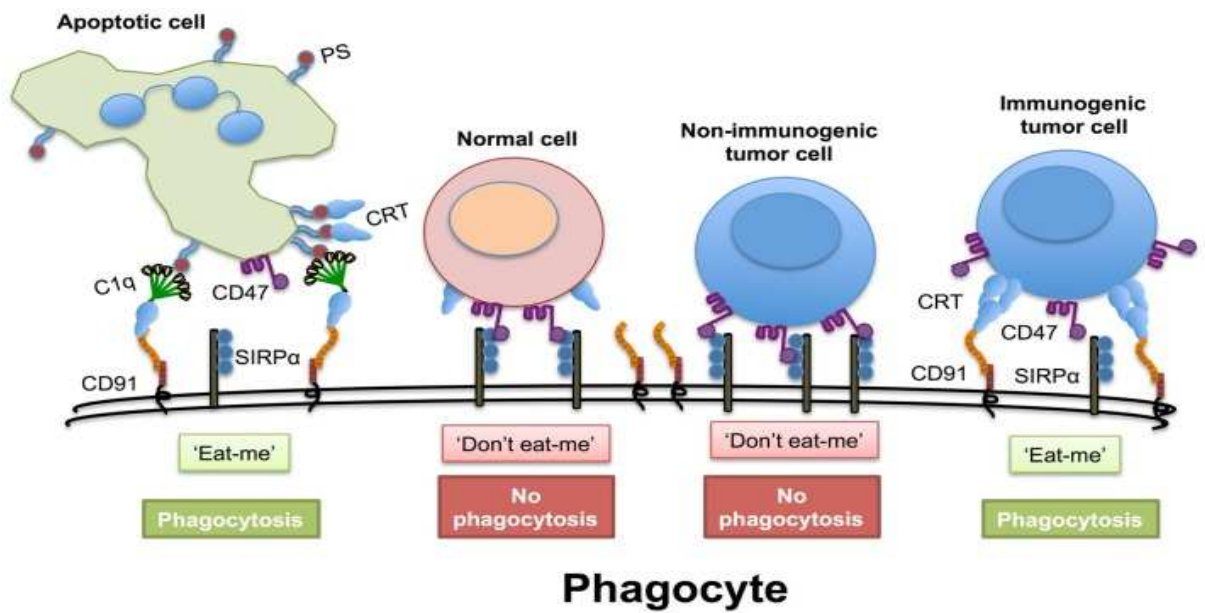


**Figure 1.7. Disruption of the “don’t eat me” signal by CRT.** Cells express a high amount of CD47 “don’t eat me” signalling molecule which binds SIRP $\alpha$  on phagocytes. During apoptosis PS translocates from inside the cell to the outer section of the cell membrane, and with the CRT on the cell surface, works as a bridge molecule between C1q and CD91 on phagocytes. In immunogenic cancer cell death, cells treated with certain chemotherapeutic drugs and ER stress-inducing drugs have up-regulation of surface exposed CRT, which enhances phagocytic uptake by DCs via a mechanism that is at least partially CRT-dependent. Non-immunogenic cells have a high amount of CD47 but it’s not enough to avoid phagocytosis in these cells (Wiersma et al., 2015)

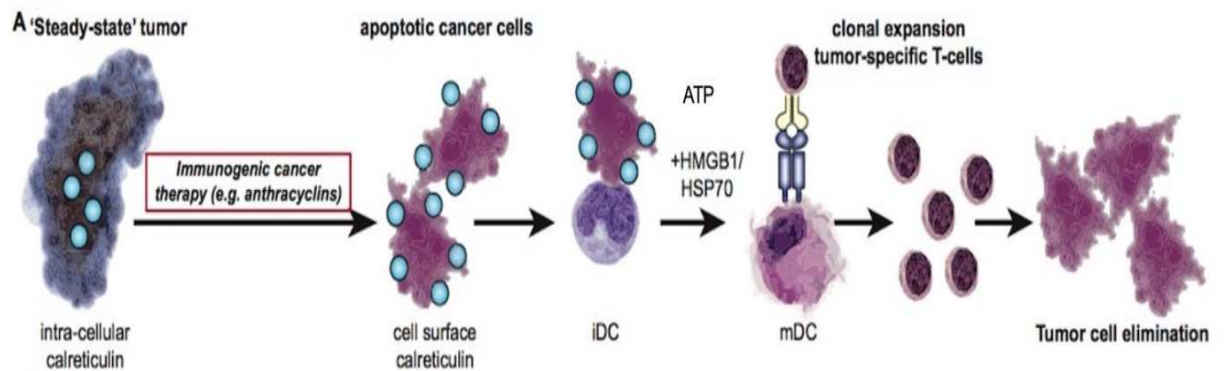


**Figure 1.8. Immunogenic cell death and DAMPS.** In tumour cells, CRT normally resides in the lumen of the ER. However, upon induction of immunogenic cell death (ICD), CRT translocates to the surface of pre-apoptotic cells, whereupon these apoptotic cells are taken up by dendritic cells (DCs). Immature DC (iDC) maturation to mature DCs (mDC) and clonal T-cell expansion are enhanced by additional DAMP signals such as HMGB1, ATP and HSP70. DAMPs are derived from different compartments of the cells. For example, they can come from mitochondria (ATP), nucleus (HMGB1, high mobility group box 1 protein; HMGN1), ER (CRT and ATP) and cytoplasm (HSP70, heat shock protein 70) (Kaczmarek et al., 2013, Krysko et al., 2011).

### **1.7.7. CRT as a therapeutic agent**

The accumulated evidence has suggested that manipulation of CRT levels may have important therapeutic potential through its pro-immunogenic role in ICD (Zitvogel et al., 2010). Chemotherapy such as anthracycline and irradiation could be planned to enhance CRT translocation to the cell surface of pre-apoptotic cells allowing them to be recognised and removed by phagocytosis and enhancing the elimination of tumour cells (Eggleton et al., 2016).

Additionally, CRT has shown potential as a wound-healing therapeutic and this is only just starting to be explored. Dr Leslie Gold and her team in New York, have identified that CRT accelerates and enhances wound healing in both porcine (heals like humans) and diabetic murine experimental models of skin injury (Gold et al., 2010). Indeed when applied topically, CRT repaired the wound of porcine skin far better than Regranex which is the only current treatment used for diabetic foot ulcers (Gold et al., 2010). When applied topically CRT enhances epithelial migration and granulation tissue formation and, importantly increases number of phagocytic cells in the wound, such as macrophages, thus aiding removal of dead cells (Gold et al., 2006). It has also been reported that CRT aids wound healing by reducing bacterial infection and these multifunctional effects have suggested a potential therapeutic role for exogenous CRT in patients such as those with diabetic ulcers who have with delayed wound healing (Gold et al., 2006).

### **1.8. ER stress inducers**

It is clear from the previous discussion that inducing ER stress in cancer cells is a possible strategy for enhancing surface exposure of cellular CRT and triggering subsequent cell removal by macrophages and/or by ICD mechanisms. A number of drugs have been reported to induce cell surface CRT expression and the resulting immunological consequences (Michalak et al., 2009). In this thesis ER stress is induced by doxorubicin and thapsigargin to examine mechanisms of CRT translocation in ovarian cancer cell ICD. Thus, this section briefly describes the mechanisms by which doxorubicin and thapsigargin may cause stress to the ER

resulting in increased cellular CRT production and surface translocation (also see Table 1.4).

### **1.8.1. Doxorubicin**

Doxorubicin is a cytotoxic drug that is used to treat many different types of cancer, including solid tumors, leukemia, lymphomas and breast cancer (Holmgren et al., 2015). It is an antibiotic, a secondary metabolite of *Streptomyces peucetius* var. *Caesius*, and along with daunorubicin, epirubicin, and idarubicin, it belongs to the family of anthracyclines (Yu et al., 2018).

Doxorubicin and other anthracycline drugs have been intensively examined during the last several decades. Doxorubicin has been reported to exert its anti-neoplastic effect by intercalation into DNA, inhibition of the enzyme topoisomerase II, and formation of ROS (Tewey et al., 1984, Renu et al., 2018). All of these have a harmful effect on DNA synthesis and DNA repair mechanisms and lead to mutagenesis and chromosomal aberrations (Momparker et al., 1976, Malla et al., 2009). At the molecular level, doxorubicin is incorporated in-between two nitric bases of the double DNA helix, thus causing the inhibition of DNA dependent DNA and RNA polymerases (Zunina et al., 1975). The successful use of doxorubicin has been hampered by toxicities such as hematopoietic suppression, nausea, vomiting, extravasation, and alopecia, yet the most feared side-effect is cardiotoxicity (Fu et al., 2016).

The ability of doxorubicin to induce the pre-apoptotic surface exposure of CRT which is required for ICD is very specific i.e. it is not observed in all chemotherapeutic agents (Obeid et al., 2007). Doxorubicin has been suggested to induce ER stress by interfering with (via its topoisomerase inhibition) the unfolded protein response (UPR) at the level of transcription of key components such as ATF4 transcription (sulfate, Kim et al., 2006). The cell responds to doxorubicin by initial activation of the ER membrane protein kinase RNA-like endoplasmic reticulum kinase (PERK) which phosphorylates eukaryotic initiation factor 2 (eIF2 $\alpha$ ). This is a normal UPR and usually protects cells from ER stress by attenuating protein synthesis and reducing ER protein load. However, in the presence of doxorubicin these initial events occur in conjunction with pre-apoptotic partial activation of caspase-8 and the intrinsic apoptotic pathway

which ultimately results in changes in ER membrane  $\text{Ca}^{2+}$  fluxes and exocytosis of CRT via Golgi apparatus-derived vesicles (Panaretakis et al., 2009) .

As mentioned previously a major side effect of doxorubicin is cardiac toxicity, at least partly due to mitochondrial damage as a result of generation of mitochondrial ROS (Oliveira, 2016). If doxorubicin could be used to induce ICD at lower dosages than required for its conventional cytotoxic effects then it may show improved therapeutic benefit, but with lower toxicity.

### **1.8.2. Thapsigargin**

Thapsigargin is a naturally occurring tumour promoter derived from the plant *Thapsia garganica*. It affects cells by emptying the intracellular calcium stores, which leads to a chain of events that causes apoptosis.

In basic research, thapsigargin is the most widely used inhibitor of the ubiquitous sarcoplasmic reticulum/ER  $\text{Ca}^{2+}$  ATPase (SERCA). SERCA pumps calcium ions from the cytoplasm into the lumen of the ER and thapsigargin, by preventing this, causes a decrease in calcium in the ER while depleting ER stores. This, in turn, decreases the activity of  $\text{Ca}^{2+}$  dependent chaperones, leading to an increase in unfolded proteins and the corresponding induction of UPR signalling (Janssen et al., 2006).

Thapsigargin also interferes with mechanisms of autophagy by inhibiting fusion of autophagosomes to lysosomes. Thus, increased calcium level along with dysregulated autophagy leads to ER stress, which ultimately progresses to apoptosis and cell death (Ganley et al., 2011).

ER inducers	Indication	On-target effect	ER effect	DAMPs	Mechanism of DAMPs
Anthracyclines (doxorubicin)	Multiple haematological and solid tumours	DNA-Intercalating agent	Associate with cellular Membranes (including ER)	CRT, ATP, IFN, HSP70, HMGB1	DAMPs are danger molecules and released from necrotic and late apoptotic tumour dying cells, causing trigger inflammatory cytokines
Thapsigargin	Ca-dependent chaperones leading to an increase in unfolded proteins and the corresponding induction of UPR signalling	Inhibitor of the Sarcoplasmic reticulum/Endoplasmic reticulum Ca <sup>++</sup> ATPase (SERCA).	inhibits ER Ca <sup>2+</sup> -dependent ATPase, leading to a depletion of ER Ca <sup>2+</sup> storage.	CRT, ATP	

**Table 1.4 Characteristics of clinically relevant ER stressors (info.emea@bio-techne.com, 2108).** (UPR) unfolded protein response, (ATPase) adenosine triphosphates', (DAMPs) damage -associated molecular pattern, (HSP70) heat shock protein, (HMGB1) high mobility group box 1 protein) and (INF) interferon.

### 1.8.3. Tauroursodeoxycholate (TUDCA) reduces ER stress

In recent studies, several small molecules commonly referred to as “chemical chaperones” (e.g., 4-phenylbutyric acid or 4-PBA, a modified fatty acid or TUDCA, a bile acid) have been identified that function to attenuate cellular stress and enhance protein processing (Vega et al., 2016). TUDCA is an amphiphilic bile acid that has been shown to control the growth of a variety of epithelial cells, including cholangiocytes (Alpini et al., 2001). TUDCA has been used effectively for the treatment of cholestatic liver diseases and its efficacy has been attributed to its cytoprotective effects on hepatocytes by increasing bile flow, biliary acid secretion, and hepatocellular vesicular exocytosis (Boyer, 2013). Recent studies have showed that

TUDCA is effective in protecting hepatocytes and restoring glucose homeostasis by reduction of ER stress (Gentile et al., 2011). Thus, there is evidence indicating that TUDCA can modulate signalling of the UPR coping response by promoting protein folding and, by activating transcription programs leading to increased expression of chaperone genes, which may increase the activity of molecular chaperones or folding enzymes in the ER, thereby increasing ER folding capacity (Ozcan et al., 2006).

TUDCA reduces BiP upregulation, protein kinase R-like ER kinase and JNK phosphorylation, expression of the ER stress protein CHOP, caspase 3 activation and apoptosis in following cholecystokinin treatment (Malo et al., 2010).

### **1.9. Overview of research presented and aims of this study**

Ovarian cancer is the fifth most common cancer among women worldwide and the most common cause of death due to a gynaecological malignancy, causing ~125,000 deaths worldwide/year (Carolina Vera Castillo, 2016). Conventional treatment of EOC is radical surgery, typically followed by chemo/radiotherapy. Unfortunately, late stage of diagnosis and intrinsic/acquired resistance to therapy leads to a limited 5-year survival rate of only 45%. This survival rate needs to be improved. Immunotherapy, designed to boost the body's natural defences against cancer, appears to be a promising option against ovarian cancer. Extracellular cell surface associated CRT promotes the immunogenicity of early apoptotic cancer cells and boosts adaptive immunity, a finding that has set CRT at a centre stage for cancer immunology in recent years. Elucidation of mechanisms by which ovarian cancer cell surface levels of CRT can be enhanced to encourage cell phagocytosis and induction of ICD is important in developing novel CRT-based therapeutics for this disease. Therefore, this thesis examines strategies to increase CRT surface levels in ovarian cancer cells, either from endogenous stores (by inducing cellular ER stress) or by adding exogenous CRT. The ability of cells treated in this way to enhance immune responses, specifically DC maturation and T-cell activation, are then examined. The data indicate that exogenous and endogenously translocated CRT bind to cancer cells and that the latter cells with externalised CRT were then able to induce DC maturation and subsequently T-cell activation and proliferation.



The overall aim of this thesis was to examine the hypothesis that enhancement of CRT on the surface of EOC could induce immunogenic responses, potentially leading to targeted cancer cell death and immunotherapy.

Specific aims:

- Purification of both bacterial (*Escherichia. coli*) and yeast (*Pichia pastoris*) expressed human full length CRT (Chapter 3).
- Fluorescent labelling of purified CRT to enable CRT-binding studies in EOC cells (Chapter 4a)
- To determine whether exogenous CRT binds to the surface of EOC under resting or stressed conditions (Chapter 4a).
- To examine the conditions of ER stress that give rise to endogenous cell surface expression of CRT on cancer cells (Chapter 4b).
- To examine whether CRT alone or surface bound can activate immune responses i.e. DC maturation and T-cell activation.

## **Chapter 2. Materials and general methods**

### **2.1. Suppliers and sources of experimental materials**

Abcam, Cambridge, UK: Goat anti-rabbit IgG H&L (Alexa Fluor® 488), Anti-EpCAM antibody.

Alpha laboratories Limited, Hampshire, UK: LW1154 Tip 0.1-10µl universal micro ultrafine tip, graduated, loose non sterile 32mm in length, APV000100 single channel pipettes 0.5-10 µl; APV002000 single channel pipettes 20-200 µl, APV010000 single channel pipettes 100-1000 µl.

BD Biosciences, Oxford, UK: Syringe luer 1ml.

Cambridge Bioscience, Cambridge, UK: PluriStrainers 30µm.

Bio Legend, Cambridge, UK: Alexa Fluor® 647 annexin V; annexin V binding buffer; PE anti-human CD16 antibody; Alexa Fluor® 488 anti-human CD14 antibody; PE anti-human CD11c antibody; PE anti-human CD80 antibody; PE anti-human CD83 antibody; PE anti-human CD86 antibody; PE anti-human HLA-DR antibody; IL-12/23 (p40) ELISA MAX™ Deluxe; mouse IgG1; anti-CD3-PerCP-Cyanine5.5; anti-human CD3.

Bio-Rad Laboratories, Hemel Hempstead, UK: 10% Mini-PROTEAN® TGX™ precast protein gels; 10-well; precision plus protein all blue standard; Bio-Safe Coomassie Stain; 4x Laemmli sample buffer, 8-16% 15 well mini protean TGX precast gels.

Fisher Scientific, Loughborough, UK: ProLong® Diamond antifade mountant; P36931 ProLong® Gold antifade mountant with DAPI; microscope slide super frost plus adhesion, glass grounded edges with white marking area 25mm x 75mm x 1mm; Cover slip best borosilicate glass 22mm x 22mm 0.13mm to 0.17mm thick; gloves, latex; syringe filter, diameter (Metric 25mm, pore size 0.45µm); DPBS (Dulbecco's Phosphate Buffered Saline) 1x without calcium, magnesium; microscope slide box (165mm x 210mm x 35mm); foetal bovine serum (FBS) heat incubated; trypsin

0.05%(w/v) EDTA, Tris base; test tube DNA LoBind 1.5mL; Nalgene™ 25mm syringe filters (CA; 0.8µm pore); calreticulin antibody (PA3-900); DMSO (dimethyl sulfoxide), Penicillin-Streptomycin solution liquid, clinical waste bins; Cryovial 1 degree freezing container; protease inhibitor tablets EDTA-free; syringe hypodermic with needle 1mL; pipette tip, blue; racked, to fit Gilson P1000; Dynabeads™ Human T-Activator CD3/CD28 for T Cell expansion and activation.

Greiner Bio-One Ltd, Gloucestershire, UK: Cryovial, 2.0ml, skirted, internal thread, natural cap, sterile; aspiration pipette, 2ml, sterile, individually wrapped; 15ml centrifuge tube, graduated, bagged, sterile; 50ml centrifuge tube, conical base, bagged, sterile; 6 well tissue culture treated plate with lid, sterile; serological pipette 10ml; serological pipette, 5ml; cryovial, 2.0ml, skirted, internal thread; aspiration pipette 2ml; 15ml centrifuge tube; 50ml centrifuge tube; pipette tip, yellow, racked, to fit Gilson P20/P200; pipette tip, to fit Gilson P2/P10, racked, sterile.

Invitrogen, Paisley, UK: CFSE (Carboxyfluorescein succinimidyl ester); cell proliferation kit.

LI-COR Biosciences, Cambridge, UK: 800CW goat anti-rabbit IgG, 680RD goat anti-mouse IgG.

Lonza, Wokingham, UK: RPMI 1640 without L-glutamine; gentamycin sulfate L-glutamine solution, 200 mM suitable for cell culture.

Miltenyi Biotec, Bisley, UK: Pan monocyte isolation kit, human; midi MACS separator, LS+ positive selection column; CD8+ T Cell isolation kit human.

PeproTech, London, UK: Recombinant human GM-CSF; recombinant Human IL-4.

Sartorius, Epsom, UK: 75cm<sup>2</sup> cell culture flasks; serological pipette 5ml, 10 ml, 25 ml individually wrapped sterile; syringe filter 28mm diameter sterile, N Nylon (N membrane filter

Sigma Aldrich, Gillingham, UK: Paque plus GE17-1440-02; Roche Dapi (4', 6-Diamidine-2'-phenylindole dihydrochloride); monoclonal anti-actin antibody produced in mouse, Doxorubicin; thapsigargin; sodium tauroursodeoxycholate (TUDCA); Tris buffered saline (TBS); propidium iodide; Guava Instrument Cleaning Fluid (ICF); Fluorescein isothiocyanate (FITC); BSA (bovine serum albumin).

Promo Cell, Heidelberg, Germany: Endothelial cell basal medium MV-2.

VH Bio, Gateshead, England: hCMEC/D3 (human cerebral microvascular endothelial cell line)

## 2.2. Buffers and Solutions

### **Tris buffered saline + CaCl<sub>2</sub> (CRT binding buffer) pH=7.6**

CaCl <sub>2</sub>	5 mM
Tris buffered saline	100 ml

### **RPMI complete medium for OVcar3, SKOV3, A2780, FaDu cells**

RPMI	500 ml
FBS	10% v/v
L-glutamine	2mM
Gentamicin	50µg/ml

### **Freezing solution for OVcar3, SKOV3, A2780, FaDu cells**

Growth medium	20% (v/v)
FBS	70% (v/v)
DMSO	10% (v/v)

### **Complete medium for hCMEC/D3 (human cerebral microvascular endothelial cell line)**

Endothelial cell basal medium MV-2

FBS (heat inactivated) 5% v/v  
Endothelial cell growth MV-2 bullet kit

**Collagen solution (for coating flask).**

Collagen solution, type I from rat tail 4mg/ml  
Diluted stock 1:30 in PBS

**MACS-Buffer**

PBS 100 ml  
BSA 0.5 g  
EDTA 2 mM (0.744g)

**Staining buffer (for use in immunofluorescent staining protocols of cells in suspension)**

PBS  
FBS 1 % (v/v)  
NaN<sub>3</sub> 0.09 % (w/v)

**10x sodium carbonate buffer for CRT ELISA**

Use 6ml of ddH<sub>2</sub>O initially to dissolve powder in tube

Na<sub>2</sub>CO<sub>3</sub> 0.1575g

NaHCO<sub>3</sub> 0.294g

pH solution to 9.6 using HCl

Make up final volume to 10ml

**0.1% (v/v) PBST -Tween 20 for ELISA**

500µl Tween-20

500ml PBS

**5% (w/v) BSA blocking buffer**

Bovine serum albumin 1g

0.1% PBST 20ml

## **2.3. Cell culture**

### **2.3.1. Cell culture conditions**

#### **SKOV3, A2780, OVcar3, FaDu cancer cells**

For all experiments cancer cells were maintained at 37°C in a humidified incubator with 5% CO<sub>2</sub>. Cancer cells were cultured in media as follows (unless otherwise specified).

SKOV3, A2780, OVcar3, FaDu cells provided by collaborators/supervisors (Dr Jacqueline Whatmore, Exeter University & Dr Edwin Bremer; University of Groningen) were grown in RPMI medium supplemented with 10% (v/v) FBS and gentamicin (50µg/ml)

Ovarian cancer cells were passaged by trypsinisation when they reached confluency in the tissue culture flasks/dishes. The medium was removed and the cells were washed once with warmed PBS followed by addition of 2 ml trypsin solution (0.05%) (w/v). The cells were placed in the incubator at 37°C for 3-5 minutes. Detachment was monitored by microscope until cells could be seen floating in the trypsin solution. Trypsin was then neutralized by the addition of 8 ml of growth medium (containing 10% (v/v) FBS) and the cell suspension was transferred to a tube and centrifuged at 1500rpm for 5 minutes. The supernatant was removed and the cells were resuspended in complete growth medium. Required number of cells was transferred into tissue culture flask (25cm [T25] or 75cm [T75]) and the total volume of medium was filled up to 10ml for T75 or 4ml for T25.

#### **2.3.2. THP-1 cell (human monocytic cell line)**

THP-1 cells were a kind gift from Dr Chris Scotton.

Cells were cultured in RPMI 1640 supplemented with 10% (v/v) FBS and 2-mercaptoethanol to a final concentration of 50µM. Cells grow in suspension and were sub-cultured when cell concentration reached approximately 1 x10<sup>6</sup> cells/ml by centrifugation and resuspension at 2-4 X 10<sup>4</sup> cells/ml. Media was changed every 2 to 3 days by centrifugation and resuspension.

### **2.3.3. HCMEC/D3 human cerebral microvascular endothelial cells**

Primary HCMEC/D3 cells were maintained at 37°C in 5% CO<sub>2</sub> in culture media (Endothelial Cell complete Media MV 2). For progressive passages, cells were trypsinised as in (2.3.1) with 0.05% (w/v) trypsin-EDTA and these cells were seeded in collagen type I (100µg/ml) coated tissue culture flasks and cultured in supplemented MV-2 endothelial growth medium. Cells were passaged at a ratio of 1:3 and fed every 2-3 days. After removing the culture medium, cells were washed twice with PBS and trypsinised. To collagen coat the flasks diluted collagen solution (3ml) was evenly distributed across the bottom of a T75 tissue culture flask and incubated at 37°C for at least 1 hour. Any remaining collagen was aspirated and the flask was washed twice with PBS prior to adding the HCMEC/D3 cell suspension.

### **2.3.4. Freezing cells**

Cells were trypsinised (2.3.1), centrifuged and resuspended (~2x10<sup>6</sup> cells) in 1ml freezing medium (as described for each cell type in 2.2.1). The cell suspension was transferred into sterile labelled vials, which were then placed in a cryo-container containing isopropanol and stored at -80°C overnight for slow cooling. Frozen vials were ultimately transferred into liquid nitrogen for long term storage.

### **2.3.5. Thawing cells**

The frozen cells in cryovials were rapidly thawed by placing in a 37°C water bath. Thereafter, the cells were slowly diluted in 10mls of pre-warmed growth medium and plated in T75 flasks (collagen coated for HCMEC/D3). The medium was replaced after cell attachment (usually 24hrs) in order to remove the DMSO used during freezing.

### **2.3.6. Seeding cells into 6 well plates.**

Flasks that were fully confluent were sub-cultured into 6-well plates. The method for sub-culturing was followed as described in section in 2.3.1. For cell counting the cell pellet was re-suspended in 1 ml cell complete medium pre-warmed to 37°C. Equal volume of 0.4% (w/v) trypan blue dye was added to the cell suspension (example: 10 µl of cells to 10 µl of trypan blue) and the suspension mixed by pipetting up and down. 10 µl of the cell-suspension was removed and placed in a haemocytometer (Figure 2.1). The cells were counted under a light microscope.

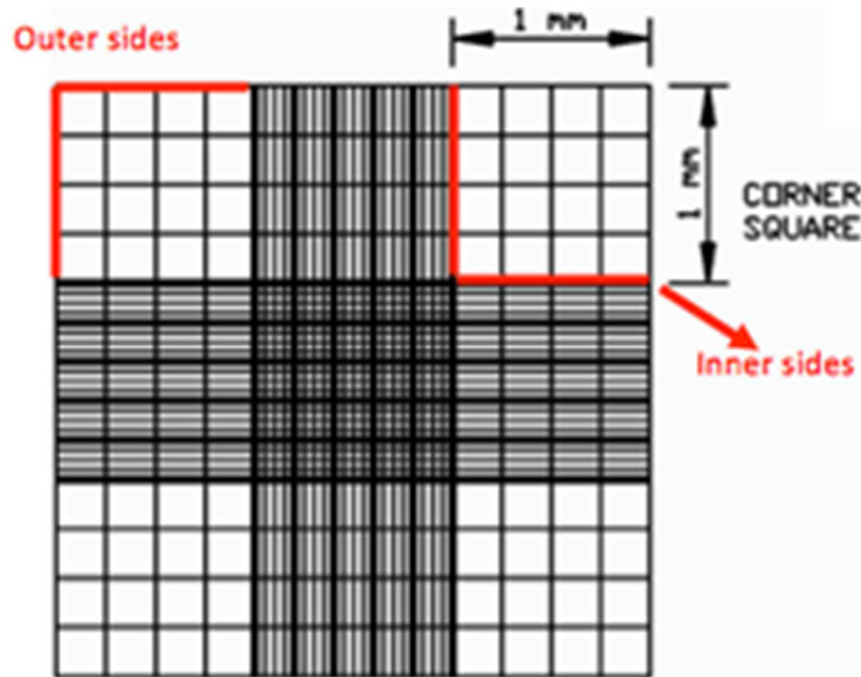


**Figure 2.1 Counting of cells on a haemocytometer (LLC, 2018)**

Trypan blue, made up in phosphate buffered saline (PBS), was used as the vital dye stain because of its ability to cross the plasma membrane and be retained within non-viable cells. A haemocytometer was used to count the number of live cells. All viable cells in the four corner squares were counted. If the cells were on the border outlining each square, only the cells on the top and left border of the square were included. This value represented the number of cells/  $\mu\text{l}$  fluid. Based on the average number of cells, the desired number of cells required for seeding could be calculated.



For example, an average of 150 cells in all four corner-squares of the haemocytometer constituted  $1.5 \times 10^6$  cells/ ml in 10 ml complete media. For the cancer cells,  $0.5 \times 10^6$  cells were seeded in each well of a 6 well plate. To obtain the correct seeding density, the cell suspension was diluted, see equations and calculations below:

$$C1 \times V1 = C2 \times V2$$

Whereby:

C1 = number of cells  $\times 10^6$ / ml;

V1 = initial volume of complete medium added to cells to create cell suspension;

C2 = desired number of cells/ ml in final cell suspension;

V2 = final volume of complete medium used to resuspend cells.

Example:

$$V2 = \frac{(1.5 \times 10^6 \times 1 \text{ ml complete media})}{(0.5 \times 10^6 \text{ cells/ ml})}$$

$$(0.5 \times 10^6 \text{ cells/ ml})$$

$$V2 = 3 \text{ ml}$$

## **2.4. Flow cytometry**

Flow cytometry is a method that allows the measurement of the properties individual cells, and their in-depth analysis by specific software programmes, as they flow in a fluid stream through a beam of light. The properties measured include a particle's relative size, relative granularity or internal complexity, and relative fluorescence intensity after specific staining. These characteristics are determined using an optical-to-electronic coupling system that records how the cell or particle scatters incident laser light and emits fluorescence.

A flow cytometer is made up of three main systems: fluidics, optics, and electronics:

- a) The fluidics system transports particles in a stream to the laser beam for interrogation.
- b) The optics system consists of lasers to illuminate the particles in the sample stream and optical filters to direct the resulting light signals to the appropriate detectors.
- c) The electronics system converts the detected light signals into electronic signals that can be processed by the computer.

### **2.4.1 Gating for live cells**

After preparation cells in suspension are passed through the narrowing channel. Each cell passes the laser beam, allowing individual analysis. The laser beam scatters in multiple directions and the flow cytometer detects light scatter as forward scatter and side scatter. Forward scatter (FSC) is proportional to cell-surface area or size. It is a measurement of mostly diffracted light and is detected just off the axis of the incident laser beam in the forward direction by a photodiode. The other detector measures scatter at a ninety degree angle relative to the laser. This parameter is called side scatter (SSC) and is a measure of the granularity of a cell. When measured together, these allow for differentiation in a heterogeneous cell population (Figure 2.2). This allows a gating strategy to eliminate cell debris from further analysis because it has lower forward scatter levels, FSC and SSC can also be used to assess cell death, specifically live cells are typically larger than dead cells and are also less granular.

However, flow cytometry can be coupled with fluorescent labels to give more detailed analysis.

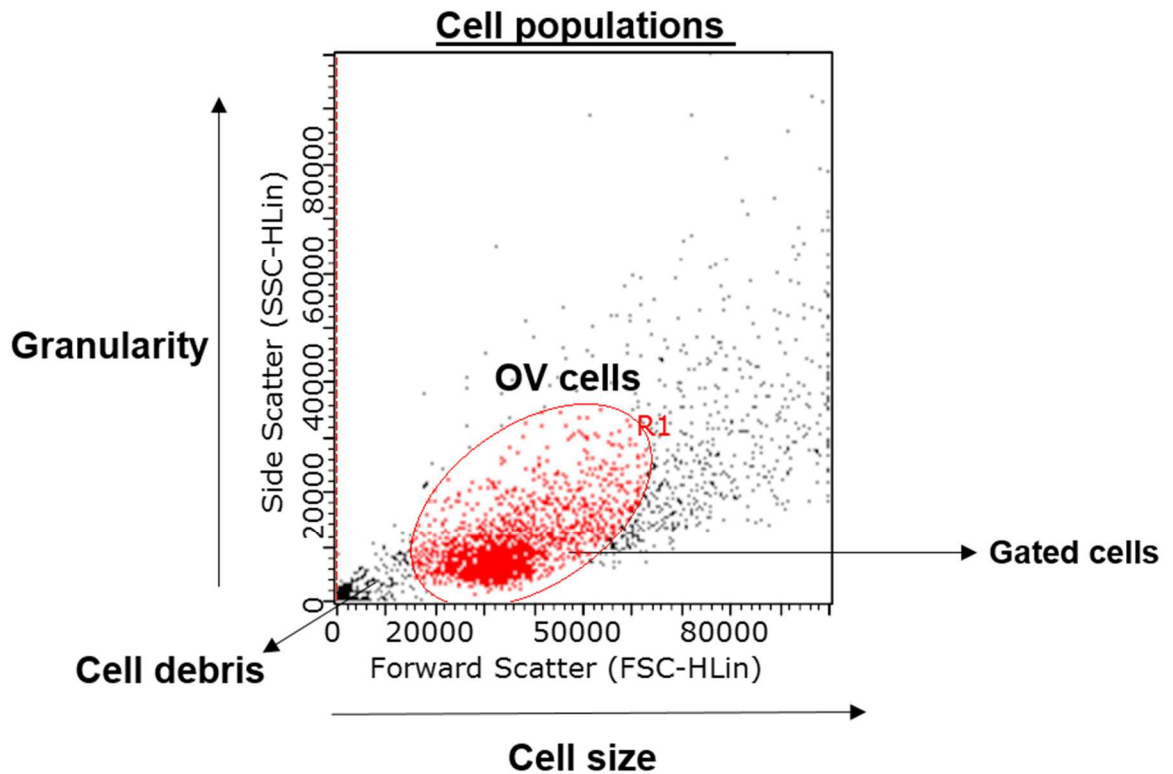


**Figure 2.2.** This graph displays two measurement parameters. Cell size on the x-axis (FSC) and granularity on the y-axis (SSC) and the events are shown as a density (or dot) plot. The gating strategy eliminates cell debris because it has lower forward scatter levels. Gated cells are often found at the bottom left corner of the FSC vs SSC density plot. The plot shows typical side scatter (SSC) and forward scatter (FSC) gating of cancer cells at gate of an ovarian cells population (R1).

### **2.4.2. Compensation**

Where more than one fluorophore is used there is a possibility of overlap between the emission spectra that may influence the data and require correction through data processing i.e. compensation. The Guava flow cytometer and associated software used here automatically calculates accurate compensation values for each fluorochrome combination and so it is not necessary to do this manually. However, for confirmatory purposes this was checked for the fluorophore combinations used in Chapter 5 i.e. Cy-5 (far red excitation/emission approximately 650/670), PE (yellow, excitation/emission approximately 496 nm/578 nm) or FITC (green, excitation/emission approximately 495 nm/519 nm).

Briefly, cells were stained with pairs of antibodies with different fluorophore combinations analysed by flow cytometry. Figure 2.3 Indicates that positively stained cells labelled with the fluorophore identified on the x axis of each image do not show any overlap with the fluorophore identified on the y axis. These data confirm that no further compensation is required.

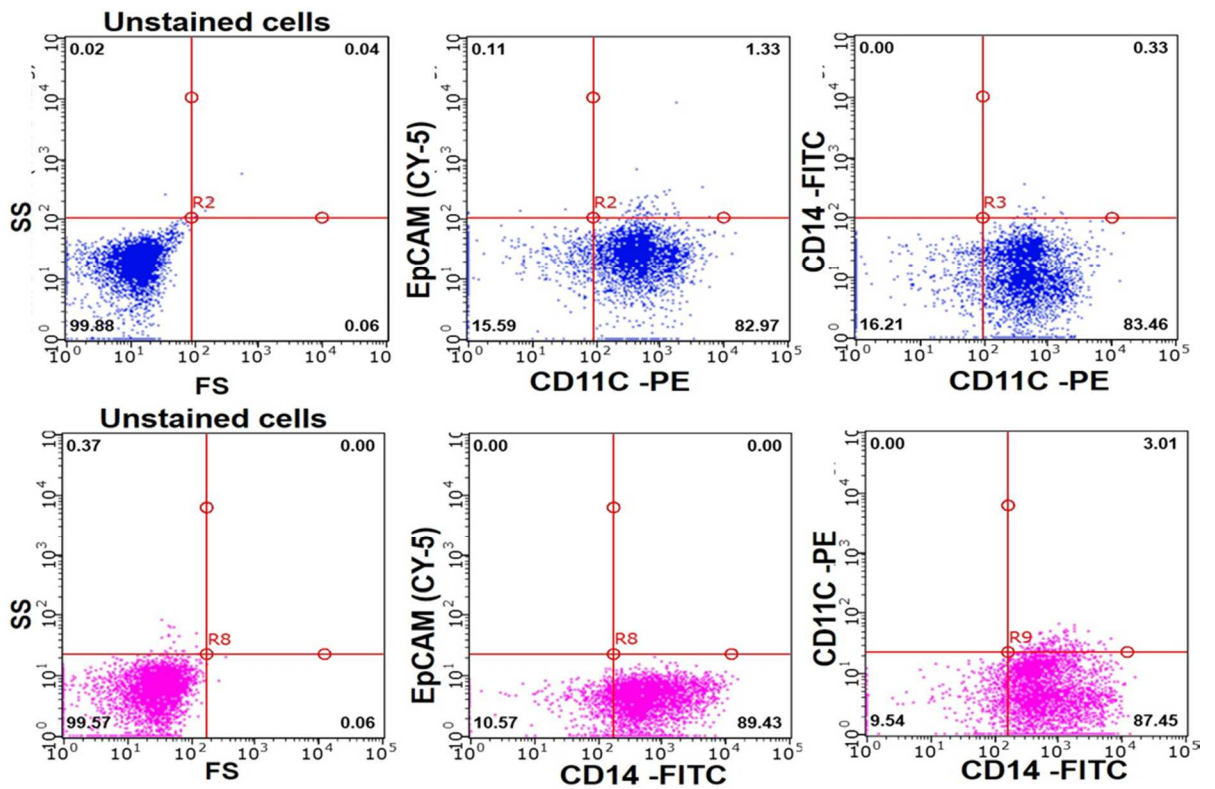


**Figure 2.3. EpCAM-cy5 fluorescence did not overlap with FITC or PE staining.** iDCs and mDCs derived from THP-1 cells (as described in the Materials and Methods) were stained with pairs of antibodies as indicated i.e. CD11c-PE + EpCam-cy5 or CD14-FITC (upper panel) or CD14-FITC + CD11c-PE or EpCan-cy5 (lower panel), and then assessed for the relevant fluorophore by flow cytometry to examine any overlap in the emission spectra.

### **2.4.3. Flow cytometry to assess cell apoptosis and necrosis**

Annexin V and PI propidium iodide can be used to detect cell death as described in the Introduction. PI is a nuclear stain which does not stain live and early apoptotic cells due to the presence of an intact plasma membrane but in late apoptosis and necrosis the plasma integrity decreases and PI can enter the cell. PI is therefore only incorporated into the DNA of dying and dead cells. These cells are described as 'PI positive cells'. The results can provide information regarding cell viability (i.e. the percentage of dead and live cells). As PI cannot enter live cells, flow cytometry can only indirectly detect these cells. Such cells are referred to as 'PI negative cells'. In contrast, annexin V is a marker to detect apoptosis. It specifically recognises PS that is exposed on the cells during apoptosis.

Cell apoptosis and necrosis were examined using the annexin V and PI staining and flow cytometry. Flow cytometry was performed using a Guava flow cytometer instrument (Millipore, Hertfordshire, UK). The data was analysed using Guava 3.1.1 software. The criteria for early and late apoptotic cells were annexin V-positive, PI-negative and annexin V-positive, and PI-positive, respectively. Signals were detected using Alexa Fluor® 647 which is a bright, far-red-fluorescent dye with excitation ideally suited for the excited at 633nm / 635nm; maximum emission of 668 nm. PI is yellow-fluorescent dye with excitation ideally suited to the excitation 540 nm; emission 608 nm laser line.

#### **Sample preparation**

Cells were trypsinised as in section (2.3.1), washed 1 x by centrifugation in annexin V binding buffer and resuspended at  $1 \times 10^5$  cells in 100- $\mu$ l of annexin V binding buffer in a 1.5-ml Eppendorf tube. 5  $\mu$ l Alexa Fluor® 647-annexin V and 10  $\mu$ l PI were added and cells were incubated for 15 min in the dark at room temperature. Finally, the volume was adjusted to 500  $\mu$ l with 1x binding buffer and analysed by flow cytometry immediately (Figure 2.4).

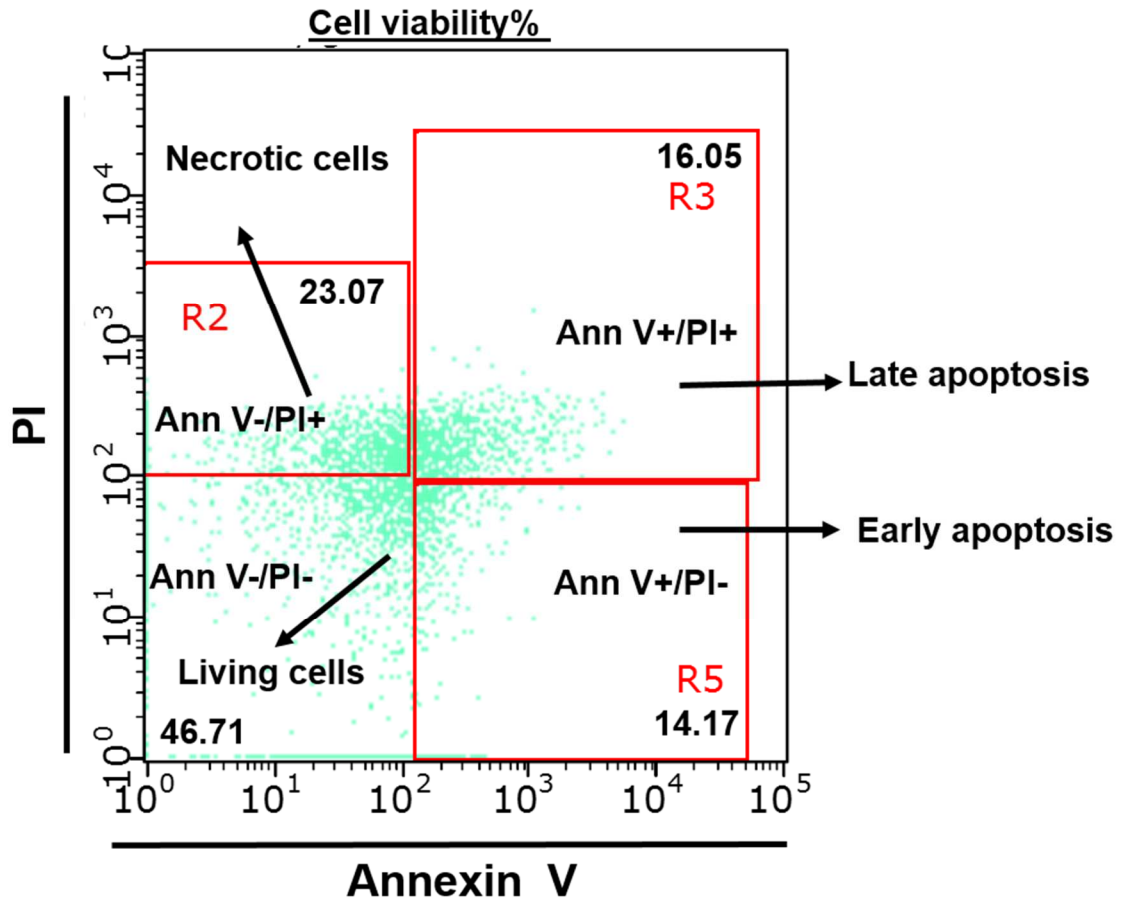


**Figure 2.4. Representative plot of cell viability of SKov3 ovarian cancer cells assessed by flow cytometry following dual staining with annexin V (Ann V) and propidium iodide (PI).** Cells were trypsinised, washed 1 x by centrifugation in annexin V binding buffer and resuspended at  $1 \times 10^5$  cells in 100- $\mu$ l of annexin V binding buffer in a 1.5-ml Eppendorf tube. 5  $\mu$ l Alexa Fluor® 647-annexin V and 10  $\mu$ l PI were added and cells were incubated for 15 min in the dark at room temperature and analysed by flow cytometry immediately. Data are presented as percentage of the cell population and interpreted showing the possible combinations of positive and negative staining for two different dyes as follows: annexin V-ve/PI-ve cells (lower left quadrant) are considered healthy cells, AnnV+ve/PI-ve cells (lower right quadrant) are considered early apoptosis, AnnV+ve/PI+ve (upper right quadrant) are considered late apoptosis, and AnnV-ve/PI+ve (upper left quadrant) are considered as necrotic cells.

In some experiments extracellular CRT was also assessed. Cells were treated as above to label annexin V and PI, resuspended in 1 ml PBS containing 0.5% w/v BSA and immediately incubated with rabbit anti-human-CRT Ab (1:200) for 1 h, followed by further washing x 3 and then stained with a 1:2000 dilution of a secondary antibody - goat anti-rabbit IgG in the dark for 30 minutes at room temperature. Finally, the volume was adjusted to 500  $\mu$ l with 1x binding buffer and analysed by flow cytometry immediately. Additional flow cytometry protocols are described in the relevant data chapter.

## **2.5. ELISAs**

### **2.5.1. CRT ELISA**

An enzyme-linked immunosorbent assay (ELISA) was used to quantify the CRT protein in cell culture media (Donnelly et al., 2006). Briefly, 153  $\mu$ l of cell-free supernatant fraction was placed into wells of a 96-well ELISA plate with 17  $\mu$ l of 10x carbonate buffer, pH 9.6 (section 2.2.). The protein was left to bind at 4°C overnight. The plates were then washed four times with PBS containing 0.1% v/v Tween 20 (PBST). Remaining binding sites were blocked with 5% (w/v) BSA in PBST at 37°C for 30 minutes. Wells were washed a further four times with PBST. Next 100 $\mu$ l of 1:2000 dilution of rabbit anti-human CRT antibody (PA3-900) diluted in PBST was added to each well for 2 hours in 37°C. The wells were washed again as described above, and a 100  $\mu$ l of 1:2000 dilution of secondary anti-rabbit HRP-conjugated antibody was added to the wells and the plate incubated for 1 hour at 37°C. The reaction was developed for 15 minutes at room temperature in the dark and was terminated by adding 50  $\mu$ l 2N H<sub>2</sub>SO<sub>4</sub> to each well. The optical density at 450 nm (OD<sub>45nm</sub>) of each sample was measured on a BMG Labtech FLUORostar™ plate reader and protein concentration estimated from a standard. A standard curve of known concentration of CRT yeast (*Pichia pastoris*) was constructed each time the ELISA was performed. A typical standard curve is shown in figure 2.5.



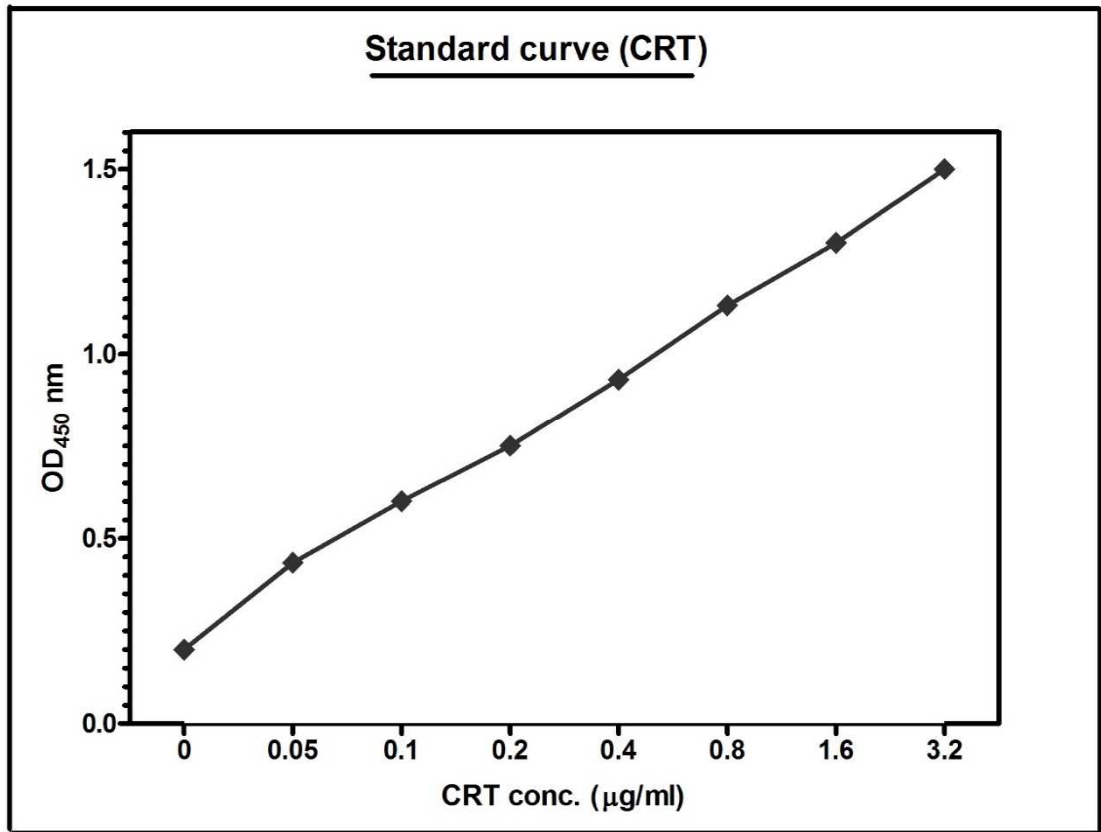


**Figure 2.5. CRT ELISA standard curve.** Standards of CRT at a known concentration (0.05 µg/ml -3.2 µg/ml) generated from a 2.5 µg/ml CRT stock serially diluted with binding buffer were assessed by ELISA (see Methods – section 2.5.1) and the data plotted as concentration vs OD<sub>450</sub>nm to provide a reference for calculation of CRT levels in test samples. The dilution buffer was used as a blank.

### **2.5.2. ELISA for IL-12/IL-23p40**

IL-12/IL-23p40, levels were determined in cell culture supernatants using enzyme-linked immunosorbent assay (ELISA) kits according to the manufacturer's instructions. IL-12 is secreted by activated B lymphocytes and macrophages as a 70 kD heterodimeric glycoprotein comprised of disulfide-bonded 35 kD and 40 kD subunits. IL-23 is a heterodimeric cytokine composed of two disulfide-linked subunits, a p19 subunit that is unique to IL-23, and a p40 subunit that is shared with IL-12. IL-23 is secreted by activated macrophages and dendritic cells. The antibodies in the Human IL-12/IL-23 (p40) ELISA MAX™ set react with the p40 subunit of human IL-12 and IL-23, as monomer and homodimer.

An anti-human IL-12/IL-23 p40 capture antibody was added to wells of a 96-well plate. The plate was sealed and incubated overnight (16-18 hrs) at 4°C. The plate was washed 4 times with at least 300 µL wash buffer per well and the residual buffer was removed by firmly tapping the plate upside down on absorbent paper. Assay volume diluent was added to each well to block non-specific binding, the plate sealed and incubated at room temperature for 1 hour with shaking at 200 rpm on a plate shaker. The plate was washed 4 times as above and 100 µL/well of standards or samples added to the appropriate wells, the plate sealed and incubated at room temperature for 2 hours with shaking. After washing 4 times as above, 100 µL of diluted biotinylated detection antibody solution was added to each well, the plate was sealed and incubated at room temperature for 1 hour with shaking. 100 µL of diluted avidin-HRP solution was added to each well, the plate sealed and incubated at room temperature for 30 minutes with shaking. The avidin-HRP solution was removed during a wash step, and 100 µL of freshly mixed TMB substrate solution was added and incubated in the dark for 15 minutes and 100 µL of stop solution added. Absorbance was read at 450 nm within 30 minutes.

## **2.6. Determination of protein concentration**

The bicinchoninic acid (BCA) assay (Thermo Fisher, Cramlington, UK) was used to determine protein concentration in a solution. The working range of the assay is 25-2000  $\mu\text{g/mL}$ . The BCA assay uses the Biuret reaction (reduction of copper (II) to copper oxide (I), in alkali conditions, by the peptide bond), which is then followed by the formation of a complex between copper oxide (I) and BCA which has an absorbance maximum at 562 nm (Smith et al., 1985). BSA was used to make a 6 point standard curve with a range of 25-2000  $\mu\text{g/mL}$ . Clear, flat bottom, 96-well microtiter plates were used and 25  $\mu\text{l}$  of the sample/standard was mixed with 200  $\mu\text{l}$  of BCA reagent. Each sample standard was measured in triplicate. The plate was covered and incubated at 37°C for 30 minutes before measuring the absorbance on a Fluostar Optima plate reader (BMG Labtech, Ortenberg, Germany), with a 550 excitation filter. Calculated concentrations (from the standard curve) were then multiplied by the relevant dilution factor to give a final concentration. A typical standard curve from this assay is shown in Figure 2.6.

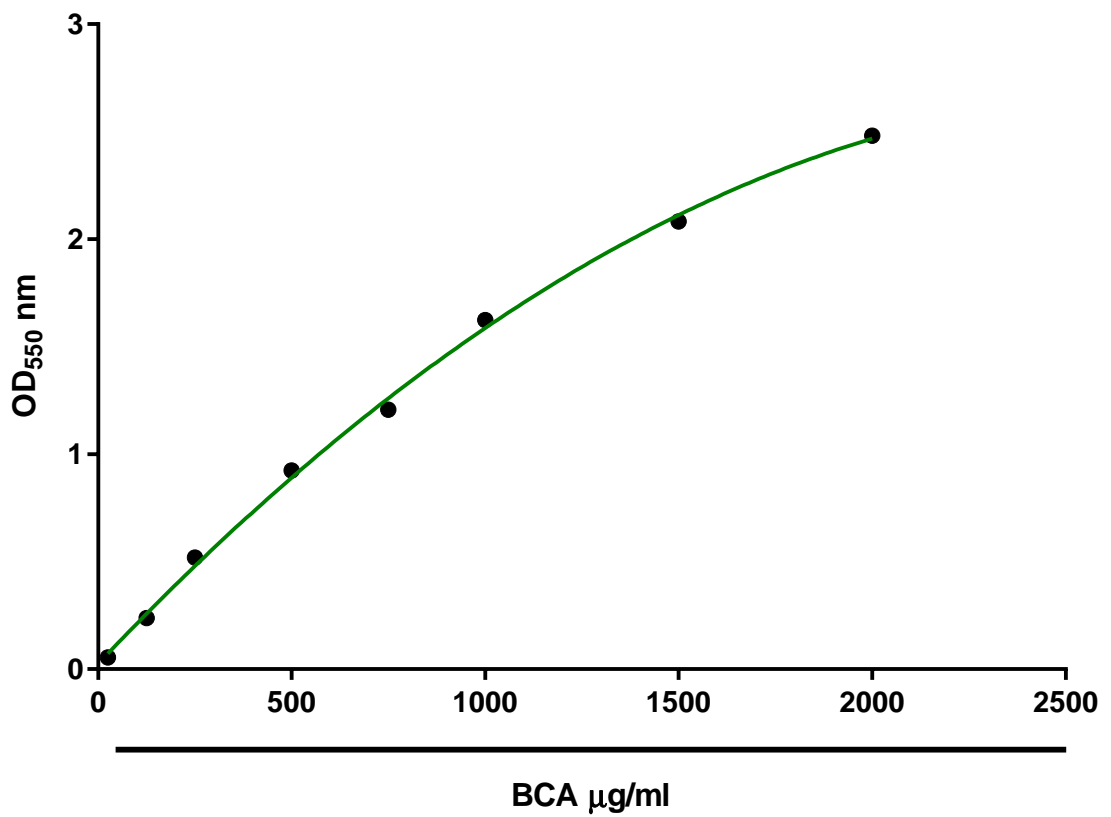


**Figure 2.6. BCA assay standard curve.** Standards of bovine serum albumin (BSA) at a range of 25 – 2500 μg/ml of known concentrations were assessed using the BCA protein assay and the data plotted as concentration vs OD<sub>550</sub> nm to provide a reference for calculation of protein levels in tested samples. 25 μl of the protein standards (diluted in H<sub>2</sub>O) was incubated with 200 μl BCA reagent at 37°C for 30 minutes before measuring the absorbance on a Fluostar Optima plate reader, with a 550-10 excitation filter.

## **2.7. SDS-PAGE (sodium dodecyl sulfate polyacrylamide gel electrophoresis) and western blotting.**

SDS-PAGE can be used to separate proteins in a sample by mass. Protein samples were denatured by addition of Laemmli buffer and heating. Laemmli buffer contains SDS and a reducing agent. SDS is both denaturing and an ionic detergent that binds evenly to proteins in a mixture giving them all an equivalent negative charge and allowing separation by mass only in the gel. DTT was used as a reducing agent; breaking the disulphide bonds so that proteins were no longer in their tertiary or quaternary structures. Samples then underwent electrophoresis; this process uses a positive charge to draw the proteins through the pores in the polyacrylamide gel. A 12% acrylamide gel was used as this has a small pore size.

### **2.7.1. SDS PAGE to determine protein molecular weight under reducing conditions.**

7.5 $\mu$ L of 3x Laemmli buffer (with DTT to give a final concentration of 350 mM) was added to 15  $\mu$ L of each protein sample, boiled for 5 min at 95°C and resolved by SDS-PAGE using a 12 %, 15 $\mu$ L/well gradient gel immersed in running buffer (25 mM Tris, 192 mM Glycine pH 8.3). Samples were electrophoresed at constant voltage of 75 V for 20 min and 100 V for 45 minutes. The gel was then removed and washed twice with ddH<sub>2</sub>O and stained with Bio-safe Coomassie Blue G-250 stain on a low speed orbital shaker for about an hour. The gel was then washed with ddH<sub>2</sub>O water then left to de-stain in ddH<sub>2</sub>O overnight.

### **2.7.2 Western blotting for CRT**

Western blotting is a widely used method to identify the presence and relevant abundance of a specific protein (using specific antibodies) in a sample following the transfer of proteins from the SDS-PAGE gel to a membrane. This technique was described and named by (Burnette, 1981) and the main principles of the procedure have not changed since.

## **Transfer**

Transfer from the SDS-PAGE gel to a nitrocellulose (0.45 µm) membrane was performed using the 'wet' tank electro transfer method. The gel was carefully removed from the running operation. After trimming off the top and bottom the gel was then placed on the top of membrane in a Trans-blot® Turbo™ blotting system (Bio-Rad). A roller was used to remove bubbles and enhance transfer. The transfer was completed in seven minutes, and the membrane processed to identify the proteins.

## **Blocking the membrane**

The nitrocellulose membrane has a high affinity for protein and therefore would bind the antibodies non-specifically if not 'blocked' first. Pierce protein free blocking buffer was used, rather than the common BSA blocking solution, as nitrated tyrosine could be expected to be present in albumin. This step was performed for one hour at 4°C with gentle rocking.

## **Antibody incubation.**

After blocking the membranes were probed with primary antibodies as indicated, washed and incubated at room temperature in the dark for 1 h with secondary antibodies conjugated to fluorophores that emit in near-infrared, wavelengths (680 and 800 nm). These fluorophores produce a signal directly proportional to the antigen and are stable over time. 2.9.3.4. Protein bands were imaged using the LiCor Odyssey CLx system (LI-COR Biosciences UK Ltd Cambridge, UK), this platform has an infrared laser for excitation. The Image Studio Lite (LI-COR Biosciences UK Ltd Cambridge, UK) software was then used to analyse the images. This software allows for the image to be edited (e.g. cropped, flipped, brightened) without changing the actual signal intensities (numerical data) collected so that comparisons between bands are valid.

## Chapter 3. Purification of calreticulin and preparation of monomeric CRT

### 3.1. Introduction

In recent years knowledge of the functional complexity of CRT has expanded, resulting in CRT being implicated in many aspects of normal physiological and pathological cell function, including important roles in health, disease, and the regulation of cell death (Eggleton and Michalak, 2013). As previously mentioned CRT is a 46 KDa protein with three defined regions; the amino and carboxy regions make up the N-C globular domain and the middle segment is comprised of the proline-rich P-domain. The N-C globular domain of CRT contains eight antiparallel  $\beta$ -strands (Michalak et al., 2002). It interacts with  $\alpha$ -integrins (Rojiani et al., 1991) and the DNA-binding site of the steroid receptor. Cysteine residues form the disulfide bond in the N-domain and the N- and P-domains are reported to have an important role in the chaperone function of CRT (Figure 3.1) (Krause and Michalak, 1997, Martin et al., 2006). The P-domain has three repetitive regions (Krause and Michalak, 1997) with repeated amino acid sequences and is thought to contribute to the protein-protein binding functions of CRT. The P-domain of CRT also has two  $\text{Ca}^{2+}$ -binding sites (high-affinity, low-capacity) (Tjoelker et al., 1994) and acts as a bridge to the co-receptor on phagocytic cells (Chouquet et al., 2011). The Carboxy terminal region of CRT contains a highly acidic, negatively charged segment which is important for  $\text{Ca}^{2+}$  buffering functions (Nakamura et al., 2001). This region interacts with other chaperone proteins in the ER (Michalak et al., 1999). Additionally, there is considerable evidence indicated that the Carboxyl region of CRT has a critical role in re-translocation of CRT from the ER lumen to the cytosol, a process that can be triggered by ER  $\text{Ca}^{2+}$  becoming depleted (Labriola et al., 2010). The globular domain of CRT interacts with PS on the cell surface of apoptotic cells (Chouquet et al., 2011).

The increasing recognition of CRT as a multifunctional protein has led to a requirement for purified CRT for experimental purposes. Thus, recombinant human CRT (rCRT) preparations have now been produced using a wide range of expression systems including bacteria and yeasts (Pandya et al., 2019). The CRT obtained can then be further purified using techniques, such as FPLC, which separate the protein from contaminants based on the characteristics of the CRT e.g. the fact that it is highly

negatively charged. However, it has emerged that CRT purified in this way from bacterial expression systems can be complexed with lipopolysaccharides (LPS or endotoxin) (Pockley et al., 2008). LPS is the most predominant lipid on the outer layer of Gram-negative bacteria, such as *E.coli*, and it is capable of triggering cellular immune responses including phagocytosis and cytokine release (Kelley et al., 2013). LPS is composed of three major portions; a lipid A portion which is responsible for its virulence and two polysaccharide components O and R (Todar, 2018). It has been reported that LPS-free CRT induced the expression of cell surface maturation markers and cytokine release by dendritic cells via NFκB signalling (Bajor et al., 2011). In contrast, LPS-free CRT in other studies was shown to prevent upregulation of dendritic cell surface activation markers, such as MHCII and CD86, and pro-inflammatory cytokine production (Bak et al., 2008). These contrasting results may be due to incomplete removal of LPS from the CRT preparations used, highlighting that it is sometimes difficult to distinguish the cellular effects of the CRT from the LPS. Thus, it is clearly important to ensure that the CRT preparations used for experimentation are LPS free. However, this is technically very difficult to achieve completely.

This chapter describes the preparation of purified full length human rCRT expressed in both the bacterium *E. coli* and the yeast *Pichia pastoris* (as previously described; (Andrin et al., 2000, Baksh and Michalak, 1991) CRT from both sources was received from collaborators or commercial sources and subsequently further purified to remove any impurities) by FPLC using anion exchange (Mono Q) chromatography (Tarr et al., 2010a). Since recombinant forms of CRT at high concentrations in solution can form monomers, dimers and multimers which might influence the ability of CRT to bind to cells, monomeric CRT was subsequently purified using size exclusion chromatography. Additionally the CRT preparation from *E Coli* was treated using the antibiotic polymyxin B to neutralise LPS activity (Domingues et al., 2012). Since the CRT from *Pichia pastoris* was expressed in yeast this preparation was not treated with polymyxin B since it should not contain LPS.



### 3.2. Aims of this chapter:

- To purify monomeric CRT expressed in both *E. coli* and *Pichia pastoris* using anion exchange chromatography followed by size exclusion chromatography (Figure 3.2).
- To investigate the purity, size and complexity of rCRT in terms of aggregates.
- To remove LPS from the purified *E. coli* CRT using polymyxin B

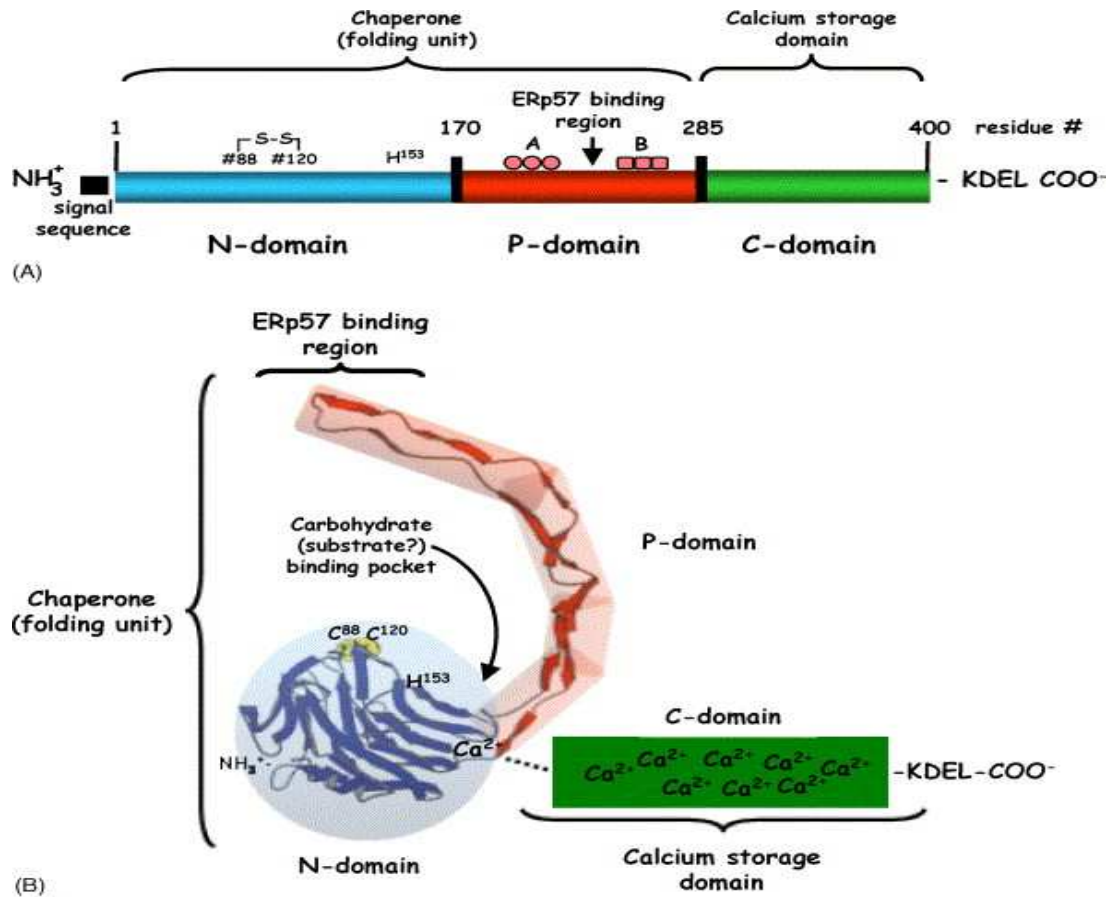


**Figure 3.1. A schematic diagram of calreticulin;** (A) The N-domain of CRT has a signal sequence peptide that is cleaved off to allow the protein to be retained in the endoplasmic reticulum; the C-terminal has a KDEL ER retrieval signal, calcium storage (buffering) domain and is highly acidic and negatively charged. This region interacts with other chaperons in the ER, and it has an important role in re-translocation of CRT from ER to the cytosol and interacts with PS on the apoptotic cells. The P-terminal is the ERp57 binding region. (B) A schematic of the 3D structure of CRT N, P and C domain organisation (Gelebart et al., 2005).

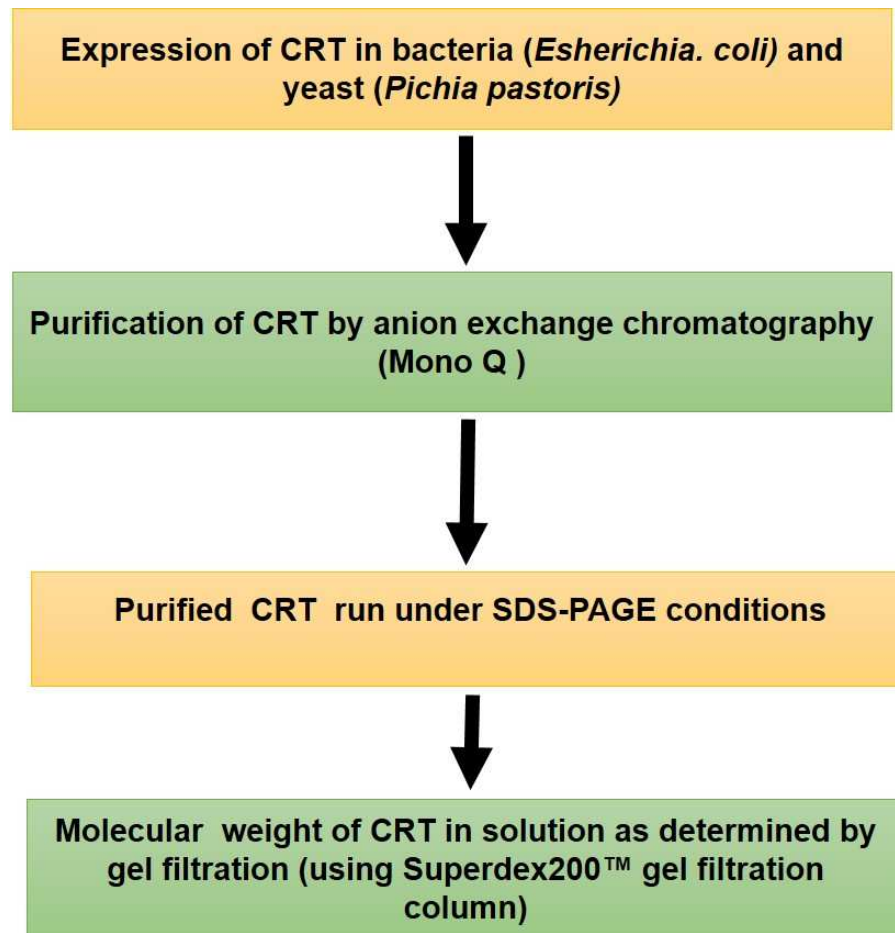


**Figure 3.2. Summary of CRT purification steps.** Both bacterial (*E. coli*) and yeast (*P. pastoris*) pellets expressing human full-length CRT were lysed and the soluble lysates containing CRT were further purified using FPLC (fast protein liquid chromatography). As CRT is highly negatively charged (pI 4.6) at pH 8.0, initial purification used an anion exchange Mono Q column. All eluted fractions were examined for purity on SDS-PAGE under reducing conditions. MonoQ fractions containing CRT were collected and subjected to size exclusion chromatography to estimate the molecular weight of CRT and the complexity of the purified protein in terms of aggregates of recombinant CRT. A Superdex200™ gel filtration column was used with molecular weight standards to calibrate the column (range 2 million Daltons to < 20 thousand Da).

### **3.3. Methods**

#### **3.3.1. Source of CRT**

Human full length CRT was obtained from the following sources: (i) expressed in *Pichia pastoris* and a gift from Dr Evaldas Ciplys and Dr Rimantas Slibinskas (Vilnius University, Lithuania) (Ciplys et al., 2015) (Nagata et al., 2016) cloned into the pBAD plasmid vector, expressed, and purified from *E. coli* BL21 (DE3), as previously described (Baksh et al., 1992) and purchased from Intas Pharmaceuticals Ltd. (Ahmedabad, India) . All CRT was prepared and stored in CRT buffer (0.01 M Tris, 3 mM Ca, pH 7.6). Further purification of CRT was carried out as described (Pandya et al., 2019)

#### **3.3.2. Ion exchange chromatography (Mono Q)**

Both recombinant CRT preparations were further purified using anion exchange chromatography which depends upon the reversible adsorption of negatively charged solute molecules to an immobilised group of opposite charge. Briefly, 100 µg human rCRT was suspended in 400 µl of Buffer A (50 mM Tris-HCl, 50 mM NaCl, 0.005M K-EDTA) and injected onto an AKTA MonoQ (Q-Sepharose) HR 5/5 anion exchange column and the sample was subjected to gradient elution with Buffer A and Buffer B (50 mM Tris-HCl, 1.0 M NaCl, 0.005M K-EDTA). The experiments were performed in four main steps; column equilibration, sample application and wash, elution.

**Table 3.1. Preparation of MonoQ buffer A, pH 8**

<b>Reagent</b>	<b>Quantity (1 l)</b>
50 mM Tris-HCl	<b>7.88 g</b>
20 mM NaCl	<b>1.17 g</b>
5 mM K-EDTA	<b>2.02 g</b>
H <sub>2</sub> O	<b>Made up to 1000 ml</b>

**Table 3.2. Preparation of MonoQ buffer B, pH 8**

<b>Reagent</b>	<b>Quantity (1 l)</b>
50 mM Tris-HCl	7.88 g
1 M NaCl	58.44 g
5 mM K-EDTA	2.02 g
H <sub>2</sub> O	<b>Made up to 1000 ml</b>

### **3.3.3. MonoQ column cleaning and equilibration**

To ensure the anion exchange column was clean and sterile, it was routinely flushed with filter sterilized water and ethanol. In addition the column was run in the reverse direction of flow during column cleaning so that any contaminants accumulating near the top of the column do not pass through the entire length of the column.

Flow: 0.5 ml/min at room temperature

1. Column was washed with: 2 column volumes (CV) of 2 M NaCl; 4 CV of 1 M NaOH; at least 2 CV of 2 M NaCl.
2. The column was then rinsed with at least 2 CV of distilled water until the eluent pH was stable and then washed with at least 4 CV of start buffer or storage buffer until pH and conductivity values reached stability. Routinely the column was clean with 70% ethanol and stored in 20% ethanol prepared in sterile filtered H<sub>2</sub>O.

### **3.3.4. Mono-Q sample application**

Aliquots of 100 µl of 1 mg/ml CRT was taken and mixed with 400 µl of buffer A. The 500 µl sample was then injected (using a 10 ml injection loop onto the AKTA FPLC loaded with a MonoQ HR 5/5 anion exchange column, using a pre-written Programme 'MonoQ2015'. This procedure ran for approximately 38 min and 0.5 ml fractions were collected from the eluted proteins peaks from 25-50 mls.

Unbound sample was eluted over 3 CV, then a linear gradient of Buffer B (0-1 M NaCl) was introduced (prepared using Buffer A and Buffer B in the AKTA pumps A and B respectively) and the protein fractions collected. The column was then washed with 100 % buffer B then re-equilibrated in buffer A. Fractions were monitored for protein concentration by optical density at 280 nm and for salt concentration using conductivity. Fractions containing protein which eluted from the column at a salt gradient of 150 – 400 mM as this was the conductivity that we had previously shown was optimum for CRT elution (ref - Purification, isolation and characterization of calreticulin (Andrin et al., 2000).

### 3.3.5. SDS PAGE to determine MW of eluted proteins under reducing conditions

SDS-PAGE was performed as described in Chapter 2 section (2.10.1).

### 3.3.6. Gel Filtration of recombinant CRT

To ensure preparation of high quality calreticulin relevant fractions were further purified by size exclusion chromatography to determine the size of the protein aggregations and to obtain monomeric CRT. The multimeric status and molecular weight of both the *E.coli*- and *Pichia pastoris*- expressed CRT were examined using size exclusion chromatography to assess aggregates of recombinant CRT (using a Superdex200™ gel filtration column).

Commercial molecular weight standards (Sigma) were individually applied (200 µl via the injection loop) to calibrate the column and allow accurate determination of the precise molecular weight of CRT.

Specifically;

- I. Carbonic Anhydrase (bovine erythrocytes) MW = 29 kDa
- II. Albumin (bovine serum) MW= 66 kDa
- II. Alcohol Dehydrogenase (yeast) MW= 150 kDa
- III. Beta-amylase (sweet potato) MW=200 kDa
- IV. Apoferrin (horse spleen) MW=443 kDa
- V. Blue dextran MW= 2000 kDa

50 µl of CRT plus 250 µl of PBS was then chromatographed by size exclusion using a Superdex-200 pre-packed commercial column 10/300 GL at a flow rate of 1 ml/min on an AKTA FPLC system (separation capacity between 600 kDa to 10 kDa). 0.2ml fractions were collected and the progress of the protein through the column was monitored for absorbance at 280 nm.

### **3.3.7. Treatment of *E -Coli* expressed CRT monomeric protein fractions (from Mono Q) with polymyxin B (PMB)**

1. PMB stock was prepared at 1mg/ml in sterile endotoxin-free PBS and subsequently diluted 1/100 in Tris buffered saline (2.2.1.).
2. 4 volumes of PBS was added to the combined fractions containing the *E Coli* CRT protein peak collected at lower salt concentrations (monomeric CRT).
3. A buffer exchange procedure was performed on the CRT by spinning the protein through a 50,000 KDa cut off centrifugal separation unit (Amicon) spun at 3000 x g for 30 minutes at 4°C.
4. The waste buffer in the lower reservoir was discarded and the protein resuspended in PMB in TBS prepared as in 1 above.
5. The treated protein sample was then washed using the steps described in 3 with 4 times with fresh TBS.
6. The final protein was resuspended in TBS and
7. 5 µl was removed to determine the protein concentration using NanoDrop microvolume Spectrophotometer (ThermFisher Scientific)..

### **3.4. Results**

#### **3.4.1. CRT elutes in two separate peaks using anion chromatography**

CRT has an isoelectric point (pI) of ~4.6 with a net negative charge at pH 8.0, so an anion exchange Mono Q column was initially used to separate it from any impurities (Eggleton et al., 2016). A pure single peak of rCRT eluted from the column at 240 mM NaCl in protein expressed in both *E. coli* and *Pichia pastoris*. A second minor protein peak eluting at a higher salt concentration (>300 mM NaCl) was observed in *E. coli* CRT preparations, but this was less pronounced in *Pichia pastoris* rCRT (Figure 3.3). All fractions containing protein from these two major peaks were collected and subjected to further purification using gel filtration chromatography.



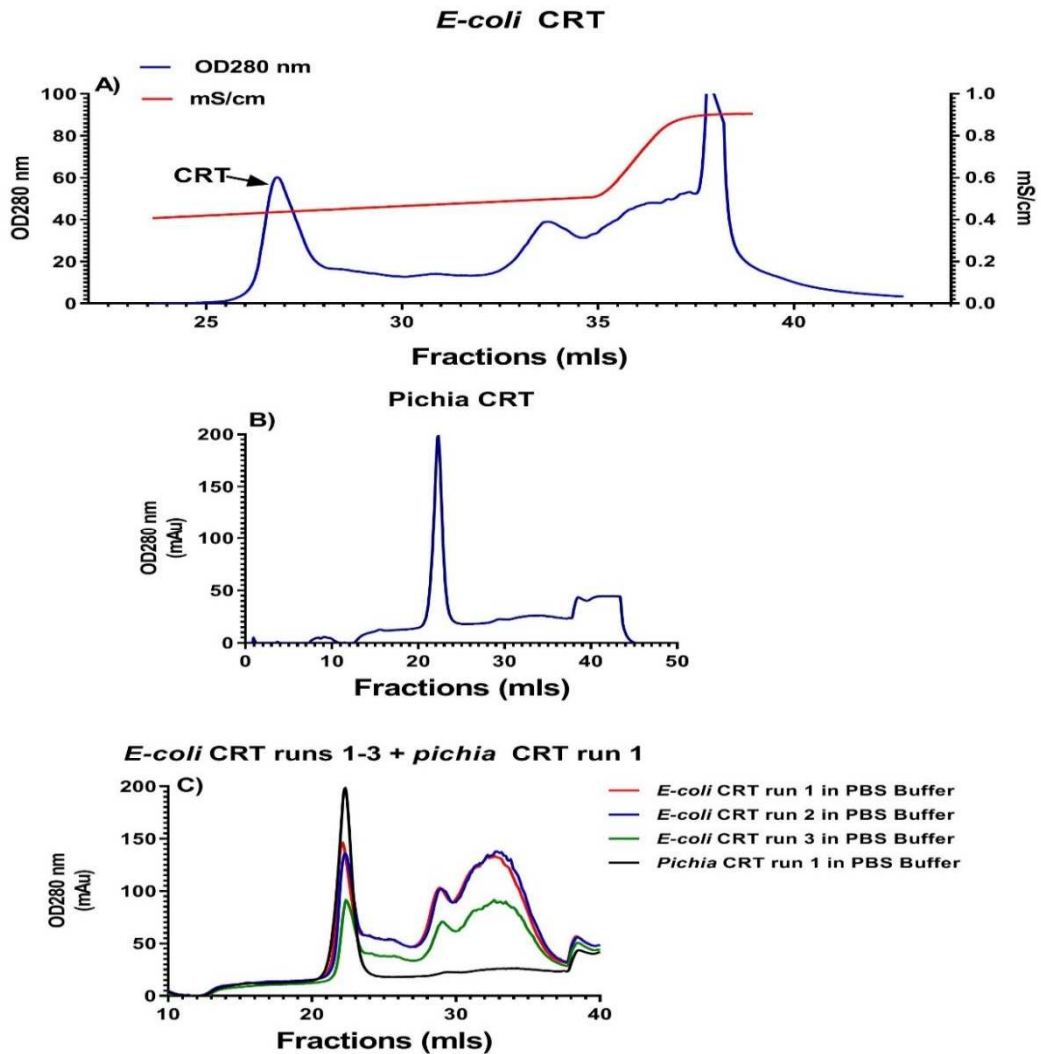


**Figure 3.3. Mono Q chromatographic analysis of human rCRT from *E. coli* and *Pichia pastoris*.** A) *E. coli* expressed human rCRT was routinely separated by anion exchange chromatography and eluted from the column with a 0-1 M NaCl buffer gradient rCRT consistently eluted with 240 mM NaCl (as depicted by arrow) as expected. A second protein peak eluted with at >300 mM NaCl. The red line shows the conductivity (concentration of NaCl) and the blue line shows the optical density (OD280 nm, concentration of protein). B) *Pichia pastoris* expressed human rCRT also eluted as one major protein peak in the presence of 240 mM NaCl (as assessed monitored at OD280nm). C) Comparison of the Mono Q chromatograph for human CRT isolated from *Pichia pastoris* and *E. coli* expression systems. Note the extra higher negatively charged protein contaminants eluting from the *E. coli* expressed system. A and B show representative chromatograms from a single FPLC run; C indicates the reproducibility of the purification protocol.

### 3.4.2. SDS PAGE to determine MW under reducing conditions

Mono Q fractions containing both CRT protein peaks from *E Coli* were examined for protein purity using SDS PAGE and Coomassie blue staining. It can be seen from (Figure 3.4) that a single protein band at a molecular weight of approx. 55-58 KDa was observed in all fractions tested. This corresponded to the reported relative molecular weight of CRT on SDS PAGE (Figure 3.4).

### 3.4.3. Gel filtration of recombinant CRT

Figure 4 clearly shows that the only protein detected in all fractions collected was CRT. It has been demonstrated that recombinant forms of CRT can form monomers, dimers and multimers (Pandya et al., 2019). This raised the possibility that these complexes may be responsible for the additional CRT peak that eluted at higher salt concentrations (Andrin et al., 2000). CRT aggregates with greater overall negative charge might require a greater salt concentration to elute from the anion exchange column. CRT does have the propensity to form complexes that might influence the ability of CRT to bind to cells (Andrin et al., 2000) and so the CRT was further purified by size exclusion chromatography to both confirm this hypothesis and to obtain pure monomeric CRT.

Size exclusion chromatography was performed using a Sephadex 200 column following calibration of the column using a number of proteins of known molecular weight between 20 to >2million KDa. Their approximate elution positions are shown in Figure 3.5. It can be seen that *E Coli* CRT shows two protein peaks on gel filtration, one at ~ 120 kDa and another at a very high molecular weight (<669 KDa (Figure 3.5 B) which is many times the reported molecular mass of CRT (approx. 48 KDa), suggesting the presence of protein aggregates. In comparison, *Pichia pastoris* CRT ('Lith-CRT') ran on gel filtration showed a single peak with a molecular weight of approximately 120 kDa (Figure 3.5 A). CRT is comprised of a globular head and elongated hair-pinned looped P-domain. It is known to characteristically run as a 120 kDa species due to retardation in its migration through gel filtration columns in solution, due to its comma shaped appearance ( ref as a above:((Young et al., 2006)) Calcium Binding Protein).

## Fractions of *E-coli* CRT

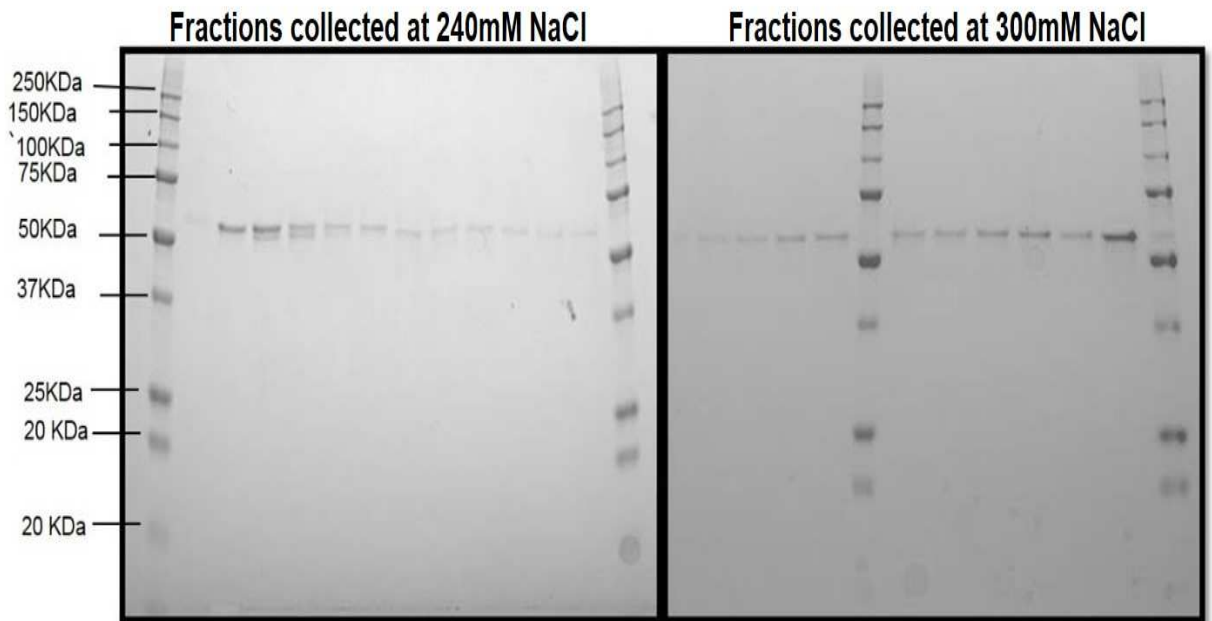


**Figure 3.4. *E Coli* CRT detected by SDS PAGE in fractions collected following Mono Q chromatography (both panels).** Protein fractions from both protein peaks were collected, concentrated were mixed with sample buffer, heated and analysed using a 12% SDS-PAGE gel under reducing conditions. Separated proteins were stained with Coomassie Brilliant Blue. A single protein band of similar relative molecular weight was obtained from both peaks.

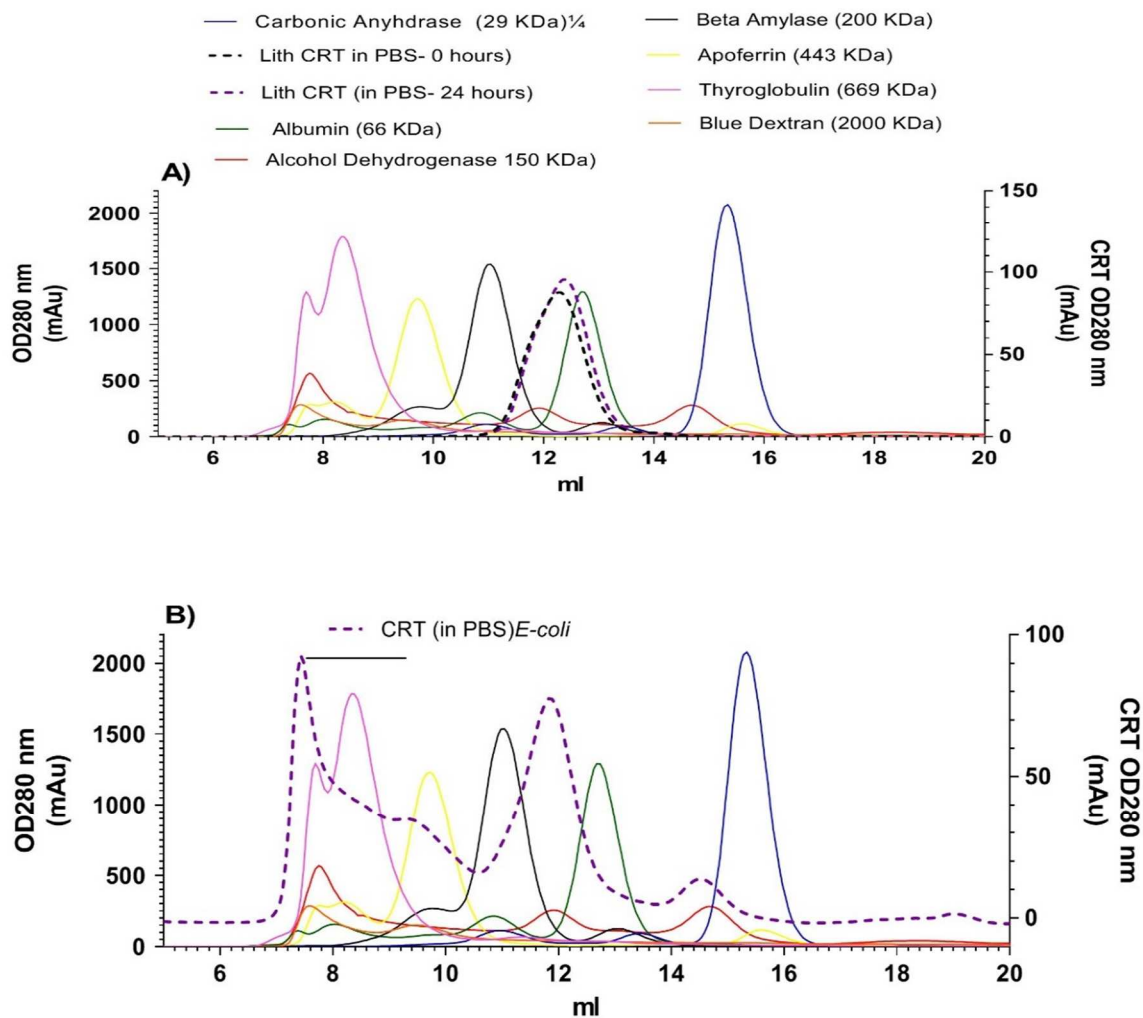


**Figure 3.5. Size exclusion chromatography of (A) *Pichia* expressed and (B) *E. coli* expressed human calreticulin.** Gel filtration of CRT-containing fractions (collected following anion exchange and eluted with 240 mM NaCl) was performed using a Superdex 200 column to determine the precise molecular weight of CRT. Calibration of the column was performed with number of molecular weight species from >2million Daltons to 20 KDa their approximate position is shown. *Pichia* expressed CRT (A, dotted lines) eluted as a single peak whereas E-Coli CRT (B, dotted line) eluted in multiple peaks suggesting the E.coli purified protein was comprised of a number of a number of molecular weight species possibly reflecting misfolded or aggregated protein .

### 3.5. Discussion

In this study human rCRT was received from two sources and expressed in either *E coli* or *Pichia pastoris*. Since CRT is highly negatively charged (pI 4.6) to ensure a pure preparation for future studies CRT was initially purified from any impurities by FPLC using a Mono Q HR 5/5 anion exchange column as previously described (Tarr et al., 2010a). For rCRT expressed in *E coli* two clear peaks of protein eluting at approximately at 240 mM NaCl and 300 mM NaCl salt concentration were observed. These data agree with those published in the literature (Pandya et al., 2019) and it has been hypothesised that the peak eluting at the high salt concentrations is CRT present in the form of multimers. Indeed recombinant forms of CRT can form monomers, dimers and multimers (Andrin et al., 2000). This was supported here by the observation that SDS-PAGE confirmed the presence of only one protein, with a molecular weight equivalent to that reported for CRT (approx. 55 KDa) in all fractions collected (Baksh et al., 1992). In contrast to the *E coli* expressed CRT, anion exchange analysis of *Pichia pastoris* showed only one peak (at 240 mM NaCl salt), suggesting that CRT expressed in this system was less prone to forming multimers.

Therefore, for all further studies *Pichia pastoris* expressed CRT was used. The observation that it did not form multimers a) suggests that it is folded correctly and does not form aggregates and b) as a monomer it is easier to interpret binding interactions with cells as it is not a complex of unknown size. Additionally, since it is not expressed in a bacterium LPS contamination was not considered to be an issue. Finally, *Pichia pastoris* CRT was shown to be stable in a 20 mM Tris base and 5mM Na-EDTA over 24 hours (Figure 5A).

Since this work was carried out further investigation suggested that even the *Pichia pastoris* CRT preparation contained very low levels of LPS, perhaps due to contamination from the buffers used (Pandya et al., 2019). This is discussed further in later chapters.

### **3.6. Conclusion**

In this study, purification of rCRT expressed in *E coli* and *Pichia pastoris* was performed by anion exchange and gel filtration chromatography. Due to its non-bacterial source and the observation that it did not form multimers *Pichia pastoris* was used for all further experiments in this thesis. The *E coli* rCRT was sent to collaborators in the USA for further analysis.

## **Chapter 4. An investigation into the conditions required for ovarian cancer cell surface association with either endogenous or exogenous CRT calreticulin**

Although CRT is mainly an ER chaperone protein, as discussed in the Introduction, cell surface-associated CRT is now recognized as an important DAMP molecule, identifying distressed cells to local immune cells. As such CRT promotes the immunogenicity of early apoptotic cancer cells and boosts adaptive immunity in the process of ICD. Cell surface CRT acts as an “eat-me” signal, enhancing phagocytic uptake of cancer cells (Gardai et al., 2005) by blocking the ability of the CD47 ('don't-eat-me' signal) to bind to its ligand SIRP- $\alpha$  (Krysko et al., 2018). Additionally, CRT has binding partners on immune cells that trigger innate immunity such as complement C1q (Donnelly et al., 2006, Verneret et al., 2014). In this case cell surface exposed CRT enhances complement-mediated phagocytosis of cells. These functional characteristics have increased the interest in surface expressed CRT in cancer immunology in recent years and it has been observed to have an anti-tumour role (Martins et al., 2010). Cell associated levels of CRT can be increased by either adding exogenous CRT or by inducing translocation of intracellular CRT to the cell surface. This chapter describes studies which examined strategies to increase ovarian cancer cell surface CRT from both sources.

### **Chapter 4a. Examination of the conditions required for binding of exogenous calreticulin to ovarian cancer cells.**

#### **4a.1. Introduction.**

Recent studies at the messenger RNA level suggest that lack of CRT expression correlated with lower cytotoxic T cell infiltration into tumour sites in ovarian cancer patients, negatively impacting their survival (Stoll et al., 2016). This highlights the requirement for cancer cells to express surface CRT to maintain immune surveillance. It is possible that surface CRT levels could be enhanced by exogenous CRT. Extracellular CRT was first reported over a decade ago when it was detected in human plasma although its origins and function were unclear (Gardai et al., 2005, Sueyoshi et al., 1991). It has since been reported that exogenously added CRT can enhance tumour cell death in various systems e.g. by augmenting the antitumour effect of

photodynamic therapy in a mouse squamous cell carcinoma model (Korbelik et al., 2015) and cytotoxic T-lymphocyte lysis of various irradiated human carcinoma cells (Bernstein et al., 2014). However, there is no available data on whether exogenous CRT interacts with ovarian cancer cells either under resting conditions or in cells treated with cytotoxic therapies. Determination of this would allow an insight into whether exogenous CRT could be used therapeutically to enhance immune mediated death of ovarian cancer cells induced by these traditional therapies.

As previously discussed in the Introduction, doxorubicin is an anthracycline chemotherapy widely used to treat ovarian cancer. Doxorubicin is known to induce ER stress and early apoptosis initiate ICD in some cell types (Panaretakis et al., 2009). However, doxorubicin is relatively toxic and is known to cause DNA damage, oxidative stress and cell death (Thorn et al., 2011). If the immunogenicity of cancer cells treated with doxorubicin could be enhanced by binding of exogenous CRT this may increase the efficiency of lower doses of doxorubicin to induce ICD, reducing off target toxicity.

Thapsigargin can be used experimentally to induce ER stress by inhibiting SERCA1 which in turn decreases ER calcium levels. This form of ER-stress leads to changes in the activity of chaperones, including CRT and accumulation of unfolded proteins (Peters and Raghavan, 2011), resulting in CRT translocation to the cell surface. Both doxorubicin and thapsigargin were used here to induce ER stress in ovarian cancer cells. Additionally the impact of co-treatment with TUDCA, a chemical chaperone that inhibits ER stress, reducing the unfolded protein response (Ozcan et al., 2006) was studied.

Chapter 3 demonstrated the purification of monomeric CRT from *Pichia pastoris*. This CRT preparation was used here to examine the binding of exogenous CRT to OVcar3 SKOV3, A2780 and FaDu cancer cells in both untreated conditions and conditions of ER stress and cell death induced by doxorubicin and thapsigargin. The impact of preventing ER stress with TUDCA was also examined to further understand the mechanisms that influence extracellular CRT binding.



## **4a.2. Aim**

The aims of this chapter were to determine whether extracellular CRT binds directly to ovarian cancer cells, potentially identifying these cells for immune-mediated eradication.

The specific objectives were:

1. To examine whether extracellular CRT was able to bind to ovarian cancer cells under normal and stress conditions induced by doxorubicin and thapsigargin.
2. To examine whether exogenous CRT preferentially bound to ovarian cancer cells in certain stages of cell death
3. To examine whether TUDCA was able to inhibit doxorubicin and/or thapsigargin induced extracellular CRT binding to ovarian cancer cells.

## **4a.3. Methods**

The ability of fluorescently labelled extracellular CRT, human serum albumin (Positive control) (Nakamura et al., 2001), and IgG (negative control) to bind cancer cells under resting and drug-treatment conditions was analysed in a panel of ovarian cancer cell lines (SKov3/OVcar3/A2780) and a1 pharyngeal cancer cell line for comparison (FaDu). Cells were treated with different concentrations of the above proteins and analysed by flow cytometry and immunofluorescence microscopy. FITC and HSA were conjugated to fluorescein isothiocyanate (FITC) for detection. Commercially purchased IgG–FITC from human serum was used as a negative control.

### **4a.3.1. Conjugation of CRT or HSA with FITC.**

CRT and HSA were conjugated to FITC according to the manufacturer's instructions. Briefly, a 54  $\mu$ M solution of CRT or HSA in 200  $\mu$ l of conjugation buffer (0.1 M sodium carbonate buffer - pH 9.0) was incubated with 50  $\mu$ l of 0.5 mg/ml (128  $\mu$ M) FITC solution in conjugation buffer for 2 hours at room temperature in the dark. The resulting FITC-protein was separated from free FITC and buffer exchanged into PBS (pH 7.4) through a 5 ml capacity desalting G-25 Sephadex column attached to an AKTA FPLC

purifier (GE Healthcare). Elution of the FITC-conjugated protein was followed by measuring absorbance at 280nm (<https://www.thermofisher.com/uk/en/home/life-science/protein-biology/protein-assays-analysis/immunoprecipitation/magnets-immunoprecipitation-co-ip-pull-down.html>) and 495nm (FITC). 0.2 ml fractions were collected and fractions containing the conjugated protein (approx. 2 – 6) were collected and pooled. Protein concentration was determined by Nano-drop spectroscopy and adjusted to 0.5 mg /ml.

The FITC/protein ratio was calculated using the following equation:

$$\text{Molar F/P} = \frac{\text{MW}}{389} \times \frac{A_{495}/195}{A_{280} - \{(0.35 \times A_{495})\}} = \frac{A_{495} \times C}{A_{280} - (0.35 \times A_{495})}$$

$$\text{Where } C = \frac{\text{MW} \times E^{0.1\%}_{280}}{389 \times 195}$$

C is a constant value given for a particular protein

MW is the molecular weight of the protein HSA = 66500

MW is the molecular weight of the protein CRT= 46000

389 is the molecular weight of FITC

195 is the absorption  $E^{0.1\%}$  of bound FITC at 490 nm at pH 13.0

$(0.35 \times A_{495})$  is the correction factor due to the absorbance of FITC at 280 nm

$E^{0.1\%}$  is the absorption at 280 nm of a protein HSA at 1.0 mg/ml.

$E^{0.1\%}$  is the absorption at 280 nm of a protein CRT at 1.0 mg/ml.

The prepared FITC-CRT had a F/P ratio of 2.1

The prepared FITC-HSA had a F/P ratio of 3.16

#### **4a.3.2. Culture of cancer cells**

OVcar3, SKov3, A2780 cells and FaDu cells (all adherent cell lines) were cultured as described in Chapter 2. Binding of FITC labelled proteins was assessed by flow cytometry or immunocytochemistry as described.

#### **4a.3.3. Exogenous CRT binding to ovarian cancer cells assessed by flow cytometry.**

Cells were trypsinised, resuspended in 1ml growth media and counted in a haemocytometer.  $4 \times 10^6$  cells/ml were resuspended in 500 $\mu$ l of Tris buffered saline with 5mM CaCl<sub>2</sub>. Different concentrations from 1-8 $\mu$ g/ml of FITC labelled protein were added to different tubes i.e. CRT-FITC, HSA-FITC and IgG –FITC. All treatments were incubated for 30 minutes in the dark at room temperature and analysed by flow cytometry to determine binding of FITC proteins to the cell surface (Figure 4a.1).

#### **4a.3.4. Staining for cell morphology**

100  $\mu$ l of  $4 \times 10^6$  cell suspension was prepared on a slide using a cytospin. The slides were then fixed with 4% (w/v) paraformaldehyde for 10 minutes followed by a Diffquik stain i.e. the slide was fixed in methanol for 10 seconds, stained with eosin G for 10 seconds, followed by staining with methylene blue dye for 10 seconds. The slides were washed and then imaged via light microscopy.

#### **4a.3.5. immunofluorescent cell staining**

The FITC labelled cell population was also examined by fluorescence microscopy. Cells were prepared as above using a cytospin and fixed with fixed with 4% (w/v) paraformaldehyde for 10 minutes. Cells were mounted in gold anti-fade reagent containing the nuclear stain DAPI and imaged using a LEICA DM4000 fluorescent microscope (figure 4a.2).

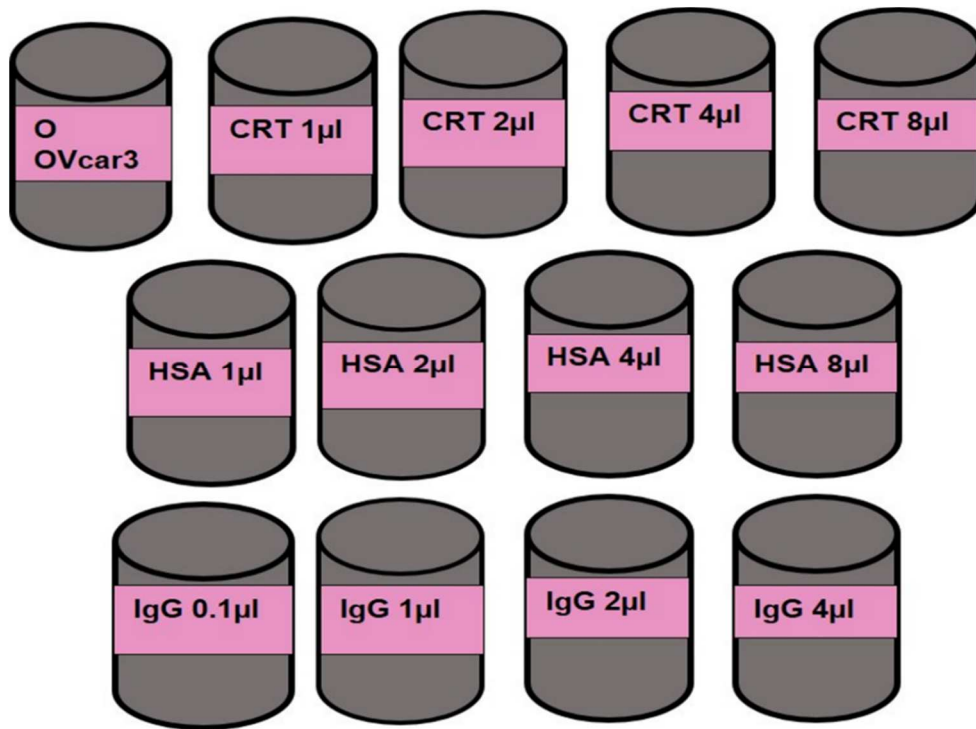


**Figure 4a.1. An example of the experimental set up of the CRT binding (in this case to OVcar3 cells).** Ovarian cancer cells were resuspended in 1 ml media and counted in a haemocytometer.  $4 \times 10^6$  cells were mixed with increasing concentrations (from 1-8µg/ml) of FITC labelled protein i.e. CRT-FITC, HSA-FITC and IgG-FITC. All treatments were incubated for 30 minutes in the dark at room temperature and analysed by flow cytometry to determine binding of FITC proteins to the cell surface.

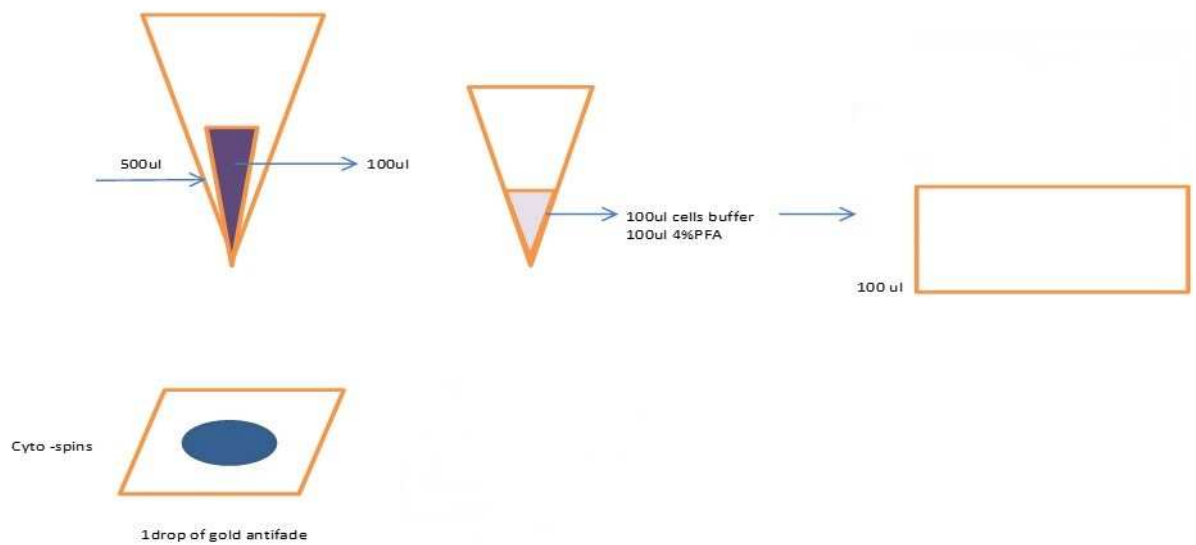


**Figure 4a.2. Workflow figure showing methodology followed for cells treated with labelled proteins and analysed by fluorescence microscopy.** 100  $\mu$ l of  $4 \times 10^6$  cell suspension mixed with either FITC-CRT, HSA-FITC or IgG-FITC was subsequently plated onto a microscope slide using a cytopspin centrifuge. Cell were fixed with 100  $\mu$ l 4% (w/v) paraformaldehyde, washed, mounted in gold anti-fade reagent containing the nuclear stain DAPI and imaged using a LEICA DM4000 fluorescent microscope.

#### 4a.3.6. Treatment of cancer cells

Doxorubicin was supplied as a lyophilized powder. Working concentrations and length of treatments varied depending on the desired effect. Briefly,  $1 \times 10^5$  cancer cells were seeded onto chamber slides (for microscopy) or into each well of a 6-well plate (for flow cytometry) and grown to 80% confluence in complete media. Cells were then treated with: 0.25, 6.3, 12.5 and 25  $\mu\text{M}$ ; 0.2, 0.5  $\mu\text{M}$  thapsigargin  $\pm$  2.5  $\mu\text{M}$  doxorubicin or 200, 400 $\mu\text{M}$  TUDCA  $\pm$  2.5 $\mu\text{M}$  doxorubicin or 0.2  $\mu\text{M}$  thapsigargin as indicated. After 16 h cells were stained for analysis using immunocytochemistry or flow cytometry as indicated. A typical experimental scheme is shown in Figure 4a.3.

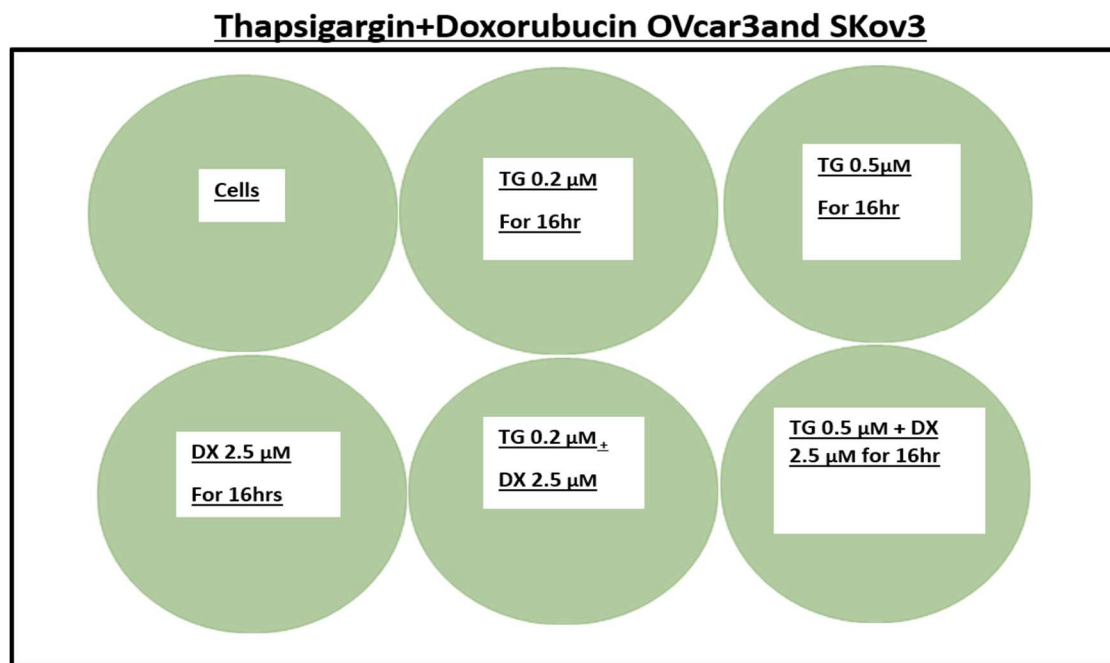


**Figure 4a.3. Experimental design of the studies examining CRT binding to cancer cells pre-treated with thapsigargin or doxorubicin (DX).** Cancer cells were plated into each well of a 6-well plate and treated with varying concentrations of thapsigargin (0.2, 0.5  $\mu\text{M}$ ) in the absence or presence of 2.5  $\mu\text{M}$  doxorubicin before being exposed to FITC-CRT for 30 minutes in the dark. The cells were then washed three times in PBS, trypsinised, placed in 1 ml annexin V binding buffer and co-stained with 5  $\mu\text{l}$  Alexa Fluor® 647 Annexin V to monitor apoptosis and 10  $\mu\text{l}$  propidium iodide-Yellow to assess necrosis. Finally, the volume was adjusted to 500  $\mu\text{l}$  with 1x binding buffer and analysed by flow cytometry immediately without fixation.

#### **4a.3.7. Assessment of surface bound CRT on cells undergoing apoptosis and necrosis.**

Cells were triple stained with FITC labelled protein and Alexa Fluor® 647 annexin V and PI to distinguish apoptotic and necrotic cells respectively.

1. After treatment as above cells were harvested by EDTA-trypsin, pelleted by centrifugation at 1500 rpm for 5 minutes and resuspended in 1 ml of PBS.
2. After counting by haemocytometer cells were double labelled with annexin V and PI. Specifically, 100- $\mu$ l of cell suspension (containing  $1 \times 10^5$  cells in total) was mixed with 5  $\mu$ l annexin V-FITC and 10  $\mu$ l PI.
3. The cells were incubated for 15 min in the dark at room temperature. 400- $\mu$ l 1x binding buffer was added and they were analysed by flow cytometry as described in the general methods section with FITC-conjugated protein F1 (green), ALEXA Fluorescent 647 annexin V (apoptosis) F2 (red), propidium iodide (necrosis) F3 (yellow).
4. The cells were initially gated using FSC-A and SSC-A to gate out any cell debris.
5. Cells were then gated on the dot plot by their PI and annexin V staining to give four populations: annexin V-ve/PI-ve (lower left quadrant) were considered as living cells, annexin V+ve/PI-ve (lower right quadrant) were early apoptotic cells, annexin V+ve/PI+ve (upper right quadrant) were late apoptotic cells, and annexin V-ve/PI+ve (upper left quadrant) were necrotic cells. FITC signal e.g. bound FTC-CRT was assessed on each of the four cell populations and could be expressed as mean fluorescence intensity (MFI). A high signal of the FITC fluorophore indicated high binding of CRT to cells (Figure 4a.4. Shows an example).

#### **4a.3.8. Immunocytochemistry**

Cells were plated onto coverslips and treated with doxorubicin, thapsigargin and TUDCA as indicated and then fixed with 4% (w/v) PFA in PBS for 30 minutes. Cells were then washed twice in PBS, and blocked in 2% (w/v) BSA for 20 minutes. Cells were exposed to FITC-CRT (2 $\mu$ g/ml) for 30 min at 37°C in the dark. Subsequently, cells were washed with PBS and liquid was removed from the coverslip by touching the corner on a paper towel. The slide was inverted on a drop of anti-fade Gold mounting media with the use of forceps. Cover slips were left for 20 min to dry and then sealed with clear nail polish and fluorescence digital images of cells were

captured either on a Leica DM4000 B LED fluorescent microscope or Leica DMi8 TCS SP8 Confocal microscope at x10, x20 and x40 magnification using LAS X digital software.

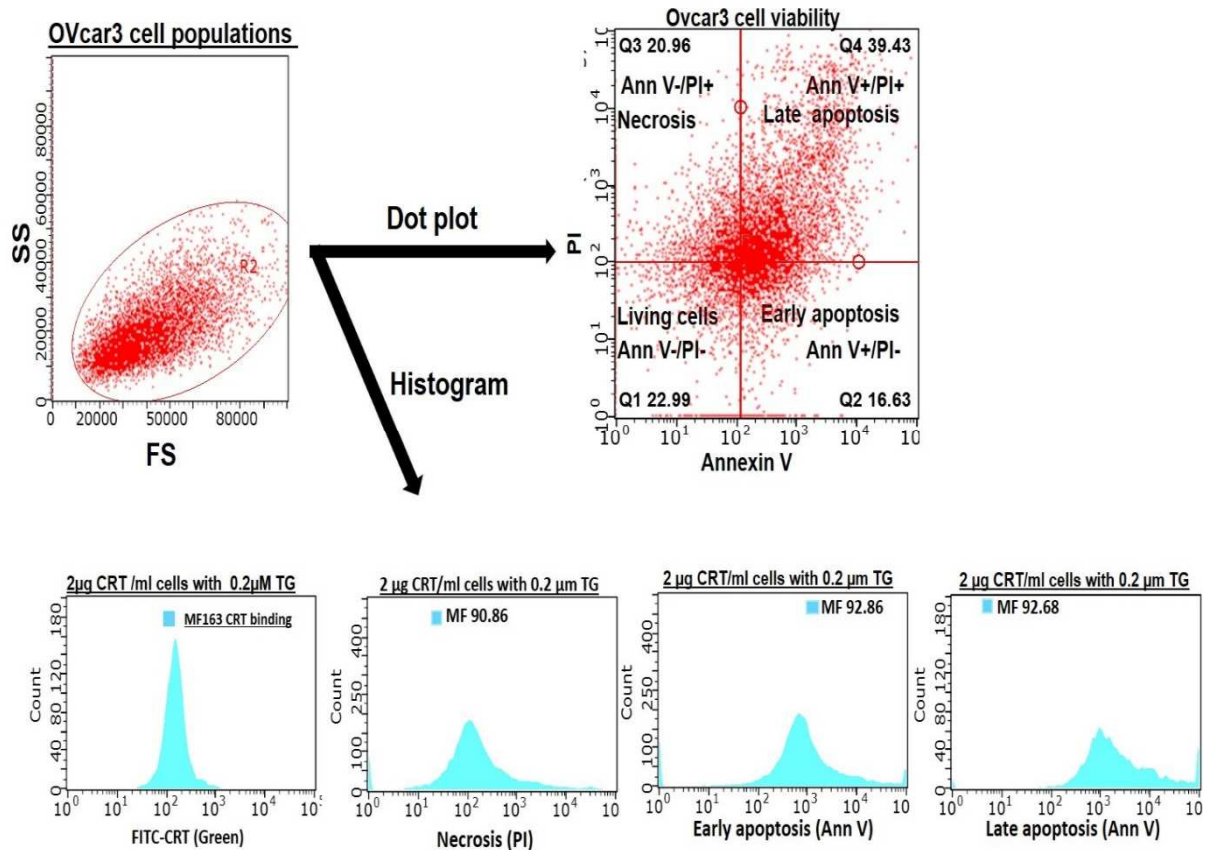


**Figure 4a.4. Gating of Ovar3 cancer cells treated with thapsigargin.** Ovar3 cells were triple stained with FITC-conjugated protein F1 (green), ALEXA Fluorescent 647 annexin V (apoptosis) F2 (red), propidium iodide (necrosis) F3 (yellow). The dot plots represent the gating out of cell debris using forward and side scatter and the percentage of the cell population detected as living cells, early apoptotic cells, late apoptotic cells, and necrotic cells. The histogram represents the mean fluorescence intensity of FITC-CRT binding to pre-apoptotic, apoptotic and necrotic Ovar3 cells gated into the 4 cell populations based on the dot plot (after treatment with the ER stressor thapsigargin).



#### **4a.3.9. Data analysis**

The data sets obtained from individual experiments were averaged and their mean values were statistically analysed using the non-parametric Mann Whitney test or one-way ANOVA (with post-hoc Tukeys' multiple comparison test) for three or more groups.

#### **4a.4. Results**

Identification of CRT and cell surface association of extracellular CRT is almost exclusively performed by fluorescent-based assays such as flow cytometry or immunofluorescence staining of cells (Goicoechea et al., 2000). Therefore, CRT and a positive control protein HSA were conjugated to FITC and purified and concentrated by FLPC employing a Hi-trap desalting column. The fractions containing the eluted FITC-conjugated protein were determined by monitoring at OD280nm and OD495nm and pooled for future use (Figure 4a.5).

##### **4a.4.1. Binding of CRT to cancer cells under non-stress conditions.**

In order to examine variations in the ability of exogenous CRT to bind to various human cancer cells, a number of epithelial cancer cell lines were obtained from the supervisory team. These were three ovarian cell lines (SKov3, OVcar3 and A2780) and a pharyngeal cancer cell line (FaDu), which was included for comparison. The morphological features of these cultured cells are shown in Figure 4a.6.

##### **4a.4.2. CRT-FITC binds to the surface of cancer cells as assessed by flow cytometry**

Initial studies were carried out to examine whether exogenous CRT could bind to the cell surface of otherwise untreated cancer cells. Cells were treated with different concentrations (1- $\mu$ g - 8 $\mu$ g/ml) of FITC-CRT, the positive control FITC-HSA and the negative control FITC-IgG and binding was studied by flow cytometry (Figure 4a.7)

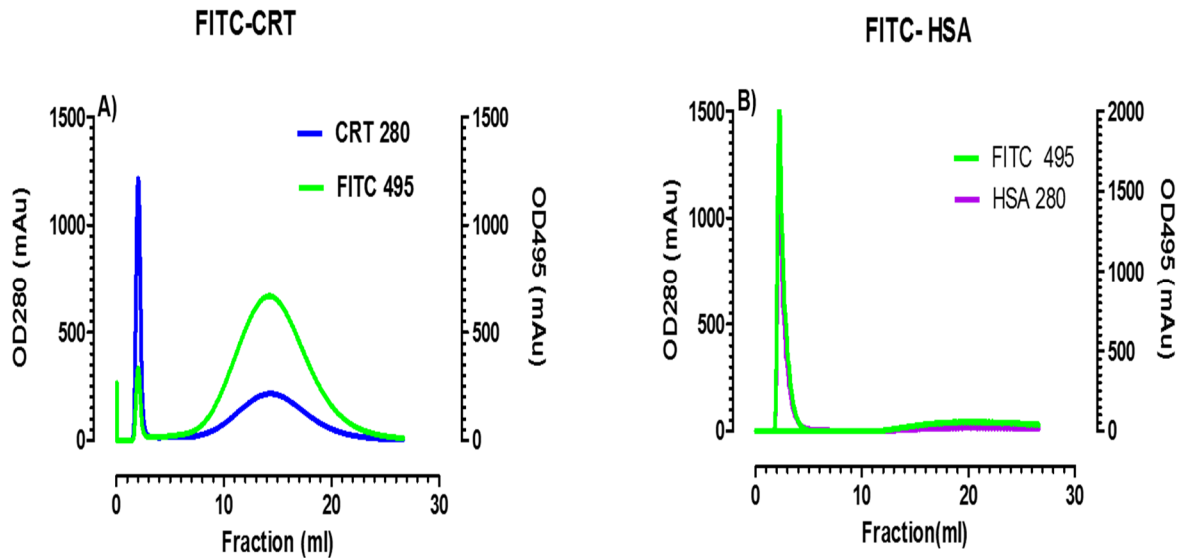


**Figure 4a.5. Sample FPLC traces showing FITC-conjugation to CRT and HSA.** (A) FITC bound to calreticulin. (B) FITC bound to albumin. CRT and human serum albumin (HSA) were conjugated to fluorescein isothiocyanate (FITC) and purified and concentrated using FLPC employing a Hi-trap desalting column. The eluted fractions were monitoring for FITC at OD495nm and protein at OD280nm. Note: the fractions containing the highest absorbance at 495 nm should overlap with a similar peak of fluorescence at 280 nm to indicate the successful labelling.

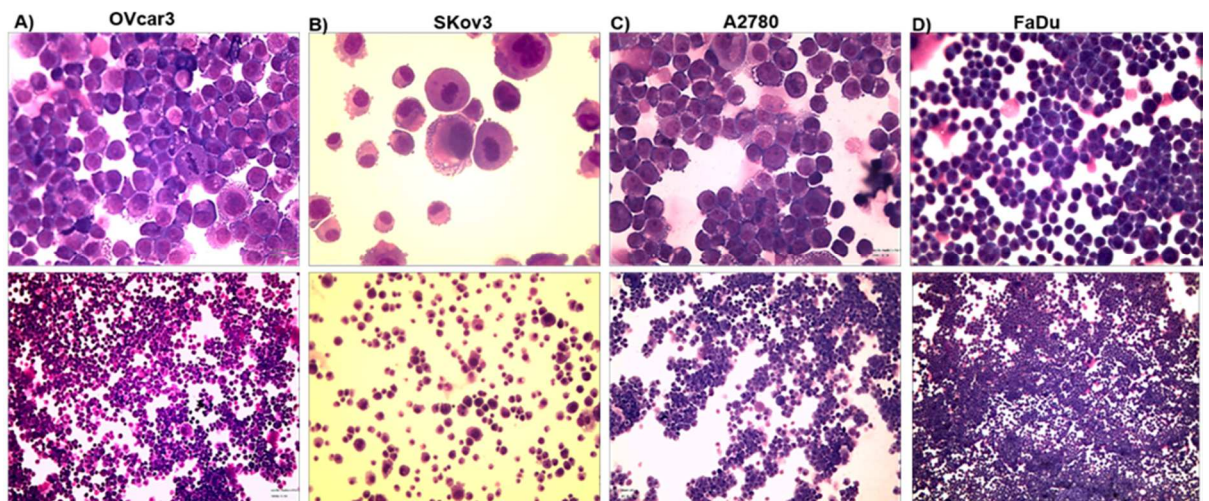


**Figure 4a.6. Morphological characteristics of the cancer cell lines studies.** Cultured cells were stained Diff-Quick and observed by light microscopy at 10x magnification (lower panels) and 40 x magnifications (upper panels). (A) OVcar3, (B) SKov3 (C) A2780 (D) FaDu.

Incubation of OVcar3 cells with all concentrations of FITC-CRT studied resulted in significant binding of exogenous CRT to the cells. For instance at 1µg/ml the MFI of bound FITC-CRT increased from controls levels of  $19.5 \pm 6.403$  to  $96.75 \pm 17.93$  (Figure 4a.8(b)). The level of binding was concentration dependent i.e. MFI of FITC-CRT treated cells was  $136.8 \pm 17.56$  at 2µg/ml treatment and  $162.5 \pm 5.745$  and  $233.5 \pm 52$  at 4 µg/ml and 8µg/ml respectively after 30-minutes exposure (Figure 4a.8). A similar binding pattern was observed for HSA which was included as a positive control. In contrast MFI of FITC-IgG (negative control) binding was significantly lower than both the CRT and HSA binding at all concentrations tested above 1 µg/ml (Figure 4a.8). These data indicate that exogenous CRT bound to the surface of OVcar3 ovarian cancer cells.

Similar data was found for all three ovarian cancer lines (Figure 4a.8) i.e. CRT-FITC bound to cells at all concentrations tested, but FITC-IgG binding was low. Interestingly, MFI of bound FITC-CRT was higher for SKov3 cells than all of the other cancer cell lines tested at all concentrations of CRT tested, suggesting that these cells bind more CRT. For instance, in cells treated with 1µg/ml FITC-CRT, there was a 4-fold increase in the MFI compared with control cells i.e. from  $25.75 \pm 5.058$  to  $201.3 \pm 93.82$  ( $p < 0.025$ ). A significant dose dependent increase of CRT binding was observed at higher CRT concentrations with an MFI of  $215.8 \pm 60.98$  2µg/ml,  $242.5 \pm 76.57$  at 4µg/ml and  $348 \pm 70.39$  at 8µg/ml ( $p < 0.05$  for all vs control).

Since OVcar3, A2780 and SKov3 cells all significantly bound exogenous CRT, FaDu pharyngeal tumour cells were also examined to determine whether this effect is limited to ovarian cancer cells. Again, incubation with increasing FITC-CRT resulted in a dramatic increase surface bound CRT at all concentrations tested. For instance, the two highest concentrations of FITC-CRT, 4 and 8µg/ml significantly enhanced CRT binding by 3.1- and 3.6-fold (to  $192.8 \pm 24.62$  MFI and  $245.3 \pm 41.31$  MFI) ( $***p < 0.001$ ) (Figure 4a.8 (d,e)) respectively in comparison to the control. Experiments were also performed to determine whether unconjugated FITC alone bound to cells to i.e. to ensure that the CRT-FITC was binding via CRT and not FITC. No background staining was observed (data not shown).

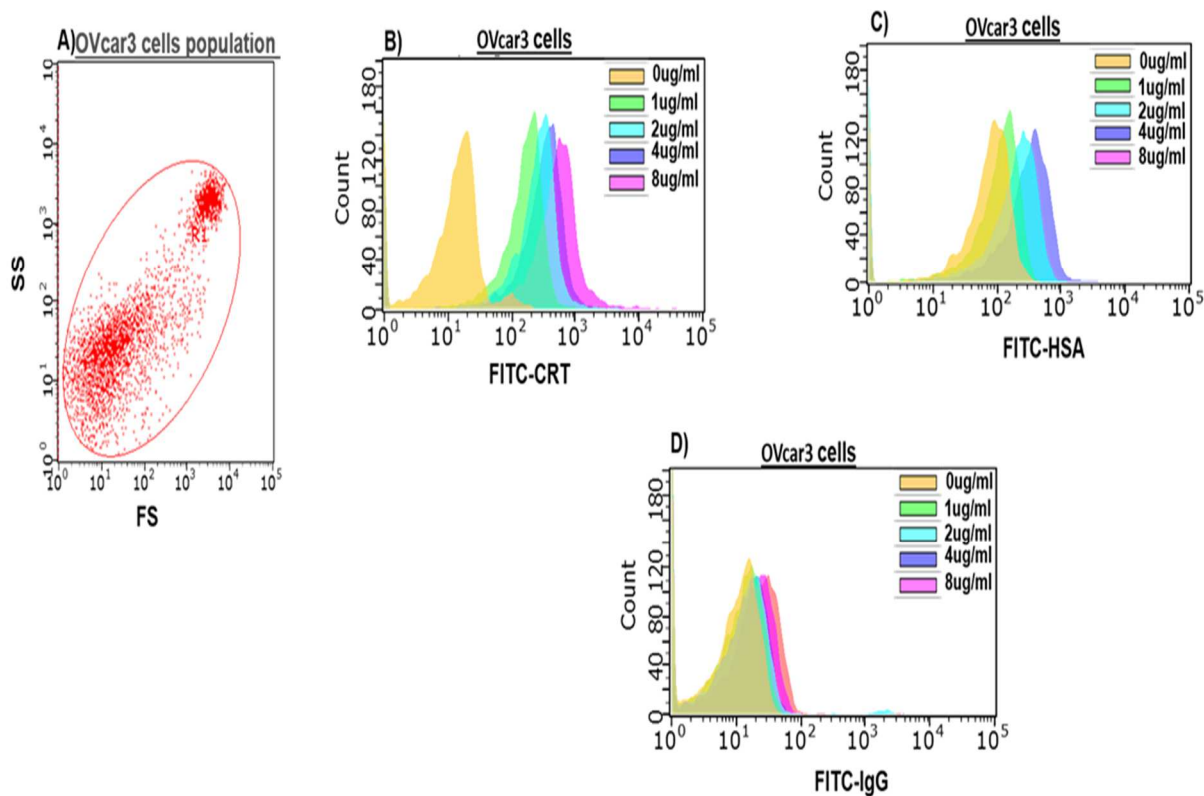


**Figure 4a.7. Demonstration of FITC-CRT, FITC-HSA and FITC-IgG binding to OVcar3 cancer cells by flow cytometry.** OVcar3 cells were treated with different concentrations (1- $\mu\text{g}$  - 8 $\mu\text{g}/\text{ml}$ ) of FITC protein or untreated (0, auto-fluorescence control) and analysed by flow cytometry (A) Typical dot plot of the cells showing their size (forward scatter-FSC) and granularity (side scatter-SS). (B) CRT (C) HSA (positive control) (D) IgG (negative control). Representative graphs from at least three independent experiments are shown.

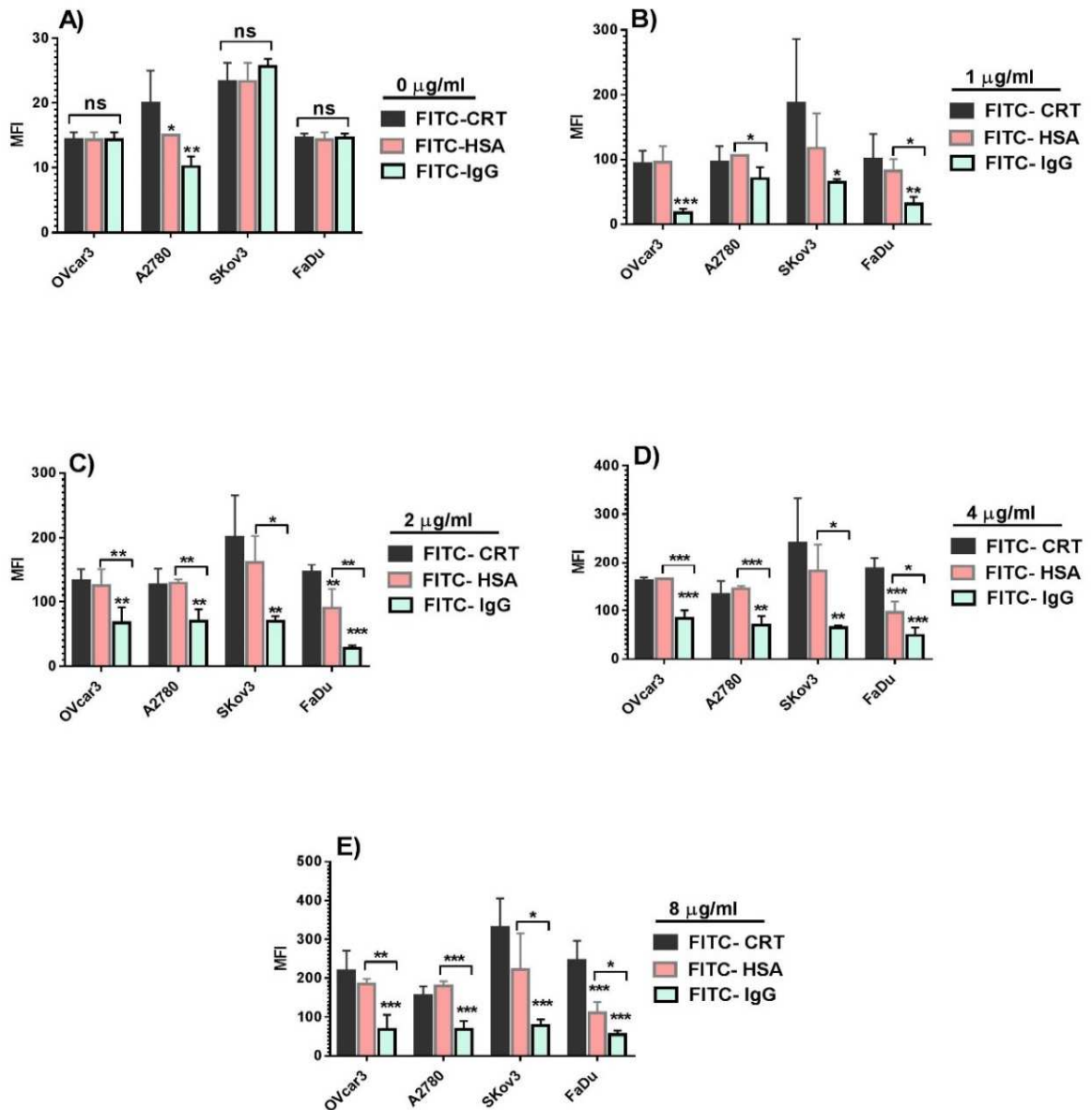


**Figure 4a.8. FITC-CRT binds to four cancer cell lines at all concentrations tested.**

Cancer cells were incubated with increasing concentrations (0-8  $\mu\text{g/ml}$ ) of FITC-CRT, FITC-HSA (positive control) or FITC-IgG (negative control) for 30 min at 37°C in the dark. After incubation the amount of FITC-conjugated protein bound to cells was assessed by flow cytometry. (A), (B), (C), (D) and (E) cells treated with 0 (buffer alone), 1, 2, 4, 8  $\mu\text{g/ml}$  FITC-CRT, HSA-FITC and IgG-FITC, respectively. Data are mean  $\pm$  SD) and analysed by one-way ANOVA and Tukey's multiple comparison test \*\*\*  $p < 0.001$ ,  $n = 6$ . Significance is between HSA and IgG where indicated and between CRT and IgG where not specified. Note the difference in the range of the y axis on (A) compared with B-E.

#### **4a.4.3. CRT-FITC binds to the surface of cancer cells as assessed by immunofluorescence microscopy.**

To further test the ability of extracellular CRT, IgG and HSA to bind to cancer cells under resting conditions, cells were also analysed by immunofluorescence microscopy. Both FITC-CRT and FITC-HSA bound to cancer cells, but there was negligible staining with FITC-IgG (Figure 4a.9). All of the data above confirm that exogenously added CRT binds to the surface of cancer cells under resting conditions i.e. standard cell culture.

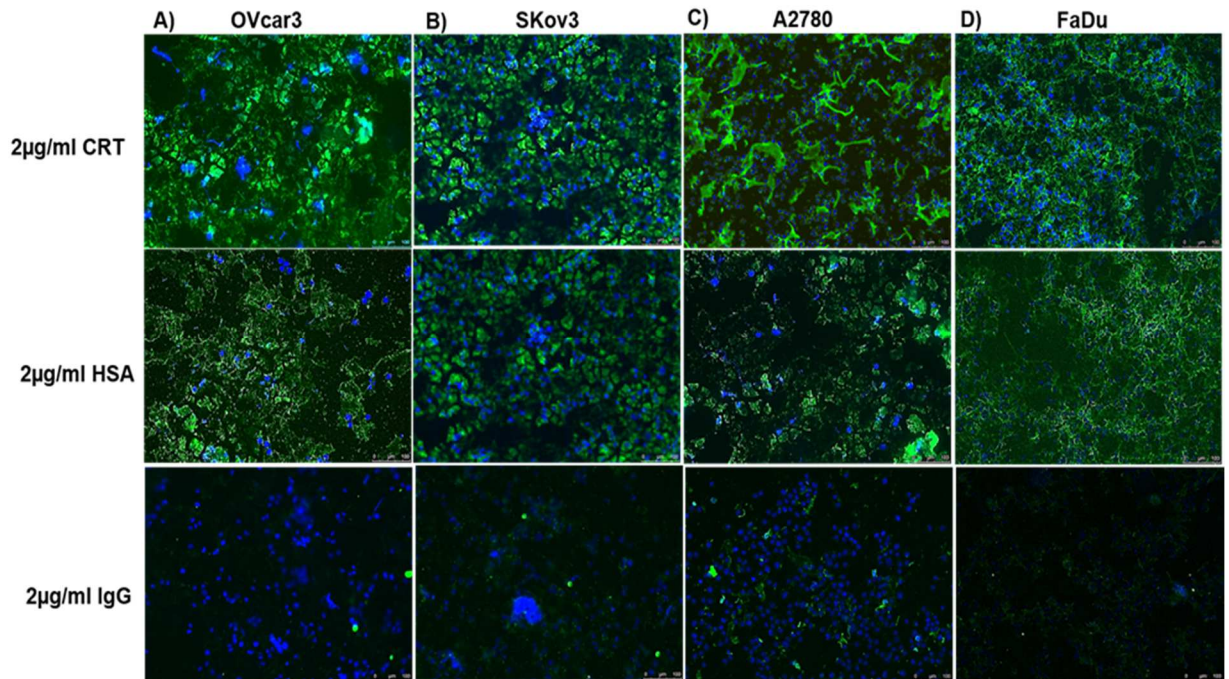
#### **4a.4.4. Binding of CRT to cancer cells under stress and ER stress conditions.**

A series of experiments were then carried out to examine whether extracellular binding of exogenous CRT could be enhanced in cells subjected to cellular stress. Initial studies were carried out to examine the effect of doxorubicin on cell viability. OVCar3, SKov3, A2780 and FaDu cells were treated with increasing concentrations of doxorubicin (2.5 $\mu$ M, 6.3 $\mu$ M, and 12.5 $\mu$ M, 25 $\mu$ M, based on values obtained from the literature) (Inoue et al., 2014). After incubation, cell viability was assessed by staining with annexin V and PI and flow cytometry analysis.

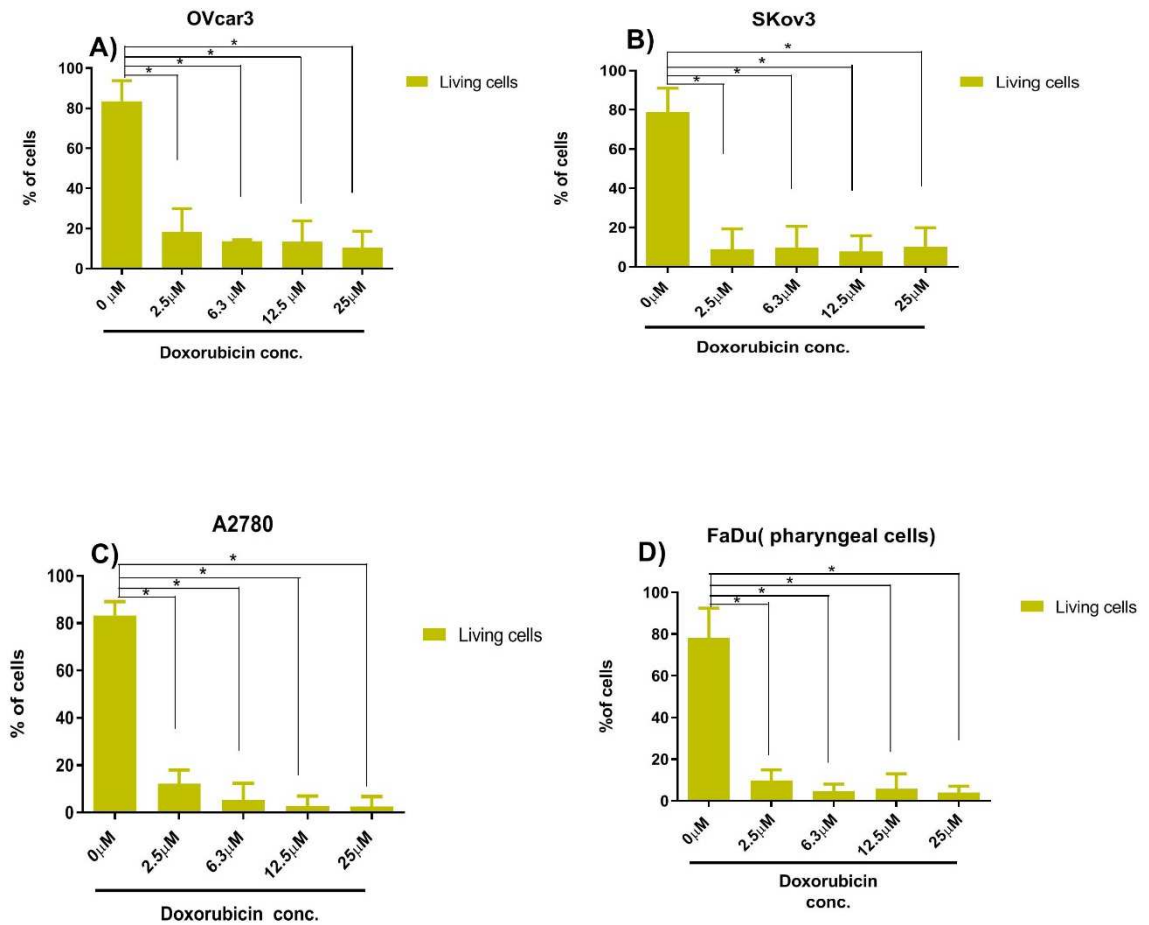
Doxorubicin significantly induced cell death in all four cancer cell types at all concentrations compared with vehicle only treated cells. For instance, in OVCar3 cells viability decreased from 85.41+ 9.17 % in control cells to 21.55  $\pm$  11.37%, 13.72  $\pm$  0.737%, 15.66  $\pm$  9.455% and 11.82  $\pm$  7.271% in cells treated with 2.5, 6.3, 12.5 and 25  $\mu$ M respectively (Figure 4a.10(a)).

Figure 4a.11. Shows a typical flow cytometry dot plot for doxorubicin treated OVCar3 showing analysis of living, early apoptotic, late apoptotic or necrotic cells based on annexin V or PI staining. Similar analyses were carried for SKOV3, A2780 and FaDu cells. Interestingly, although doxorubicin significantly reduced cell viability in all cell lines tested the proportion of cells in the different phases of cell death differed between the cell lines. For instance, in SKov3 early apoptotic cells formed the largest cell population at all concentrations of doxorubicin tested, whereas in OVCar3 cells late apoptotic cells formed the major cell population (Figure 4a.12. Table 4a.1). In A2780

and FaDu cells virtually no early apoptotic cells were observed. Most cells were either late apoptotic or necrotic in all cell types except SKov3.



**Figure 4a.9. FITC-CRT and FITC-HSA bind to the surface of cancer cells as assessed by fluorescence microscopy.** Cancer cells were incubated with FITC labelled proteins and the nuclear stain DAPI and fixed and imaged by fluorescence microscopy. Images show FITC-CRT binding (upper panel), FITC-HSA (positive control, middle panel) and FITC-IgG (negative control, lower panel). (A) OVcar3, (B) SKov3, (C) A2780 and (D) FaDu cells. Green labelling represents CRT, HSA or IgG individually binding to cancer cells; blue labelling represents DAPI stain of cell nuclei. 10x magnification images shown. Representative images of experiments carried out at least 3 times with similar results are shown.



**Figure 4a.10. Dose response effect of doxorubicin on cancer cell survival.** Various cancer cells were treated with doxorubicin and the percentage of living cells (annexin V<sup>-ve</sup>/PI<sup>-ve</sup>) were assessed. (A) OVcar3 cells (B) SKov3 cells, (C) A2780 cells, (D) FaDu. Data show the mean + SD. Experiments were repeated three times. Mann-Whitney analysis, \*p= 0.0286 vs control. All concentrations of doxorubicin used significantly decreased cell viability in all cell types.



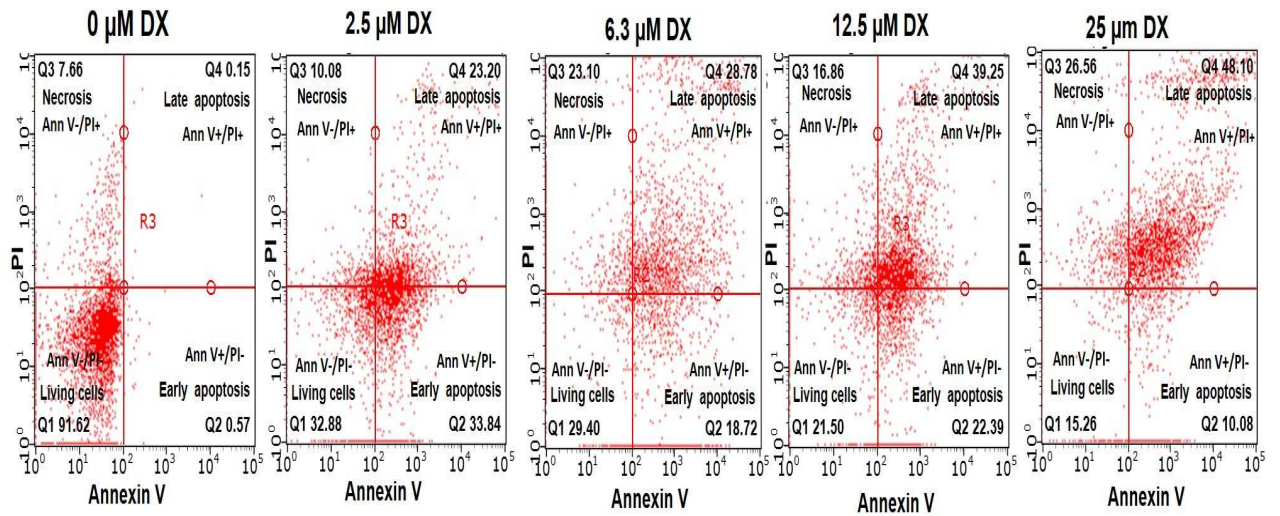


**Figure 4a.11. Doxorubicin treatment of OVcar3 ovarian cancer cells induces cell apoptosis (early and late) and necrosis as quantified by flow cytometry using Annexin V and PI.** OVcar3 cells were treated with increasing concentrations (0, 2.5, 6.3, 12.5, 25 μM) of doxorubicin (DX) and then harvested by trypsinisation. To discriminate between early and late apoptosis and necrosis, the cells were simultaneously stained with annexin V and PI and analysed by flow cytometry using guava 3.1.1 software. At least 5000 cells were counted in each sample. Experiments were performed and interpreted as follows: cells that were annexin (Ann) V<sup>-ve</sup>/PI<sup>-ve</sup> (lower left quadrant) were considered as living cells, AnnV<sup>+ve</sup>/PI<sup>-ve</sup> cells (lower right quadrant) as early apoptotic cells, AnnV<sup>+ve</sup>/PI<sup>+ve</sup> (upper right quadrant) cells as late apoptotic cells, and AnnV<sup>-ve</sup>/PI<sup>+ve</sup> (upper left quadrant) as necrotic cells. A representative analysis is shown.

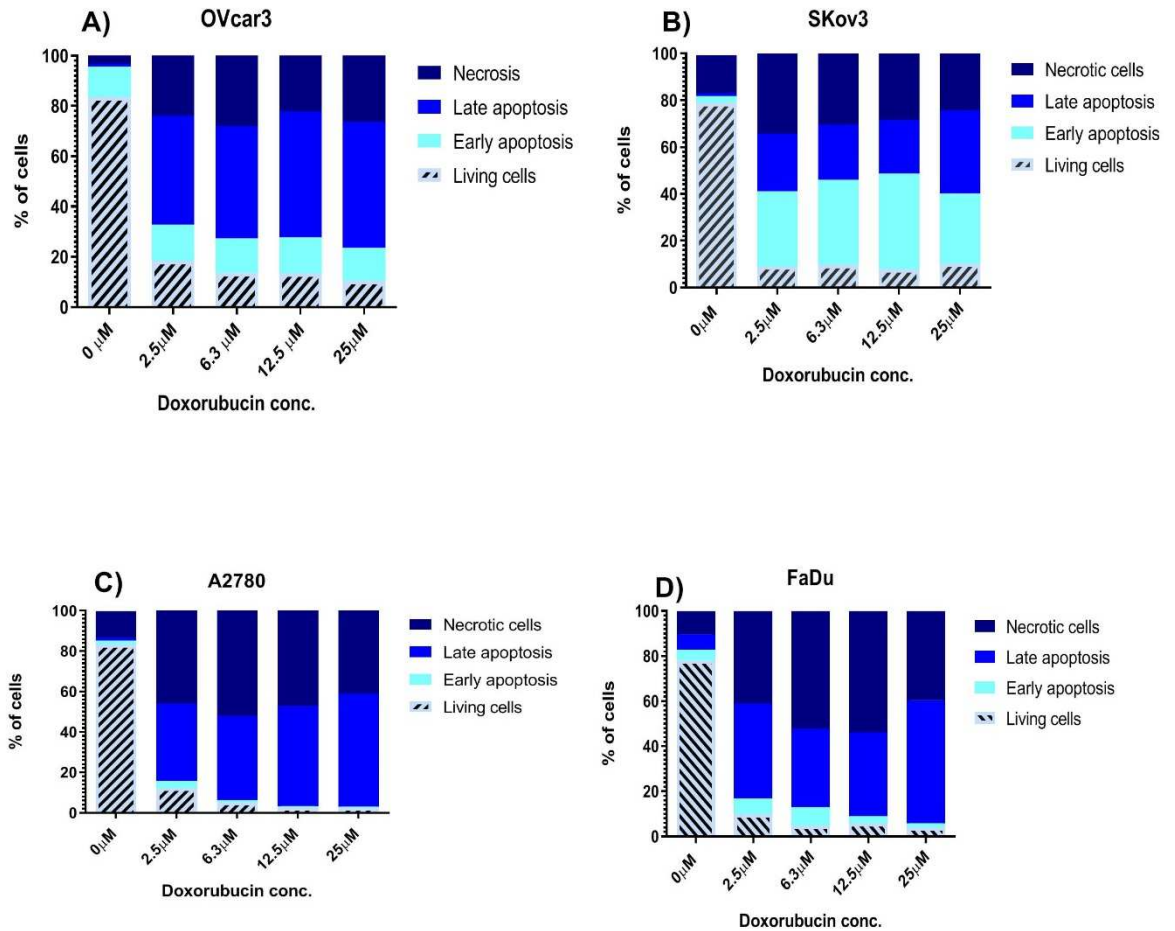


**Figure 4a.12. The percentage of living and dying cancer cells pre and post doxorubicin treatment.** Cells were treated with increasing concentrations of doxorubicin as indicated. To discriminate between early and late apoptosis and necrosis, the cells were simultaneously stained with annexin V and PI and analysed by flow cytometry. (A) OVcar3 cells (B) SKov3 cells, (C) A2780 cells, (D) FaDu cells. Data show the mean from three experiments. Mann-Whitney analysis, \* $p= 0.0265$  vs control.

OVcar3 %	Control	Early apoptosis	Late apoptosis	Necrosis
2.5 $\mu$ M	21.55 $\pm$ 11.37	16.07 $\pm$ 8.913	47.26 $\pm$ 21.16	30.63 $\pm$ 23.72
6.3 $\mu$ M	13.72 $\pm$ 0.737	15.34 $\pm$ 9.613	49.19 $\pm$ 22.91 *	33.25 $\pm$ 18.67
12.5 $\mu$ M	15.66 $\pm$ 9.455	16.44 $\pm$ 11.06	61.89 $\pm$ 42.13	29.02 $\pm$ 25.1
25 $\mu$ M	11.82 $\pm$ 7.271	15.06 $\pm$ 9.991	57.98 $\pm$ 32.19	31.89 $\pm$ 20.21

SKov3 %	Control	Early apoptosis	Late apoptosis	Necrosis
2.5 $\mu$ M	9.065 $\pm$ 10.34	32.16 $\pm$ 24.59	24.59 $\pm$ 8.632	34.19 $\pm$ 25.66
6.3 $\mu$ M	9.758 $\pm$ 10.85	36.32 $\pm$ 26.35	23.56 $\pm$ 10.06	30.36 $\pm$ 29.09
12.5 $\mu$ M	7.795 $\pm$ 8.106	40.97 $\pm$ 29.78	22.97 $\pm$ 15.46	28.27 $\pm$ 26.55
25 $\mu$ M	10.3 $\pm$ 9.672	29.92 $\pm$ 29.27	35.58 $\pm$ 27.79	24.2 $\pm$ 24.16

A2780 %	Control	Early apoptosis	Late apoptosis	Necrosis
2.5 $\mu$ M	13.13 $\pm$ 5.116	4.185 $\pm$ 1.778 *	43.76 $\pm$ 19.3 *	49.43 $\pm$ 14.86 *
6.3 $\mu$ M	7.17 $\pm$ 6.985	1.303 $\pm$ 1.345 *	48.77 $\pm$ 24.63 *	56.01 $\pm$ 18.32 *
12.5 $\mu$ M	3.78 $\pm$ 4.101	0.7675 $\pm$ 0.8526	56.74 $\pm$ 24.95 *	51.46 $\pm$ 20.76 *
25 $\mu$ M	3.663 $\pm$ 4.049	0.6875 $\pm$ 0.7192	63.49 $\pm$ 26.33 *	44.91 $\pm$ 21.15 *

FaDu %	Control	Early apoptosis	Late apoptosis	Necrosis
2.5 $\mu$ M	10.6 $\pm$ 4.481	8.723 $\pm$ 6.104	44.91 $\pm$ 9.971 *	43.52 $\pm$ 15.68 *
6.3 $\mu$ M	5.31 $\pm$ 2.896	11.43 $\pm$ 11.05	35.38 $\pm$ 2.359 *	54.13 $\pm$ 9.562 *
12.5 $\mu$ M	7.84 $\pm$ 7.185	2.538 $\pm$ 2.979	40.18 $\pm$ 10.2 *	57.2 $\pm$ 18.21 *
25 $\mu$ M	4.738 $\pm$ 2.943	1.698 $\pm$ 1.191	54.11 $\pm$ 1.32 *	40.21 $\pm$ 3.191 *

**Table 4a.1. Dose-dependent effects of doxorubicin in tumour cells.** Cells were treated for 16 hours with doxorubicin. To discriminate between early and late apoptosis and necrosis, the cells were simultaneously stained with annexin V and PI and analysed by flow cytometry. Pooled data from 3 different experiments, were statistically analysed using the Mann Whitney test ( $n \geq 12$ , mean  $\pm$  S.D,  $*p \leq 0.0143$ , vs control).

Experiments were then carried out to examine whether CRT bound to the surface of these dying cells. Initially, A2780 tumour cells were treated with 2.5 and 25  $\mu\text{M}$  doxorubicin. It was evident that increasing doses of doxorubicin increased the binding of exogenous FITC-CRT to apoptotic and necrotic cells (Figure 4a.13.). Based on this result all four cancer cell lines were treated with increasing concentrations of doxorubicin (0, 2.5, 6.3, 12.5 and 25  $\mu\text{M}$ ) followed by exposure to FITC-CRT. The MFI of FITC-CRT binding to apoptotic and necrotic cells (gated by co-staining with annexin V and PI) was analysed by flow cytometry.

From (Figure 4a.14. and Table 4a.2), it can be seen that CRT binding (assessed by MFI) was lowest in the living cell population for all four cancer cell types. Interestingly, this was observed in the remaining living cells even in doxorubicin treated populations, suggesting that the presence of doxorubicin alone is not sufficient to enhance CRT binding i.e. cell death is required. Highly enhanced CRT binding was observed in cells at all stages of cell death examined i.e. early apoptosis, late apoptosis and necrosis in all cell types. However, these increases did not consistently seem to be dependent on the dose of doxorubicin used in early or late apoptotic cells suggesting that even the lowest concentration i.e. 2.5  $\mu\text{M}$  was enough to induce maximum CRT binding in these stages of cell death. For instance MFI of CRT binding to early apoptotic SKov3 cells was  $731 \pm 870$ ,  $424 \pm 98$ ,  $846 \pm 995$  and  $857 \pm 1254$  for cells treated with 2.5, 6.3, 12.5 and 25  $\mu\text{M}$  doxorubicin respectively. MFI of CRT binding to late apoptotic SKov3 cells was  $793 \pm 858$ ,  $1422 \pm 1731$ ,  $920 \pm 956$  and  $1044 \pm 1152$  following treatment with 2.5, 6.3, 12.5 and 25  $\mu\text{M}$  doxorubicin respectively (Table 4a.2), MFI of CRT binding to necrotic cells did show a dose dependent effect in all cells except A2780. It can also be observed that in SKov3 and FaDu cells CRT binding was greatest in necrotic cells, whereas in A2780 CRT binding was greatest in late apoptotic cells.

These effects were investigated further on OVcar3 cells treated in the same way and examined for cell morphology and FITC-CRT binding by microscopy. The images shown in Figure 4a.15 support the flow cytometry data that doxorubicin treatment enhances CRT binding to ovarian cancer cells.

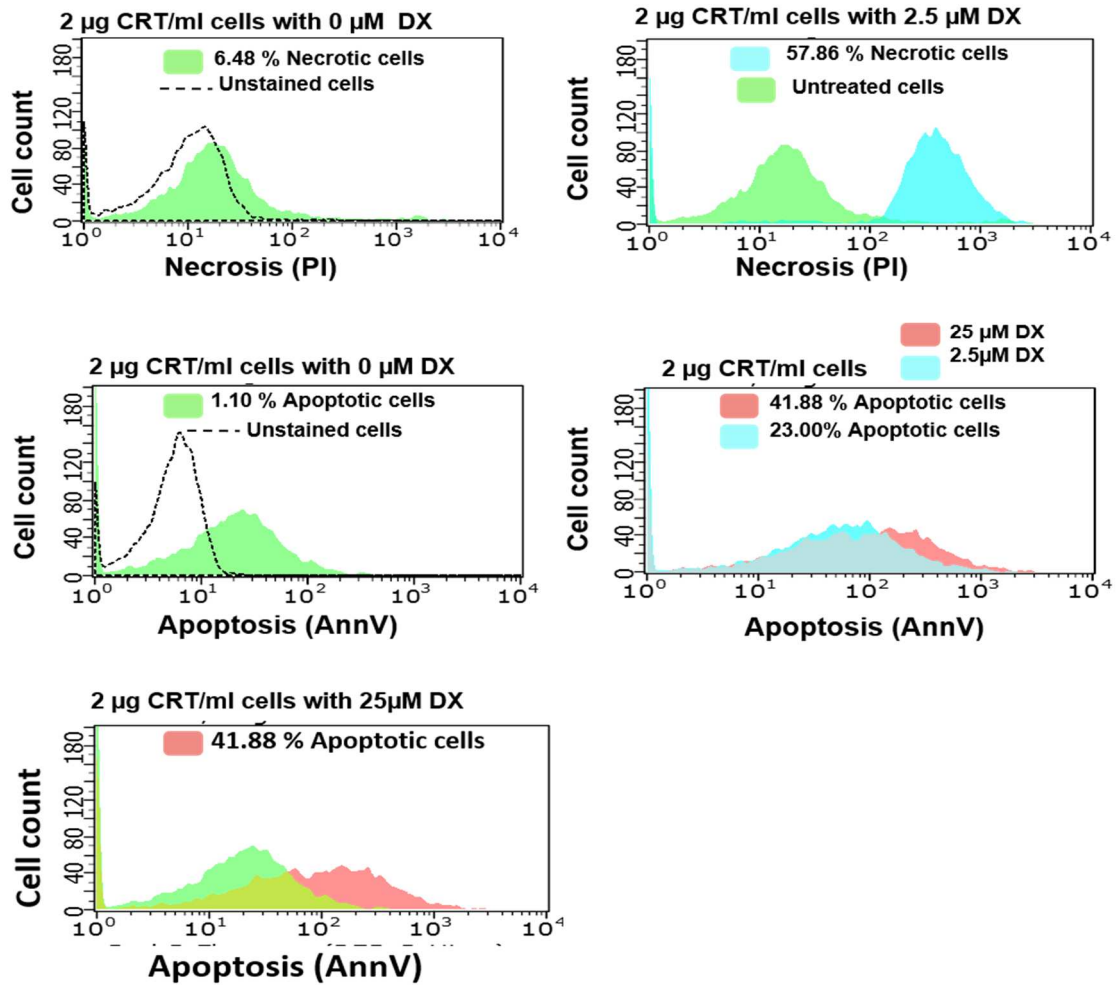


**Figure 4a.13. Degree of FITC-CRT binding to A2780 ovarian cancer cells before and after treatment with doxorubicin.** A2780 cells were initially treated with 0, 2.5 or 25 µM doxorubicin (DX) and then incubated with FITC-CRT at 2µg/ml. The MFI of FITC-CRT on apoptotic and necrotic gated cells (determined by co-staining with Alexa Fluor® 647 annexin V and PI) was assessed by flow cytometry. CRT fluorescence intensity (at the indicated stages of cell death) is plotted on the x axis. CRT-FITC fluorescence is increased on necrotic and apoptotic cells indicating enhanced binding.

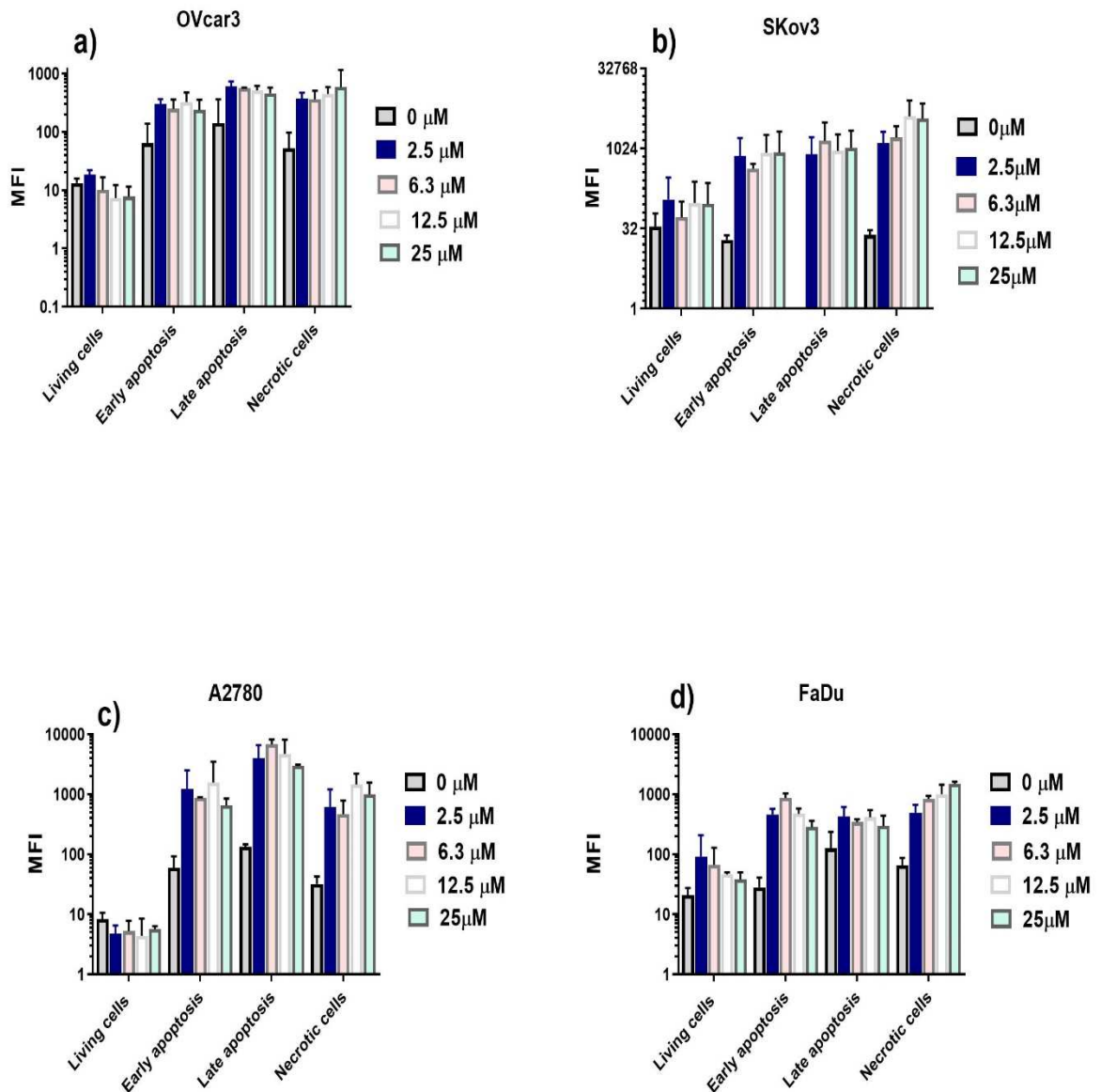


**Figure 4a.14. Mean fluorescence intensity (MFI) of FITC-CRT binding to living and dying cells pre and post treatment with doxorubicin.** Cancer cells were treated with increasing concentrations of doxorubicin (0, 2.5, 6.3, 12.5 and 25  $\mu\text{M}$ ) and then with FITC-CRT at  $2\mu\text{g/ml}$ . The MFI of FITC-CRT on early and late apoptotic and necrotic cells (gated by co-staining with annexin V and PI) was analysed by flow cytometry. (A) OVcar3 cells (B) SKov3 cells, (C) A2780 cells, (D) FaDu cells. Data show the mean + SD from 4 experiments.

OVcar3 MFI	0µM	2.5 µM	6.3 µM	12.5 µM	25 µM
Living cells	13.89 ± 2.627	19.41 ± 3.384	10.1 ± 6.587	8.538 ± 4.592	8.365 ± 3.189 *
Early apoptosis	50.48 ± 66.27	298.8 ± 53.44 *	246.4 ± 89.58 *	344.8 ± 125.8 *	253.8 ± 100.2
Late apoptosis	179.8 ± 197	626.9 ± 114.9 *	561.2 ± 8.624 *	535.1 ± 92.64 *	494.8 ± 114.5
Necrosis	56.5 ± 38.2	400.7 ± 106.3*	419.7 ± 171.9 *	508.5 ± 173.4 *	691.2 ± 510.1 *

SKov3 MFI	0µM	2.5 µM	6.3 µM	12.5 µM	25 µM
Living cells	35.03 ± 26.39	111.4 ± 178.7	51.56 ± 50.66	51.56 ± 50.66	96.91 ± 145.4
Early apoptosis	19.63 ± 4.3	731.1 ± 870.9 *	424.8 ± 98.41 *	846 ± 995.1 *	857.3 ± 1254 *
Late apoptosis	0 ± 0	793 ± 858.6 *	1422 ± 1731 *	920.8 ± 956 *	1044 ± 1153
Necrosis	24.22 ± 5.41	1286 ± 798.4*	1644 ± 1032*	4078 ± 4073 *	3695 ± 3427 *

A2780 MFI	0µM	2.5 µM	6.3 µM	12.5 µM	25 µM
Living cells	8.64 ± 1.897	5.06 ± 1.586 *	5.745 ± 2.298	5.28 ± 3.804 *	5.8 ± 0.6505 *
Early apoptosis	49.5 ± 32.91 *	1411 ± 1116 *	877 ± 27.11 *	1927 ± 1722 *	662.8 ± 162.2 *
Late apoptosis	132.1 ± 11	3726 ± 2208 *	7092 ± 1284 *	5530 ± 3213 *	2975 ± 136.4
Necrosis	29.18 ± 10.16	754.6 ± 571.2 *	523.3 ± 286.2 *	1342 ± 649.4 *	1070 ± 494.8 *

FaDu MFI	0µM	2.5 µM	6.3 µM	12.5 µM	25 µM
Living cells	21.71 ± 6.063	124.7 ± 116.3	84.12 ± 60.83	46.91 ± 3.259 *	38.81 ± 10.05*
Early apoptosis	30.8 ± 11.9	443.2 ± 97.87 *	903.2 ± 151.8 *	501.5 ± 103.4 *	305.4 ± 77.27 *
Late apoptosis	143.5 ± 95.89	403.3 ± 160.7 *	353.6 ± 34.85 *	448.1 ± 131.2 *	326 ± 131.5
Necrosis	59.37 ± 21.1	538.9 ± 174.4*	858.3 ± 92.7*	1102 ± 407.9 *	1525 ± 111.8 *

**Table 4a.2. Mean fluorescent intensity (MFI) of FITC-CRT binding to OVcar3, SKov3, A2870 and FaDu tumour cells pre- and post- doxorubicin treatment.** Cancer cells were treated with increasing concentrations of doxorubicin (0, 2.5, 6.3, 12.5 and 25 µM) and then incubated with FITC-CRT at 2µg/ml. The MFI of FITC-CRT binding to early and late apoptotic and necrotic cells (gated by co-staining with annexin V and PI) was analysed by flow cytometry. Pooled data from 4 different experiments were statistically analysed using the Mann Whitney test (n≥12, mean ± S.D, \*p≤0.0143, vs control 0µM).

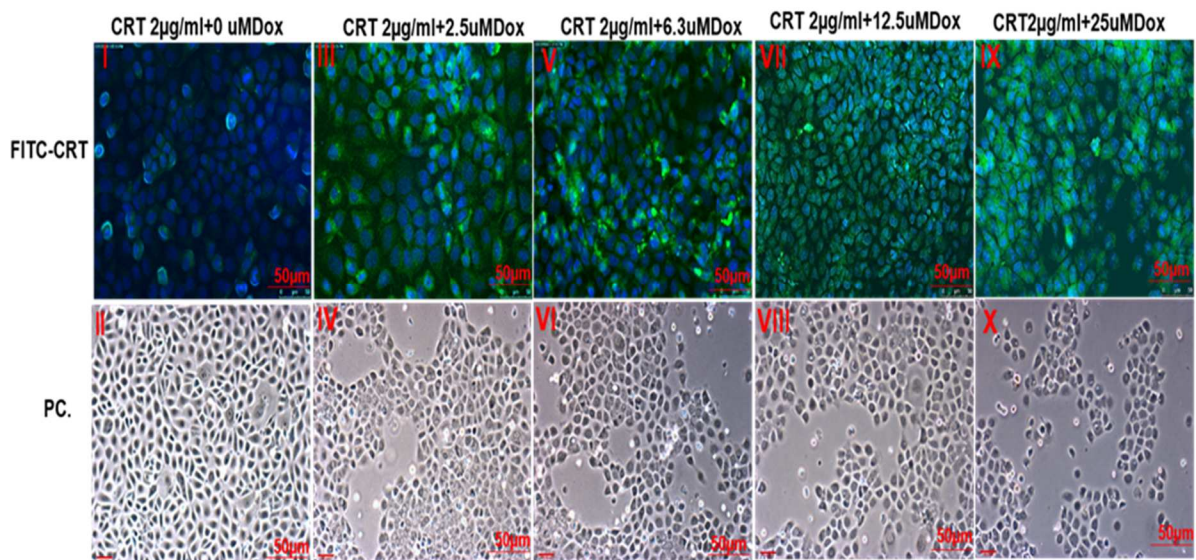


**Figure 4a.15. Doxorubicin treatment of OVcar3 ovarian cancer cells enhances CRT binding.** Upper row - cells were treated with different concentrations of doxorubicin (0, 2.5, 6.3, 12.5 and 25 $\mu$ M; I, III, V, VII, IX respectively), fixed, stained with FITC-CRT (green, 2 $\mu$ g/ml) and DAPI (blue, nuclear stain) and observed under fluorescence microscopy. Lower row - cells treated as for upper row and imaged with phase contrast microscopy (PC), (0, 2.5, 6.3, 12.5 and 25 $\mu$ M doxorubicin = I, III, V, VII, IX respectively) Scale bar = 50  $\mu$ m. Representative images from three similar data sets are shown.



#### **4a.4.5. Treatment of both OVcar3 and SKov3 cells with thapsigargin and doxorubicin treatment alone, and combined, increases CRT binding to dying cells.**

It is evident from the previous experiments that inducing cancer cell stress with doxorubicin enhances their exogenous CRT binding. It was hypothesised that subjecting cells to additional stress induced by an ER stressor might enhance CRT binding further, which could be therapeutically beneficial i.e. further enhance CRT-mediated ICD. Additionally, examining the impact of another ER stressor could provide mechanistic data on the effects of doxorubicin.

OVcar3 and SKov3 cells were treated with doxorubicin alone (0, 2.5, 6.3, 12.5, 25  $\mu$ M) or thapsigargin (0.2, 0.5 $\mu$ M) alone, or in combination with 2.5 $\mu$ M doxorubicin, and cell death was monitored by annexin V and PI staining and CRT binding was monitored by FITC-CRT binding. The highest concentration of 0.5  $\mu$ M thapsigargin was chosen based on previous studies where this concentration was employed (Mlynarczyk and Fahraeus, 2014). Both doses of thapsigargin used (0.2, 0.5  $\mu$ M) significantly reduced cell viability in both OVcar3 and SKov3 to similar levels observed with doxorubicin alone (Figure 4a.16.). Combined treatment with thapsigargin and doxorubicin did not induce further cell death. Interestingly, both treatments induced a high proportion of late apoptotic cells in OVcar3 cells whereas in SKov3 necrotic cells were the largest cell population (Figure 4a.17 (a, b)).

Exogenous FITC-CRT binding to cancer cells was increased under stress conditions induced by doxorubicin and thapsigargin, similar to the previous data on doxorubicin (Figure 4a.17(c, d)). The amount of CRT on the external surface of all apoptotic (early and late) and necrotic cells was statistically significantly greater in treated cells compared with living cells (AnnV-ve/PI-ve) treated under the same conditions. For instance, (Figure 4a.17(d)) MFI of CRT binding to SKov3 cells treated with 0.5  $\mu$ M thapsigargin was  $17.41 \pm 2.314$  for living cells but increased to  $317.8 \pm 28.6$ ,  $701.1 \pm 58.6$  and  $309 \pm 203.2$  in cells undergoing early apoptosis, late apoptosis and necrosis respectively ( $p < 0.05$  for all,  $n=3$ ). Cells treated with thapsigargin and doxorubicin alone showed increased cell surface CRT on early apoptotic (annexin V+ve / PI-ve), late apoptotic (annexin V+ve / PI+ve), and necrotic cells (annexin V-ve / PI+ve).

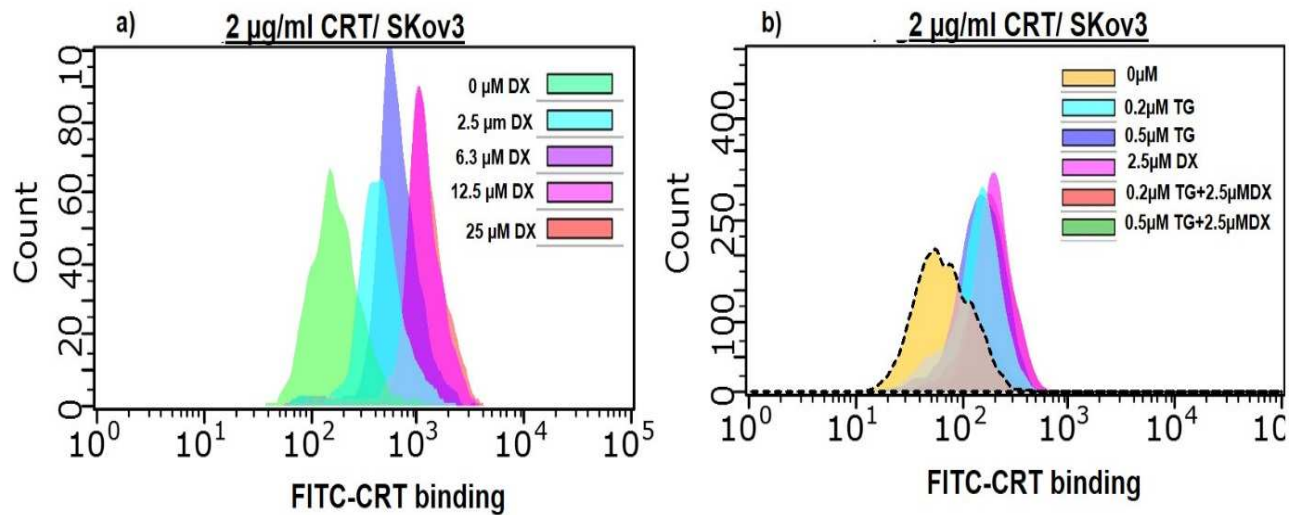


**Figure 4a.16. Representative flow cytometry histograms showing that exogenous FITC-CRT binding to SKov3 ovarian cancer cells is increased under stress conditions using the ER-stressors doxorubicin and thapsigargin.** SKov3 cells were treated with 0, 2.5, 6.3, 12.5, 25  $\mu\text{M}$  doxorubicin or 0.2 or 0.5  $\mu\text{M}$  thapsigargin  $\pm$  2.5  $\mu\text{M}$  doxorubicin and then incubated with FITC-CRT at 2  $\mu\text{g/ml}$ . The fluorescence intensity of FITC-CRT binding was analysed by flow cytometry. (a) Flow cytometry histogram of fluorescence of FITC-CRT binding after treatment with doxorubicin. (B) Flow cytometry histogram of fluorescence of FITC-CRT binding after treatment with doxorubicin and thapsigargin. Representative histograms of one of at least three independent experiments are shown.

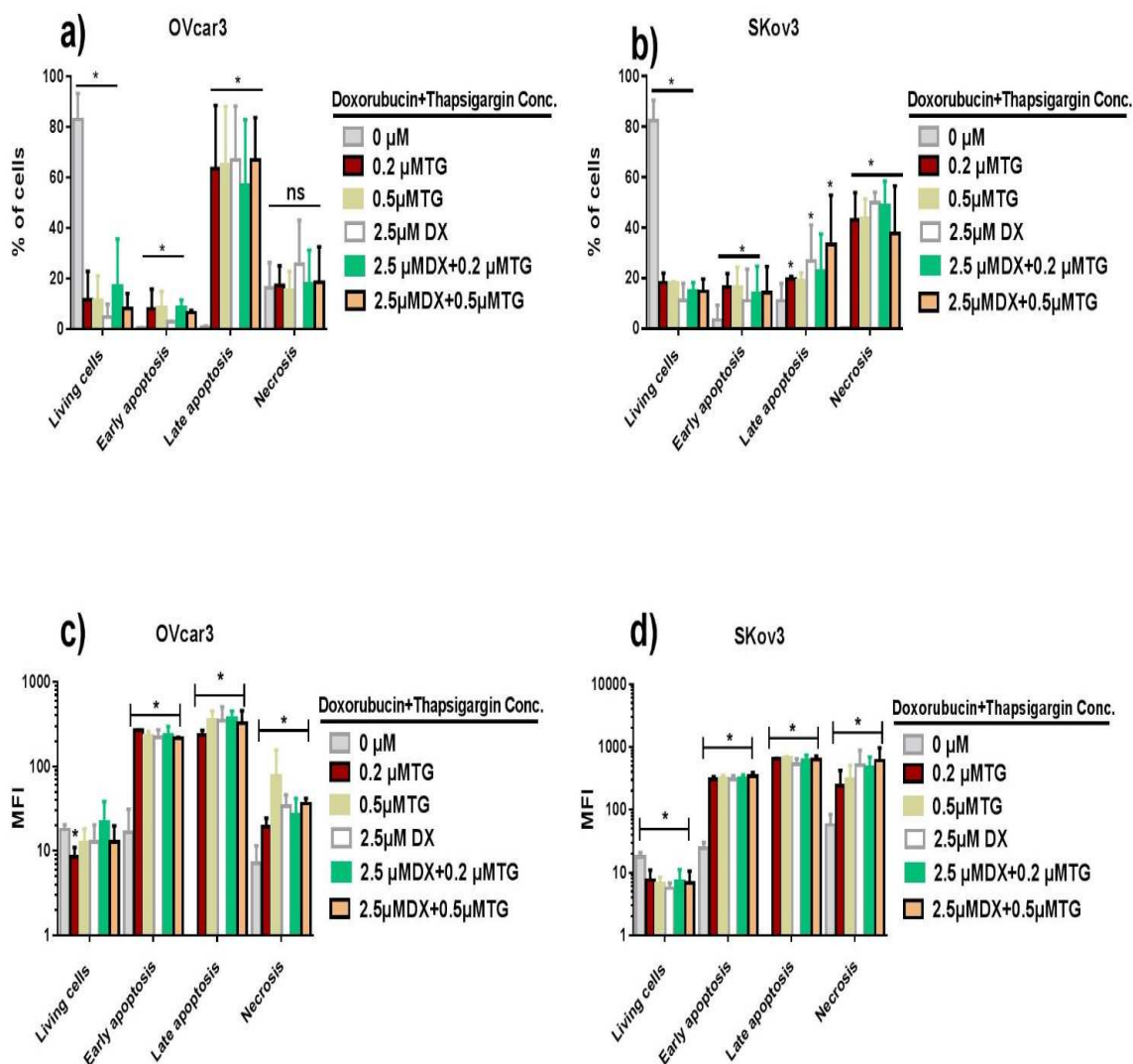


**Figure 4a.17. Doxorubicin and thapsigargin can induce cell death in ovarian cancer cells and exogenous CRT preferentially binds to cancer cells undergoing apoptosis after treatment with thapsigargin and doxorubicin.** Cancer cells were treated with 0.2 and 0.5  $\mu\text{M}$  thapsigargin  $\pm$  2.5  $\mu\text{M}$  doxorubicin (DX) and then with FITC-CRT at 2 $\mu\text{g}/\text{ml}$ . The early and late apoptotic and necrotic cells (gated by co-staining with annexin V and PI) were analysed by flow cytometry. (a, b) The percentage of OVcar3 and SKov3 cells in each phase of cell death; (c, d) Mean fluorescence intensity (MFI) of FITC-CRT binding to OVcar3, SKov3 cancer cells pre and post-doxorubicin treatment. Data show the mean + SD. \* $p < 0.5$ . Experiments were repeated three times.

Combined treatment of cancer cells with thapsigargin and doxorubicin did not lead to the greater surface binding of CRT on apoptotic (early and late) or necrotic cells in either OVcar3 or SKov3. Indeed no significant difference in FITC-CRT binding was observed between thapsigargin alone and thapsigargin at the same dose plus doxorubicin for any stage of cell death in either cell type.

#### **4a.4.6. Inhibition of ER stress reduced binding of exogenous CRT in doxorubicin and thapsigargin treated cells.**

To clarify whether the ER stress-inducing properties of doxorubicin and thapsigargin were related to their induction of cell death and enhanced exogenous CRT binding, the effect of tauroursodeoxycholic acid (TUDCA) on doxorubicin and thapsigargin treated cells was examined. TUDCA is known to reduce ER stress, prevent the dysfunction caused by UFP response, and stabilise mitochondria (Vang et al., 2014).

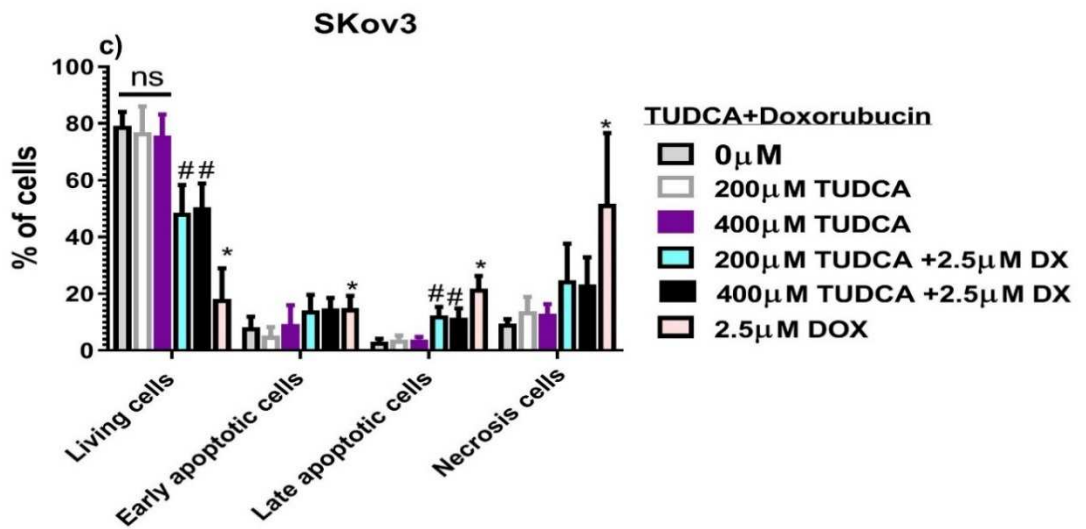
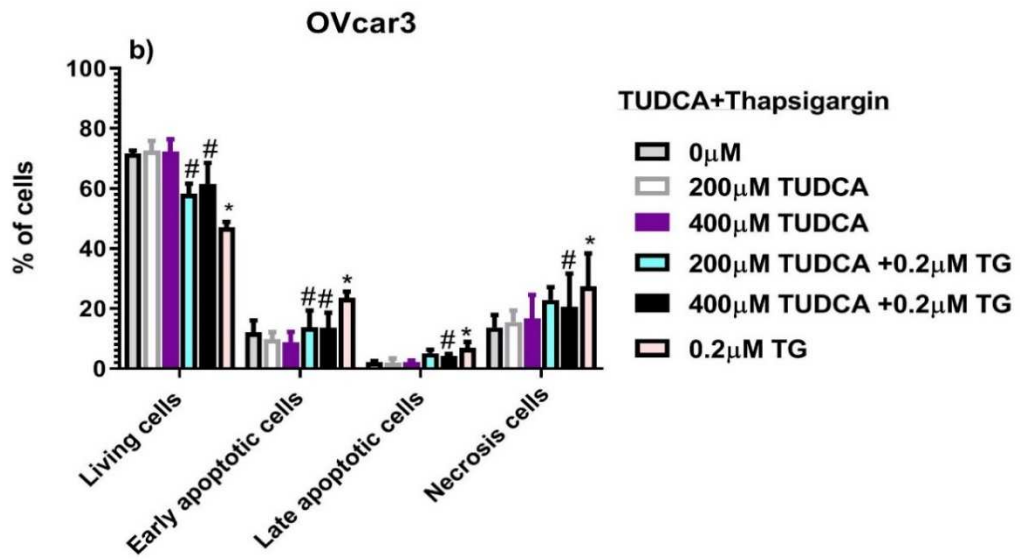
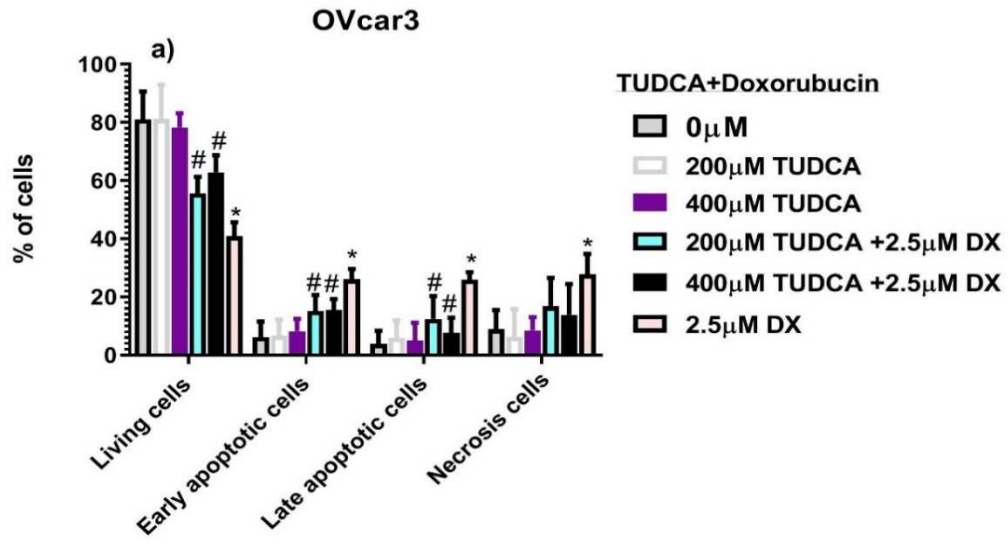
SKov3 and OVcar3 cells were pre-treated with 200  $\mu$ M or 400  $\mu$ M TUDCA. Cells were then incubated in the absence or presence of doxorubicin or thapsigargin to examine the impact of TUDCA on cell death by these two agents (as assessed by annexin V and PI staining) induced (Figure 4a.18.). TUDCA alone did not reduce cell viability at either concentration used in either cell type. However, toxicity of both ER stressors, as assessed by percentage of live cells, was partially, but significantly reduced by pre-treatment with TUDCA. In SKov3 cells there did not appear to be any dose effect of the concentration of TUDCA used, whereas in OVcar3 cells 400  $\mu$ M was slightly more effective, although this difference did not reach significance.

Further analysis of PI and annexin V status indicated that TUDCA reduced doxorubicin-mediated apoptosis and necrosis in both OVcar3 (Figure 4a.18), and SKOV3 cells. This did not always reach significance, but was highly significant in both cells types for doxorubicin induction of late apoptosis. TUDCA significantly reduced thapsigargin-mediated induction of CRT in early and late apoptotic and necrotic cells in OVcar3, but interestingly this reduction failed to reach significance in SKov3 cells. These data indicate that thapsigargin is able to partially protect against cell death induced by ER stressors.

Examination of the effect of TUDCA on doxorubicin and thapsigargin mediated binding of exogenous CRT showed a similar trend (Figures 4a.19 and 4a.20). Figure 4a.20 shows the effect of TUDCA pre-treatment on the MFI of FITC-CRT binding to OVcar3 and SKov3 undergoing different stages of cell death induced by doxorubicin or thapsigargin. TUDCA significantly inhibited exogenous CRT binding facilitated by ER stressors. Doxorubicin and thapsigargin -mediated late apoptotic and necrotic OVcar3 and SKov3 cells had significantly reduced cell surface CRT in the presence of TUDCA. These findings indicated that treatment with TUDCA attenuated exogenous CRT binding to dying cells under ER-stress conditions. For instance, MFI of late apoptotic OVcar3 cells treated with 2.5  $\mu$ M doxorubicin + 400  $\mu$ M TUDCA was  $481.9 \pm 25.94$  compared with  $697.9 \pm 72$  in doxorubicin treatment alone ( $n=3$ ;  $p<0.05$ , Figure 4a.20 (a)) and MFI of exogenous CRT in necrotic cells was  $185.5 \pm 8.6$  vs  $1383 \pm 39.21$  with the same treatments.

Similarly, in SKov3 cells treated with TUDCA (200  $\mu$ M) and thapsigargin (0.5  $\mu$ M) the data revealed that there was a significant reduction in MFI of exogenous FITC-CRT on necrotic cells from  $269.6 \pm 50.01$  with thapsigargin alone compared with  $103.5 \pm 10.12$  in cells treated with both, (Figure 4a.20. (d)). These flow cytometry data were supported by direct immunofluorescence visualisation of FITC-CRT bound to treated cells (figure 4a.21).

These combined data suggest that ER stress on ovarian cancer cells is associated with induction of apoptotic and necrotic cell death and enhanced binding of exogenous CRT which can be partially reversed by agents which protect against ER stress.



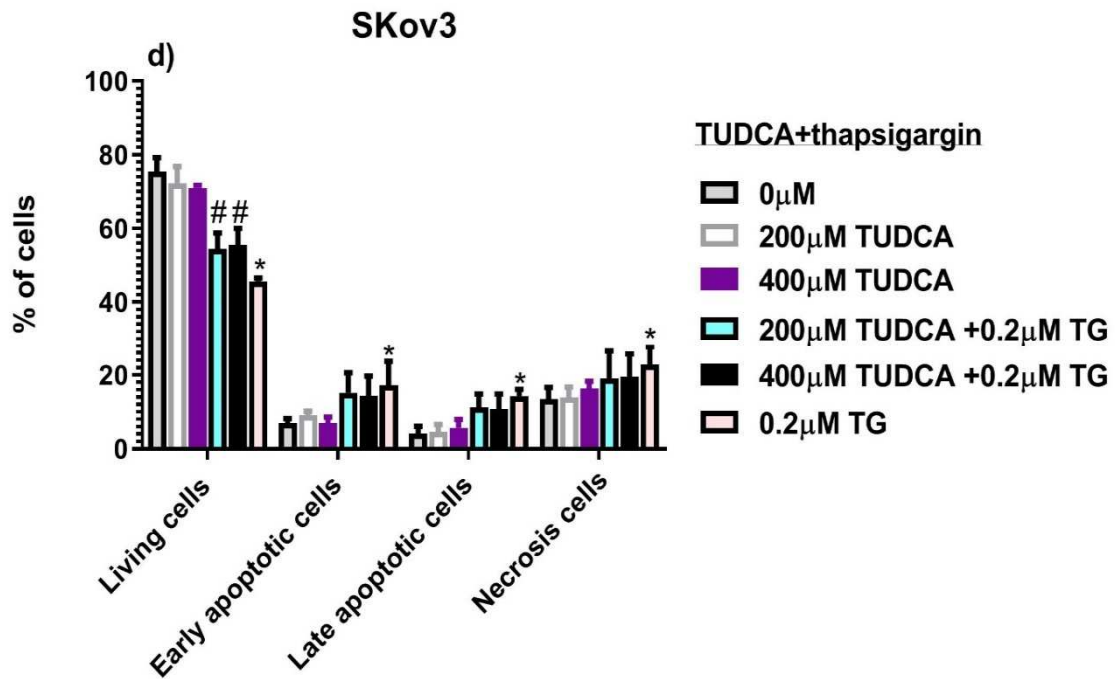


**Figure 4a.18. TUDCA does not induce cell death, and protects against doxorubicin and thapsigargin induced toxicity, in ovarian cancer cells.** SKov3 and OVcar3 cancer cells were treated with TUDCA (200  $\mu$ M or 400  $\mu$ M), doxorubicin (DX, 2.5  $\mu$ M) or thapsigargin (TG, 0.2  $\mu$ M) or in combination as indicated, and stained with annexin V and PI to assess apoptosis and necrosis by flow cytometry. Data show % of cells in different stages of cell death. (a) OVcar3 treated with TUDCA  $\pm$  DX or DX alone, (b) OVcar3 treated with TUDCA  $\pm$  TG or TG alone, (c), SKov3 treated with TUDCA  $\pm$  DX or DX alone, (d) SKOV3 treated with TUDCA  $\pm$  TG or TG alone. Data show the mean + SD. Experiments were repeated three times. \* =0  $\mu$ M vs. 2.5  $\mu$ M DX, 200  $\mu$ M TUDCA and 400  $\mu$ M TUDCA (a & c), \* =0  $\mu$ M vs. 0.2  $\mu$ M TG, 200  $\mu$ M TUDCA and 400  $\mu$ M TUDCA (b & d). # = 2.5  $\mu$ M DX vs. 2.5  $\mu$ M DX + 200, 400  $\mu$ M TUDCA (a & c), # = 0.2 TG  $\mu$ M vs. 0.2 TG  $\mu$ M +200, 400  $\mu$ M TUDCA (b & d).  $p = <0.0143$  for all.

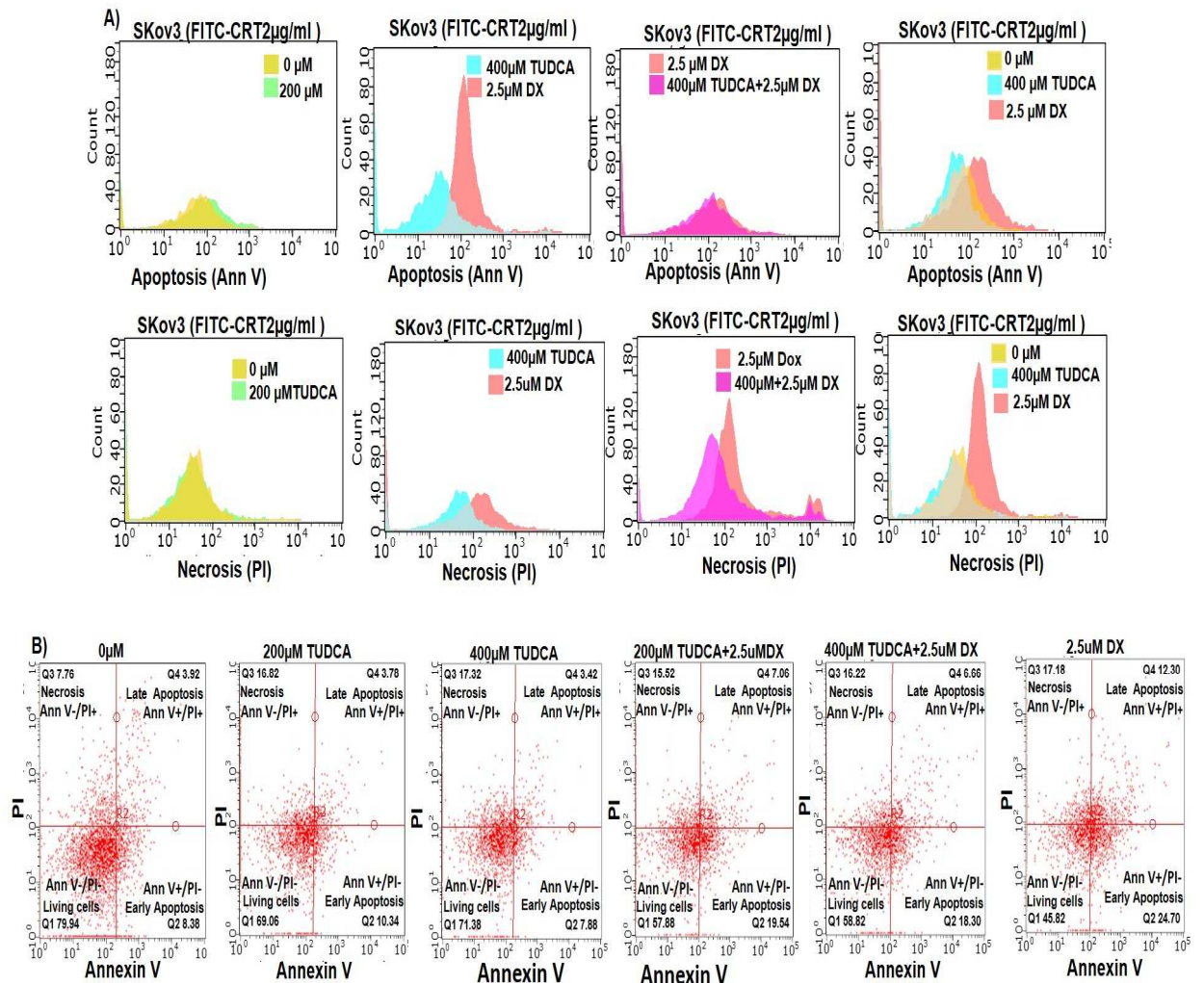
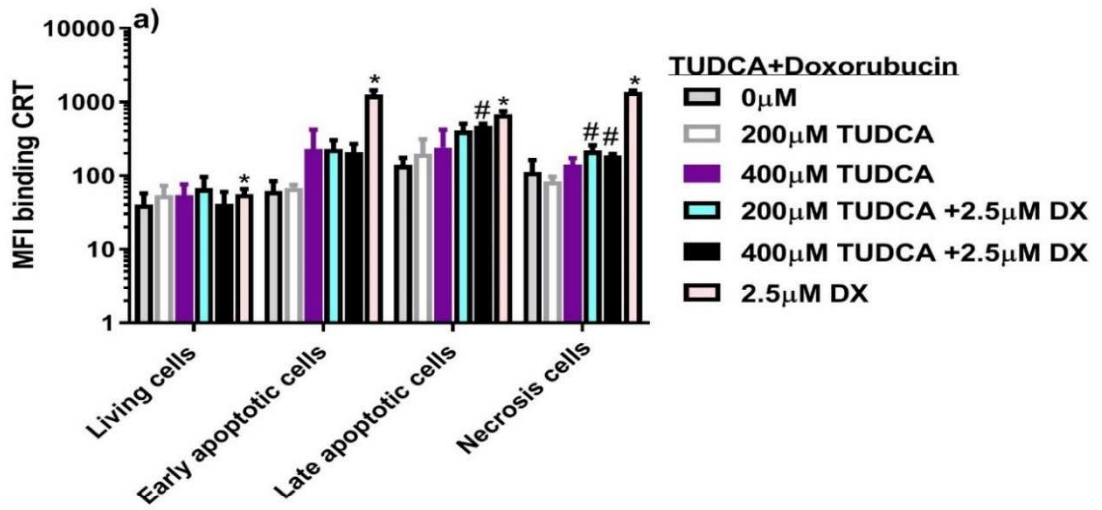


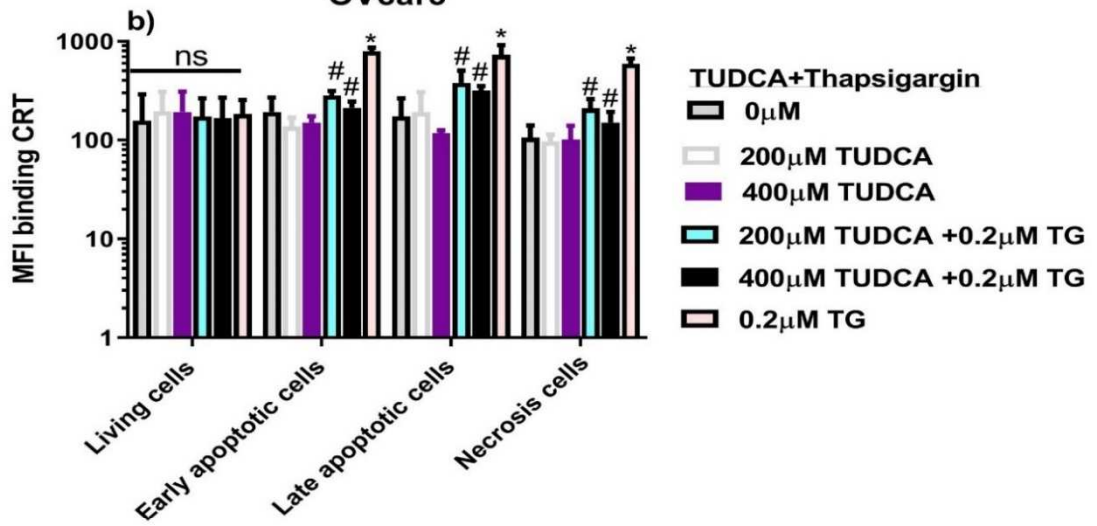
**Figure 4a.19. TUDCA promoted a decrease in exogenous CRT binding to doxorubicin (DX) treated ovarian cancer cells.** SKov3 cancer cells were treated with doxorubicin (2.5  $\mu$ M), TUDCA (200  $\mu$ M or 400  $\mu$ M) or a combination of both for 16 hours followed by exposure to FITC-CRT (2 $\mu$ g/ml) and staining with annexin V/PI to assess apoptosis and necrosis. (A) Fluorescence intensity of exogenous FITC-CRT binding to SKov3 cancer cells undergoing different stages of cell death (gated by annexin and PI staining). (B) Representative flow cytometry dot plot illustrating percentage of cells undergoing apoptosis and necrosis with the different treatments. Lower right quadrant (annexin V +ve / PI -ve) represents early apoptosis; upper right quadrant (annexin V +ve / PI +ve) represents late-apoptosis; upper left quadrant (annexin V -ve / PI +ve) represents necrosis. Representative data are shown from three experiments with similar results.



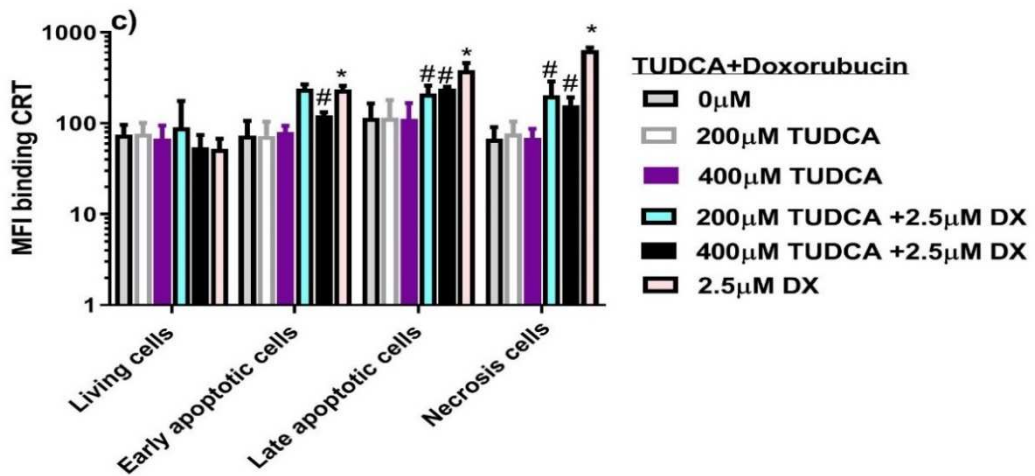
### OVcar3



### OVcar3



### SKov3



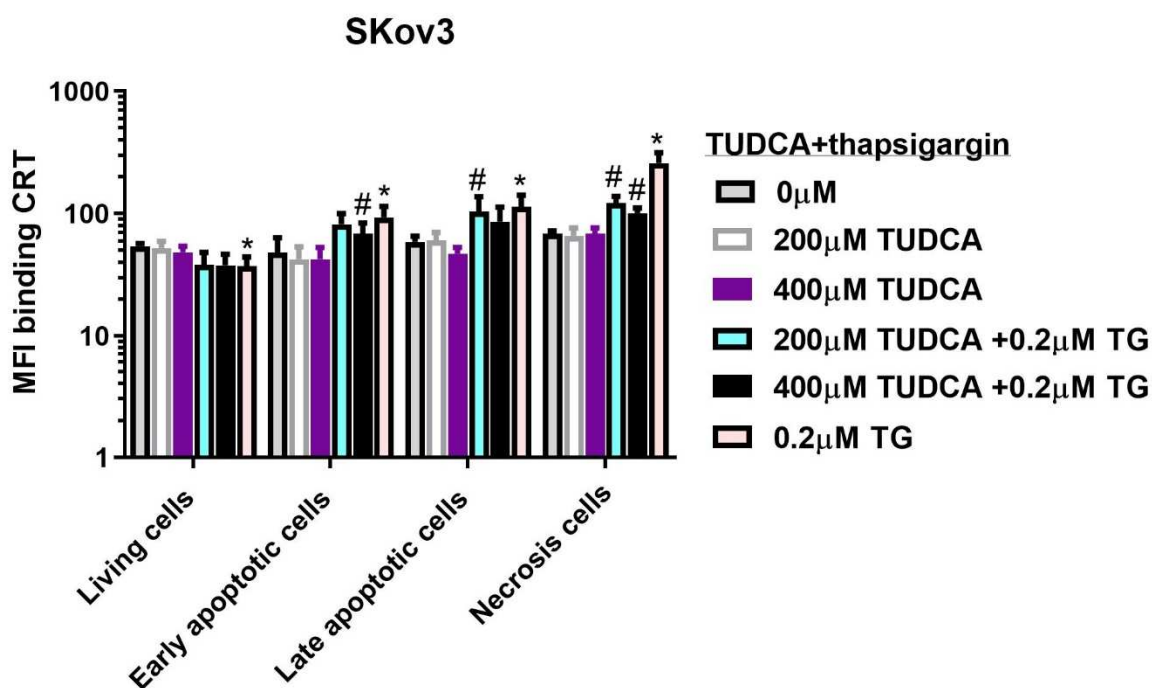


**Figure 4a.20. Treatment with TUDCA reduced the exogenous FITC-CRT binding to ovarian cancer cells when compared with cells treated with doxorubicin and thapsigargin.** SKov3 and OVcar3 cancer cells were treated with TUDCA (200 µM or 400 µM), doxorubicin (DX, 2.5 µM) or thapsigargin (TG, 0.2 µM) or in combination as indicated. Cells were then incubated with FITC-CRT and stained with annexin V and PI to assess apoptosis and necrosis by flow cytometry. Data show mean fluorescence intensity (MFI) of FITC-CRT binding to cells undergoing different stages of cell death as gated by annexin V and PI staining. (a) OVcar3 treated with TUDCA ± DX or DX alone, (b) OVcar3 treated with TUDCA ± TG or TG alone, (c), SKov3 treated with TUDCA ± DX or DX alone, (d) SKOV3 treated with TUDCA ± TG or TG alone. Data show the mean + SD. Experiments were repeated three times. \* =0 µM vs. 2.5 µM DX, 200 µM TUDCA and 400 µM TUDCA (a & c), \* =0 µM vs. 0.2 µM TG, 200 µM TUDCA and 400 µM TUDCA (b & d). # = 2.5 DX vs. 2.5 µM DX + 200, 400 µM TUDCA (a & c), # = 0.2 TG µM vs. 0.2 TG µM +200, 400 µM TUDCA (b & d). p = <0.0143 for all.

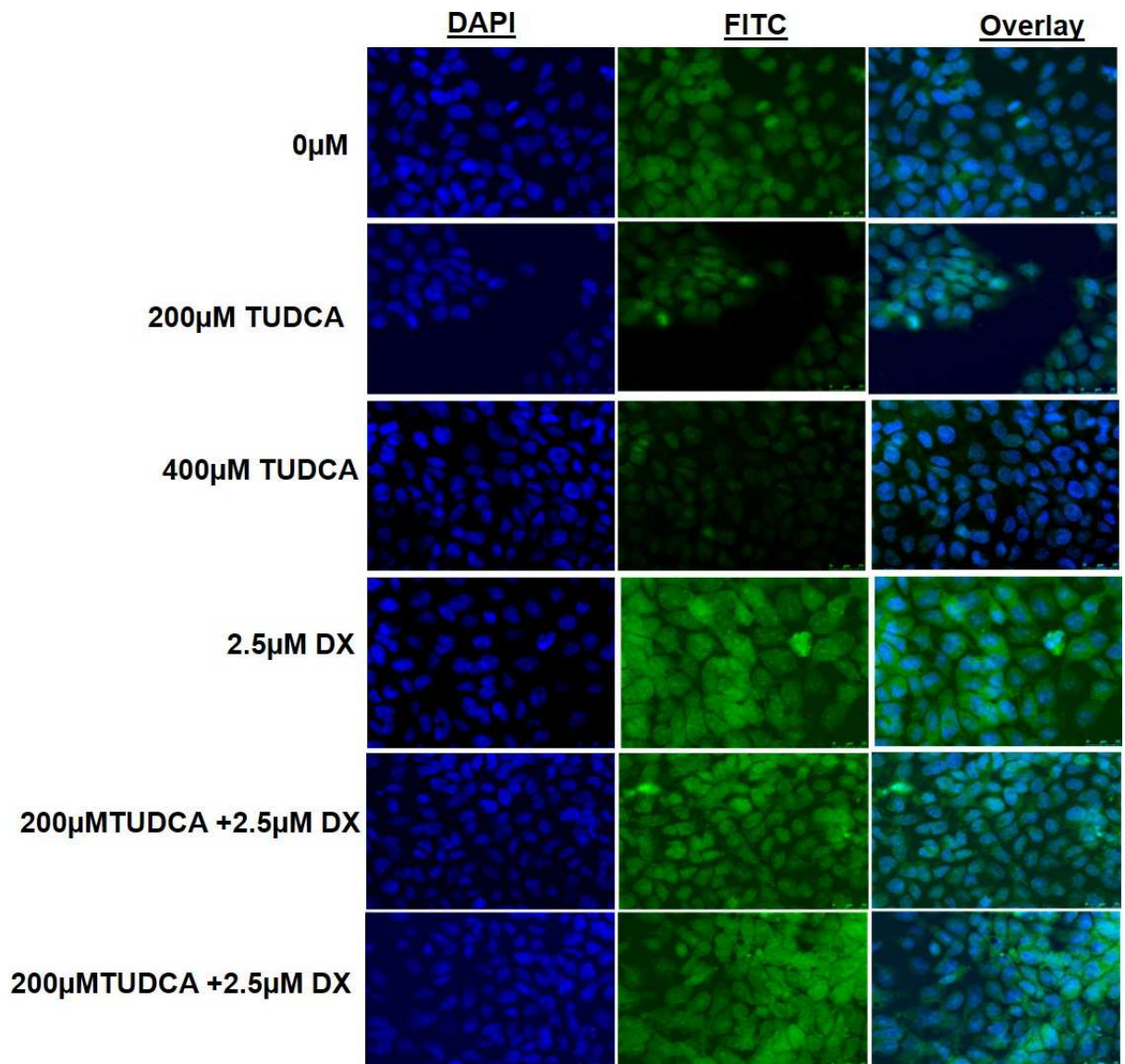


**Figure 4a.21. TUDCA reduces binding of exogenous CRT to doxorubicin (DX) treated OVcar3 ovarian cancer cells as assessed by immunofluorescent staining.** OVcar3 cells were treated with TUDCA (200  $\mu$ M or 400  $\mu$ M)  $\pm$  doxorubicin (2.5  $\mu$ M) or doxorubicin alone (2.5  $\mu$ M). Cells were fixed in 4% (w/v) paraformaldehyde, stained with  $\pm$  FITC-CRT (2 $\mu$ g/ml) and DAPI and observed under confocal microscopy. FITC-CRT = green labelling, blue labelling represents DAPI stain of cell nuclei. Scale bar equals 25  $\mu$ m. Representative images are shown from experiments carried out three times with similar data.

## **Chapter 4b. Examination of the conditions required for surface exposure of translocated endogenous calreticulin in ovarian cancer cells.**

### **4b.1 Introduction**

Chapter 4a described studies that demonstrated that exogenous CRT could bind to the surface of ovarian cancer cells and that this binding was increased in cells undergoing cell death induced by ER stressors such as doxorubicin. It is now known that chemotherapies such as doxorubicin also induce translocation of CRT to the cell surface of some tumour cells (Obeid et al., 2007) The possibility that this CRT enhances the immunogenicity of early apoptotic cancer cells by triggering ICD has set CRT at centre stage for aiding our understanding of cancer immunology in recent years (Panaretakis et al., 2009). Translocation of endogenous CRT to the cell surface of dying tumour cells is now thought to enhance their recognition and engulfment by DC (Raghavan et al., 2013). Although not fully established, the importance of this mechanism operating in ovarian cancer is supported by recent studies at the messenger RNA level that suggest that lack of CRT message correlated negatively with cytotoxic T cell infiltration into tumour sites in ovarian cancer patients influencing survival (Stoll et al., 2016).

The aims of this section were to determine the conditions that give rise to endogenous CRT cell surface expression under stress conditions in ovarian cancer. Elucidation of the conditions required may aid targeted immunotherapy for immune-mediated eradication of ovarian cancer. Briefly, cancer cells were treated with the ER stressors doxorubicin and thapsigargin in the presence or absence of TUDCA which has been reported to protect against ER damage. Cells were analysed for externalised CRT by staining with specific antibodies followed by flow cytometry and immunofluorescence. Additionally, levels of secreted CRT were assessed by ELISA western blotting.

## **4b.2 Aim**

The aims of this section were to determine whether intracellular CRT becomes externalised in ovarian cancer cells, potentially identifying these cells for immune-mediated eradication.

The specific objectives were:

1. To examine whether endogenous CRT was translocated to the surface of ovarian cancer cells and/or secreted under stress conditions induced by doxorubicin and thapsigargin.
2. To examine whether endogenous CRT preferentially became externalised in ovarian cancer cells in certain stages of cell death
3. To examine whether TUDCA was able to inhibit doxorubicin and/or thapsigargin induced translocation and secretion of intracellular CRT in ovarian cancer cells.

## **4b.3 Methods**

### **4b.3.1. Treatment of cancer cells with doxorubicin.**

Ovarian cancer cells were cultured as described in Chapter 2 (Materials and Methods).  $1 \times 10^5$  cells/well were plated in 6-well plates and cultured to 80% confluence (approximated 48 hours) in complete media. Cells were treated with 2.5  $\mu\text{M}$  doxorubicin for (0, 2, 4, 6, 8, 16, 24 h), harvested prepared for using flow cytometry. Externalised CRT was quantified using a rabbit anti-human-CRT primary antibody (1:200, 1 hour) followed by washing and incubation with a goat anti-rabbit IgG H&L secondary antibody (Alexa Fluor® 488) (green color) (1/2000, 30 minutes).

### **4b.3.2. Treatment of cancer cells with thapsigargin**

Ovarian cancer cells  $1 \times 10^5$  cells/well were plated in 6-well plates and cultured to 80% confluence (approximated 48 hours) in complete media. Cells were then treated with varying concentrations of thapsigargin (0.2, 0.5  $\mu\text{M}$ ) in the absence or presence of 2.5  $\mu\text{M}$  doxorubicin. After washing twice in PBS, cells were harvested, stained for externalised CRT as above and with annexin V and PI as previously described in Chapter 2 (Materials and Methods). Cells were resuspended in 100  $\mu\text{l}$  of binding buffer

in each sample and analysed by flow cytometer then the fluorescent intensity of stained cells was gated on propidium iodide (PI), annexin V by flow cytometry.

#### **4b.3.3. Treatment of cancer cells with TUDCA**

$1 \times 10^5$  ovarian cancer cells, SKov3 and OVcar3, were plated in each well of a 6-well plate and treated with different concentrations (200  $\mu$ M, 400 $\mu$ M) of TUDCA, 2.5 $\mu$ M doxorubicin and thapsigargin for 16 h. After washing twice in PBS, cells were stained for externalised CRT and annexin V and PI as above. Cells were harvested, resuspended in 100  $\mu$ l of binding buffer and analysed by flow cytometry with the fluorescent intensity of stained cells gated on propidium iodide (PI), annexin V by flow cytometry.

#### **4b.3.4. Immunocytochemistry**

Immunocytochemistry was carried out as described in section 4a.3.7.

#### **4b.3.5. HCMEC/D3**

HCMEC/D3 cells were cultured as described in Chapter 2 section (2.3.3). Cells were treated, stained for externalised CRT and prepared for flow cytometry and as in section 4a.3.6.

#### **4b.3.6. CRT ELISA**

Secreted CRT was quantified by ELISA as described in chapter 2 (2.5.1).

#### **4b.3.7. Preparation of cell lysates for western blotting**

Following treatment cells were immediately solubilized in 200  $\mu$ l of ice-cold lysis buffer containing 1% (w/v) SDS, 1% (v/v) triton X 100, 50 mM Tris (pH 7.5), 150 mM NaCl, and 1 protease inhibitor tablet. After lysis on ice for 30 minutes samples were centrifuged at 340g at 4°C for 20 minutes and the supernatant collected. Protein content of the lysates was determined by BCA assay. Samples were then assessed for their CRT content by western blotting according to the method of Osman (Osman et al. 2017). Beta actin was quantified as a loading control.

#### **4b.3.8. Western blotting**

Changes in CRT protein levels were examined by western blotting as described in Chapter 2 (2.7). Membranes were incubated with 1:1000 dilution of a 1 µg/ml rabbit anti-human-CRT (A3-900) in PBS-0.2% (v/v) Tween-20 on a rocker overnight at 4°C. After washing the membranes were incubated at room temperature in the dark for 1 h with a 1:15000 dilution of IRDye 800CW goat anti-rabbit IgG. Blots were washed twice in PBS-0.2% (v/v) Tween-20 and once in PBS alone and were analysed on an Odyssey CLx Imager.

#### **4b.3.9. Assessment of apoptosis and necrosis**

Apoptosis and necrosis were assessed as described in section 4a.3.7.

## **4b.4 Results.**

### **4b.4.1 Doxorubicin treatment of cancer cells increased release of endogenous CRT.**

Initial experiments were carried out to examine whether doxorubicin treatment could induce externalisation of CRT on ovarian cancer cells. To test this, SKov3 cells were treated with 2.5 $\mu$ M doxorubicin for a maximum of 24 hours and cell surface CRT and cell apoptosis and necrosis were assessed by immunocytochemistry and flow cytometry. Doxorubicin induced a robust expression of CRT on the cell surface as assessed immunocytochemistry (Figure 4b.1). This was accompanied by induction of cell death (Figure 4b.1 (b, c)). Doxorubicin treatment led to a rapid decrease in live cells and a steady increase in late apoptotic cells and a transient increase in early apoptotic and necrotic cells over 24 hour treatment. Notably, late apoptotic cells increased from 0.3% to 56% of the cell population after 24 hours doxorubicin treatment. When CRT exposure on the different cell populations was examined it was observed that cells undergoing early and late apoptosis, as well as necrosis had a marked increase in cell surface CRT expression compared with living cells (Figure 4b.1 (d)). For instance MFI of externalised CRT after 2 hours of treatment was 12.25  $\pm$  0.96 in living cells; 94.25  $\pm$  0.96 in cells undergoing early apoptosis; 188.8  $\pm$  25.51 in cells in late apoptosis and 151.3  $\pm$  10.11 in necrotic cells, ( $p$ =<0.05 for all,  $n$ =3). At later time points necrotic cells had the highest MFI of CRT staining suggesting that necrotic cells have high levels of CRT on their surface.



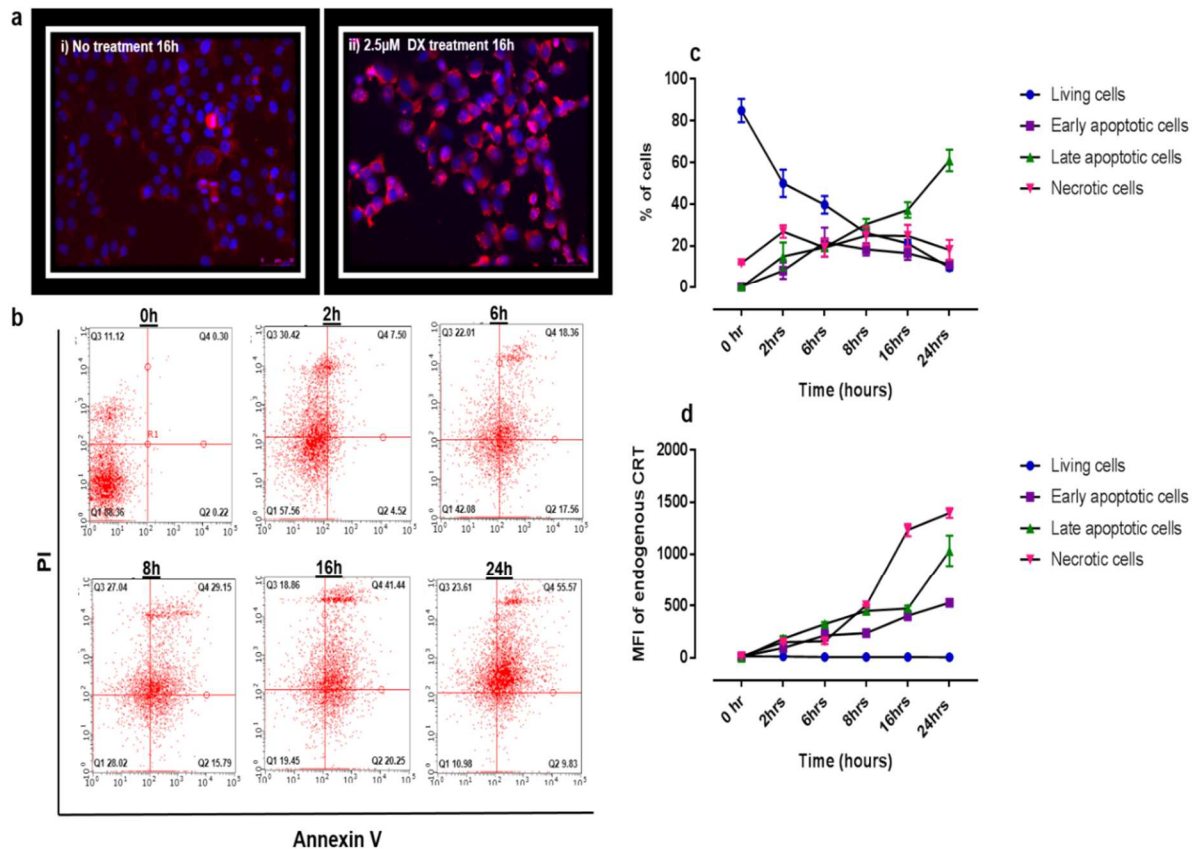


**Figure 4b.1. Doxorubicin treatment increases surface expression of endogenous CRT on non-permeabilised SKOV3 cancer cells.** SKOV3 cells were treated with 2.5  $\mu$ M doxorubicin for times as indicated. Extracellular CRT was assessed by immunocytochemistry and flow cytometry (after staining with fluorescent anti-CRT antibody) and apoptosis and necrosis were assessed using annexin V and PI. MFI of externalised CRT in live, apoptotic and necrotic cells was measured after gating cell population based on their PI and annexin V staining. (a) Representative image showing expression of surface CRT detected by immunofluorescence on untreated and 2.5  $\mu$ M doxorubicin treated SKOV3 post-16 h treatment (x20 magnification). (b) Representative flow cytometry histograms of SVOV3 cells treated with 2.5  $\mu$ M doxorubicin for 0-24 hours and assessed for cell death. (c) Percentage of living, apoptotic and necrotic cells pre and post doxorubicin treatment. (d) MFI of surface CRT on SKOV3 cell population's pre and post- 2.5  $\mu$ M doxorubicin. Figures a-d are representative images of three experiments carried out with similar results.

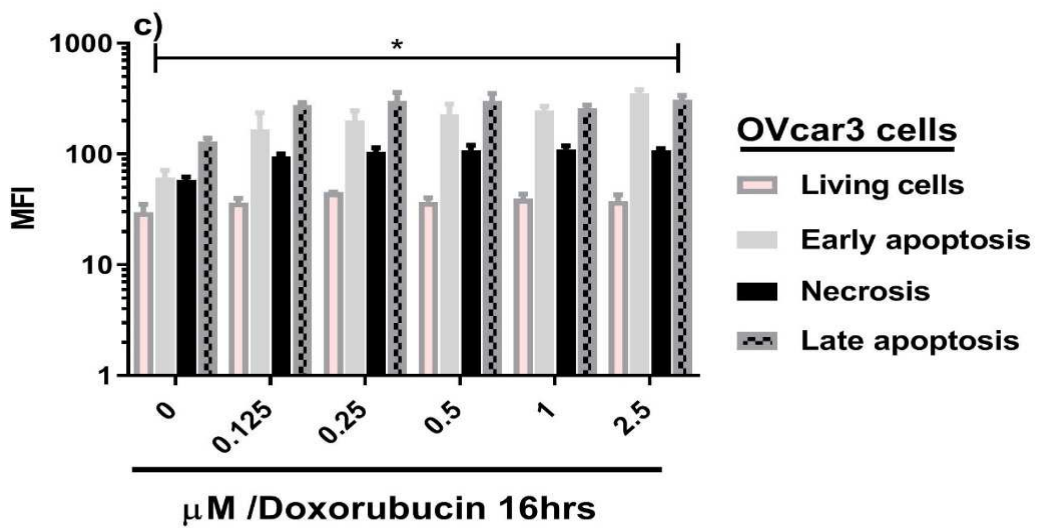
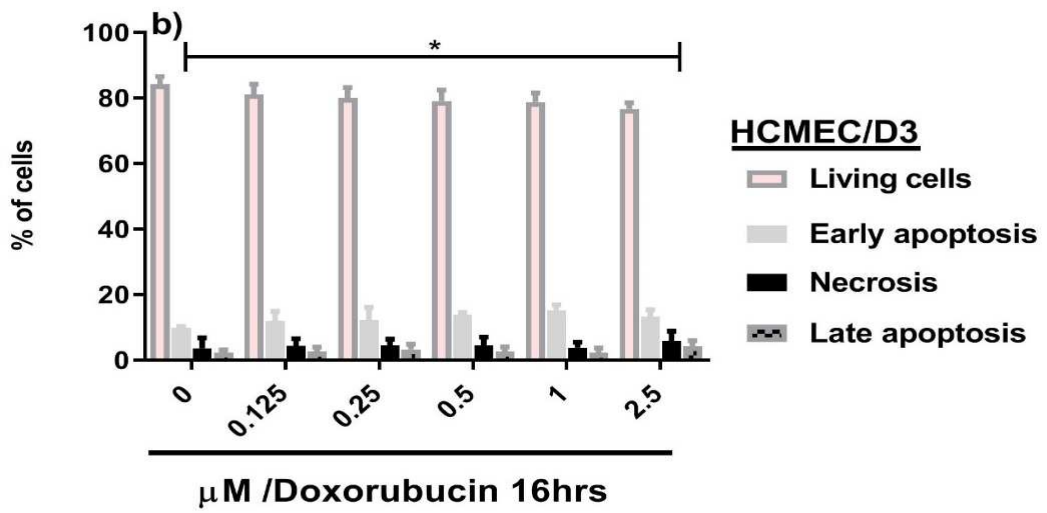
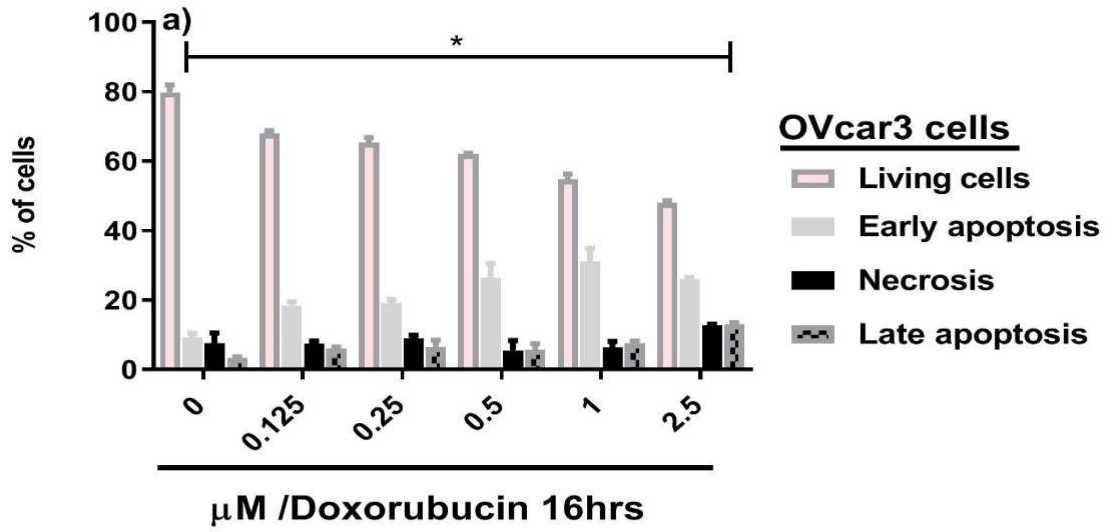
#### **4b.4.2. The effect of doxorubicin on cell death and CRT externalisation on non-cancer cells.**

The data in section 4b.4.1. Indicate that ovarian cancer cells treated with doxorubicin externalise CRT. To examine whether this observation is only seen in cancer cells or is a wide spread effect, similar experiments were carried out on human endothelial cells (HCMEC/D3) and a different ovarian cancer cell line, OVcar3. Additionally the dose response to doxorubicin was tested. HCMEC/D3 and OVcar3 cells were treated with increasing concentrations of doxorubicin (0, 0.125, 0.25, 0.5, 1, 2.5  $\mu$ M) for 16 hours and apoptosis and necrosis and MFI of externalised CRT were examined (Figure 4b.2 and Table 4b.1). As shown in (Figure 4b.2. (a)) treatment with doxorubicin for 16 hours markedly reduced cell viability in OVcar3 cell compared with untreated cells ( $p < 0.05$  all concentrations tested), but only minimally altered cell viability in HCMEC/D3 (Figure 4b.2 (b)), suggesting that doxorubicin is preferentially toxic to cancer cells.

OVcar3 cancer cells undergoing doxorubicin-induced cell death had significantly increased surface CRT at all stages of cell death (Figure 4b.2 (c)). After 16 hours of treatment CRT MFI was  $31.5 \pm 8.963$  in living cells;  $261.5 \pm 30.65$  in early apoptotic cells;  $255.5 \pm 16.11$  in late apoptotic cells and  $109.5 \pm 3$  in necrotic cells ( $p = < 0.05$  vs untreated for all,  $n = 3$ ). In contrast there was virtually no change in MFI of CRT with time across the different stages of cell death in the HCMEC/D3 cells (Figure 4b.2 (d)). These data indicate that doxorubicin does not induce CRT exposure in these cells. It also appears that doxorubicin induced externalisation of CRT is associated with cell death. It is not possible from these results to determine whether doxorubicin induces ER stress without cell death in the HCMEC/D3, but if CRT exposure is due to ER stress then this would suggest that either the non-cancer cells are resistant to doxorubicin induced cell death or that ER stress is not linked to CRT surface translocation in these cells.

#### **4b.4.3 Treatment of both OVcar3 and SKov3 cells with thapsigargin and doxorubicin alone and in combination increases surface exposure of endogenous CRT.**

Since surface translocation of CRT in various cancer cells has been reported to occur following ER stress this was examined in ovarian cancer cells. Initial immunocytochemistry studies were carried out in SKov3 cells treated with the ER stressors doxorubicin and thapsigargin individually and in combination. It was evident that both thapsigargin and doxorubicin alone, and in combination, enhanced surface exposure of endogenous CRT compared with untreated cells (Figure 4b.5). This was further examined in OVcar3 and SKov3 cells undergoing different stages of apoptosis or necrosis using flow cytometry. Representative data are shown in (Figure 4b.3) and combined data in (Figure 4b.4). Doxorubicin and thapsigargin significantly altered the MFI of fluorescently labelled, externalised, endogenous CRT in both cell types at all stages of cell death. For instance in SKov3 cells treated with 2.5  $\mu$ M doxorubicin 0.5  $\mu$ M thapsigargin MFI was  $4 \pm 4$  in living cells and  $619 \pm 46$ ,  $856 \pm 316$  and  $5459 \pm 4654$



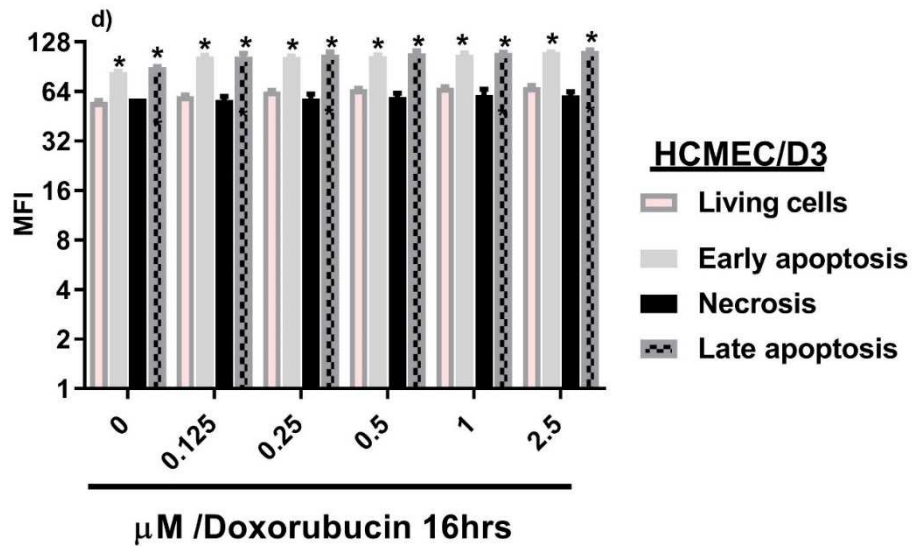


**Figure 4b.2. Doxorubicin dose-dependently induces apoptosis and necrosis in OVcar3 ovarian cancer cells, but not HCMEC/D3 human endothelial cells.** OVcar3 and HCMEC/D3 cells were treated with increasing concentrations (0, 0.125, 0.25, 0.5, 1, 2.5  $\mu\text{M}$ ) of doxorubicin for 16 hours. Externalised CRT and apoptosis and necrosis were detected by flow cytometry. (a) and (b) the percentage of OVcar3 and HCMEC/D3 cells undergoing apoptosis and necrosis as determined by annexin V and PI staining. (c) and (d) MFI of CRT staining in OVcar3 and HCMEC/D3 cells at different stages of cell death (cells gated on PI and annexin V staining). Note different y axis scales in (c) and (d) Data show the mean + SD. Experiments were repeated three times. \* $p < 0.05$  vs control.

HCMEC/D3 %	Control	Early apoptosis	Late apoptosis	Necrosis
0 $\mu$ M	83.93 $\pm$ 1.953	9.853 $\pm$ 0.4242 *	2.225 $\pm$ 0.7113 *	4.24 $\pm$ 2.807*
0.125 $\mu$ M DX	81.87 $\pm$ 2.849	12 $\pm$ 2.38 *	3.148 $\pm$ 1.704 *	4.983 $\pm$ 2.249 *
0.25 $\mu$ M DX	80.78 $\pm$ 2.957	12.9 $\pm$ 3.49*	3.698 $\pm$ 1.573 *	4.625 $\pm$ 1.582 *
0.5 $\mu$ M DX	79.85 $\pm$ 3.041	13.64 $\pm$ 0.732*	2.633 $\pm$ 1.246 *	5.13 $\pm$ 2.394 *
1 $\mu$ M DX	79.36 $\pm$ 2.467	14.66 $\pm$ 1.75*	2.388 $\pm$ 1.341 *	4.348 $\pm$ 1.722 *
2.5 $\mu$ M DX	76.31 $\pm$ 1.722	12.7 $\pm$ 2.046*	4.625 $\pm$ 1.698 *	5.873 $\pm$ 2.401 *

OVcar3 %	Control	Early apoptosis	Late apoptosis	Necrosis
0 $\mu$ M	79.36 $\pm$ 1.966	9.485 $\pm$ 0.9857 *	3.375 $\pm$ 0.25 *	7.905 $\pm$ 2.54*
0.125 $\mu$ M DX	68.03 $\pm$ 0.6006	18.12 $\pm$ 1.114 *	6.28 $\pm$ 0.616 *	7.57 $\pm$ 0.7 *
0.25 $\mu$ M DX	65.51 $\pm$ 1.208	19.12 $\pm$ 0.8386*	6.66 $\pm$ 1.571 *	9.21 $\pm$ 0.9282 *
0.5 $\mu$ M DX	62.12 $\pm$ 0.1558	25.34 $\pm$ 4.013*	6.36 $\pm$ 1.729 *	6.435 $\pm$ 2.879 *
1 $\mu$ M DX	54.59 $\pm$ 1.268	31.93 $\pm$ 3.299*	31.93 $\pm$ 3.299 *	6.805 $\pm$ 1.593 *
2.5 $\mu$ M DX	48.11 $\pm$ 0.3743	25.75 $\pm$ 0.6206*	13.11 $\pm$ 0.3288 *	12.54 $\pm$ 0.4795 *

HCMEC/D3 MFI	Control	Early apoptosis	Late apoptosis	Necrosis
0 $\mu$ M	55.33 $\pm$ 1.155	84 $\pm$ 1 *	90 $\pm$ 0.8165 *	58 $\pm$ 0*
0.125 $\mu$ M DX	60.25 $\pm$ 0.9574	115.8 $\pm$ 22.9 *	113.3 $\pm$ 18.28 *	75.25 $\pm$ 36.56
0.25 $\mu$ M DX	64 $\pm$ 0.8165	115.5 $\pm$ 23.01*	107.3 $\pm$ 4.163 *	68.5 $\pm$ 21.21
0.5 $\mu$ M DX	65.5 $\pm$ 1.291	113.5 $\pm$ 17.75*	109 $\pm$ 4.359 *	69.5 $\pm$ 20.5
1 $\mu$ M DX	67.67 $\pm$ 0.5774	107 $\pm$ 2.646*	109.3 $\pm$ 1.528 *	61 $\pm$ 5.196
2.5 $\mu$ M DX	68 $\pm$ 1.732	110.7 $\pm$ 0.5774*	112.7 $\pm$ 2.082 *	60.74 $\pm$ 2.96 *

OVcar3 MFI	Control	Early apoptosis	Late apoptosis	Necrosis
0 $\mu$ M	31.17 $\pm$ 5.029	64.25 $\pm$ 10.18 *	131.5 $\pm$ 8.963 *	59 $\pm$ 3.367*
0.125 $\mu$ M DX	37.26 $\pm$ 3.374	185.8 $\pm$ 67.11 *	277.3 $\pm$ 9.979 *	96.25 $\pm$ 4.787 *
0.25 $\mu$ M DX	45.25 $\pm$ 0.1908	200.3 $\pm$ 46.37*	300.3 $\pm$ 59.28 *	105.0 $\pm$ 8.660 *
0.5 $\mu$ M DX	45.19 $\pm$ 0.1997	213 $\pm$ 45.56*	310.3 $\pm$ 52.31 *	103.8 $\pm$ 7.5 *
1 $\mu$ M DX	39.86 $\pm$ 2.966	261.5 $\pm$ 30.65*	255.5 $\pm$ 16.11 *	112.3 $\pm$ 8.958 *
2.5 $\mu$ M DX	36.32 $\pm$ 5.06	352 $\pm$ 22.02*	317.5 $\pm$ 29.91 *	109.5 $\pm$ 3 *

**Table 4b.1. Doxorubicin induces apoptosis and necrosis in OVcar3 ovarian cancer cells, but not HCMEC/D3 human endothelial cells.** OVcar3 and HCMEC/D3 cells were treated with increasing concentrations of doxorubicin for 16 hours. Externalised CRT and apoptosis and necrosis were detected by flow cytometry. Upper panel = % of HCMEC/D3 cells undergoing apoptosis and necrosis; second from top panel = % of OVcar3 cell undergoing apoptosis and necrosis; third from top = MFI of CRT staining in HCMEC/D3 cells at different stages of cell death; bottom panel = MFI of CRT staining in OVcar3 cells at different stages of cell death. Data are mean + SD \*p-<0.05 vs control. Experiments were repeated three times.

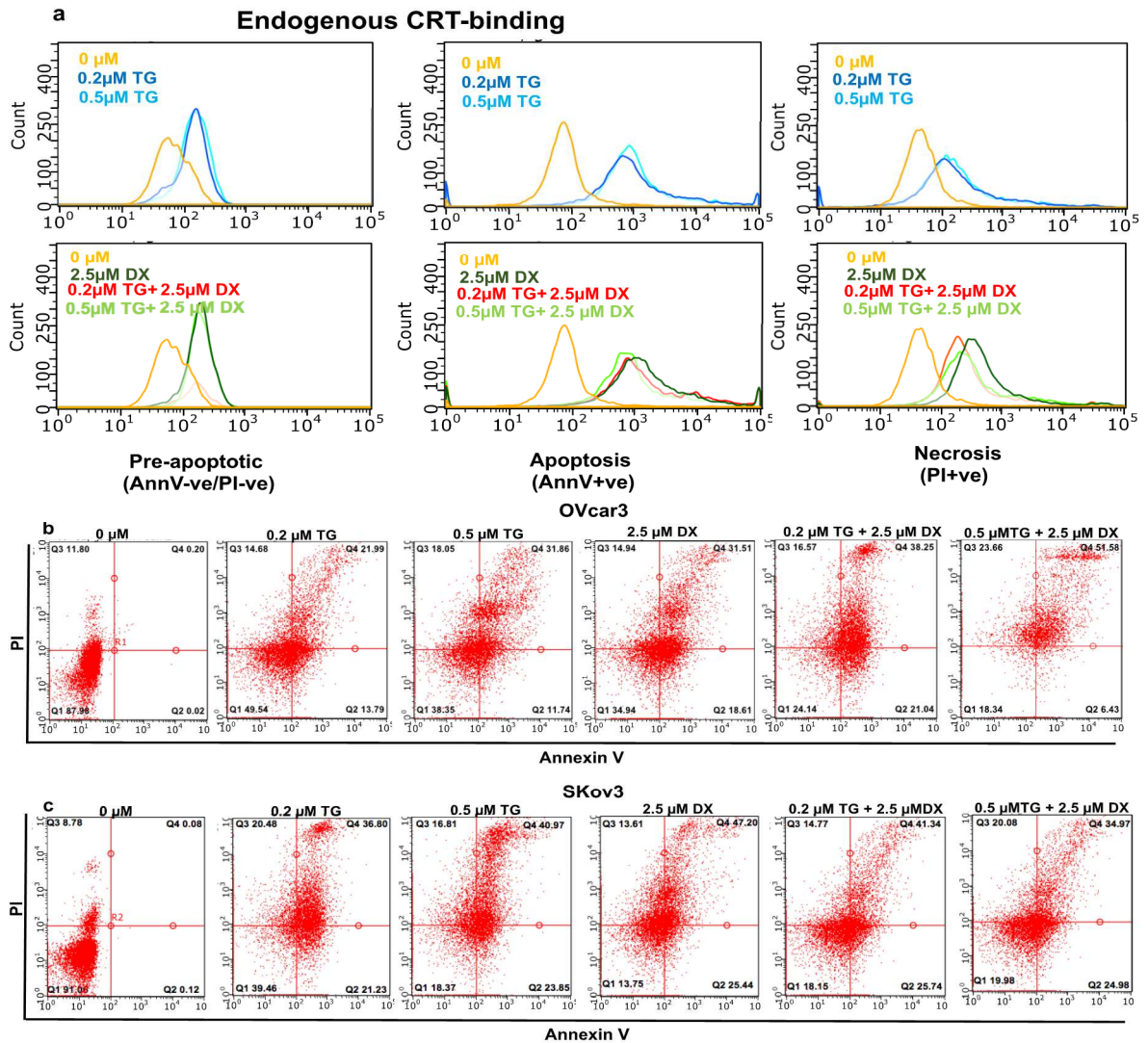


**Figure 4b.3. The ER stressors doxorubicin and thapsigargin alone and in combination induce CRT exposure in SKov3 and OVcar3 ovarian cancer cells.** Cells were treated with doxorubicin (DX, 2.5  $\mu$ M),  $\pm$  thapsigargin (TG, 0.2, 0.5  $\mu$ M) for 16 h and their apoptosis/necrosis status was determined by flow cytometry using annexin v (annV) and PI staining before and after treatment. (a) Differences in cell surface CRT expression as monitored by changes in fluorescent intensity on pre-apoptotic, apoptotic and necrotic OVcar3 cells. (b) and (c) Dot plot graphs show the changes in the percentage of viable cells (lower left quadrant), early apoptotic cells (lower right quadrant), late apoptotic cells (upper right quadrant) and necrotic cells (upper left quadrant) of (b) SKov3 and (c) OVcar3 cancer cells respectively. The bolded numbers represent the percentage of apoptosis and necrosis in the right, left lower or upper quadrant, respectively. Representative data from experiments performed at least three times are shown.

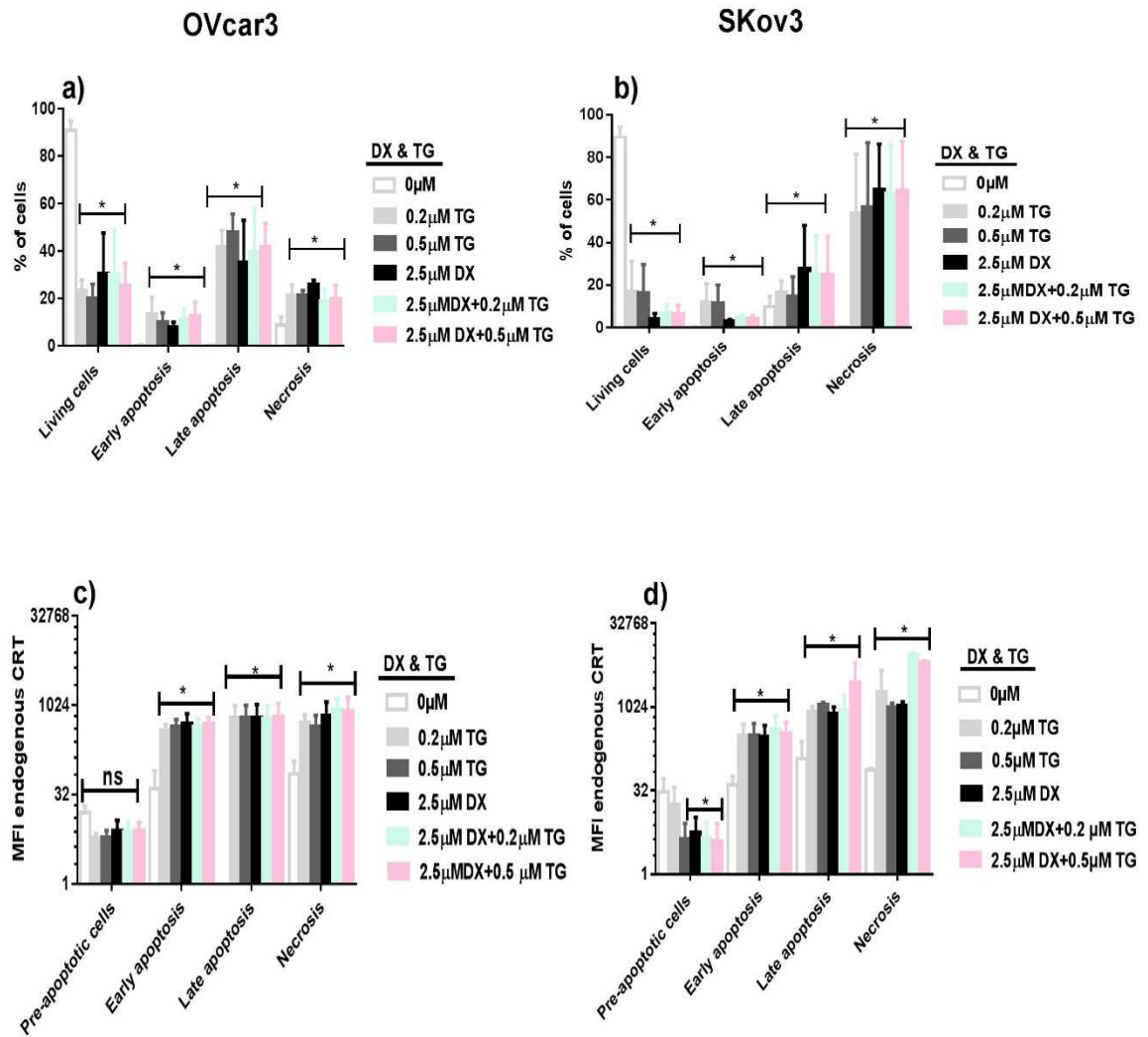


**Figure 4b.4. Surface expression of endogenous CRT is significantly increased in ovarian cancer cells in varying stages of apoptosis and necrosis in cells treated with doxorubicin and/or thapsigargin.** OVcar3 (a,c) and SKov3 cells (b,d) were treated ± doxorubicin (DX, 2.5 µM) and/or thapsigargin (TG, 0.2, 0.5 µM) for 16 h. Extracellular CRT was assessed by flow cytometry after staining with specific antibodies. Apoptosis and necrosis were assessed using annexin V and PI, with the fluorescent intensity of CRT stained cells on different cell populations gated on PI and annexin V. (a), (b) the percentage of OVcar3 and SKov3 at different stages of cell death (c), (d) the MFI of externalised CRT in OVcar3 and SKov3 in the different stages of cell death. Data show the mean + SD of three separate experiments. \* $p < 0.05$  vs control untreated cells.



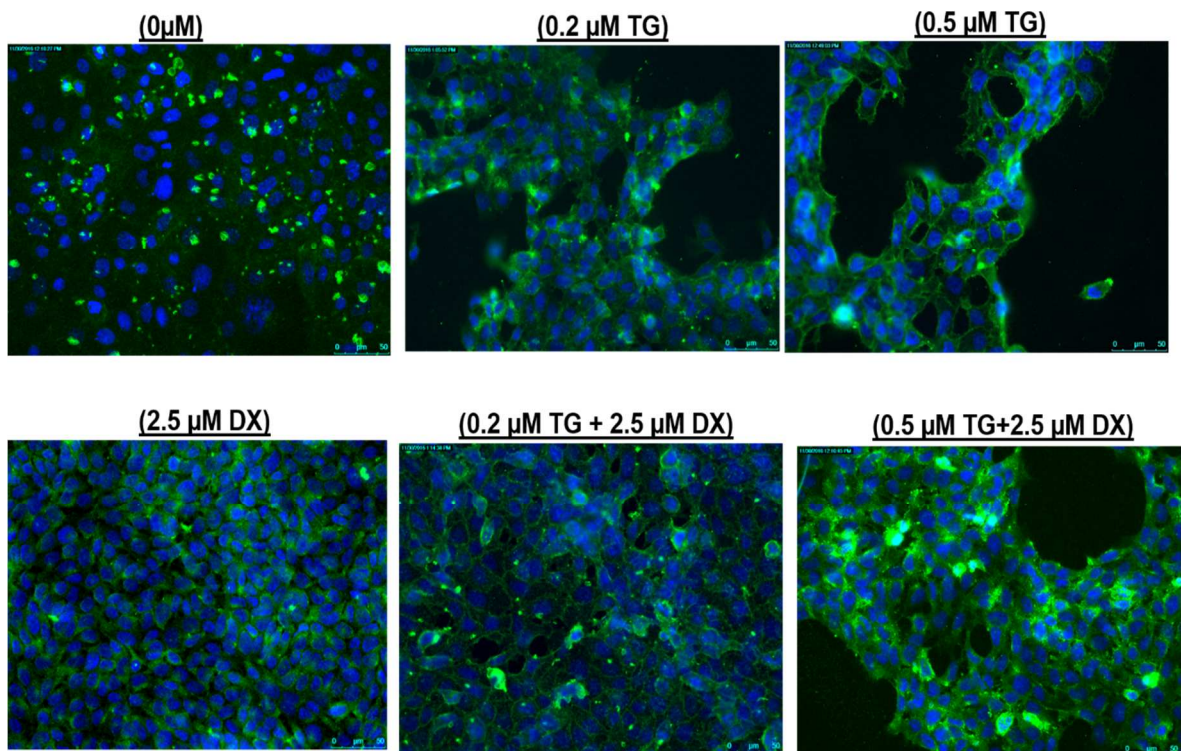


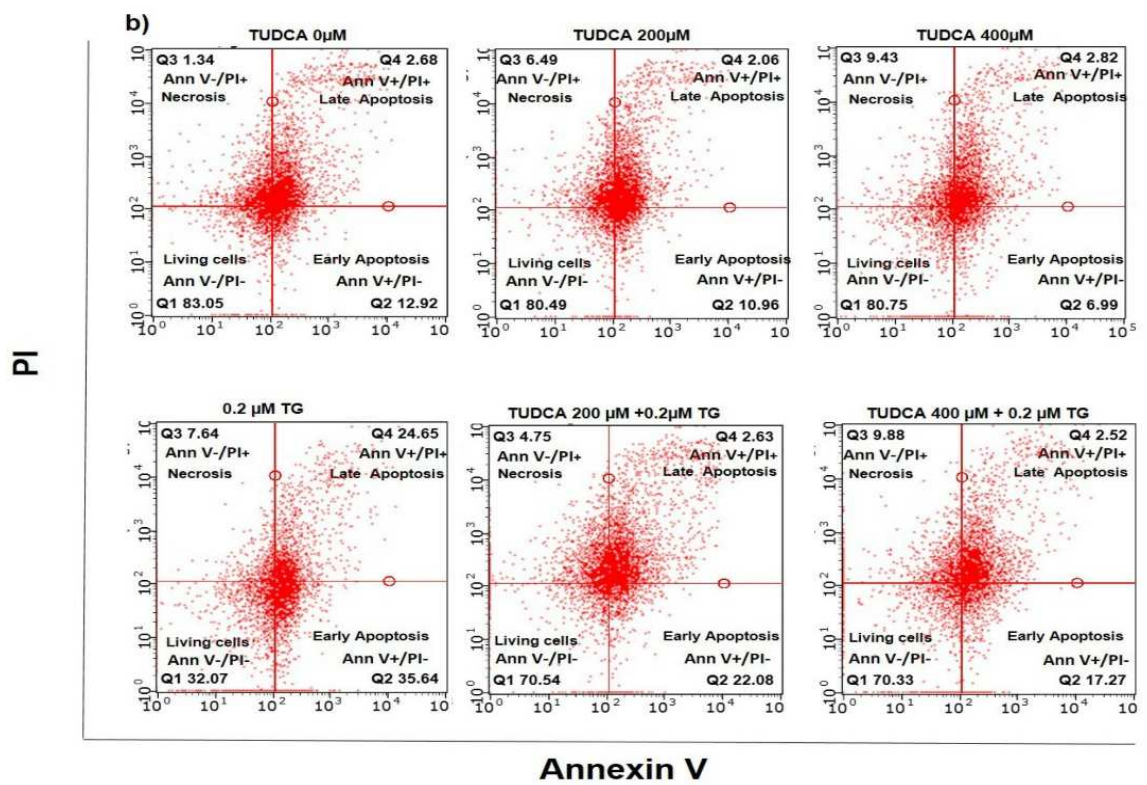
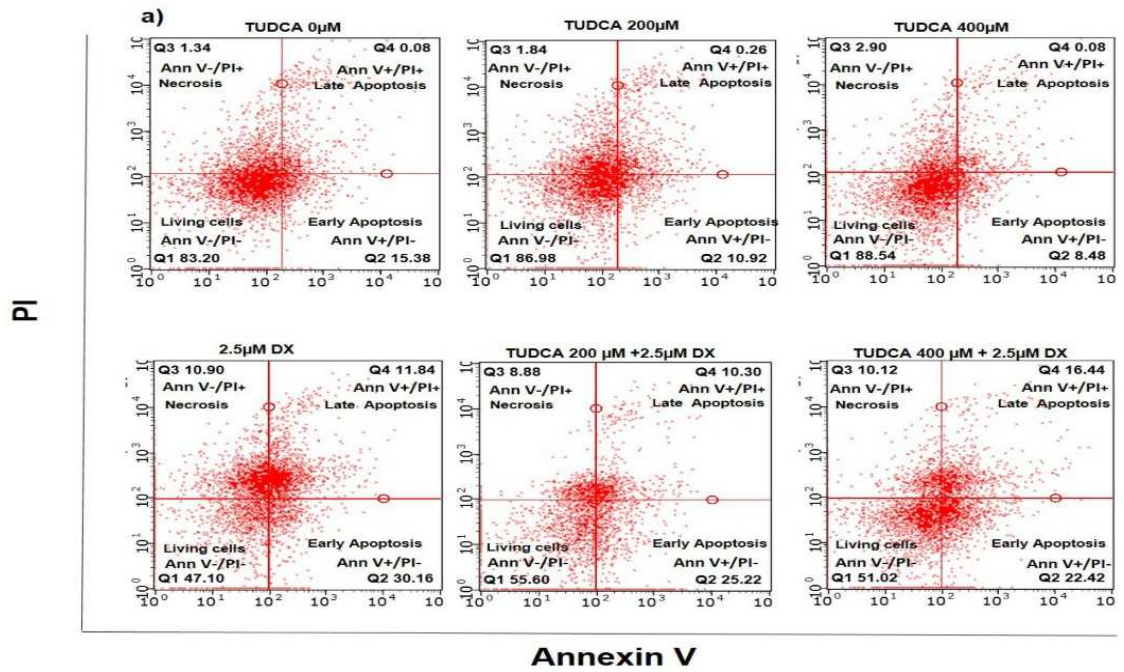
**Figure 4b.5. Surface exposure of CRT from cancer cells is induced by doxorubicin and thapsigargin individually and enhanced by treatment with both together.** SKov3 cells were treated  $\pm$  doxorubicin DX (2.5 $\mu$ M)  $\pm$  thapsigargin TG (0.2, 0.5 $\mu$ M) for 16 hours, fixed with 4% (w/v) paraformaldehyde and surface CRT was visualised by immunocytochemistry staining using rabbit anti-human-CRT Ab and goat anti-rabbit IgG-FITC antibodies respectively. Green labelling represents externalised endogenous CRT; blue labelling represents DAPI stain of cell nuclei. Images are representative from at least three experiments showing similar results and were taken at x40 magnification.

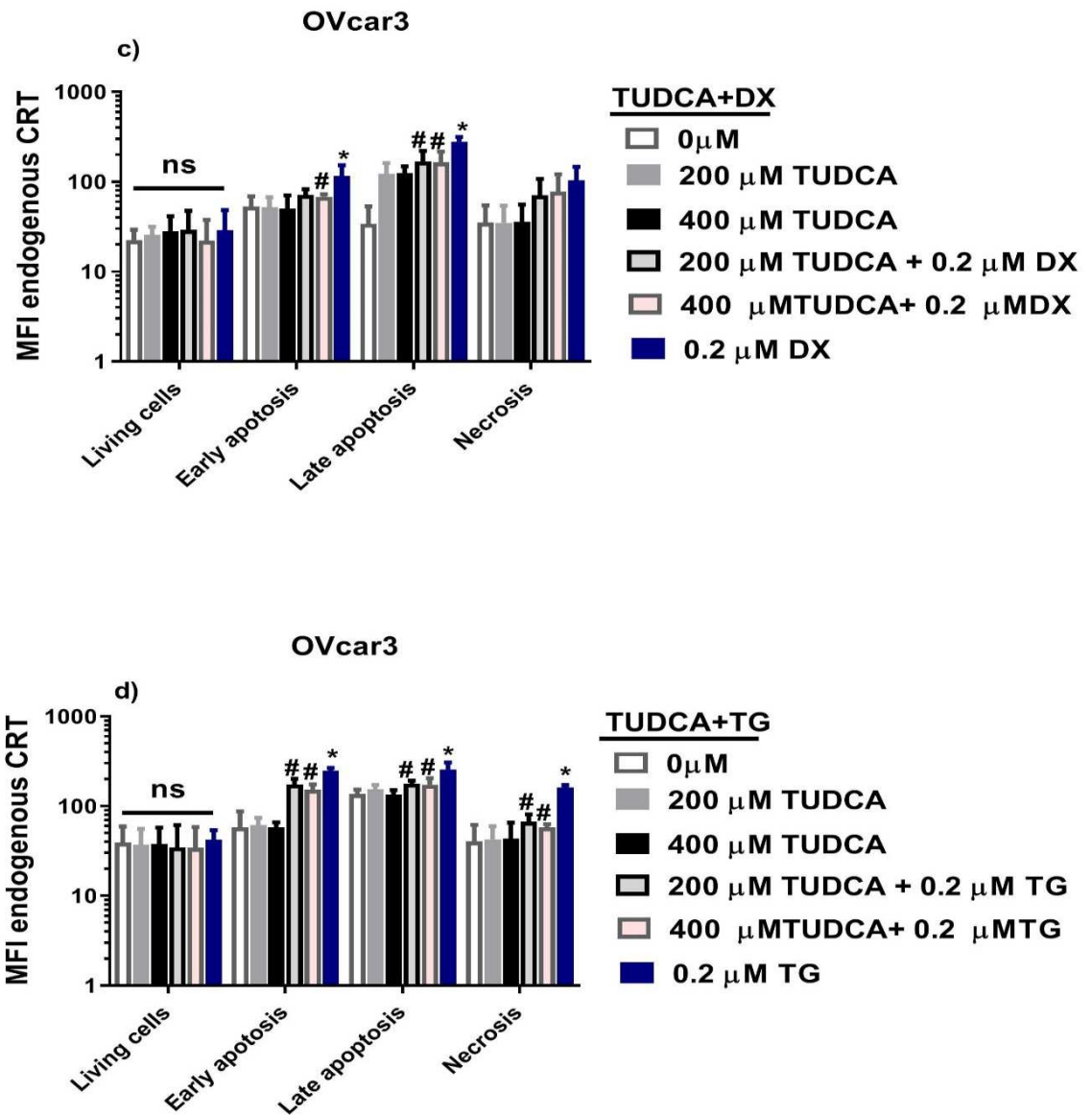
in early apoptotic, late apoptotic and necrotic cells respectively ( $p < 0.05$  for all,  $n=3$ ) (Figure 4b.4 (d)). In similarly treated OVCAR3 cells the MFI was  $6.0 \pm 0.84$ ,  $484 \pm 150$ ,  $599.3 \pm 317.9$  and  $804.1 \pm 381.2$  in living, early apoptotic, late apoptotic and necrotic cells respectively ( $p < 0.05$  for all,  $n=3$ ) (Figure 4b.4(c)).

#### **4b.4.4 Inhibition of ER stress by TUDCA reduced externalization of CRT from doxorubicin treated ovarian cancer cells.**

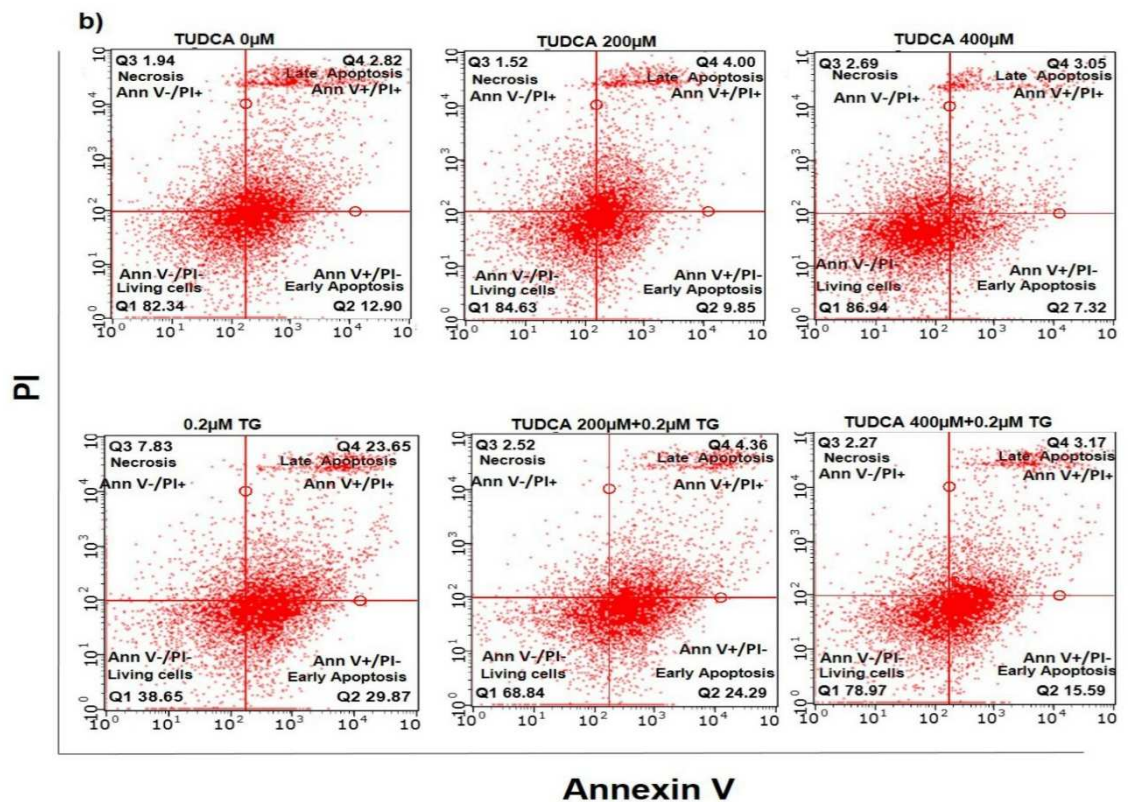
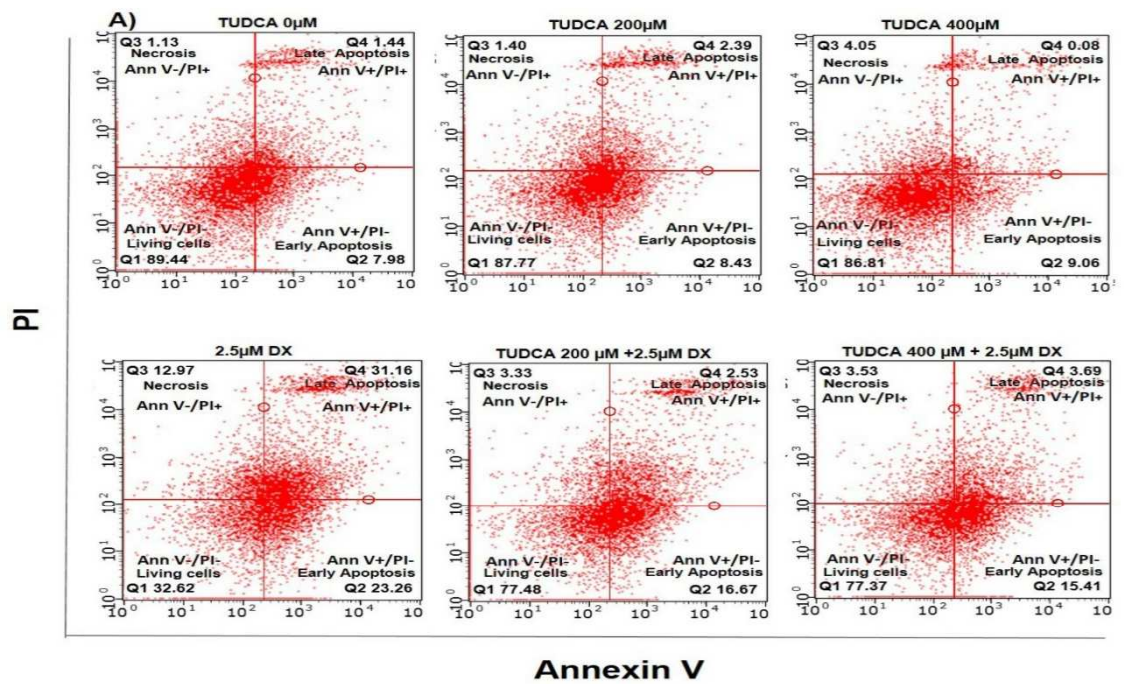
The previous data indicate that cell death induced by agents reported to induce ER stress is accompanied by externalisation of endogenous CRT. The role of ER stress in this CRT translocation was examined further using TUDCA. OVCAR3 and SKOV3 cells were treated with TUDCA (200 or 400  $\mu\text{M}$ )  $\pm$  doxorubicin or thapsigargin and cell viability status and levels of externalised endogenous CRT binding were determined by flow-cytometry. In OVCAR3 cells treated with ER stressors both concentrations of TUDCA consistently partially reduced the MFI of detected externalised CRT at all stages of cell death (Figure 4b.6). This reduction only failed to reach significance in necrotic cells induced by doxorubicin treatment. For instance, in late apoptotic cells MFI was reduced from  $231.6 \pm 21.21\mu\text{M}$  in doxorubicin alone treated cells to  $188.7 \pm 23.67\mu\text{M}$  in the presence of TUDCA ( $p < 0.05$ ,  $n=6$ ) (Figure 4b.6 (c, d)). No dose dependent effect of TUDCA was observed.

Similar results were obtained for SKOV3 cells; TUDCA induced a significant decrease in externalised CRT at all stages of cell death induced by both doxorubicin and thapsigargin (Figure 4b.7) Interestingly, in these cells the higher concentration of TUDCA (400  $\mu\text{M}$ ) did appear to be more effective at reducing CRT translocation. The data indicate that again TUDCA was only partially effective. This may reflect that either TUDCA is not fully effective at inhibiting ER stress induced by the two agents used here or that more than one pathway can induce CRT translocation. The former could be assessed by following expression of the ER stress proteins BiP/GRP78 e.g. using commercially available kits or by assessment of intracellular calcium using cell permeable calcium dyes which increase in fluorescence when bound to  $\text{Ca}^{2+}$ . These results were confirmed in OVCAR3 cells by immunocytochemistry staining and fluorescent microscopy (Figure 4b.8.).





**Figure 4b.6. TUDCA reduces cell death and externalisation of endogenous CRT in doxorubicin or thapsigargin treated OVcar3.** Cells were treated with TUDCA (200  $\mu$ M) and/or either doxorubicin (DX, 2.5  $\mu$ M) or thapsigargin (TG, 0.2 $\mu$ M) for 16hr. Extracellular CRT and apoptosis and necrosis were assessed by flow cytometry with fluorescent intensity of CRT stained cells gated on PI and annexin V. (a) and (b) Flow cytometry dot plots showing the protective effect of TUDCA on (a) doxorubicin and (b) thapsigargin induced OVcar3 cell death. (c) and (d) MFI of CRT staining at different stages of cell death. The results shown are representative of three independent experiments. \* =0  $\mu$ M vs. 2.5  $\mu$ M DX, 200  $\mu$ M TUDCA and 400  $\mu$ M TUDCA (c), \* =0  $\mu$ M vs. 0.2  $\mu$ M TG, 200  $\mu$ M TUDCA and 400  $\mu$ M TUDCA (d). # 2.5  $\mu$ M DX vs. 2.5  $\mu$ M DX +200,400  $\mu$ M TUDCA, # 0.2  $\mu$ M TG vs. 0.2  $\mu$ M TG +200,400  $\mu$ M TUDCA (c,d respectively).  $P < 0.05$  for all.



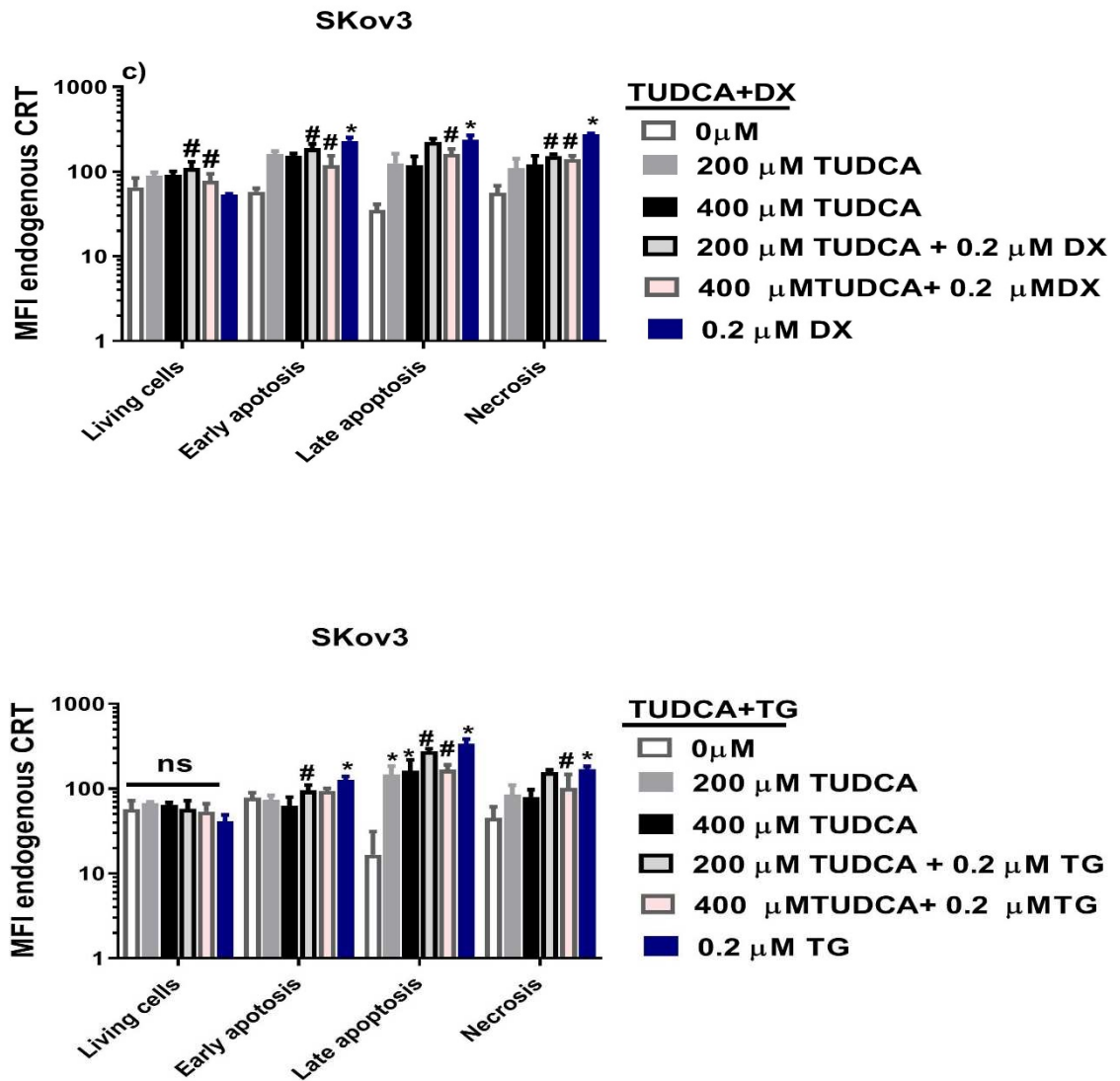


**Figure 4b.7. TUDCA reduces cell death and externalisation of endogenous CRT in doxorubicin or thapsigargin treated SKov3.** Cells were treated with TUDCA (200  $\mu$ M) and/or either doxorubicin (DX, 2.5  $\mu$ M) or thapsigargin (TG, 0.2 $\mu$ M) for 16hr. Extracellular CRT and apoptosis and necrosis were assessed by flow cytometry with fluorescent intensity of CRT stained cells gated on PI and annexin V. (a) and (b) Flow cytometry dot plots showing the protective effect of TUDCA on (a) doxorubicin and (b) thapsigargin induced SKov3 cell death. (c) and (d) MFI of CRT staining at different stages of cell death. The results shown are representative of three independent experiments. \* =0  $\mu$ M vs. 2.5  $\mu$ M DX, 200  $\mu$ M TUDCA and 400  $\mu$ M TUDCA (c), \* =0  $\mu$ M vs. 0.2  $\mu$ M TG, 200  $\mu$ M TUDCA and 400  $\mu$ M TUDCA (d), # 2.5  $\mu$ M DX vs. 2.5  $\mu$ M DX +200,400  $\mu$ M TUDCA, # 0.2  $\mu$ M TG vs. 0.2  $\mu$ M TG +200,400  $\mu$ M TUDCA (c,d respectively).  $P < 0.05$  for all.

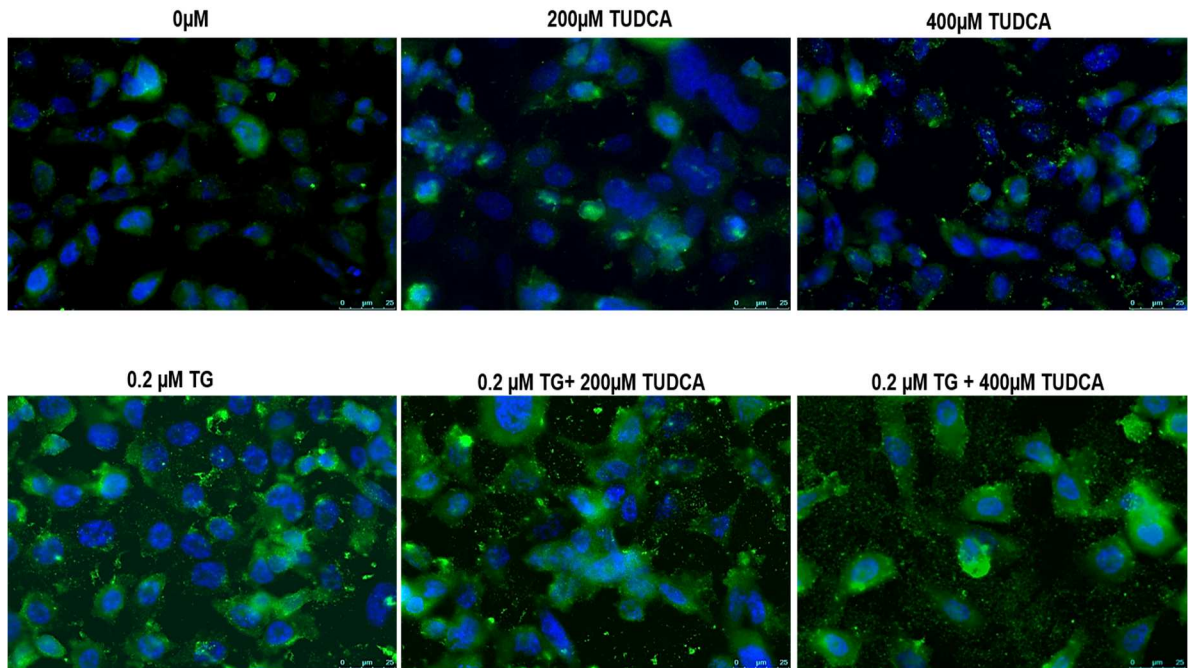


**Figure 4b.8. TUDCA reduced the amount of endogenous CRT externalised on the cell surface of OVcar3 ovarian cancer cells treated with the ER stressor thapsigargin.** OVcar3 cells were treated with control media, TUDCA (200, 400  $\mu$ M)  $\pm$  thapsigargin (TG, 0.2, 0.5 $\mu$ M) or thapsigargin alone for 16 hours and fixed with 4% (w/v) paraformaldehyde. Surface CRT was visualised by immunocytochemistry staining using rabbit anti-human-CRT Ab and goat anti-rabbit IgG-FITC antibodies respectively. Green labelling represents externalised CRT binding to cancer cells; blue labelling represents DAPI stain of cell nuclei. Images are representative from at least three experiments showing similar results and were taken at x40 magnification.

#### **4b.4.5 Effect of ER-stressors and inhibitors on CRT expression and release from OVcar3 cells.**

The previous data suggest that doxorubicin and thapsigargin stimulate CRT translocation to the cell surface at least partially via induction of ER stress. It is also possible that this translocation is associated secretion of CRT from the cells. Indeed, CRT has been considered a biomarker of elevated ER stress associated with various malignancies (Wiersma et al., 2015) including ovarian cancer (Galazis et al., 2012, Abbott et al., 2010, Bengtsson et al., 2007). Thus, CRT expression and secretion in ovarian cancer cells in response to ER stressors was examined in the cell culture system used here.

OVcar3 cells were treated with doxorubicin (0.25, 2.5 $\mu$ M) or thapsigargin (0.2 $\mu$ M)  $\pm$  TUDCA. Cell expression of CRT was examined by western blotting of cell lysates and lysates and secreted CRT in the culture medium was quantified by ELISA. Both doxorubicin and thapsigargin induced a significant increase in cellular CRT expression by at least 4 fold (Figure 4b.9 (c, d)). This was significantly decreased by pre-incubation with TUDCA, although interestingly TUDCA alone did increase CRT expression. Both doxorubicin and thapsigargin also significantly increased secretion of CRT which was again significantly decreased by pre-treatment with TUDCA (Figure 4b.9 (a, b)). These data suggest that CRT expression is increased in ovarian cancer cells in response to ER stress and that following translocation of CRT to the cell surface some of the CRT remains associated with the external surface of the cell and some is secreted.



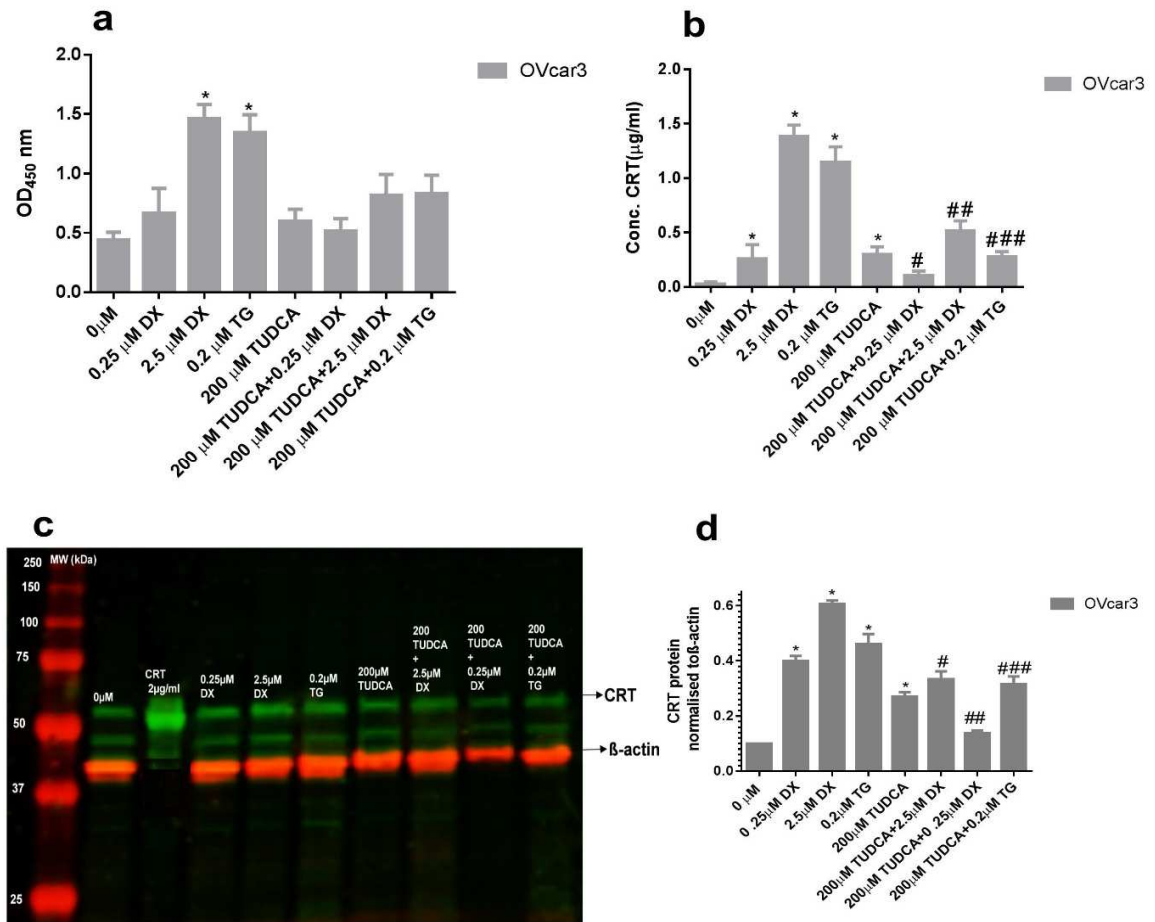


**Figure 4b.9. Effect of doxorubicin and thapsigargin on secretion and expression of CRT in OVcar3 cells.** Cells were treated with doxorubicin (DX, 0.25, 2.5 $\mu$ M), or thapsigargin (TG, 0.2 $\mu$ M) for 16 h  $\pm$  TUDCA. (200 $\mu$ M). The culture supernatant was collected for measurement of secreted CRT by ELISA and the cells were lysed and analysed by SDS-PAGE and western blotting to examine relative cellular expression of CRT. (a) and (b) ELISA of CRT release from OVcar3 cells - raw data showing mean optical density (OD) at 450nm from one experiment. (b) ELISA of CRT release from OVcar3 cells showing mean secreted concentrations calculated using a CRT standard curve - results from 6 independent experiments (c) Representative western blot of CRT expression in OVcar3 cells. (d) Densitometry plots of CRT protein expression relative to  $\beta$ -actin as the loading control. Data are mean  $\pm$  SD of 10 independent experiments. \* $p$  = 0.05 vs. control, #2.5 doxorubicin vs. 2.5  $\mu$ M+200  $\mu$ M TUDCA, ##0.25  $\mu$ M doxorubicin vs. 0.25  $\mu$ M doxorubicin+200  $\mu$ M TUDCA, ###0.2  $\mu$ M thapsigargin vs. 0.2  $\mu$ M thapsigargin+200  $\mu$ M TUDCA  $p$ =<0.02 for all.

#### **4.1. Discussion**

Apoptosis or programmed cell death is generally considered to be immunogenically silent since the dying cell contents are confined within undisrupted cell membrane-bound compartments that are efficiently cleared by phagocytes without inducing an adaptive immune response. However, it is now accepted that in certain circumstances cells dying by apoptosis can have immunogenic properties and thus trigger an adaptive immune response known as ICD. In the case of tumour cells undergoing ICD immune responses against cancer cell specific antigens or altered self-antigens can occur (Galluzzi et al., 2017). A critical aspect of ICD is surface expression of DAMPs which are required for an efficient immune response. As described in the Introduction these molecules are exposed by dying or stressed cells and are recognised by pattern recognition receptors (PRRs) on innate immune cells such as monocytes, macrophages and DCs. This interaction stimulates the activation and maturation of these cells, engaging the adaptive immune system (Matzinger, 2002) and facilitating recognition and destruction of a large number of tumour cells with minimal toxicity towards non-tumour cells.

Engagement of the adaptive immune system as cancer therapy raises the possibility that vaccine based anti-tumour therapies may be developed. This is particularly attractive for cancers that are difficult to treat such as ovarian cancer, which due to late diagnosis and a high rate of relapse, still has a 5 year survival of less than 50%.

It is now widely accepted that extracellular, surface bound CRT acts as a DAMP and has a key role in mediating ICD of tumour cells (Chaput et al., 2007) (Giglio et al., 2018). Thus, further understanding of the mechanisms involved in CRT exposure at the cell surface is required. A general consensus is that various chemical (anthracyclines, fatty acids) and physical (radiation) perturbations of tumour cells can lead to ER stress and redistribution of CRT from the ER to the cell surface (Molinari et al., 2011, Buoncervello et al., 2012). Doxorubicin can induce rapid translocation (within minutes) of CRT to the surface of pre-apoptotic cells (Obeid et al., 2007). It is proposed that this surface exposed CRT is subsequently recognised by DCs and induces immunogenic uptake of dying cancer cells by CD11c-positive DCs and ultimately tumour cell destruction by the host immune system (Son et al., 2017). Indeed doxorubicin has been shown to induce ICD (Hodge et al., 2013).

These studies suggest that therapeutic strategies designed to increase tumour cell surface CRT may aid cell destruction. An increase in extracellular, cell surface CRT could be induced by translocation of intracellular CRT from the ER or by binding of exogenously added CRT. The studies described in this chapter investigated both strategies to enhance surface levels of CRT on ovarian cancer cells.

The binding of exogenous CRT was studied using FITC-labelled protein and it could be seen that CRT bound to the surface of cancer cells even under resting cell culture conditions. This binding was significantly increased in all three ovarian cancer cell types studied, OVcar3, SKov3 and A2780, as well as FaDu pharyngeal carcinoma cells, following treatment with the ER stressors doxorubicin and thapsigargin. This suggests that the enhancement of CRT binding stimulated by these agents is a general response of cancer cells, although this could be tested further by examining other cell types. The results obtained agree with a recent report that both exogenous CRT and endogenous bind to ovarian cancer cells under stress conditions (Osman et al., 2017). The enhanced binding induced by doxorubicin and thapsigargin was associated with a decrease in cell viability and an increase in apoptotic and necrotic cells with increased mean FITC-CRT fluorescence observed on cells in all stages of cell death. This suggests that cell surface changes associated with cell death induced by these agents increases the ability of the cell surface to bind exogenous CRT.

One possible surface binding site for CRT is phosphatidylserine (PS), a membrane phospholipid that is transferred from its normal localisation, on the inner leaflet of the plasma membrane, to the outer leaflet during apoptosis. It has been reported that CRT binds PS with high affinity in a  $\text{Ca}^{2+}$ -dependent manner (Wijeyesakere et al., 2016) (Tarr et al., 2010b) and, since, as previously mentioned, measurement of early and late apoptosis by annexin V takes advantage of this PS externalisation it can be deduced that PS is present on the surface of the cells studied (Martin et al., 1995).

However, FITC-CRT also bound at high levels to necrotic cells and these do not express surface PS (as assessed by annexin V binding). This suggests that on these cells there is an alternative CRT binding site. Alternatively, it is possible that in necrotic cells the FITC-CRT can enter cells through the damaged membrane and bind to intracellular exposed PS; however this would seem unlikely due to the lack of annexin V staining in these cells. Additionally, it has been reported that CRT is released on

certain cancer cells treated with doxorubicin (e.g. mouse colon cancer cells) before PS is externally presented (Chaput et al., 2007) suggesting that PS may not be the CRT binding site on early apoptotic cells. However, the assay used here depends on PS/annexin V binding to distinguish apoptotic cells and so it is not possible to deduce whether very early apoptotic cells bind FITC-CRT.

Both thapsigargin and doxorubicin are known to induce ER stress, but by different modes of action. Thapsigargin inhibits calcium pumps leading to depletion of  $Ca^{2+}$  stores in the ER whereas doxorubicin induces ER stress (Panaretakis et al., 2009) and apoptosis by intercalating into a number of key DNA and RNA polymerases and altering the Bcl-2/Bax central checkpoint apoptosis pathways which are prevalent in different cancer cells (Reed, 2006). In order to examine whether the ER stress function of thapsigargin and doxorubicin was related to their ability to enhance exogenous CRT binding to ovarian cancer cells, TUDCA an effective ER stress-relieving drug was used. TUDCA partially protected ovarian cancer cells against both doxorubicin and thapsigargin induced cell toxicity and partially reduced FITC-CRT binding caused by these two agents. These data support the hypothesis that the degree of CRT binding is related to the cellular changes associated with apoptosis and necrosis in ovarian cancer cells.

The second part of these studies investigated the effect of doxorubicin and thapsigargin on translocation and externalisation of endogenous CRT. Again, both agents were significantly toxic and the increase in apoptotic and necrotic cells was accompanied by significantly increased cell surface exposure of CRT as assessed by the labelling of unpermeabilised cells with anti-CRT antibodies detected by fluorescence. CRT was detected by both flow cytometry and immunocytochemistry with similar results. Interestingly, control experiments using doxorubicin showed that the drug was not cytotoxic against non-cancer cells i.e. normal human endothelial cells. This lack of cell death was mirrored by a lack of enhanced surface CRT. These results suggest that in the cancer cells the externalization of CRT is associated with cell death. However, it is possible that doxorubicin does induce cell death in the non-tumour cells, but by an alternative mechanism that requires a greater time course for induction than the relatively short 16 hours studied here. For instance it has been reported that doxorubicin enhances apoptosis in a normal cells and some cancer cells

by a different mechanism. Endothelial cells and cardiomyocytes treated with 0.5  $\mu\text{M}$  doxorubicin for 72 hours showed increased apoptosis via a  $\text{H}_2\text{O}_2$ -mediated mechanism (Wang et al., 2004).

The observation that ovarian cells treated with doxorubicin and the ER stressors thapsigargin externalise endogenous CRT agrees with the existing literature in other cancer cell types. For example, doxorubicin and thapsigargin treated murine colon cancer cells had enhanced surface CRT (Obeid et al., 2007). Interestingly, a similar effect was observed in Jurkat T-lymphocytes treated with 4  $\mu\text{g}/\text{ml}$  doxorubicin for 4 hours. The doxorubicin enhanced surface translocation, but this was significantly inhibited in adherent cells engaged with integrin-mediated adhesion (Liu et al., 2016a). The authors suggest that integrins are able to reduce CRT translocation to the cell, suppressing ICD and adding complexity to the cellular environment required for doxorubicin to induce ICD. It has also been shown that other mediators can induce CRT translocation, for instance human ovarian cancer cell lines treated with nerve growth factor showed increased surface CRT (Vera et al., 2012) (Vera et al., 2017).

Since the data clearly indicated surface externalisation of CRT it was possible that this was the result of enhanced CRT expression rather than just a relocation of existing cellular CRT. Examination of this by western blotting indicated that both doxorubicin and thapsigargin increased CRT expression. This is in contrast to the results of (Liu et al., 2016a) who found that doxorubicin treatment of Jurkat T-lymphocytes resulted in a negligible change in total calreticulin. It is possible that the different cell types have differential responses to doxorubicin e.g. solid tumour vs suspension haematological cells.

The secretion of CRT from ovarian cancer cells in response to doxorubicin and thapsigargin was also studied. Both ER stressors induced significant levels of CRT release into the culture medium. This has been previously reported in A2780 ovarian cancer cells treated with 1  $\mu\text{M}$  of thapsigargin for 4 h (Vera et al., 2017). This suggests that dying cells (early, late apoptosis & necrotic), may be a source of exogenous CRT. If this CRT is able to bind to local dying cells, as suggested here, marking them for DC recognition then this may be an additional mechanism by which CRT can drive ICD. These findings highlight an important regulatory role of CRT that may be exploitable for cancer immunotherapy.

This is the first study that sought to determine whether TUDCA would inhibit cell death in tumour cells treated with doxorubicin and thapsigargin as pharmacological agents used to induce cell death. TUDCA alone was not cytotoxic, but TUDCA did partially, but significantly reduce cell death caused by both agents, suggesting that ER stress contributes to their induction of cell death in ovarian cancer cells. However, this protective effect was not complete. It is possible that doxorubicin and thapsigargin promote cell death through more than one pathway and that this second pathway is ER stress independent. Interestingly, TUDCA has also been reported to reduce tunicamycin, UV-irradiation 4- phenylbutyric acid-induced cell death in HepG2 human liver carcinoma cells via ER stress dependent and independent pathways (Uppala et al., 2017). Specifically, the authors noted a role for TUDCA inhibition of PARP (poly ADP-ribose polymerase) cleavage in the observed reduction in cell death. Additionally, they also noted that TUDCA alone was not cytotoxic, confirming the data presented here. It is also possible that the treatment conditions for TUDCA were not optimal. Although, the time and dose of TUDCA used were informed by the existing literature, further optimisation studies for the cell culture system used here could be carried out.

Importantly, the presented results also showed that the reduction in cell death induced by TUDCA was accompanied by a significant reduction in doxorubicin and thapsigargin induced exogenous CRT binding, CRT externalisation, total cellular CRT expression and CRT release in ovarian cancer cells. These data suggest that all of these functions are dependent on ER stress and/or cell death. Indeed, it has been reported that TUDCA impacts the PERK-eIF2 $\alpha$ -ATF4-CHOP arm of the UPR (Uppala et al., 2017) and that a number of these pathway components (e.g. PERK and eIF2 $\alpha$ ) are associated with ER stress influenced CRT translocation induced by thapsigargin and doxorubicin treatment of cancer cells (Martins et al., 2010).

These data demonstrate for the first time that doxorubicin and thapsigargin are able to induce secretion of CRT. CRT secretion has also been reported to be induced by thapsigargin in mouse embryonic fibroblasts, although interestingly the secreted CRT (or other secreted ER chaperones) did not contribute to induction of the innate immune response as assessed by phagocytic uptake of these fibroblasts (Peters and Raghavan, 2011).

## 4.2 Conclusion

It is thought that ICD of tumour cells is triggered when CRT is translocated to the cell surface of tumour cells where it acts as an 'eat-me' signal, enhancing phagocytic uptake of the cancer cells and consequently activation of the adaptive immune response (Gardai et al., 2005). The studies presented in this chapter show that agents that induce ER stress i.e. the cytotoxic anthracycline doxorubicin and thapsigargin, promoted cell death in ovarian cancer cells with an increase in early and late apoptotic and necrotic cells. This was associated with enhanced binding of exogenous CRT and surface externalisation of endogenous CRT as well as increased expression and cellular release of the protein. All of these cellular responses were significantly inhibited by TUDCA, an agent known to reduce ER stress by acting on components of the UPR pathway, suggesting that ER stress is at least partially responsible for the changes in CRT.

From these data it is possible to hypothesise that cytotoxic agents such as doxorubicin may act in complementary ways to induce ICD. Specifically, the CRT translocated to the cell surface may be supplemented with cell released CRT binding directly to the surface of both the immediate cell and its neighbours. This may enhance uptake by, and activation of, phagocytic cells such as DCs and thus the engagement of adaptive immunity which can act to clear multiple tumour cells. The results also raise the possibility that therapeutic strategies designed to increase extracellular CRT, either by induction of tumour cell lysis or exogenous application may be effective.

These findings highlight an important regulatory role of CRT that may be exploitable for cancer immunotherapy. The ability of tumour cells with enhanced surface CRT levels induced by endogenous translocation or exogenous application will be examined in chapter 5.

## **Chapter 5 Investigation into whether exogenous CRT or cancer cell expressing of surface CRT can induce maturation of DCs and subsequent activation of T-cells.**

### **5.1. Introduction**

As previously described immunogenic elimination of cancer cells by the host requires the innate immune system to recognise tumour antigens as non-self. Specifically, the priming of adaptive immune cells e.g. T-cells is required, which then act against cells displaying the antigens. A crucial step in this process is the presentation of the tumour antigens on the surface of APCs, with DCs being the most versatile and efficient of these. Dendritic cells are found in two main states, immature dendritic cells (imDCs) which are the normal steady state cells, and mature DCs (mDCs) which are phenotypically and functionally different and are able to present antigens to, and activate, T-lymphocytes (Dudek et al., 2013). Specifically imDCs recognise non-self-cells and internalise their antigens which triggers the maturation process. During this these antigens are processed and presented at the cell surface in association with MHC class I and II molecules, the DCs migrate to the lymph nodes and prime naïve T cells for their cytotoxic response against these antigens.

The major functional changes between imDCs and mDCs are expression of chemokine receptors that allow the DCs to become responsive to chemokines that facilitate their migration to the lymph tissue (Morelli et al., 2001). Additionally, the DCs start to secrete immunomodulatory cytokines such as IL17, IFN $\gamma$ , IL4, IL5, IL10 and TNF alpha which allow them to activate the T-lymphocytes. The T cells become cloned via mitosis, and differentiate to mature cells that help regulate and suppress the immune system (Morelli et al., 2001). DC phenotype changes include surface up-regulation of CD80, CD83, CD86 and MHC II, and the secretion of the cytokines interleukin IL-2, IL-12 and granulocyte-macrophage-colony-stimulating factor (GM-CSF) (Srivastava, 2002). Thus, imDCs and mDCs can be distinguished from each other based on their expression of these specific cell surface markers. In particular, CD80, CD83, CD86, CD11C and HLA-DR all have increased expression levels on mDCs compared to imDCs (Table 5.1).



Marker	Description
<b>CD11c</b>	CD11c is an integrin, alpha X (complement component 3 receptor 4 subunits). It is a transmembrane protein expressed exclusively on dendritic cells and monocytes.
<b>CD80</b>	CD80 is expressed on DCs. It is ligand for CD 28 and CTLA-4 on the T cell surface.
<b>CD83</b>	CD83 is expressed on DCs and plays an important role in antigen presenting cells and T- cell activation.
<b>CD86</b>	CD86 (also known as CD86 and B7-2) is expressed on APC and is a co-stimulatory molecule for T-cell activation. It is the ligand for CD28 and CD152 (CTLA-4).
<b>CD14</b>	CD14 is highly expressed on monocytes and macrophages and has a high affinity for LPS.
<b>HLA-DR</b>	HLA-DR is an MHC-II surface molecule expressed on B cells, activated T cells, monocytes, DCs and other non-professional APCs and is involved in antigen presentation to TCR complex.

**Table 5.1. Major cell surface markers on mature DCs**

The activation of T- cells by mDCs is a critical step in cell mediated immunity (Figure 5.1). T-lymphocyte production occurs in bone marrow and the cells migrate to the thymus to complete their maturation. The majority of T-cells are then found in the circulation and the lymph nodes (Germain, 2002). Most T cells are considered naïve (immature CD8+ cells) and have the potential to become cytotoxic T-cells. When activated, cells within the lymph nodes have the ability to recognise different pathogens via presentation of their antigens on the surface of migrated mDCs (Geginat et al., 2015). Once in the lymph node, the antigenic cargo of the DCs, presented via MHC molecules, is recognised by naïve T-cells which then undergo an activation period to become cytotoxic T cells. This recognition occurs initially via the T-cell receptor (TCR) on the T-cell, which engages with the MHC complex on the mDC (Tseng et al., 2013). T cell expressed CD28 interaction with co-stimulatory molecules (CD80 and CD86) on DCs leads to synthesis of interleukins (e.g.IL2 and IL6) which drives proliferation and differentiation of the T-cells, ultimately leading to their clonal expansion (Pennock et al., 2013). CD8 is a surface glycoprotein which is primarily expressed on cytotoxic T cells and acts a co-receptor for the TCR. An individual T-cell generally carries between 10,000 and 30,000 identical copies of the CD8 molecule

which functionally is usually found as dimer, usually with one CD8- alpha ( $\alpha$ ) and one CD8 - beta ( $\beta$ ) chain.

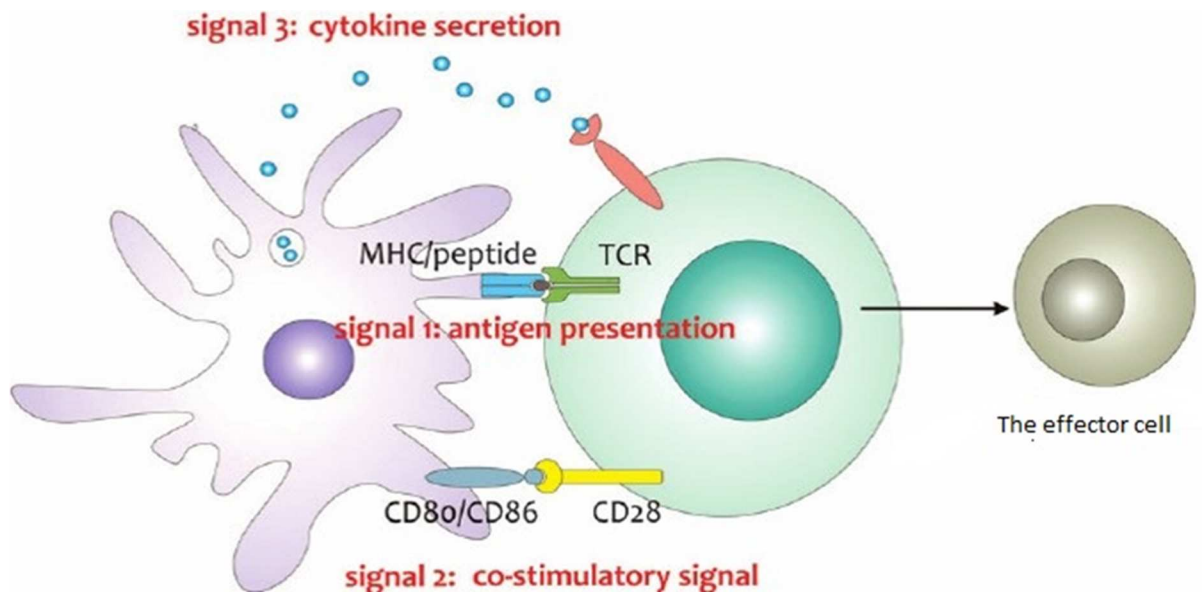


**Figure 5.1. Schematic representation of the major signals involved in activating T-cell responses (TCR = T- cell receptor).** T-cell activation requires three signal inputs: stimulation of the T- cell receptor (TCR) by MHC/peptide complexes on antigen presenting cells (APCs) e.g. dendritic cells (signal 1); interactions between co-stimulatory ligands on the APC and CD28 on the T cell which initiate T cell proliferation (signal 2); secretion of cytokines which contribute to regulation of the immune response (signal 3) (De Koker et al., 2011).

The surface of imDCs has numerous cytoplasmic processes which increase surface area, enhancing contact with non-self-cells or pathogens which the DCs can then recognise through their expression of pattern recognition receptors (PRRs). These receptors recognise conserved molecular patterns on the non-self-cell or pathogen i.e. pathogen- or damage-associated molecular patterns (PAMPs and DAMPs) (Gold et al., 2015).

As discussed in Chapter 1 (Introduction) cell surface exposed CRT acts a DAMP during ICD (Kumar et al., 2011). It is translocated to the cell surface of apoptotic and necrotic cells under different circumstances such as UVB radiation, anthracyclines,

oxaliplatin, and photodynamic therapy (Kepp et al., 2014) and can allow these cells to communicate with APCs (Feng et al., 2018). It has been reported that CRT on the surface of dying cells during irradiation and chemotherapy such as anthracyclines can induce DC uptake of tumour cells e.g. colon cancer cells (Obeid et al., 2007); inducing DC maturation and ultimately an ICD response. This interaction between CRT and imDCs enhances signalling events involved in the maturation of DCs (Kuppner et al., 2001). Thus, CRT has the ability to activate the adaptive immune system through DCs. It has also been reported that CRT additionally acts as an “eat-me” signal on apoptotic cells, lead to initiation of phagocytosis, which promotes secretion of inflammatory cytokines (e.g., IL-12) (Pandya et al., 2019).

Previous studies have shown that it is possible to study *in vitro* maturation of imDCs into mDCs using the markers described above to distinguish between the two cell types (Han et al., 2009). Two major sources of imDCs have been described in the literature to study *in vitro* maturation (a) imDCs derived from monocytes directly isolated from peripheral blood and (b) imDCs derived from THP-1 cells, an immortalised cell line derived from the peripheral blood of a childhood case of acute monocytic leukaemia (Bosshart and Heinzelmann, 2016). Differences have been found in the responses of these two preparations, in particular it has been noted that responses in monocyte-derived DCs are more variable, presumably reflecting the heterogeneity in the donor population (Patente et al., 2018).

Previous chapters of this thesis have shown that ovarian cancer cells treated with agents that induce ER stress express endogenous CRT on their cell surface and also that exogenously added CRT binds to the surface of ovarian cancer cells. This highlights two strategies by which CRT levels on the surface of ovarian cancer cells can be enhanced. Since CRT has been shown to act as a DAMP, this raises the possibility that artificially raising CRT levels on the surface of ovarian cancer cells could activate DCs, inducing DC maturation and subsequent T-cell proliferation. This could be a promising cancer therapy for ovarian cancers. Indeed a similar strategy has been utilised using the cancer antigen New York esophageal squamous cell carcinoma 1 (NY-ESO-1) which has been shown to induce the immune system in many malignancies. NY-ESO-1 is expressed on various different kinds of cancers including neuroblastoma, myeloma, metastatic melanoma, synovial sarcoma, bladder

cancer, oesophageal cancer, hepatocellular cancer, head and neck cancer, non-small cell lung cancer, ovarian cancer, prostate cancer, and breast cancer (Jungbluth et al., 2001, Sharma et al., 2003). In recent years, the first NY-ESO-1 cancer vaccine trials have been carried out and show its ability to activate T- cytotoxic cells (Thomas et al., 2018). Thus, cancer immunotherapy can be summarised as the treatment of cancer by promoting and boosting the immune response (Mellman et al., 2011) and theoretically could be an important strategy in the fight against cancer.

## 5.2. Aims

The overall objective of this chapter was to examine whether EOC cells expressing CRT could enhance DC maturation and subsequent T-cell proliferation in an *in vitro* experimental model. Ovarian cancer cells were treated with agents shown in Chapter 4 to increase CRT surface exposure. The ability of these treated cells to induce imDC cell maturation was then examined initially in imDCs derived from THP-1 cells to develop the protocol and then imDCs derived from freshly isolated peripheral blood monocytes. DC maturation was assessed by expression of key markers as described above. The ability of matured DCs to induce T-cell proliferation was then assessed in freshly isolated human T-cells from peripheral blood.

Therefore the specific aims of this chapter were:

- To establish a technique to isolate CD14+ monocytes from peripheral blood samples from healthy blood donors
- To establish a technique to derive imDCs *in vitro* from THP-1 cells and isolated CD14+ monocytes.
- To establish a technique to assess maturation of imDCs to mDCs *in vitro*
- To establish a technique to isolate CD8+ T cells from peripheral blood samples from healthy blood donors
- To investigate whether ovarian cancer cells pre-treated with doxorubicin (and expressing surface CRT) induce DC maturation
- To examine whether exogenous CRT can induce DC cell maturation.
- To study the potential of the DCs matured as above to induce T-cell proliferation
- To study the potential of CRT to active and induce proliferation of T- cells.

### **5.3. Methods**

#### **5.3.1. Cell culture**

THP-1 and OVcar3 ovarian cancer cells were cultured as described in Chapter 2 section (2.3.1.) and (2.3.2.). Where indicated OVcar3 cells were treated with 0.5, 1, 2.5  $\mu\text{M}$  doxorubicin for 16 h and harvested and co-incubated with imDCs. THP-1 cells were treated as indicated to induce differentiation to imDCs.

#### **5.3.2. Isolation of human blood mononuclear cells (Protocol 1).**

A CD14<sup>+</sup> monocyte magnetic bead separation technique was used to isolate monocytes from other leukocytes obtained from peripheral blood samples by depleting a mixed cell population of unwanted leukocyte populations i.e. negative selection. Briefly, 50 ml of blood was collected from healthy donors into EDTA vacutainer tubes after obtaining written informed consent (UEMS ethics approval number 18102/152 $\Delta$ 1). After centrifugation to collect the buffy coat the resulting leukocyte preparation was enriched for monocytes using a magnetic bead separation technique.

1. 2 volumes of room temperature PBS (without  $\text{Ca}^{2+}$  and  $\text{Mg}^{2+}$ , PBS-) was added to one volume of the blood. 15 ml Ficoll-Hypaque was added to new 50 ml centrifuge tubes and 30 ml of the diluted blood was carefully overlaid on the top. Tubes were centrifuged for 30 minutes at 900 x g at room temperature without the brake. Using a sterile transfer pipette all but 5 ml of the supernatant was removed, and kept in a separate 50 ml tube. The remaining 5 ml were vacuum aspirated, thus removing the upper layer containing most of the platelets. This was discarded.
2. Using a sterile transfer pipette the cloudy interface (buffy coat) between the plasma and red blood cells was removed and placed in new 50 ml centrifuge tubes. Cells were washed by adding 3 volumes of PBS and centrifuging for 15 minutes at 500 x g at room temperature. After removing the supernatant, a new wash was done with chilled PBS and centrifuging at 4°C. (This discarded most of the platelets and remaining Ficoll).
3. 5 ml of sterile NaCl (0.2% w/v) were added to lyse residual red blood cells. After 3 minutes, 20 ml of chilled PBS- with 2mM EDTA (PBS-E) were added and the wash repeated. Cells were resuspended in 20 ml chilled PBS-E and counted at a

100x dilution using trypan-blue, (10  $\mu$ l of cell suspension mixed with 10  $\mu$ l of trypan blue).

4. After this the cells were enriched for monocytes using the Monocyte Isolation Kit II (Miltenyi Biotec). The cell suspension was initially filtered to remove cell aggregates before starting the magnetic-activated cell sorting (MACS) procedure.
  - Cells were resuspended in 40  $\mu$ L MACS-Buffer (PBS [100 ml] with 0.5% (w/v) BSA) and 2mM EDTA) per  $10^7$  white cells.
  - 10  $\mu$ L of FcR Blocking Reagent was added per  $10^7$  total cells.
  - 10  $\mu$ L of Pan Monocyte Biotin-Antibody Cocktail, human was then added per  $10^7$  total cells to label non-CD14+ monocytes.
  - Following complete mixing the cells were incubated for 5 minutes at 4°C.
  - 30  $\mu$ L of MACS-Buffer was added per  $10^7$  total cells. 20  $\mu$ L of Anti-Biotin Microbeads was added of per  $10^7$  total cells which were then mixed well and incubated for a further 10 minutes at 4°C. Cells were then washed by adding 2 ml of buffer per  $10^7$  cells and centrifuging at 300xg for 10 minutes.
  - The supernatant was discarded completely and the cells re-suspended, up to  $10^8$  cells, in 500  $\mu$ L of Macs Buffer. A separation LS column was then placed in the magnetic field of a MAC separator column (Molinari et al., 2011)
  - The column was prepared by rinsing with 3 ml of Macs Buffer to extract bubbles. The cell suspension was then applied onto the column and the unlabeled cells (i.e. those which the antibody coated magnetic beads (monocytes) did not attach to) passed through, were collected, and the column washed with 3 x 3 ml of Macs Buffer with every wash flow-through collected. This constituted the CD14+positive cells.
  - The column was removed from the separator and placed on a centrifuge tube. Buffer was pipetted onto the column and the magnetically labeled non-monocytes were flushed out by firmly pushing the plunger into the column.
5. To confirm monocyte enrichment cells were stained with Diffquik as described in Chapter 4 and analysed by flow cytometry using antibodies against the monocyte markers CD14 and CD16 as described below (section 5.5.).

### **5.3.3. Generation of mDCs from monocytes (Protocol 2)**

#### **A- Generating imDCs from isolated peripheral monocytes.**

imDCs were generated from isolated monocytes by 7 day treatment with IL4 and GM-CSF following the protocol of (Berges et al., 2005).

1. Monocytes were seeded in 6 well plates at  $0.3 - 0.5 \times 10^6/\text{ml}$  in 2 mls of cell culture medium supplemented with 500U/ml IL-4 + 800 U/ml GM-CSF to induce differentiation.
2. Cells were incubated in a tissue culture incubator at 37°C with 5% CO<sub>2</sub>.
3. 850 µl of medium from the culture was removed at day 3 and centrifuged at 300 x g for 5 minutes at 4°C. The supernatant was aspirated and the pellet resuspended in 1 ml of cell culture medium containing 2x concentration of 500U/ml IL-4 + 800 U/ml GM-CSF i.e. 1000U/ml IL-4 + 1600 U/ml GM-CSF. This suspension was added back to the culture, diluting the GM-CSF and IL-4 to the original concentration.
4. Step 3 was repeated at day 6.
5. At 7 days cells were stained for markers of immature dendritic cells (increased CD11c, HLA-DR and CD83 compared with monocytes (Johansson et al., 2008), using flow cytometry as in section (5.5) below.

#### **B. Generation of imDCs from THP-1 cells**

THP-1 cells were harvested by centrifugation, resuspended in culture medium supplemented with 10% (v/v) FCS at a concentration of  $2 \times 10^5$  cells/ml, and transferred in a final volume of 14 ml into 75 cm<sup>2</sup> tissue culture flasks. To induce differentiation into imDCs, IL-4 (500 IU/ml) and GM-CSF (800 IU/ml) were added as above. Cells were cultured for 7 days with change of media every 2 days by substituting half of the media with fresh media containing fresh cytokines.

### **C. Generation of mDCs from imDCs**

Lipopolysaccharide (LPS) is known to activate antigen-presenting cells. Thus, LPS was added at 1 µg /ml as a positive control to induce maturation of imDCs using the protocol of (Sim et al., 2016). imDCs were cultured with LPS for a further 4 days (i.e. total of 11 from initiation of monocyte differentiation with GM-CSF and IL4). mDCs were harvested by flushing the culture dish with PBS-E. Only non-adherent cells were harvested. Maturation of DCs was assessed by surface expression of markers of maturation i.e. CD14, CD83, CD11c, CD80, HLA-DR and CD86 by flow cytometry.

#### **5.3.4. Co-culture of imDCs with doxorubicin (DX) pre-treated OVcar3 cells or purified CRT (see Figure 5.2).**

Additionally:

1. The effect of exogenous CRT alone to induce imDC maturation was examined by culture of imDCs with 0.5, 1, 2.5 µg/ml CRT for 4 days. As a positive control, 1µg/ml LPS was added as above.
2. The effect of doxorubicin-treated OVcar3 cells on DC maturation was also examined. OVcar3 cells were treated with varying concentrations of doxorubicin (0.25, 1, 2.5µM) for 16h (as determined in chapter 4) to ensure surface exposure of CRT and then washed three times with PBS to remove the doxorubicin. OVcar3 cells were then co-cultured with imDCs at a ratio of 1:1 in RPMI 1640 supplemented with GM-CSF, IL-4 (as above) and 10% (v/v) FBS for 4 days. As a control, imDCs were co-cultured with untreated OVcar3 cells. Maturation of DCs was assessed by surface expression of markers of maturation i.e. CD14, CD83, CD11c, CD80, HLA-DR and CD86 by flow cytometry. The OVcar3 cells were stained with an antibody against epithelial cell adhesion molecule (EpCAM) which is highly expressed on ovarian cancer cells (Nunna et al., 2014). i.e. anti-EpCAM CY-5 (1:50 dilution). This allowed these cells to be gated out of the analysis (see section 5.9.). For all antibodies cells were incubated for 30 min in the dark at room temperature, washed once with PBS and analysed by flow cytometry.
3. Control experiments to confirm that OVCar3 cells did not express DC markers were carried out by incubating OVCar3 cells with anti-EpCAM CY-5 and each of anti-



CD14-FITC, anti-CD83-PE, PE anti-human CD11c, PE anti-human CD80, PE anti-human CD83, anti-HLA-DR-PE and anti-CD86-PE. Cells were incubated for 30 min at room temperature and expression of EpCAM and DCs markers were analysed by flow cytometry (see section 5.9.). Similarly, DCs were stained with EpCAM to confirm that they did not express this marker which would result in them being gated out of the analysis.

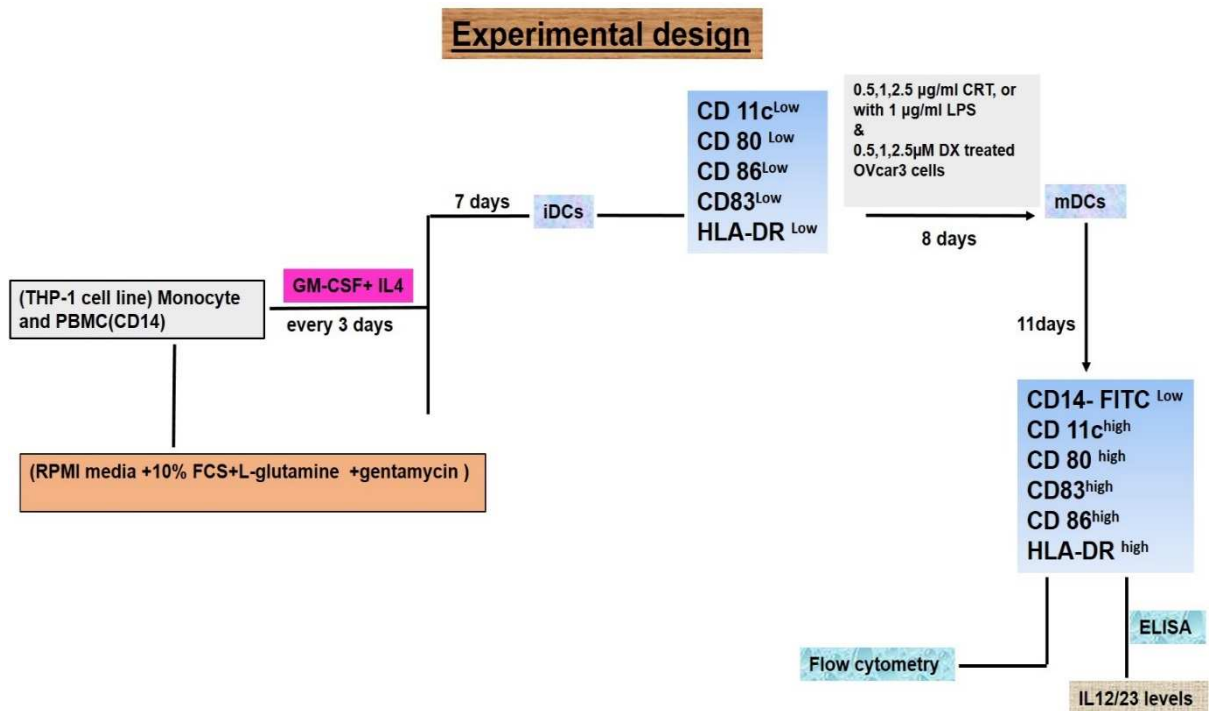


**Figure 5.2. Schematic diagram describing the experimental design of treatments potentially inducing DC maturation.** imDCs were generated from THP-1 cells or isolated monocytes by 7-day treatment with IL-4 and GM-CSF. At day 7, cells were stained for markers of immature dendritic cells CD11c, HLA-DR and CD83, CD80, CD86 (compared with monocytes). imDCs were then cultured for a further 4 days with LPS (positive control), 0.5, 1, 2.5 µg/ml CRT or OVcar3 previously treated with varying concentrations of doxorubicin (DX, 0.25, 1, 2.5µM) for 16h to ensure surface exposure of CRT. Maturation of DCs was assessed by surface expression of markers of maturation i.e. CD14, CD83, CD11c, CD80, HLA-DR and CD86 by flow cytometry and ELISA for the measurement of secreted IL-12, IL-23.

### **5.3.5. ELISA protocol**

Cell culture supernatants were collected for the measurement of secreted IL-12, IL-23 by ELISA since these cytokines have been reported to be secreted by DCs as they mature (Mayordomo et al., 2018). Supernatants were analysed for IL12/23 using a commercially available 12/23 (p40) ELISA MAX™ kit as described in Chapter 2.

### **5.3.6. Isolation of human T lymphocytes**

Human T cells were isolated by negative selection from whole blood using a magnetic bead CD8+ T Cell Isolation Kit (Miltenyi Biotec).

1. Human peripheral blood was obtained from healthy donors as described in section 5.3.2.
2. 3 ml of room temperature polymorph density gradient media was pipetted into an 8 ml round-bottom polystyrene tube. Gently, 3 ml of whole blood was added on top of the polymorph media to avoid mixing.
3. The tubes were centrifuged at 500 x g for 45 minutes at room temperature.
4. Following the centrifugation, the peripheral blood mononuclear cells (PBMC) separated from other blood components into the top cell layer appearing, from the top down, as the first cloudy band.
5. Carefully, the plasma was removed from above the PBMC layer, and a P1000 micropipette was used to transfer the PBMC layer to a fresh centrifuge tube.
  - The PBMCs were washed twice with PBS, centrifuging cells at 500g for 5 minutes each time, and then cells were counted. The cell pellet was then resuspended in 40 µL of MACS- buffer per 10<sup>7</sup> total cells.
  - 10 µL of Biotin-Antibody Cocktail was added of per 10<sup>7</sup> total cells, mixed well and the cells incubated for 5 minutes at 4°C.
  - 30 µL MACS-buffer was added of per 10<sup>7</sup> total cells.
  - 20 µL of CD8+ T Cell Microbeads Cocktail was added per 10<sup>7</sup> total cells then mixed well and incubated for 10 minutes at 4°C.
6. Labelled cells were separated using Miltenyi LS separation columns.

- The LS Column was placed in the magnetic field of a MACS separator. The columns were rinsed with 3 ml of MACS-buffer and the cell suspension was applied onto the column. Flow-through containing unlabelled cells was collected, representing the enriched CD8+T cells.
- 3 ml of buffer was washed through the column and the flow through again collected and added to the flow-through previously collected.
- Purity of the T cell population was assessed by flow cytometry using anti-CD8-FITC and anti-CD3-APC

### **5.3.7. Examination of T-cell activation by mDCs (see Figure 5.3).**

T cell activation under a range of experimental conditions was assessed by measurement of proliferation in which cells were fluorescently labelled and cell divisions were followed by assessing subsequent labelling of daughter cells using flow cytometry. T-cells were labelled with a Cell Trace carboxyfluorescein succinimidyl ester (CFSE) cell proliferation kit according to the manufacturer's protocol (Invitrogen). Briefly, harvested T cells were stained with 2.5  $\mu$ M CFSE in 0.1% w/v BSA/PBS for 10 minutes at 37°C. Subsequently, T cells were incubated in fresh medium for 10 minutes on ice and excess dye was removed by 3 washes. DCs matured as indicated (or relevant controls) were harvested, washed once, resuspended at a density of  $1 \times 10^6$  cells/ml in RPMI 1640 with 10% (v/v) FCS, 500 U/ml GM-CSF and 500 U/ml IL-4, and plated at the indicated ratios in round-bottom 96-well plates in the presence of  $1 \times 10^5$  CFSE-labelled T-cells/well. DC-T cell co-cultures were incubated for 5 days at 37°C in a humidified 5% CO<sub>2</sub> incubator. At day 5, cells were harvested and an additional staining were performed with anti-CD3-PerCP-Cyanine5.5 for 30 minutes at 4°C and the cells were analysed by flow cytometry to examine the CFSE-staining pattern. Cells were gated on CD3-positivity (to gate out the mDCs) since it is expressed almost exclusively on mature T cells.

### **5.3.8. Treatment of T cells with human T-activator CD3/CD28 Dynabeads.**

Since CD3 and CD28 are essential co-stimulatory signals for T cell expansion (Li and Kurlander, 2010) antiCD3/anti-CD28 coated magnetic beads were also incubated with freshly isolated T cells as a positive control for cell expansion (Figure 5.4).

#### **Dynabead preparation.**

Magnetic Dynabeads coated with anti-CD3/anti-CD28 (Invitrogen) were resuspended in the vial by thorough mixing and the desired volume of Dynabeads was transferred to a fresh tube and washed well with 1ml of MACS-buffer. The tube was then placed on a magnet for 1 minute and the supernatant discarded. The tube was removed from the magnet and the washed Dynabeads resuspended in the same volume of culture medium as the initial volume of Dynabeads taken from the vial.

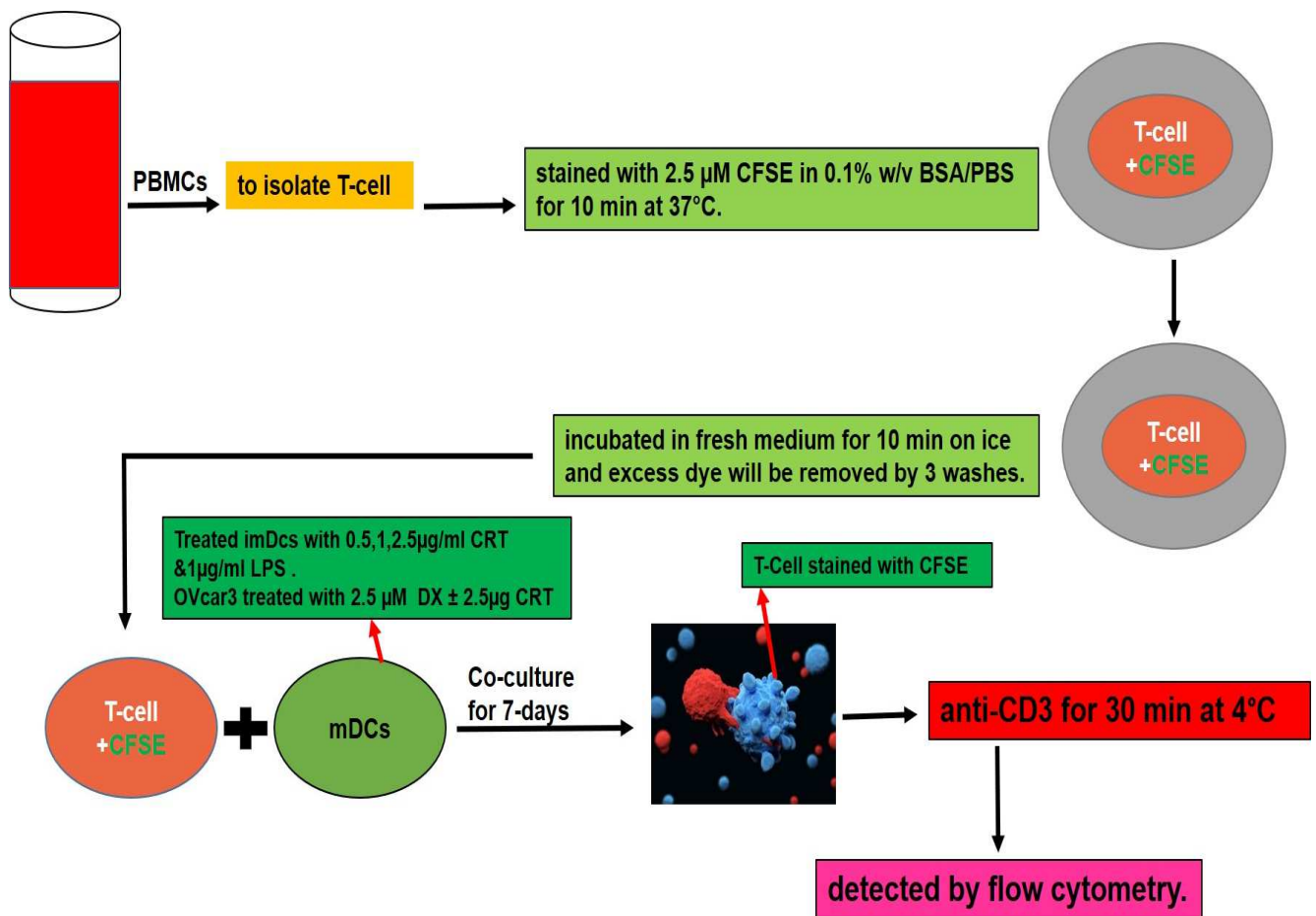


**Figure 5.3. Schematic diagram describing the experimental design of T-cell isolation and activation/proliferation as assessed by CFSE staining.** T-cells harvested from peripheral blood mononuclear cells (PBMCs) were stained with carboxyfluorescein succinimidyl ester (CFSE) to allow subsequent assessment of cell proliferation. Subsequently, T-cells were incubated with mature dendritic cells (mDCs) derived from iDCs (immature dendritic cells) treated with either 0.5, 1, or 2.5 μg/ml of CRT and 1 μg/ml LPS; OVCar3 pre-treated with 2.5 μg/ml doxorubicin (DX) or OVcar3 pre-treated with 2.5 μg/ml CRT to induce maturation. mDC-T cell co-cultures were incubated for 5 days, cells harvested, and an additional staining performed with anti-CD3-PerCP-Cy5.5 before flow cytometry analysis to examine the CFSE-staining pattern. Cells were gated on CD3-positivity (to gate out the mDCs) since it is expressed almost exclusively on mature T-cells.

### 5.3.9. Activation of human T cells with CD3/CD28 T-activator Dynabeads.

1.  $8 \times 10^4$  purified T cells in 100–200  $\mu\text{L}$  medium were placed in a 96-well tissue culture plate.
2. 2  $\mu\text{L}$  of pre-washed and resuspended Dynabeads was added to obtain a bead-to-cell ratio of 1:1 and cells incubated in a humidified  $\text{CO}_2$  incubator at  $37^\circ\text{C}$ , according to specific experimental requirements.
3. The activated T cells were harvested and used directly for further analysis.
4. For flow cytometry the beads were removed prior to staining by placing the tube on a magnet for 1–2 min to separate the beads from the solution. The supernatant containing the cells was then transferred to a fresh tube for analysis.

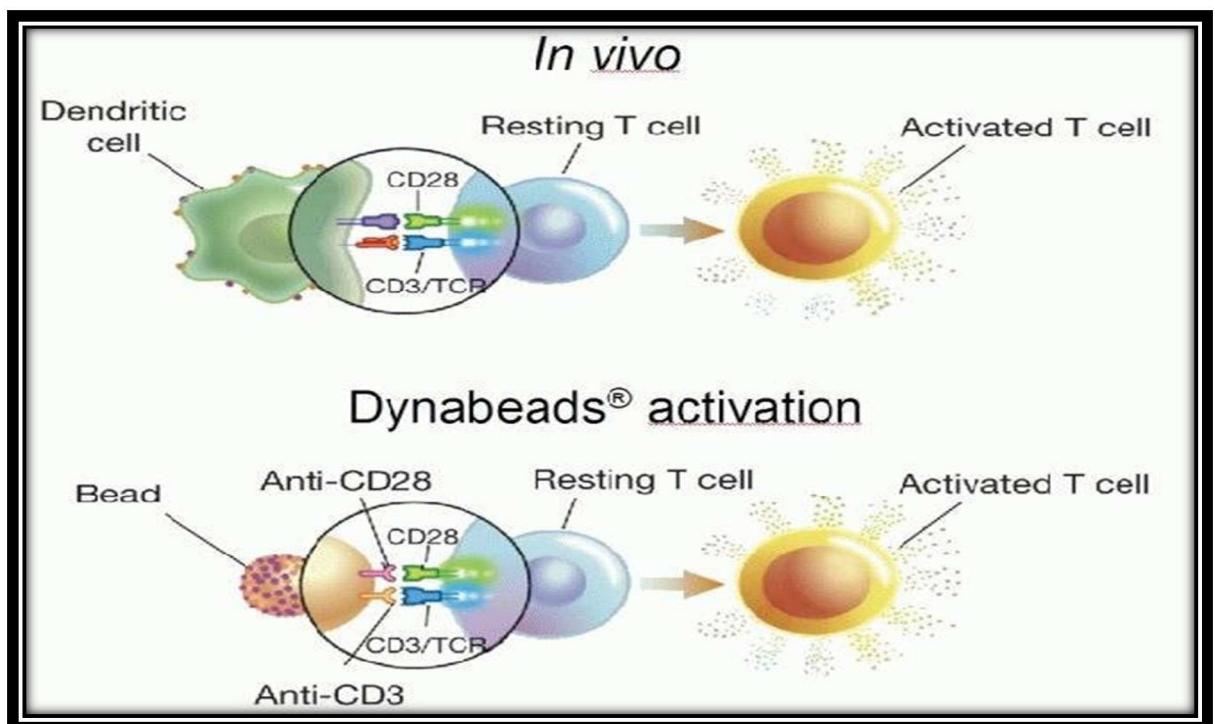


Figure 5.4. Diagram indicating the mechanism by which T cell expansion activated by anti-CD3/anti-CD28 coated Dynabeads (beads) mimics T-cell activation *in vivo* by antigen presenting cells dendritic cells.

### **5.3.10. Flow cytometry**

All flow cytometry was carried out using a Guava flow cytometer instrument (Millipore, Hertfordshire, UK) as described in Chapter 2 (Materials and Methods)

#### **Characterisation of isolated monocytes**

Isolated monocytes were fluorescently stained with Alexa Fluor® 488 anti-human CD14 antibody, PE anti-human CD16 antibody. The live cell population was gated on an FSC-A vs SSC-A plot, based on size and granularity (complexity).

#### **Cell surface marker characterization of imDCs and mDCs**

1. DCs were detached from the culture dish by pipetting, washed once with PBS/EDTA and resuspended at a concentration of  $1 \times 10^6$  cells per 100  $\mu$ l of staining buffer in 1.5 ml micro centrifuge tubes.
2. For flow cytometric analysis, 5 $\mu$ l of fluorescently-labelled monoclonal antibodies against cell surface markers were added to separate cell aliquots i.e. PE-anti-human CD11c, PE-anti-human CD80, PE- anti-human CD83, PE anti-human CD86, PE anti-human HLA-DR, Alexa Fluor 488-anti CD14.
3. Cells were incubated in the dark for 30 minutes at 4°C. Isotype-matched Alexa Fluor® 488 Mouse IgG1,  $\kappa$  Isotype Ctrl (FC), PE Mouse IgG1,  $\kappa$  Isotype Ctrl (FC), PE Mouse IgG2b,  $\kappa$  Isotype Ctrl antibodies were used as isotype controls (Table 5.2). Unstained cells were also analysed as a negative control.
4. Levels of surface marker expression were analysed using flow cytometry.

#### **Analysis of maturation of DCs incubated with doxorubicin treated ovarian cancer cells.**

The experiments examining the effect of doxorubicin treated OVCar3 cells on DC maturation involved a two cell type culture model i.e. DCs and OVCar3 and thus the OVCar3 cells were stained with anti-EpCAM CY-5 to detect EpCAM which is highly expressed on ovarian cancer cells, allowing these cells to be gated out of the analysis. Additional control experiments were carried out to ensure the reliability of this method.

These were (1) confirmation that OVcar3 cells did not express DC surface markers confirmation (2) confirmation that DCs did not express EpCAM.

Markers	Dilution factors	Isotype controls	Dilution factors
Alexa Fluor® 488 anti-human CD14 Antibody	1:50	Alexa Fluor® 488 Mouse IgG1, κ Isotype Ctrl (FC) Antibody	1:20
PE anti-human CD11c Antibody	1:50	PE Mouse IgG1, κ Isotype Ctrl (FC) Antibody	1:20
PE anti-human CD80 Antibody	1:50	PE Mouse IgG1, κ Isotype Ctrl (FC) Antibody	1:20
PE anti-human CD83 Antibody	1:25	PE Mouse IgG1, κ Isotype Ctrl (FC) Antibody	1:20
PE anti-human CD86 Antibody	1:50	PE Mouse IgG1, κ Isotype Ctrl (FC) Antibody	1:20
PE anti-human HLA-DR Antibody	1:100	PE Mouse IgG2b, κ Isotype Ctrl Antibody	1:11

**Table 5.2. Details of the antibodies and the isotype controls used for characterisation of imDCs & mDCs.**

### 5.3.11. Statistical analysis

Statistical analyses were carried out using GraphPad PRISM software 7 and Microsoft Office Excel. The Mann Whitney U test was used to test the significance of variables between the two groups.  $P < 0.05$  was considered statistically significant. The graphical representation of the data is mean  $\pm$  standard deviation (SD).

## 5.4. Results

### 5.4.1. Generation of imDCs from the human monocytic THP-1 cell line.

Human monocytic THP-1 cells (Figure 5.5) were differentiated to imDCs by incubation with GM-CSF and IL-4 for 7 days and levels of surface markers of differentiation were assessed by flow cytometry. It has been reported that imDC have relatively high surface expression of CD11c, HLA-DR and CD83 compared with monocytes (Johansson et al., 2008).



Figure 5.6 demonstrates that at day 7, THP-1 cells showed increased expression of all surface markers studied with this reaching significance for CD11c, CD86 and HLA-DR markers ( $59.4 \pm 7.592$  vs  $17.94 \pm 14.27$ ;  $65.03 \pm 18.49$  vs  $31.07 \pm 15.23$  and  $65.03 \pm 18.49$  vs) respectively (figure 5.6 c). These data indicate that THP-1 monocytes can be differentiated into cells expressing markers of imDCs.

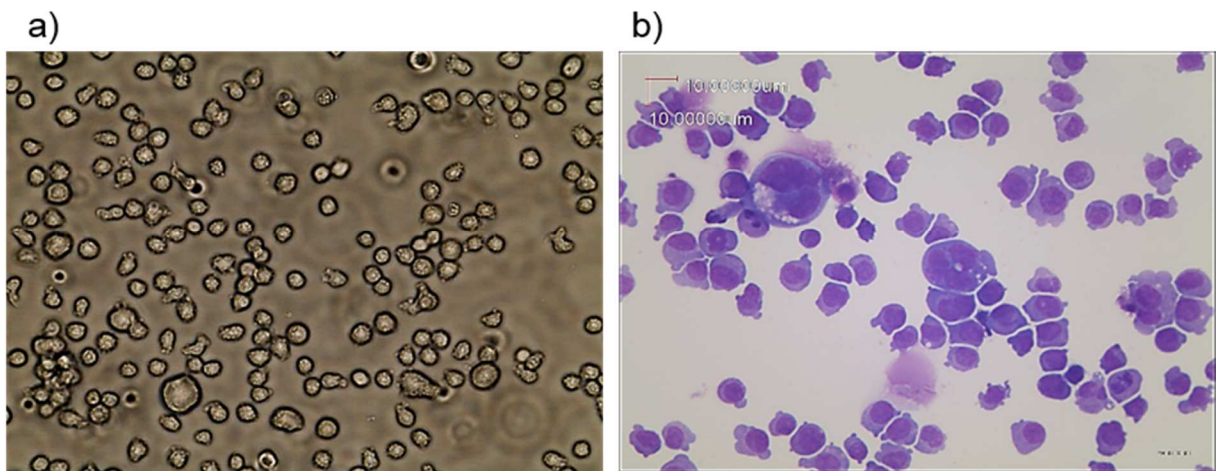
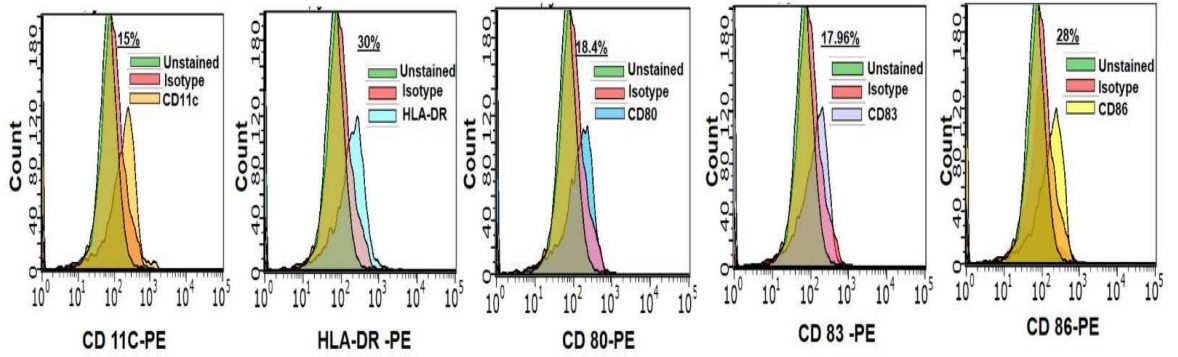


**Figure 5.5. Morphology of THP-1 cells at 0 day.** (a) The THP-1 cell line observed under bright field microscopy, (b) THP-1 cells observed under light microscope following staining by Diff-Quick stain at magnification of 40x.

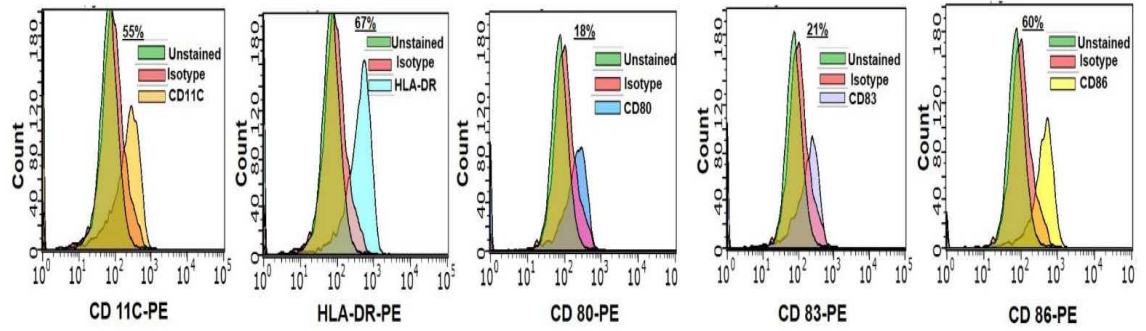
a)

0-Day



b)

7-Day



c)

Markers	THP-1 cells at 0-day	THP-1 (imDCs) at 7-day	
CD11c	17.94 ± 14.27	59.4 ± 7.592	(##)
HLA-DR	33.2 ± 5.357	58.73 ± 10.17	(##)
CD 80	21.22 ± 5.267	40.68 ± 22.58	(n.s.)
CD 83	31.01 ± 15.79	51.02 ± 21.49	(n.s.)
CD 86	31.07 ± 15.23	65.03 ± 18.49	(##)

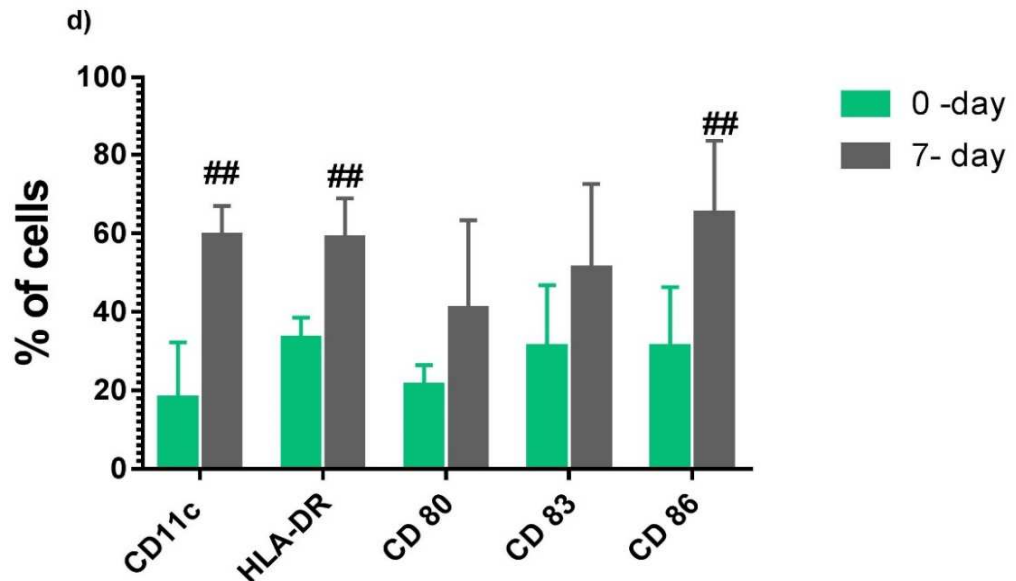


**Figure 5.6. THP-1 cells can be induced to express markers of imDCs.** THP-1 cells were treated with GM-CSF and IL-4 for 7 days and surface expression of CD11c, HLA-DR, CD80, CD 83 and CD 86 were assessed by flow cytometry before (0 days) and after (7 days) treatment. Isotype controls and unstained cells were included in all analyses. (a) Flow cytometry histograms of stained THP-1 cells at day 0 (b) flow cytometry histograms of THP-1-derived immature dendritic cells at 7 day; (c & d) table and graph showing the % of cells in each population expressing the markers assessed. Results are mean ± SD, ##p< 0.01 vs unstimulated cells at 0 day, n=5. n.s. denotes not significant. (a) and (b) are representative results from one of 5 independent experiments with similar results.

#### **5.4.2. Phenotypic maturation of imDCs derived from THP-1 monocytes to mDCs by LPS.**

The imDCs (from THP-1 cells) described above were treated with 1 µg/ml LPS for a further 4 days and then assessed for surface markers of mDCs. Figure 5.7 demonstrates that the derived cells showed characteristics of mDCs including a significant 1.6-fold increase in expression of CD11c from  $59.4 \pm 7.592$  to  $79.6 \pm 6.96$ . A similar response was observed when cells were stained for HLA-DR with a significant 1.8- fold increase from  $58.73 \pm 10.17$  to  $85.67 \pm 6.537$ . Significant upregulation of surface expression of CD80 from  $40.68 \pm 22.58$  to  $81.14 \pm 7.202$ , CD86  $65.03 \pm 18.49$  to  $84.12 \pm 4.58$  and CD83  $51.02 \pm 21.49$  to  $75.2 \pm 8.64$  were also observed. There was also a significant decrease in CD14 expression from  $69.72 \pm 15.08$  to  $23.32 \pm 19.02$  (Figure 5.7 b). These data suggest that imDCs derived from THP-1 cells can be matured to cells expressing markers of mDCs by LPS.

#### **5.4.3. The effect of CRT on maturation of THP-1 derived imDCs.**

The experiments above establish a methodology to examine DC maturation *in vitro*. Since ICD requires DC maturation, and cancer cells undergoing ICD expose CRT on their cell surface, experiments were carried out to examine whether CRT alone can induce DC maturation. Immature DCs were incubated with increasing concentrations of CRT and maturation was assessed by surface marker staining. The data presented in Figures 5.8 and 5.9 demonstrate that exogenous CRT can induce maturation of THP-1 derived imDCs. This effect appears to be dose dependent with 0.5 µg/ml CRT only inducing a significance increase in the expression level of HLA-DR, although it did induce a significant reduction in the expression level of CD14 from  $69.72 \pm 15.08$  to  $6.5 \pm 2.302$  (Figure 5.9 a). In contrast both 1 and 2.5 µg/ml CRT (Figure 5.9 b, c) induced significant changes in the maturation surface markers CD14, CD11c, CD80, CD83, and HLA-DR. For instance HLA-DR levels were increased from  $58.73 \pm 10.17$  to  $80.47 \pm 3.82$  at 1 µg/ml CRT and  $77.92 \pm 4.46$  at 2.5 µg/ml CRT. However, although CD86 levels were increased by both 1 and 2.5 µg/ml CRT these increases did not reach significance. CRT treatment also significantly reduced CD14 to  $7.04 \pm 2.628$

at 1  $\mu\text{g/ml}$  CRT, and  $5.8 \pm 2.775$  at 2.5  $\mu\text{g/ml}$  CRT respectively vs imDCs ( $69.72 \pm 15.08$ ) (Figures 5.9 a, b).

a)

Markers	THP-1 at 7-day (imDCs)	THP-1 + 1 $\mu\text{g/ml}$ LPS at 11-day (mDCs)	
CD 14	$69.72 \pm 15.08$	$23.32 \pm 19.02$	(##)
CD11c	$59.4 \pm 7.592$	$79.6 \pm 6.96$	(##)
HLA-DR	$58.73 \pm 10.17$	$85.67 \pm 6.537$	(##)
CD 80	$40.68 \pm 22.58$	$81.14 \pm 7.202$	(##)
CD 83	$51.02 \pm 21.49$	$75.2 \pm 8.643$	(#)
CD 86	$65.03 \pm 18.49$	$84.12 \pm 4.58$	(#)

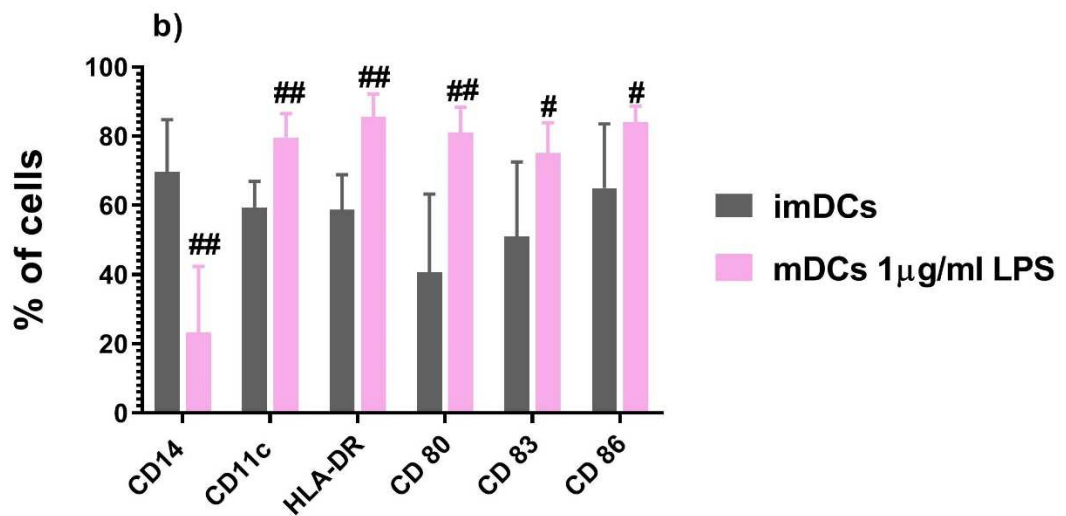


**Figure 5.7. DC maturation status examined using flow cytometry analysis of surface markers.** imDCs derived from THP-1 cells were matured by incubation with LPS for 4 days and the change in surface levels of CD11c, CD80, CD83, CD86 and HLA-DR and CD14 were measured by flow cytometry. (a) and (b) show % of cells stained for each marker before (imDC) and after (mDC) LPS treatment.  $n=5$ , #  $p < 0.05$ , ##  $< 0.01$ .

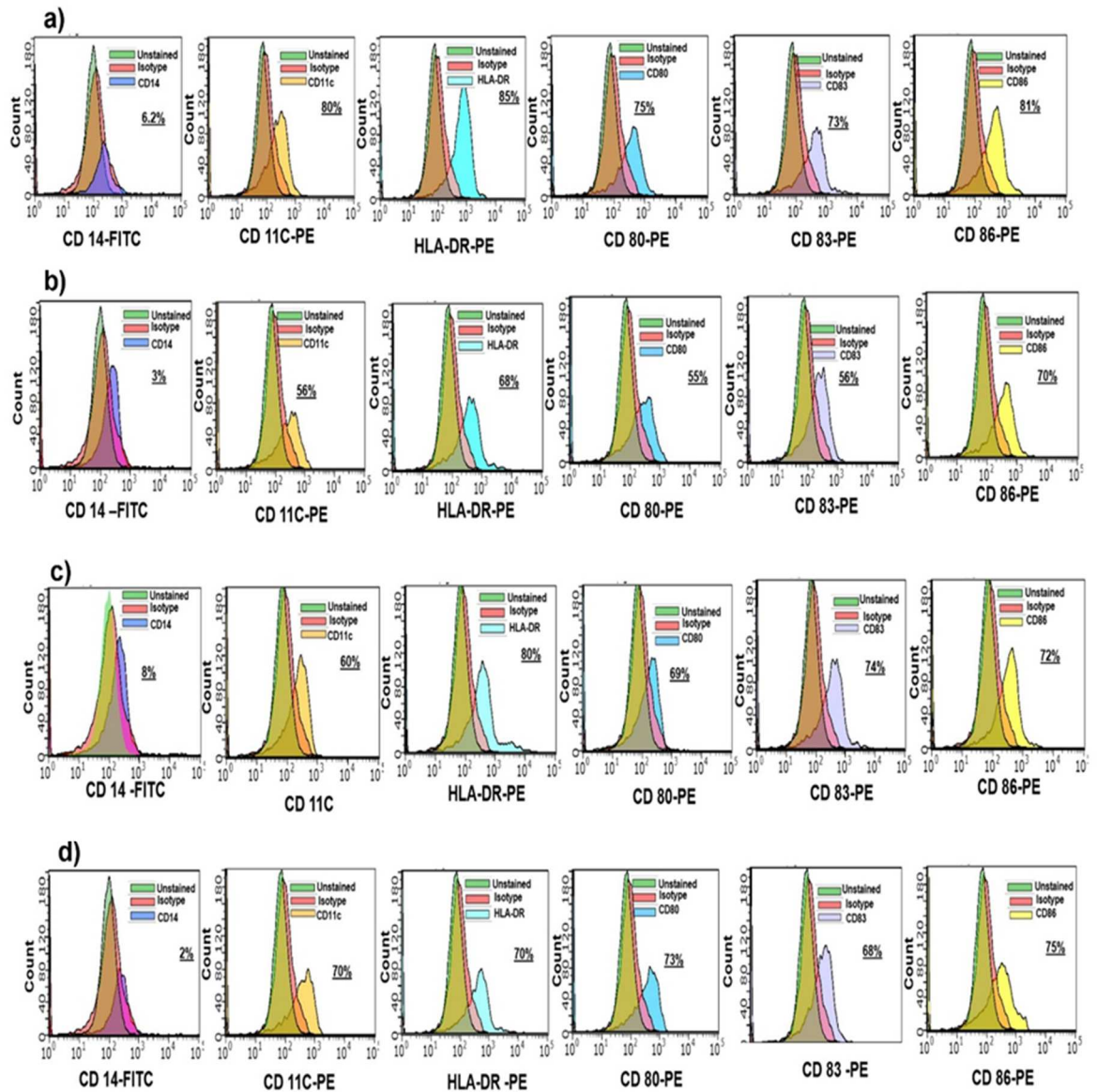


**Figure 5.8. CRT induced maturation of THP-1 derived imDCs to mDCs.** THP-1 derived imDC were stimulated with LPS (1  $\mu\text{g/ml}$ , a positive control) and increasing concentrations of CRT for 4 days. DC maturation was assessed by flow cytometric analysis of mDC surface markers. Cells were treated with (a) 1  $\mu\text{g/ml}$  LPS (b) 0.5  $\mu\text{g/ml}$  CRT (c) 1  $\mu\text{g/ml}$  CRT (d) 2.5  $\mu\text{g/ml}$  CRT. % indicated in each panel shows percentage of cell population expressing the marker measured. Representative histograms from 5 independent experiments with similar results are shown.

a)

Markers	THP-1 at 7-day (imDCs)	THP-1 + 0.5 µg/ml CRT at 11-day (mDCs)	
CD 14	69.72 ± 15.08	6.5 ± 2.302	(##)
CD11c	59.4 ± 7.592	61.2 ± 3.421	(n.s.)
HLA-DR	58.73 ± 10.17	72.23 ± 3.962	(##)
CD 80	40.68 ± 22.58	61.4 ± 4.393	(n.s.)
CD 83	51.02 ± 21.49	62.6 ± 3.912	(n.s.)
CD 86	65.03 ± 18.49	79 ± 5.292	(n.s.)

b)

Markers	THP-1 at 7-day (imDCs)	THP-1 + 1 µg/ml CRT at 11-day (mDCs)	
CD 14	69.72 ± 15.08	7.04 ± 2.628	(##)
CD11c	59.4 ± 7.592	71.8 ± 7.694	(#)
HLA-DR	58.73 ± 10.17	80.47 ± 3.82	(##)
CD 80	40.68 ± 22.58	74.2 ± 2.95	(##)
CD 83	51.02 ± 21.49	72.4 ± 5.079	(#)
CD 86	65.03 ± 18.49	79.8 ± 4.55	(n.s.)

c)

Markers	THP-1 at 7-day (imDCs)	THP-1 + 2.5 µg/ml CRT at 11-day (mDCs)	
CD 14	69.72 ± 15.08	5.8 ± 2.775	(##)
CD11c	59.4 ± 7.592	72.4 ± 3.647	(#)
HLA-DR	58.73 ± 10.17	77.92 ± 4.46	(##)
CD 80	40.68 ± 22.58	72.8 ± 1.483	(##)
CD 83	51.02 ± 21.49	74.6 ± 4.827	(#)
CD 86	65.03 ± 18.49	81.71 ± 4.424	(n.s.)

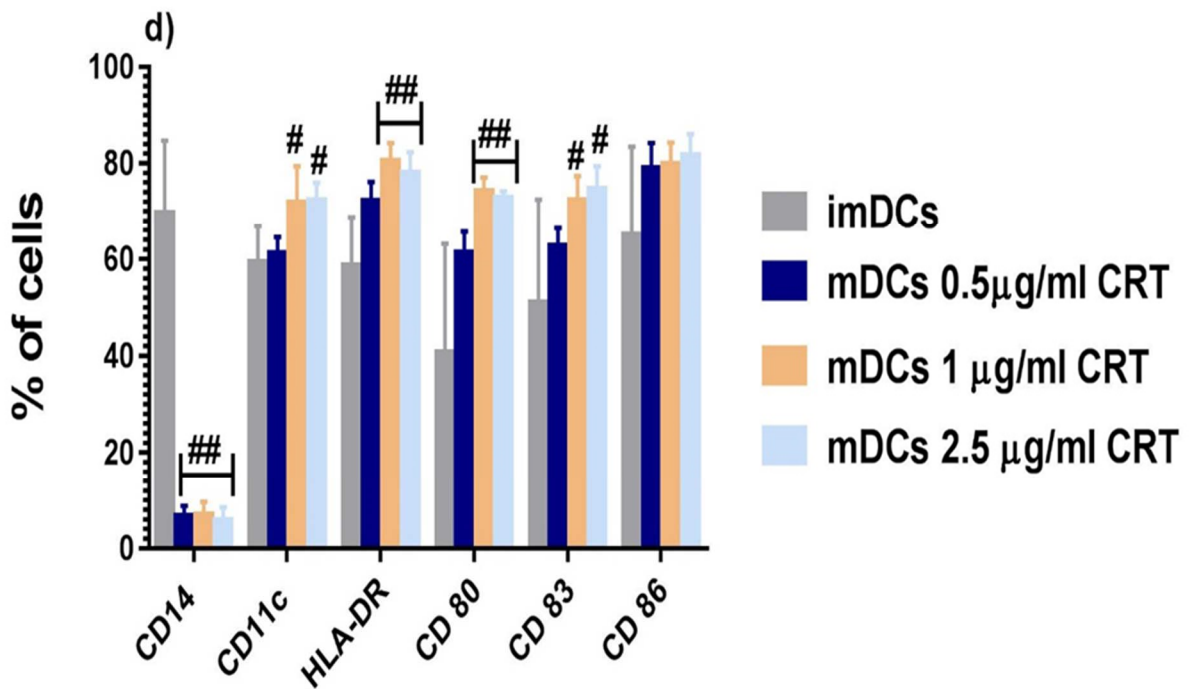


**Figure 5.9. CRT induced expression of mDC markers in THP-1 derived imDCs.** THP-1 derived imDCs were stimulated with different concentrations of CRT for 4 days. DC maturation was assessed by flow cytometric analysis of mDC surface markers. Cells were treated with (a) 0.5µg/ml CRT, (b) 1µg/ml CRT (c) 2.5µg/ml CRT. (d) Combined data for comparison. Data are shown as mean ± SD. ##p< 0.01, #p<0.05 vs imDCs at 7- day, n=5, n.s. denotes not significant.



The data presented in Figures 5.5 - 5.9 examine the responses of DCs derived from the THP-1 monocytic cell line. These experiments were performed in order to establish these techniques in the laboratory. However, it has been reported that differential responses have been observed between blood and THP-1 derived DCs (Daigneault et al., 2010) and therefore further experiments were carried out to establish a protocol to derive DCs from human peripheral blood monocytes.

#### **5.4.4. Monocyte isolation**

Monocytes were isolated from peripheral blood of healthy donors using protocol 1 (10 isolations in total). Enrichment of monocytes was achieved by magnetic separation by MACS® Technology (Miltenyi Biotec). Purification required several procedures including isolating PBMC by density centrifugation of blood into plasma, buffy coat and erythrocytes (Figure 5.10 a). The morphology of monocyte cells was initially observed using a light microscope after separation from PBMCs. Monocytes have unilobed nuclei with an amoeboid shape after staining by Diff-Quick stain (Figure 5.10 b). Isolated cells were also characterized by flow cytometry using antibodies against monocyte specific antigens i.e. anti-CD14 –FITC and anti-CD16 –PE (Figure 5.11). It can be seen that in a typical isolation approximately 85% of the isolated monocytic cells express CD14 which is considered to be the major marker of monocytes (Menck et al., 2014). CD16 allows further differentiation into monocyte subpopulations (Mandl et al., 2014). Over 50% of the monocytes isolated were CD14++ CD16– monocytes i.e. classical monocytes. These data indicate an enriched monocyte preparation.

#### **5.4.5. Generation of imDCs from isolated peripheral monocytes.**

Isolated monocytes were differentiated to imDCs as described for THP-1 cells and then stained for DC surface markers (CD80, CD83, CD86 and HLA-DR) using flow cytometry. As shown in (Figure 5.12 a, b) freshly isolated peripheral monocytes expressed low levels of all markers at day 0 (Figure 5.12 a). However, following 7 days treatment with the differentiating factors GM-CSF and IL4 the cell population showed a significantly increased expression of: CD11c (from  $14.89 \pm 1.17$  to  $64.86 \pm 7.547\%$ ), HLA-DR (from  $23.83 \pm 1.28$  to  $68.67 \pm 7.742\%$ ), CD80 (from  $11.5 \pm 0.89$  to  $64.13 \pm 9.71\%$ ); CD83 (from  $16.44 \pm 3.25$  to  $60.7 \pm 12.43\%$ ) and CD86 (from  $18.88 \pm 7.153\%$  to  $67.29 \pm 10.95\%$ ) (Figure 5.12 b, c, d).

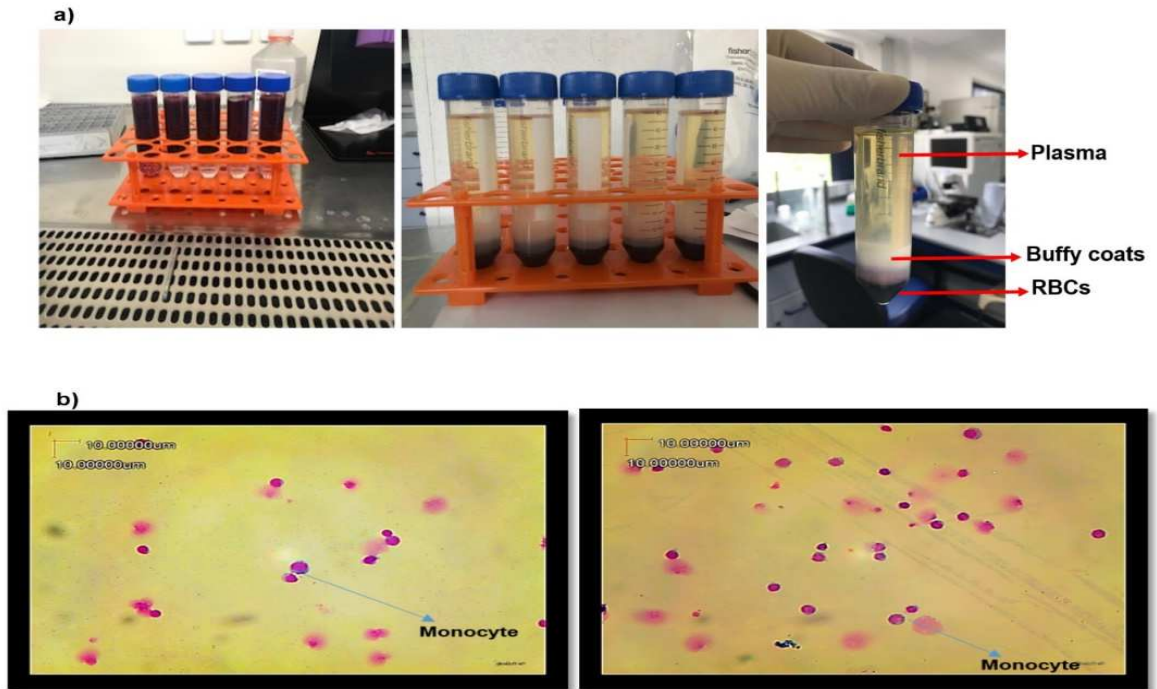


**Figure 5.10. Isolation procedure for purification of monocytes from peripheral human blood.** (a) Leukocyte buffy coat layer after separation of blood on a Ficoll gradient and (b) monocytes under light microscopy, stained by Diff-Quick stain, observed at 40 x magnification.

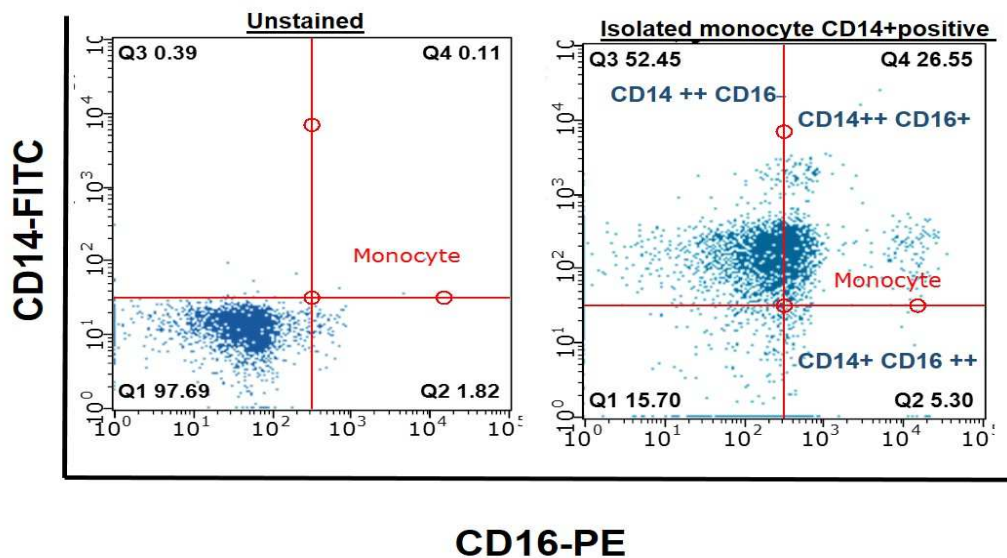
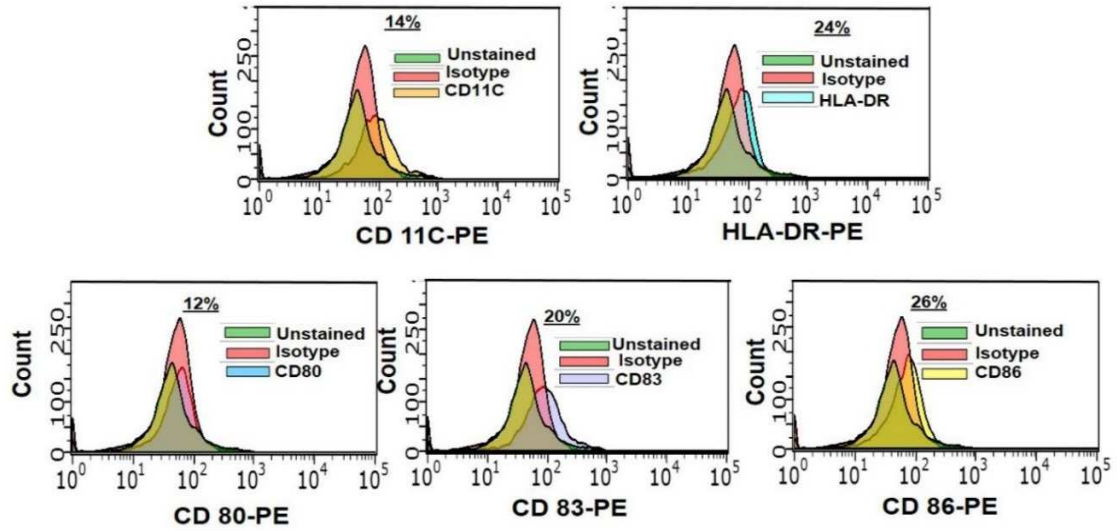
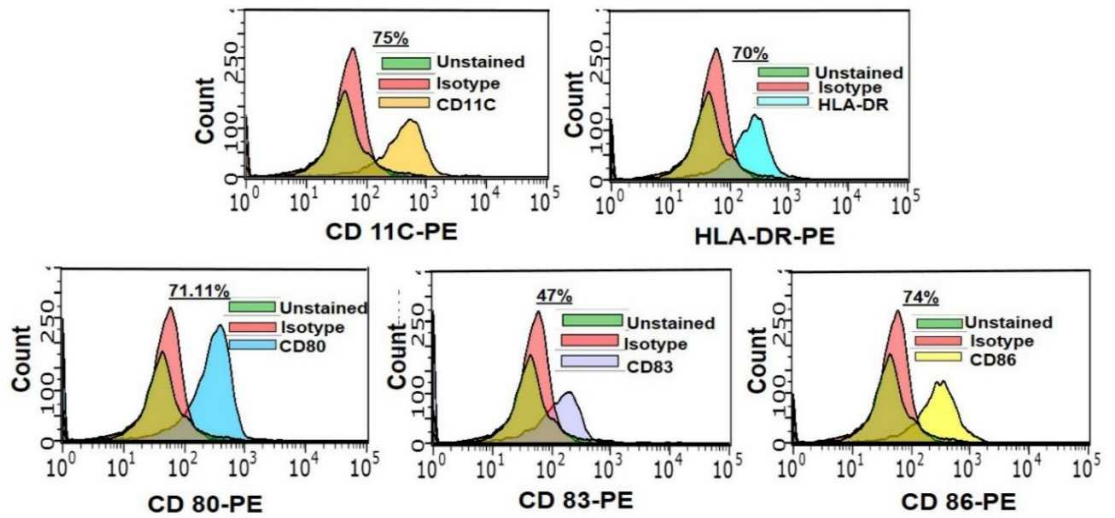


**Figure 5.11. Characterisation of enriched monocyte population.** Isolated monocytes were stained with fluorescent anti-CD16 PE and anti- CD14 FITC (monocyte markers) and analysed by flow cytometry. Representative plot from 10 isolations.

a) 0 day



b) 7 day



c)

Markers	CD14+ cells at 0-day	CD14+ (imDCs) at 7-day	
CD11c	14.89 ± 1.171	64.86 ± 7.547	(##)
HLA-DR	23.83 ± 1.281	68.67 ± 7.742	(##)
CD 80	11.5 ± 0.8944	64.13 ± 9.712	(##)
CD 83	16.44 ± 3.25	60.7 ± 12.43	(##)
CD 86	18.88 ± 7.153	67.29 ± 10.95	(##)

d)

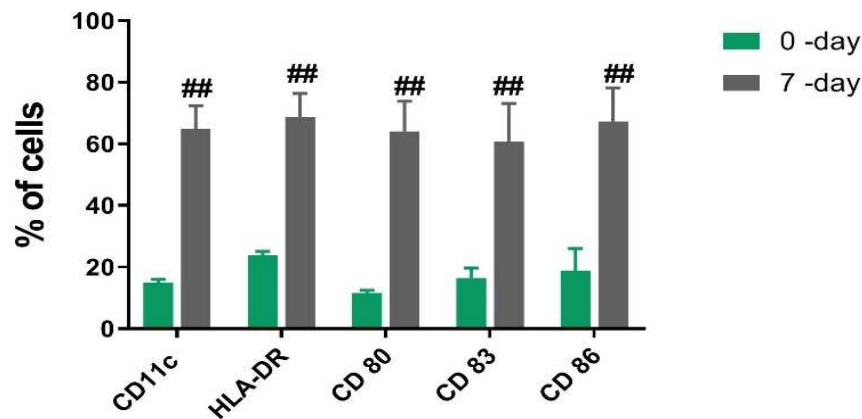


**Figure 5.12. Peripheral monocytes can be differentiated into imDCs.** Monocytes isolated from peripheral blood were incubated for 7 days in the presence of GM-CSF (800U/ml) and IL-4 (500U/ml). Cells at day 0 and 7 were analysed by flow cytometry for a panel of markers expressed on DCs. Unstained cells and isotype controls were included for all markers (a) flow cytometry histograms of monocytes analysed at day 0 day (b) flow cytometry histograms of monocyte derived imDCs at 7 day (c) and (d) expression of DC markers at day 0 and after 7 days of differentiation. Results are mean ± SD. ##p< 0.01 vs unstimulated cells at 0 day, n=5. (a) and (b) are representative data from one experiment repeated 5 times with similar results. The percentages shown indicate the percentage of the cell population expressing the marker measured.

#### **5.4.6. Generation of mDCs from imDCs derived from peripheral blood monocytes.**

imDCs derived from peripheral monocytes were stimulated with 1 µg/ml LPS to induce differentiation into mDCs. Cell surface expression of the mDC markers CD11c, CD80, CD83, CD86 and HLA-DR all significantly increased after 4 days treatment compared with the unstimulated cells. CD11c increased from  $64.86 \pm 7.55$  to  $78.22 \pm 4.58\%$ ; HLA-DR from  $68.67 \pm 7.74$  to  $80.37 \pm 7.79\%$ ; CD80 from  $64.13 \pm 9.71$  to  $79.41 \pm 3.85\%$ ; CD83 from  $56.63 \pm 6.14$  to  $73.6 \pm 4.16\%$  and CD86 from  $67.29 \pm 10.95$  to  $78.6 \pm 7.3\%$ . CD14 showed an approximately 6 -fold reduction in expression in mDCs ( $7.63 \pm 6.54\%$ ) compared with imDCs ( $65.48 \pm 14.82\%$ ). These data confirmed that monocyte derived imDCs could be matured *in vitro* to mDCs by LPS (Figure 5.13).

#### **5.4.7. CRT promotes monocyte derived imDC maturation.**

CRT was able to induce expression of DC maturation markers in THP-1 derived imDCs and so this was also tested in monocyte derived imDCs. imDCs treated with CRT at all concentrations tested (0.5, 1, 2.5 µg/ml) showed increased expression of CD11c, CD80, CD83, CD86 and HLA-DR compared with untreated monocyte derived imDCs (Figures 5.14 (a, b, c, d)). This increase was significant for HLA-DR and CD83 for cells treated with 0.5 µg/ml CRT and significant for all markers at the two higher CRT concentrations. For instance, 2.5 µg/ml CRT increased CD11c levels from  $64.86 \pm 7.55$  to  $78 \pm 2.74\%$ , HLA-DR from  $68.67 \pm 7.74$  to  $83.2 \pm 2.95\%$ , CD80 from  $64.13 \pm 9.71$  to  $83.2 \pm 7.16\%$ , CD83 from  $56.63 \pm 6.14$  to  $79.6 \pm 2.6\%$  and CD 86 from  $67.29 \pm 10.95$  to  $83.54 \pm 2.82\%$  ( $p < 0.05$ ,  $n=5$  for all) (Figures 5.15 (a, b, c, d)). CD14 expression was significantly reduced by treatment with all CRT concentrations studied. Hence, it appears from this experiment that CRT can induce maturation of imDCs derived from peripheral blood monocytes.

a)

Markers	CD14+ (imDCs) at 7-day	LPS 1µg/ml mDCs at 11- day	
CD 14	65.48 ± 14.82	7.63 ± 6.541	(##)
CD11c	64.86 ± 7.547	78.22 ± 4.583	(#)
HLA-DR	68.67 ± 7.742	80.37 ± 7.786	(#)
CD 80	64.13 ± 9.712	79.41 ± 3.85	(#)
CD 83	56.63 ± 6.137	73.6 ± 4.159	(##)
CD 86	67.29 ± 10.95	78.6 ± 7.301	(#)

b)

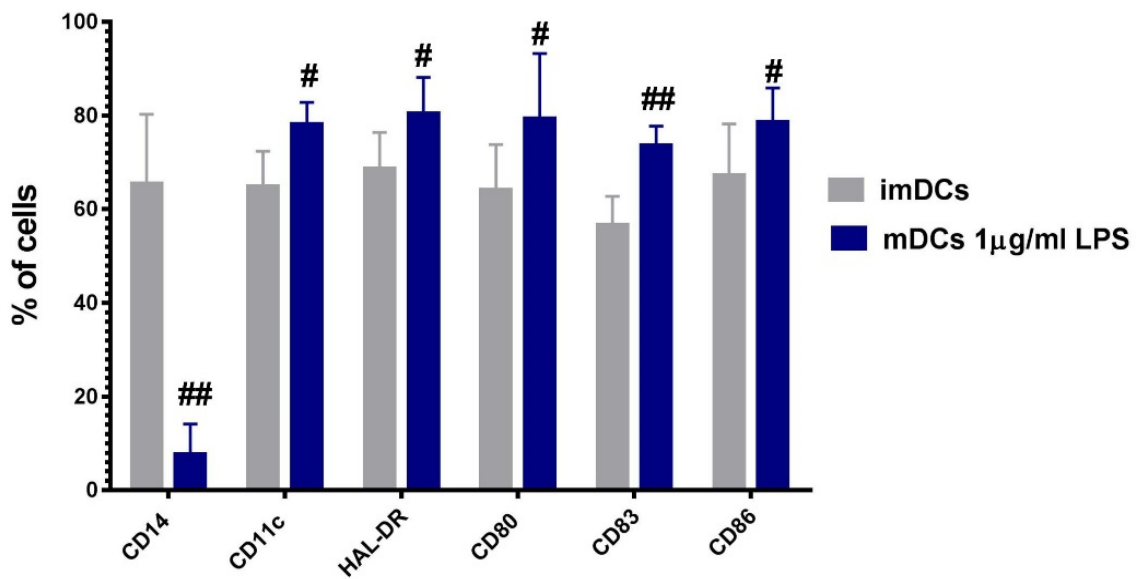


**Figure 5.13. imDCs derived from peripheral blood monocytes can be differentiated into mDC by LPS.** Monocyte-derived imDCs (cells at day 7 after isolation) were treated with 1µg/ml LPS for 4 days (cells at day 11 after isolation) and then assessed by flow cytometry for markers of DC maturation. (a) Table of average data from 5 separate isolations displayed as mean ± S.D, n=5. (b) Data presented graphically. #p<0.05, ##p<0.01

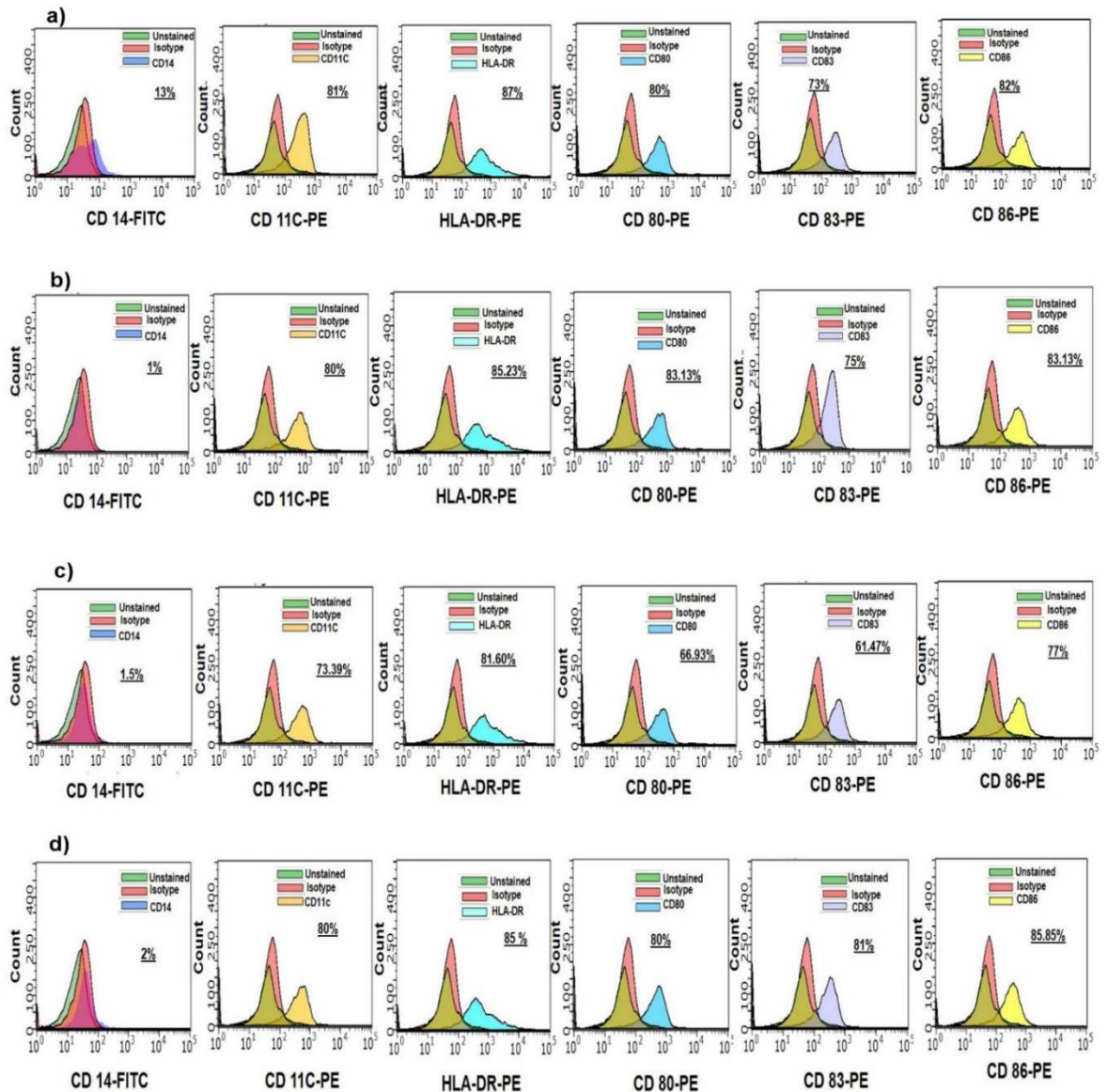


**Figure 5.14. Exogenous CRT can induce maturation of imDCs derived from peripheral monocytes.** Monocyte derived imDCs were treated for 4 days with (a) LPS (positive control), (b) 0.5, (c) 1, (d) 2.5  $\mu$ g/ml CRT and then analysed by flow cytometry for cell surface markers of DC maturation as indicated. Unstained cells and isotype controls were included as controls. Representative histograms from one experiment are shown. The experiment was repeated three times with similar results. Percentages shown in each panel indicate the percentage of the cell population expressing the marker measured.

a)

Markers	CD14+ (imDCs) at 7-day	CRT 0.5µg/ml mDCs at 11- day	
CD 14	65.48 ± 14.82	13.95 ± 17.05	(##)
CD11c	64.86 ± 7.547	69.8 ± 4.913	(n.s.)
HLA-DR	68.67 ± 7.742	83.66 ± 2.826	(##)
CD 80	64.13 ± 9.712	72.22 ± 7.246	(n.s.)
CD 83	56.63 ± 6.137	62.65 ± 1.616	(##)
CD 86	67.29 ± 10.95	71.8 ± 7.12	(n.s.)

b)

Markers	CD14+ (imDCs) at 7- day	CRT 1µg/ml mDCs at 11- day	
CD 14	65.48 ± 14.82	15.51 ± 11.51	(##)
CD11c	64.86 ± 7.547	81.99 ± 2.308	(##)
HLA-DR	68.67 ± 7.742	87.05 ± 1.944	(##)
CD 80	64.13 ± 9.712	81.67 ± 1.201	(##)
CD 83	56.63 ± 6.137	69.42 ± 5.985	(##)
CD 86	67.29 ± 10.95	82.56 ± 0.8816	(##)

c)

Markers	CD14+ (imDCs) at 7-day	CRT 2.5µg/ml mDCs at 11- day	
CD 14	65.48 ± 14.82	4.8 ± 5.805	(##)
CD11c	64.86 ± 7.547	78 ± 2.739	(#)
HLA-DR	68.67 ± 7.742	83.2 ± 2.95	(##)
CD 80	64.13 ± 9.712	83.2 ± 7.155	(##)
CD 83	56.63 ± 6.137	79.6 ± 2.608	(##)
CD 86	67.29 ± 10.95	83.54 ± 2.819	(##)



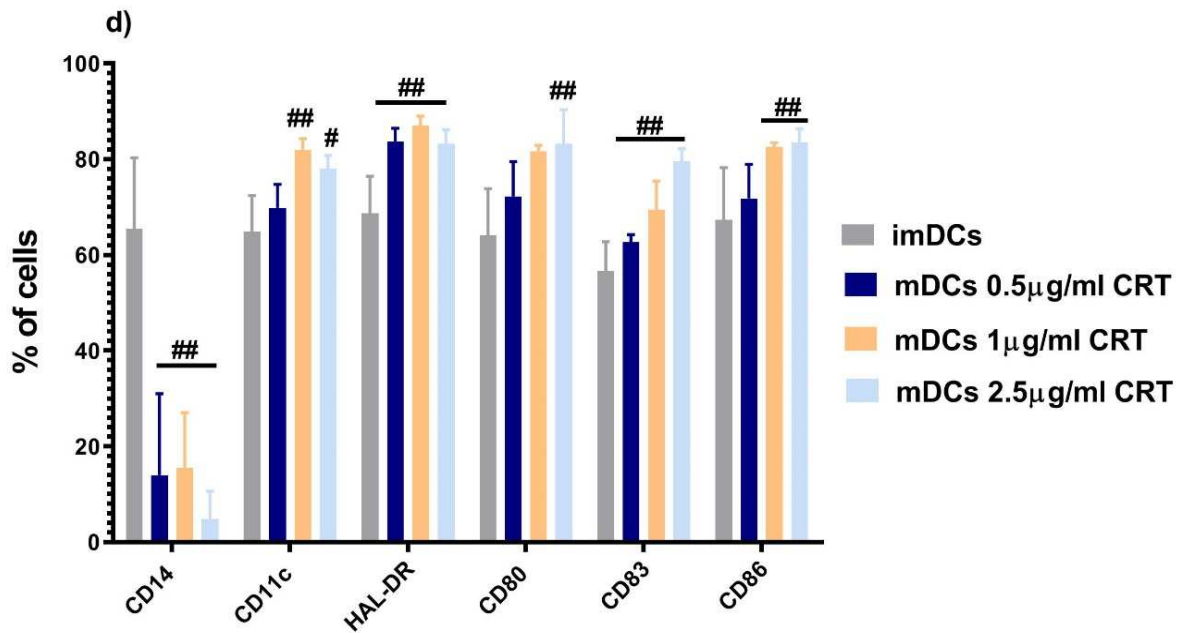


**Figure 5.15. CRT induced expression of mDC markers in peripheral blood monocyte derived imDCs.** Peripheral blood monocyte derived imDCs (cells at 7 days after isolation) were stimulated with different concentrations of CRT for 4 days (cells at 11 days after isolation). DC maturation was assessed by flow cytometric analysis of mDC surface markers. Cells were treated with (a) 0.5µg/ml CRT, (b) 1µg/ml CRT (c) 2.5µg/ml CRT (d) combined data for comparison. Data are shown as mean  $\pm$  SD ##p< 0.01, #p<0.05 vs imDCs at 7- day, n=5, n.s. denotes not significant.

#### **5.4.8. DCs derived from peripheral blood monocytes exhibit a dendritic morphology.**

Morphological examination of the isolated monocytes before and after differentiation to imDCs and subsequent maturation to mDCs supported the phenotypic changes suggested by changes in expression of surface markers (Figures 5.15). Initially, isolated monocytes had a rounded shape and adhered to the plastic surface of the flask. During treatment with GM-CSF/IL-4 to induce differentiation into imDCs the cells appeared to increase in size and the cell clusters began to become larger and non-adherent to the flask, but the numbers of cells did not expand. imDCs treated with 1 µg/ml LPS or CRT (0.5, 1, 2.5 µg/ml) to induce maturation transformed into cells with stellate processes/cytoplasmic projections and an irregular shape. mDCs showed processes that extended in different directions with numerous granules and irregular nuclei (Hart, 1997) (Figure 5.16).

#### **5.4.9. Activation of DC maturation by ovarian cancer cells (OVcar3) treated with doxorubicin to induce surface expression of CRT.**

The data above indicate that exogenous CRT induces maturation of imDCs. To examine this further, a series of experiments were carried out to investigate whether cancer cells treated with doxorubicin to induce surface expression of endogenous CRT could also stimulate DC maturation. OVcar3 cells previously treated with increasing concentrations of doxorubicin (0.25, 1, 2.5 µM for 16 hr), to induce cell surface CRT exposure, were co-cultured with imDCs derived from peripheral blood monocytes. Markers of DC maturation were then examined by flow cytometry with the OVcar3 cells gated out by staining with EpCAM. Since this co-incubation resulted in a mixed cell population initial studies examined possible cross staining of each cell type with markers of the other.

Figure 5.17 indicates that over 90% of OVcar3 cells expressed EpCAM and that the cells only expressed low levels of the DC markers. Mann Whitney test results confirmed significant differences between all DC markers when compared with EpCAM alone ( $90.95 \pm 1.123$ ) (Figure 5.18;  $n=3$ ;  $\#p<0.05$ ). These results confirm that

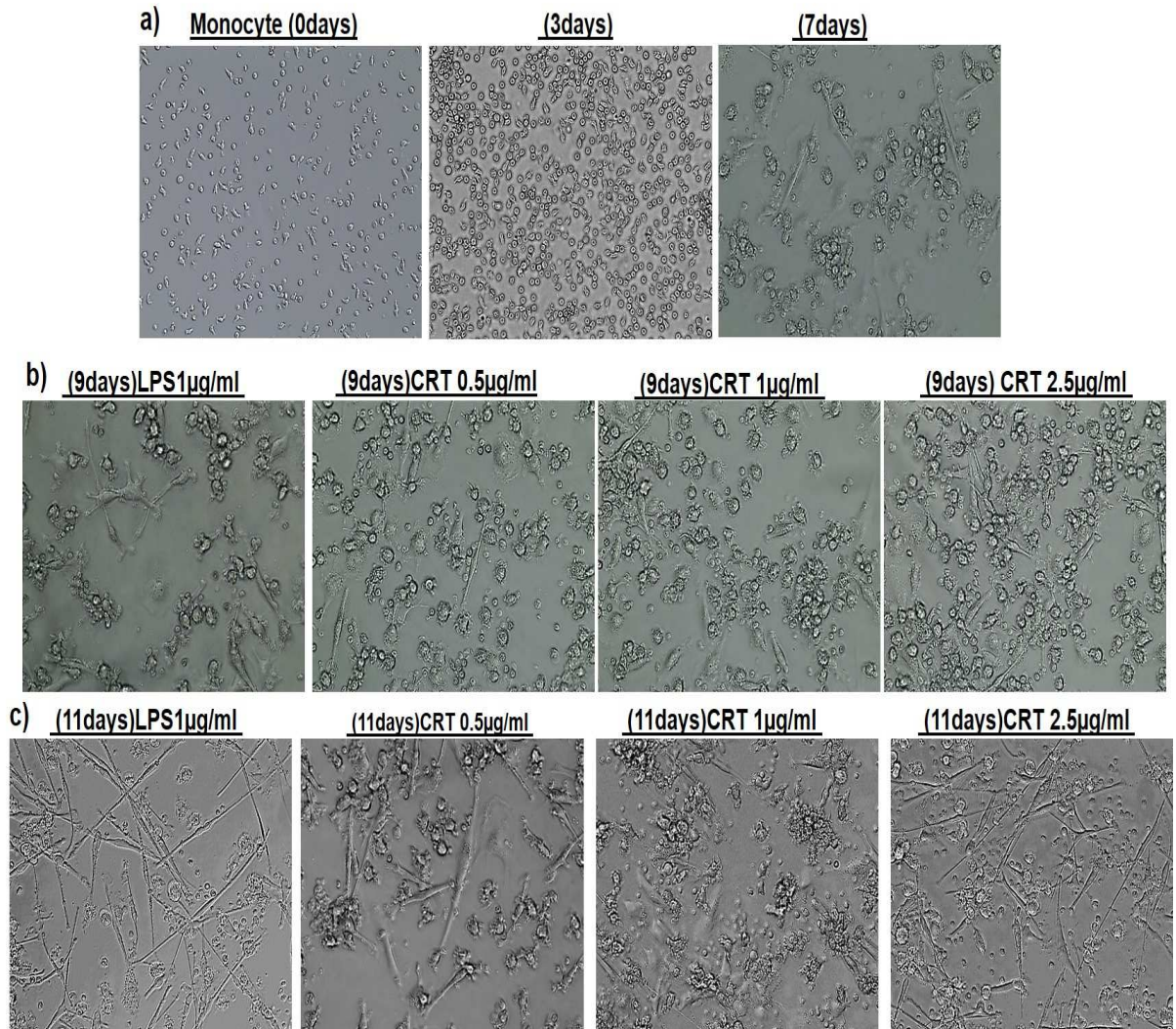


**Figure 5.16. The morphology of isolated peripheral blood monocytes changes during differentiation to imDCs and maturation to mDCs.** Isolated monocytes were treated initially with GM-CSF and IL4 to induce differentiation to imDCs and then with LPS or increasing concentrations of CRT to induce maturation to mDCs. Changes in cell morphology were observed under bright field microscopy during cell culture (40× magnification). (a) Isolated monocytes at day 0, 3 and 7 of GM-CSF and IL4 treatment, (b) imDCs observed at day 2 of treatment (i.e. day 9 after isolation) with either LPS or different concentrations CRT, (c) imDCs observed at day 4 of treatment (i.e. day 11 after isolation) with either LPS or different concentrations CRT.

EpCAM was a suitable marker for the detection of OVCAR3 cells in a mixed population with DCs.

Experiments were then performed to confirm that DC did not express EpCAM. Figure 5.19 indicates that no EpCAM fluorescence was detected on the surface of mDCs and that the presence of anti-EpCAM antibodies did not interfere with staining by DC markers.

#### **5.4.10. Doxorubicin-treated ovarian cancer cells (OVcar3) induce DC maturation**

Doxorubicin treated OVcar3-induced DC maturation was assessed by cell surface markers (Figures 5.20 and 5.21). This effect appeared to be dependent on the original concentration of doxorubicin used to treat the OVcar3 cells. Although OVcar3 treated with all doxorubicin concentrations i.e. 0.25, 1, 2.5  $\mu$ M induced a significant reduction in expression of CD14, only OVcar3 treated with higher concentrations significantly induced increased expression of the majority of the other markers studied. OVcar3 treated with both 1 and 2.5  $\mu$ M induced increased expression of CD11c, CD80, CD83, CD86 and HLA-DR compared with untreated imDCs, although this did not always reach significance (Figure 5.21). For instance in DCs co-incubated with OVcar3 treated with 2.5  $\mu$ M doxorubicin there was an increase in expression of: CD11c from  $64.86 \pm 7.55$  to  $80.8 \pm 8.7\%$ ; CD83 from  $56.63 \pm 6.14$  to  $69.2 \pm 1.92\%$ ; CD86 from  $67.29 \pm 10.9$  to  $79 \pm 3.67\%$  and HLA-DR from  $68.67 \pm 7.74$  to  $78.2 \pm 2.16\%$ .

The above experiments were also carried out using imDCs derived from THP-1 cells to allow comparison of the functional responses of the imDCs derived from the two different sources. It can be seen from figures 5.22 and figure 5.23 that OVcar3 treated with all three concentrations of doxorubicin tested (0.25, 1, 2.5  $\mu$ M) and then co-incubated with THP-1 derived imDCs induced a significant reduction in CD14 expression on the DCs. Co-incubation of imDCs with OVcar3 previously treated with 1 and 2.5  $\mu$ M doxorubicin resulted in increased expression of all other markers of DC maturation, although again this did not always reach significance (Figure 5.23).

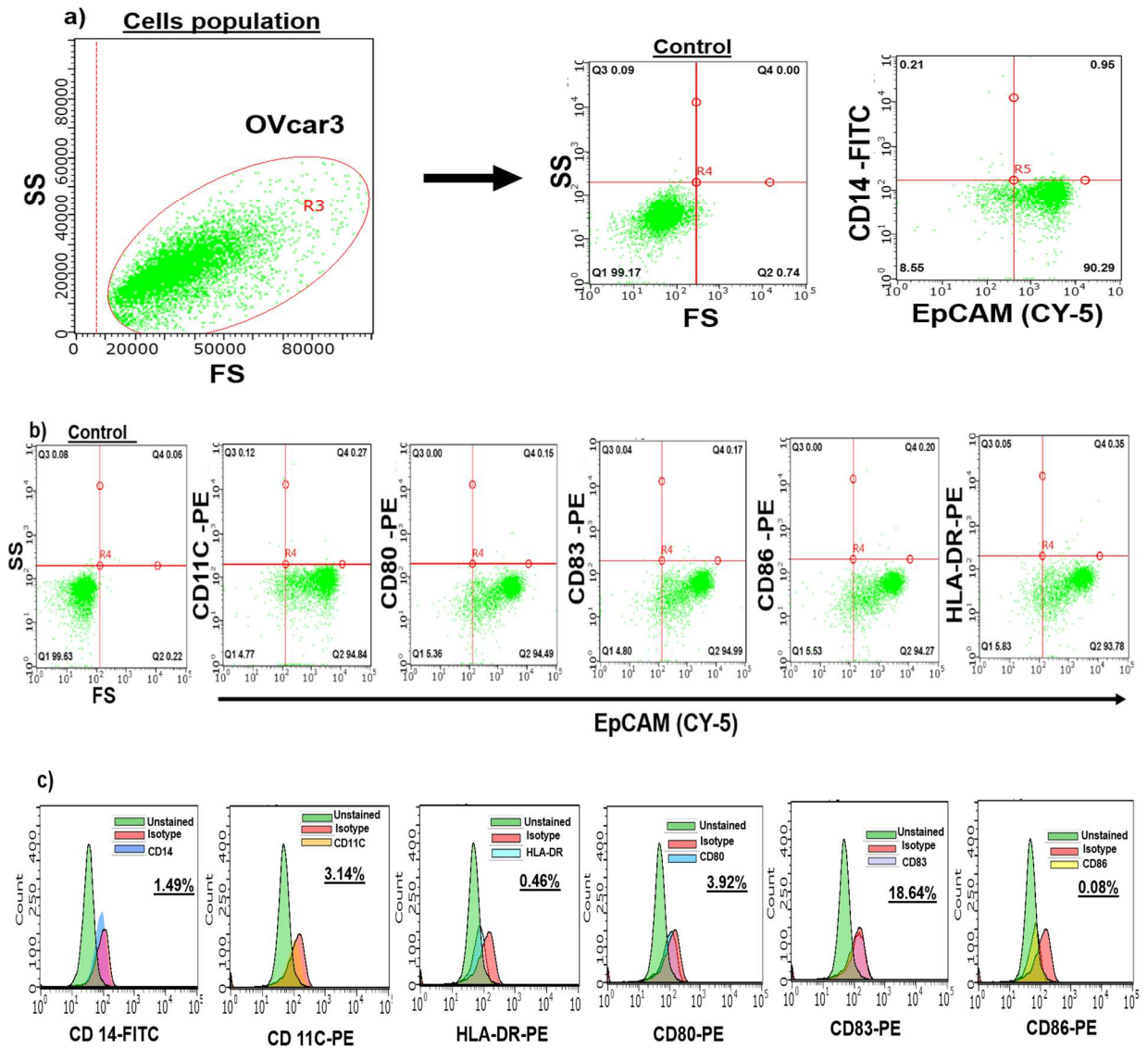


**Figure 5.17. EpCAM is expressed on ovarian cancer cells, but DC markers are not.** OVcar3 ovarian cancer cells were stained for EpCAM (anti-EpCAM-Cy5) and DC markers (PE conjugated CD11c, HLA-DR, CD80, CD83 and CD86 and CD14-FITC) for 30 minutes and surface expression of the markers was assessed by flow cytometry. Unstained cells and isotype controls were included as controls and for initial gating. (a) Gated OVcar3 cell population was over 90% positive for EpCAM expression (b), (c) EpCAM positive OVcar3 cells expressed very low levels of DC markers i.e. staining with fluorescently labelled specific antibodies is almost identical to isotype controls. Representative plots are shown from a typical experiment carried out on three occasions

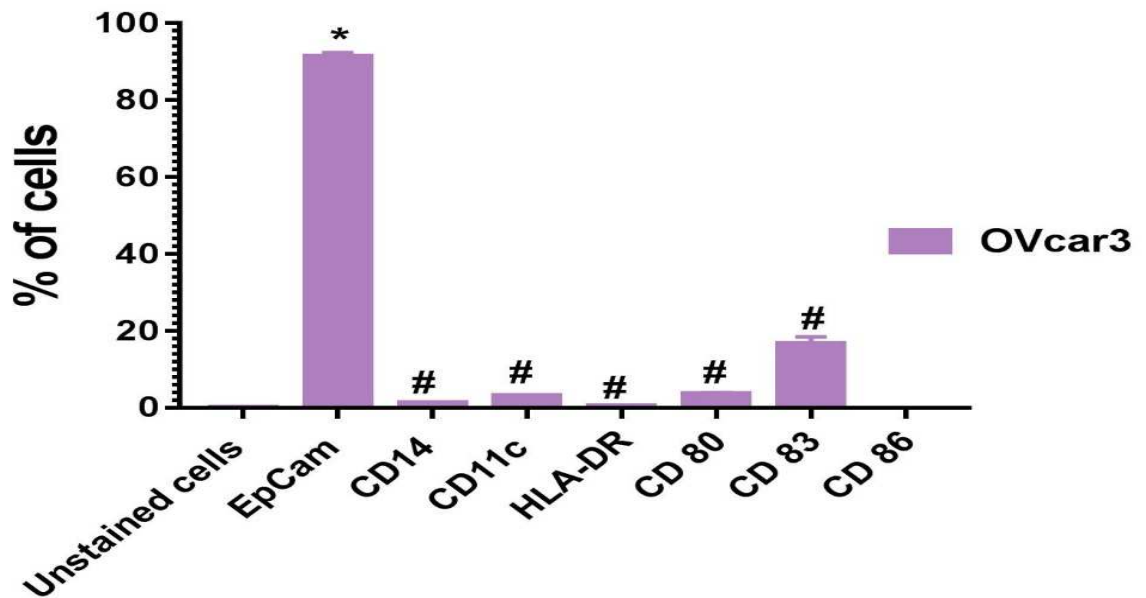


**Figure 5.18. Ovcar3 cells express high surface levels of EpCAM and low levels of DC markers.** OVcar3 cells were stained with fluorescent antibodies against EpCAM and markers of DC maturation (PE conjugated CD11c, HLA-DR, CD80, CD83 and CD86 and CD14-FITC) and expression of each marker was assessed by flow cytometry. Data show the mean  $\pm$  SD of three separate experiments. \*unstained OVcar3 cells vs. anti-EpCAM, # anti-EpCAM vs. DC markers.  $p < 0.05$  for all.

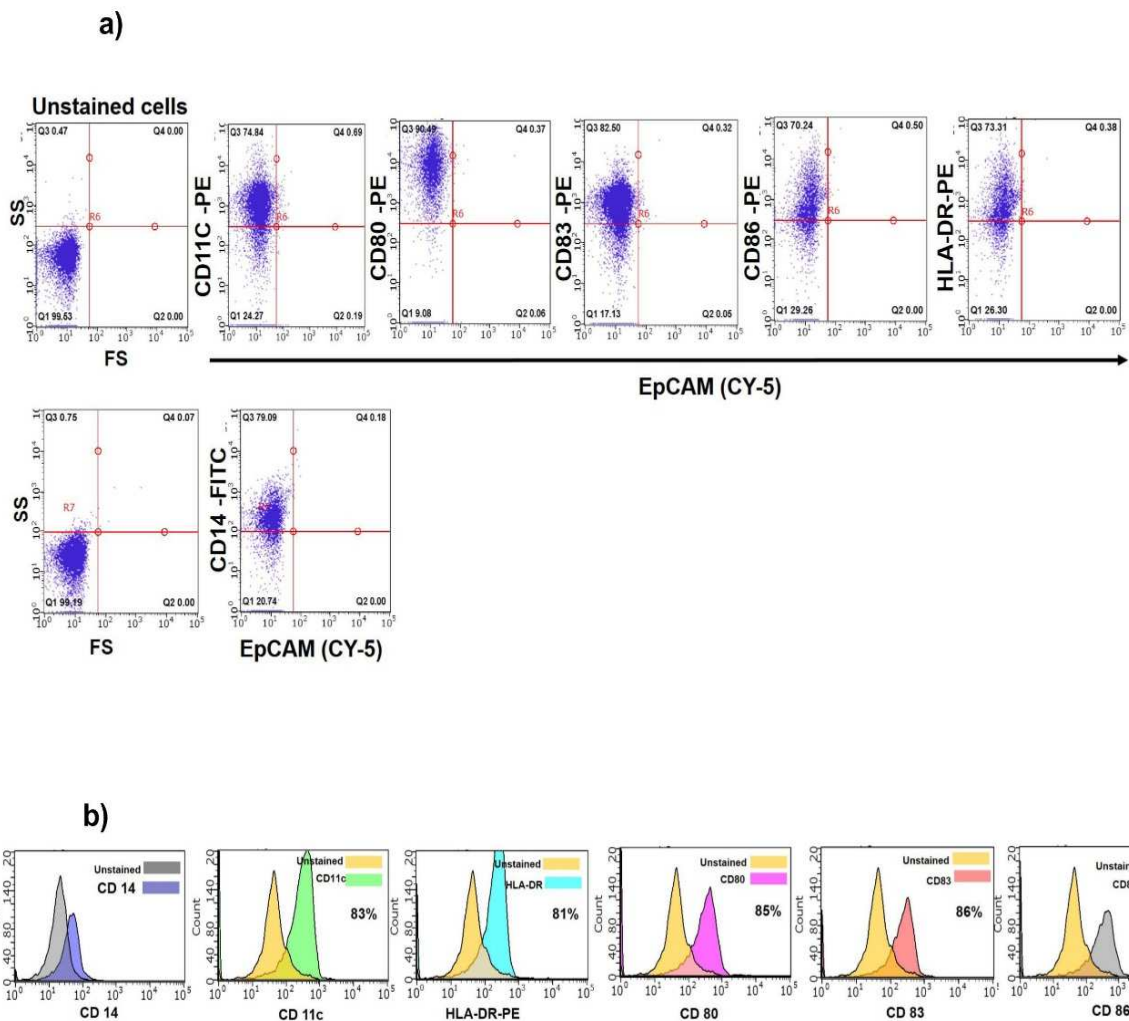


**Figure 5.19 mDCs do not express EpCAM.** mDC were stained with anti- EpCAM and DCs markers (CD14, CD11c, CD80, CD83, CD86 and HLA-DR), incubated for 30 minutes at the room temperature, then analysed by flow cytometry. (a) Dot plot showing fluorescence intensity of staining with EpCAM vs DC markers indicating that no EpCAM fluorescence was observed (b) Percentage flow cytometry histograms confirming that DCs markers were highly expressed on DC cells in the presence of anti-EpCAM. Representative plots are shown from a typical experiment carried out on three occasions. Percentages shown in each panel indicate the percentage of the cell population expressing the marker measured.

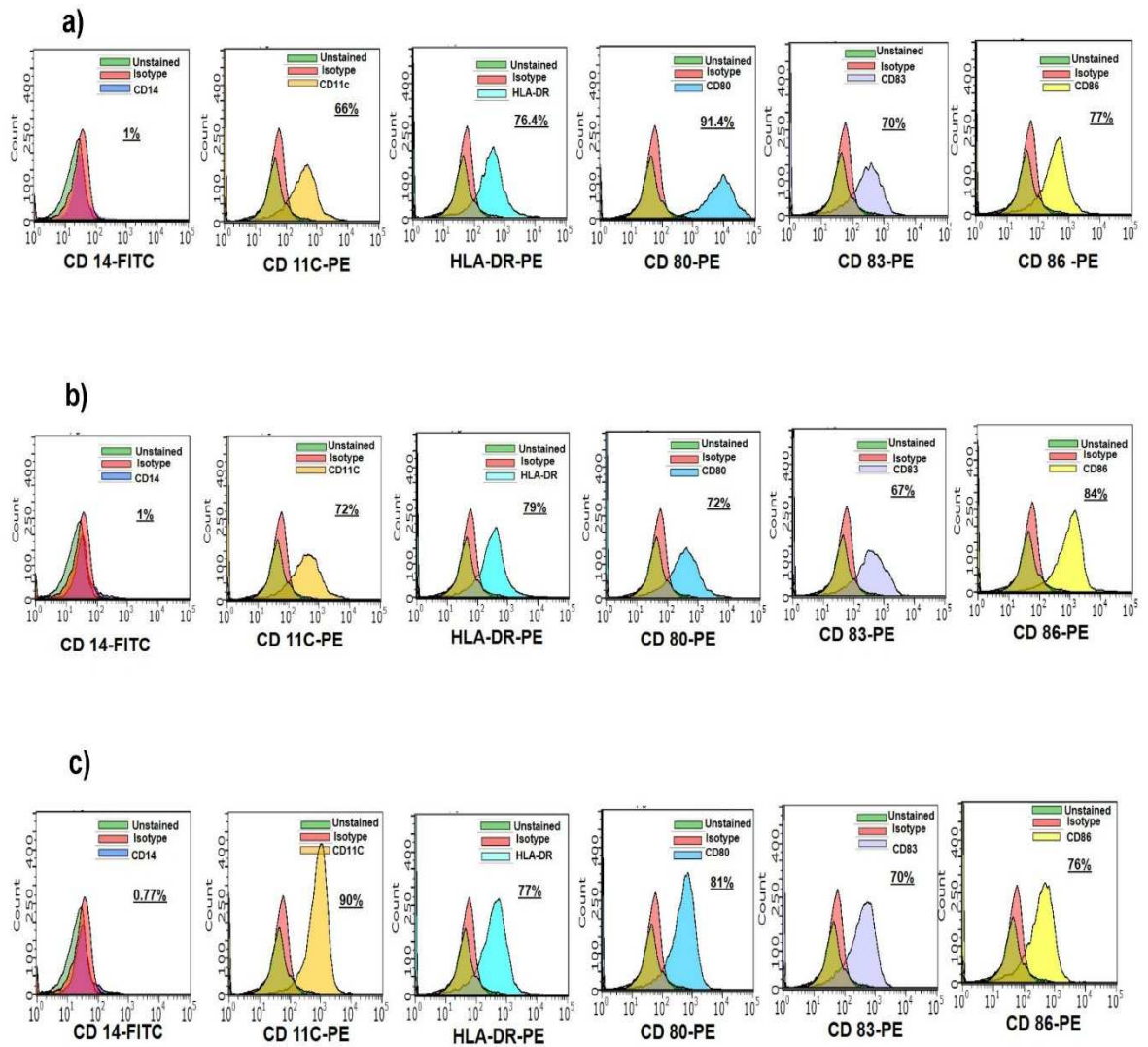


**Figure 5.20. Co-incubation of doxorubicin treated OVcar3 cells with peripheral blood derived imDCs induced DC maturation.** OVcar3 cells were treated with increasing concentrations of doxorubicin (a) 0.25  $\mu$ M, (b) 1  $\mu$ M, (c) 2.5  $\mu$ M, for 16 hours. The doxorubicin was washed off and the OVcar3 cells were co-incubated with imDCs for 4 days and markers of DC maturation (CD14, CD11c, CD80, CD83, CD86 and HLA-DR) were assessed by flow cytometry. OVcar3 cells were stained with anti-EpCAM to allow these cells to be gated out of the analysis. Representative histograms are shown from 5 independent experiments. Percentages shown in each panel indicate the percentage of the cell population expressing the marker measured.



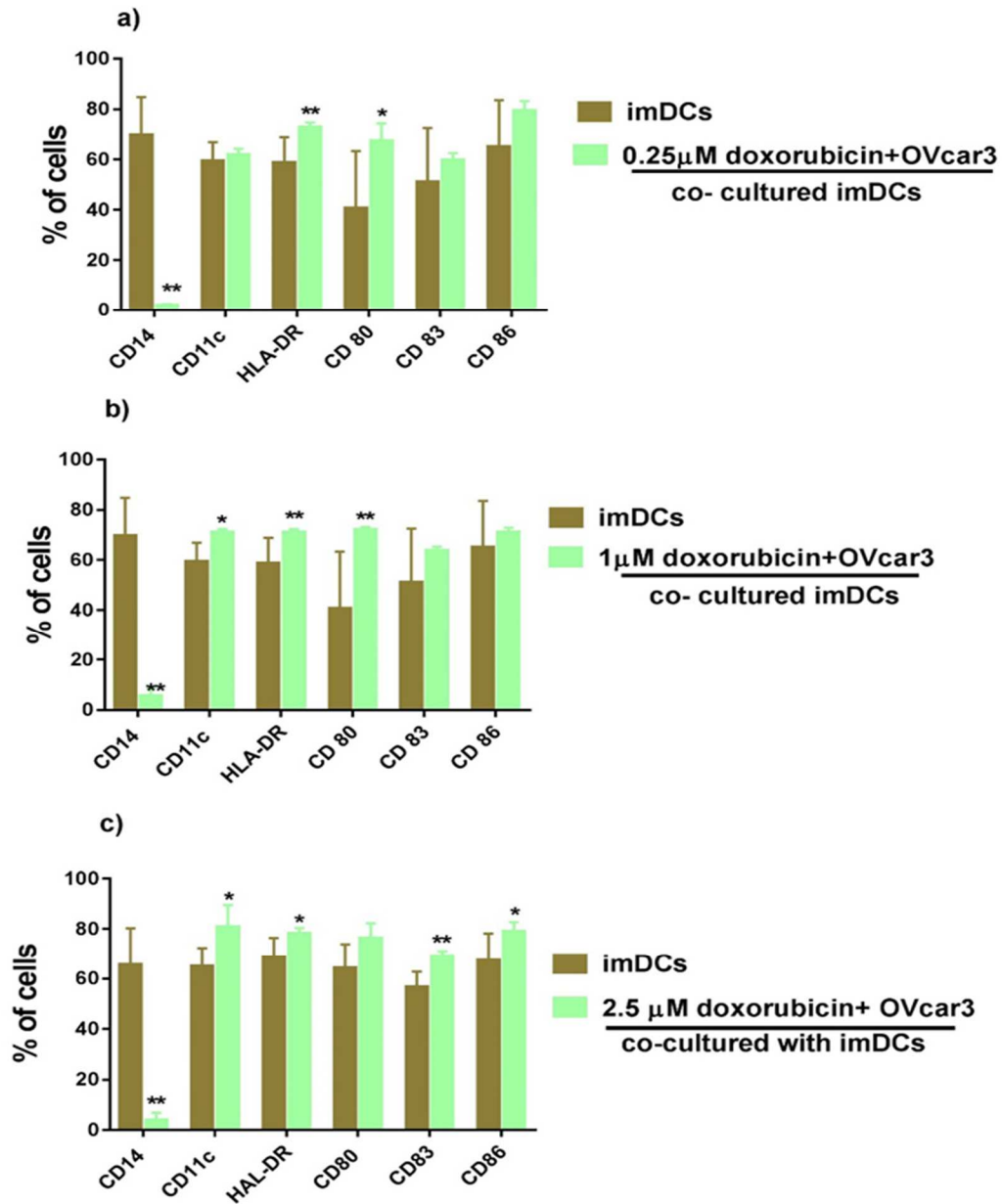


**Figure 5.21. Co-incubation of doxorubicin treated OVcar3 cells with peripheral monocyte derived imDCs induced DC maturation.** OVcar3 cells were treated with increasing concentrations of doxorubicin (a) 0.25 μM, (b) 1 μM, (c) 2.5 μM, for 16 hours and then co-incubated with peripheral monocyte derived imDCs for 4 days. The DCs were then assessed for markers of maturation (CD11c, CD80, CD83, CD86 and HLA-DR) by flow cytometry. OVcar3 cells were stained with anti-EpCAM to allow these cells to be gated out of the analysis. Results are mean ± SD, \*p < 0.05, \*\*p < 0.01 vs untreated imDCs (n = 5 independent experiments).

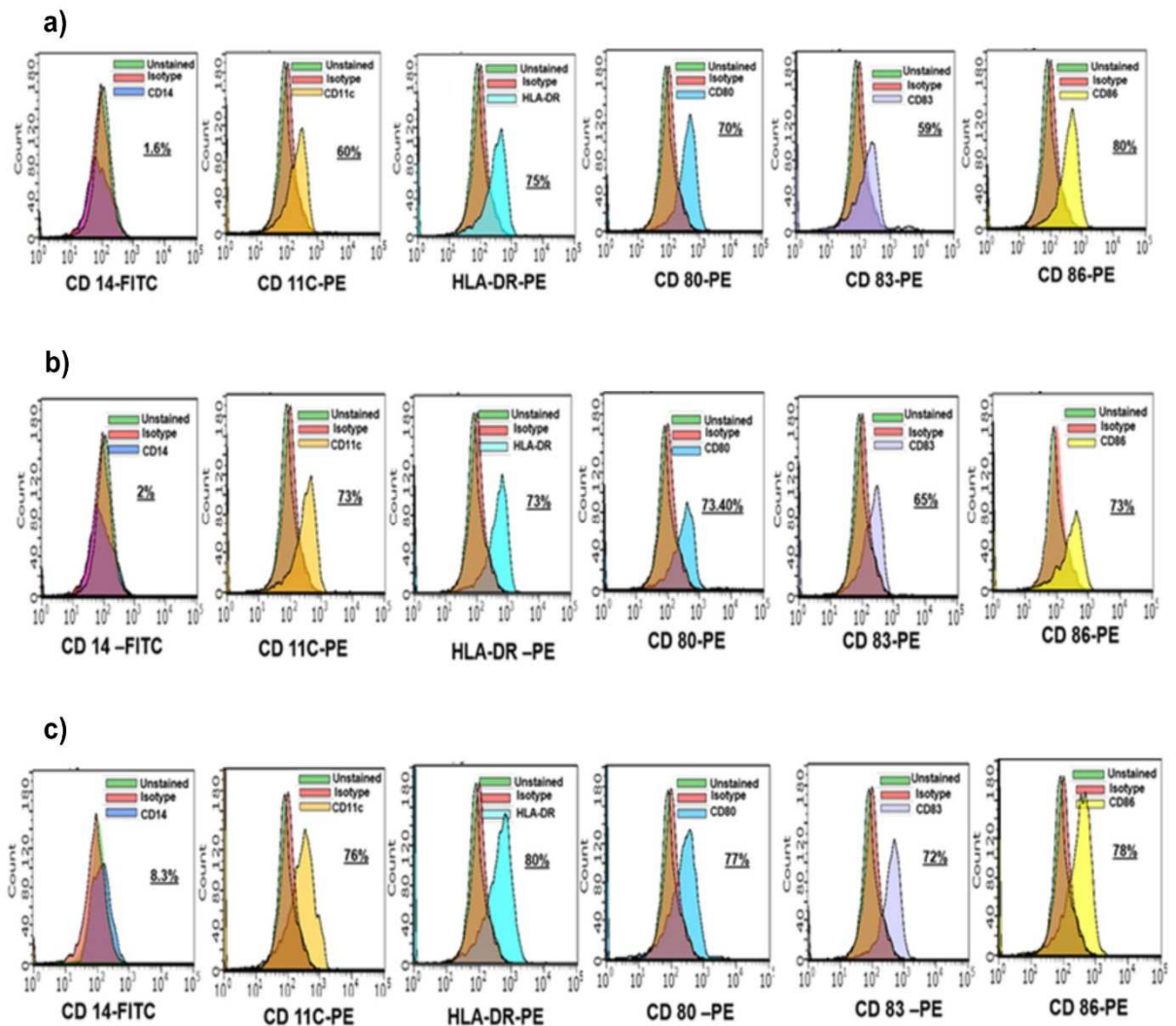


**Figure 5.22. Co-incubation of doxorubicin treated OVcar3 cells with THP-1 derived imDCs induced DC maturation.** OVcar3 cells were treated with increasing concentrations of doxorubicin (a) 0.25  $\mu\text{M}$ , (b) 1  $\mu\text{M}$ , (c) 2.5  $\mu\text{M}$ , for 16 hours. The doxorubicin was then washed off and the treated cells were co-incubated with THP-1 derived imDCs for 4 days, after which markers of DC maturation (CD14, CD11c, CD80, CD83, CD86 and HLA-DR) were assessed by flow cytometry. OVcar3 cells were stained with anti-EpCAM to allow these cells to be gated out of the analysis. Representative histograms are shown from one of 5 independent experiments. Percentages shown in each panel indicate the percentage of the cell population expressing the marker measured.

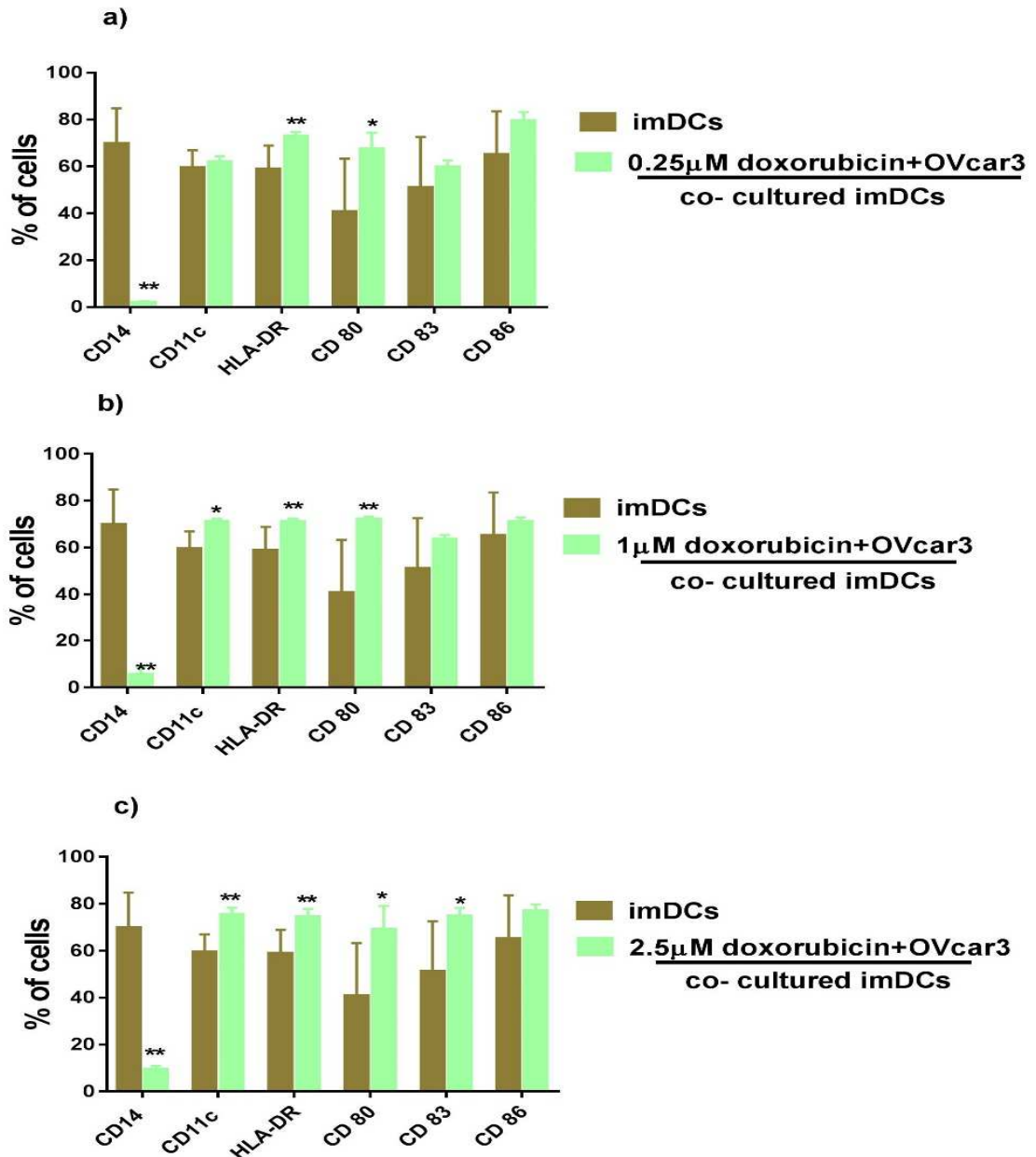


**Figure 5.23. Co-incubation of doxorubicin treated OVcar3 cells with THP-1 derived imDCs induced DC maturation.** OVcar3 cells were treated with increasing concentrations of doxorubicin (a) 0.25 μM, (b) 1 μM, (c) 2.5 μM, for 16 hours and then co-incubated with THP-1 derived imDCs for 4 days. The DCs were then assessed for markers of maturation (CD11c, CD80, CD83, CD86 and HLA-DR) by flow cytometry. OVcar3 cells were stained with anti-EpCAM to allow these cells to be gated out of the analysis. Results are mean ± SD, \*p<0.05, \*\*p<0.01 vs untreated imDCs (n = 5 independent experiments).

#### **5.4.11. Maturation of dendritic cells derived from peripheral monocytes is associated with increased secretion of IL12/IL23**

As previously mentioned it has been reported that maturation of DCs is not only characterised by changes in surface expression of maturation markers, but also by increased secretion of cytokines including IL12 and IL23 (Mayordomo et al., 2018). Therefore, as an additional marker of DC maturation in the *in vitro* system used here, levels of secreted IL12 and 23 were measured in DC culture media following cell treatments. It can be seen from (Figure 5.24 a) that IL12/23 secretion was significantly increased in the media of peripheral blood monocytes stimulated to undergo differentiation to imDCs by GM-CSF and IL4. Secreted levels increased with time over the 7 days of differentiation treatment i.e. from  $402.0 \pm 16.17$  in freshly isolated monocytes to  $631.1 \pm 67.07$  pg/ml after 3 days and  $750.4 \pm 143.9$  pg/ml after 7 days.

Secreted levels of these cytokines were also examined in the culture media of imDCs induced to mature to mDCs. Since the marker expression data suggested that exogenous CRT could induce DC maturation (Figure 5.24 b), cytokine secretion stimulated by CRT was also examined. Although LPS, the classic stimulator of imDC maturation, did induce an increase in secreted IL12/23 levels this did not reach significance. However, CRT at all concentrations tested did significantly increase IL12/23 secretion. DCs treated with 0.5, 1, 2.5  $\mu$ g/ml secreted  $1081 \pm 202.4$  pg/ml,  $1255 \pm 238\%$  pg/ml and  $1227 \pm 217.1$  pg/ml respectively in comparison to the untreated imDCs ( $750.4 \pm 143.9$  pg/ml) ( $n < 0.05$ ,  $n=3$  for all (Figure 5.24 b). These data confirm the marker expression results and suggest that exogenous CRT is a potent stimulator of DC maturation.

Maturation of imDCs (from peripheral blood monocytes) by OVcar3 ovarian cancer cells pre-treated with doxorubicin was also accompanied by increased secretion of IL12/23 (Figure 5.25). OVcar3 cells treated with 0.5, 1 or 2.5  $\mu$ M doxorubicin induced secretion of  $1221 \pm 170.7$  pg/ml,  $1219 \pm 188$  pg/ml and  $1506 \pm 60.14$  pg/ml of IL12/23 from maturing imDCs respectively, compared with  $750.4 \pm 143.9$  pg/ml secreted from untreated imDCs.

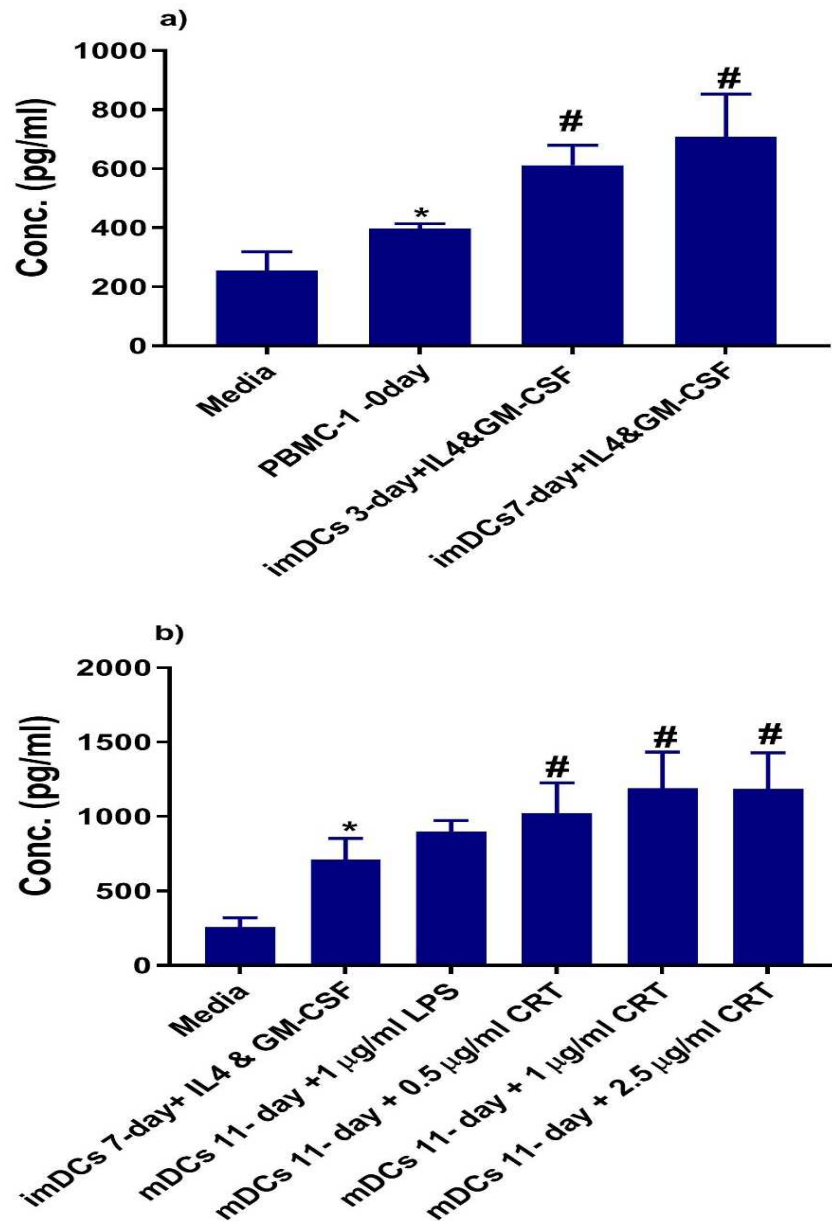


**Figure 5.24. Peripheral blood monocyte derived DC maturation by CRT is associated with secretion of the cytokines IL12 and IL23.** Peripheral blood derived monocytes were treated with (a) GM-CSF and IL4 to induce differentiation of imDCs or (b) LPS or CRT (0.5, 1, 2.5 µg/ml) to induce maturation to mDCs. Cell culture supernatants were collected and assessed for the content of IL-12/IL-23 (p40) using a commercially available ELISA kit. Data are mean ± SD, from three individual experiments with each determination performed in triplicate. \*p<0.05 basal media vs. untreated cells at day 0. #<0.05 treatments vs untreated cells at day 0 (PBMC monocytic cells).

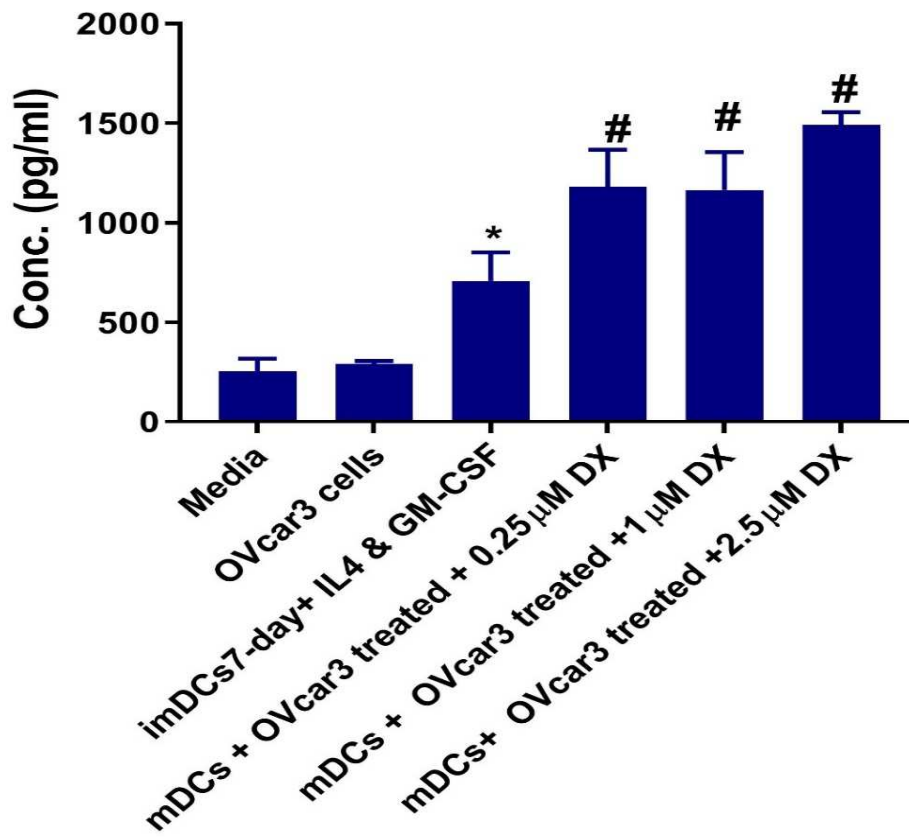


**Figure 5.25. Co-incubation of doxorubicin treated OVcar3 cells and peripheral monocyte-derived imDCs induces secretion of IL12/IL23.** imDCs derived from peripheral blood derived monocytes were co-incubated with OVcar3 ovarian cancer cells pre-treated with increasing concentrations of doxorubicin (0.25,1, 2.5 μM) to induce DC maturation. After 4 days cell culture supernatants were collected and assessed for the content of IL-12/IL-23 (p40) using a commercially available ELISA kit. Data are mean ± SD, from three individual experiments with each determination performed in triplicate. \* $p < 0.05$  basal media vs. untreated cells at day 0. # $< 0.05$  treatments vs untreated cells at day 0.

#### **5.4.12. Maturation of dendritic cells derived from THP-1 cells is also associated with increased secretion of IL12/IL23.**

The levels of secreted IL-12/IL-23 were also examined in DCs derived from THP-1 cells to allow further comparison of the functional responses of the DCs derived from the two different sources. Differentiation of THP-1 cells to imDCs was accompanied by a significant secretion of IL12/IL23 (Figure 5.26). At days 3 and 7 of maturation by GM-CSF & IL4 secreted levels were  $661 \pm 301.5$  pg/ml and  $635.9 \pm 190.1$  pg/ml compared with levels at day 0 ( $359.5 \pm 149.9$  pg/ml). These responses were similar to those seen in peripheral monocytes (Figure 5.26 a). However, in contrast to the monocyte derived DCs only maturation induced by  $1 \mu\text{g/ml}$  exogenous CRT was associated with a significant increase in IL12/23 secretion (from  $635.9 \pm 190.1$  pg/ml in control cells to  $1255 \pm 238$  pg/ml, (Figure 5.26 b,  $p < 0.05$ ,  $n=3$ ). THP-1 derived DCs treated with LPS as a positive control and  $0.5 \mu\text{g/ml}$  CRT secreted increased levels of IL12/IL23, but these were not significant. Interestingly,  $2.5 \mu\text{g/ml}$  CRT did not induce any increase in cytokine secretion which was in contrast to the results from peripheral monocyte derived DCs.

Cytokine secretion from THP-1 derived imDCs that were stimulated to mature by co-incubation with doxorubicin-treated OVcar3 cells was also different to the results observed in DCs from peripheral monocytes. Only OVcar3 treated with the highest concentration of doxorubicin ( $2.5 \mu\text{M}$ ) induced significant cytokine secretion (from  $750.4 \pm 143.9$  pg/ml to  $1227 \pm 217.1$  pg/ml,  $p < 0.05$ ,  $n=3$ ) (Figure 5.27). Although OVcar3 cells treated with  $1 \mu\text{M}$  doxorubicin did induce increased cytokine secretion this was not significant. OVcar3 pre-treated with  $0.5 \mu\text{M}$  doxorubicin had no effect on DC secretion of IL12/23 (Figure 5.27). These data confirm that DCs derived from different sources display differential responses.

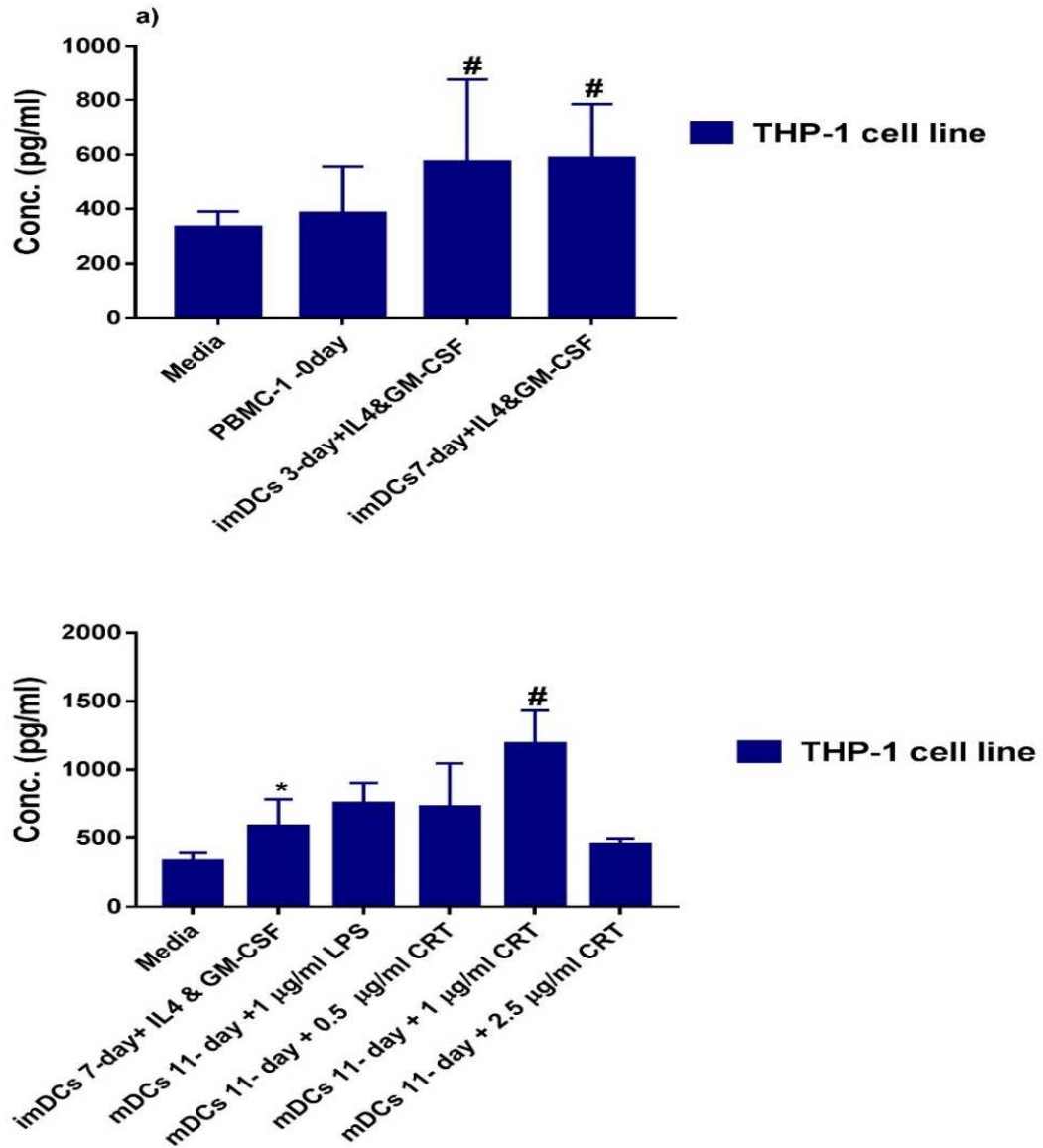


**Figure 5.26. THP-1 derived DC maturation is only associated with secretion of the cytokines IL12 and IL23 when induced by high concentrations of CRT.** THP-1 cells were treated with (a) GM-CSF and IL4 to induce differentiation imDCs or (b) either LPS or CRT (0.5, 1, 2.5 µg/ml) to induce maturation to mDCs. Cell culture supernatants were collected and assessed for the content of IL-12/IL-23 using a commercially available ELISA kit. (b) Data are mean ± SD, from three individual experiments with each determination performed in triplicate. \* $p < 0.05$  basal media vs. untreated cells at day 0. # $< 0.05$  treatments vs untreated cells at day 0.



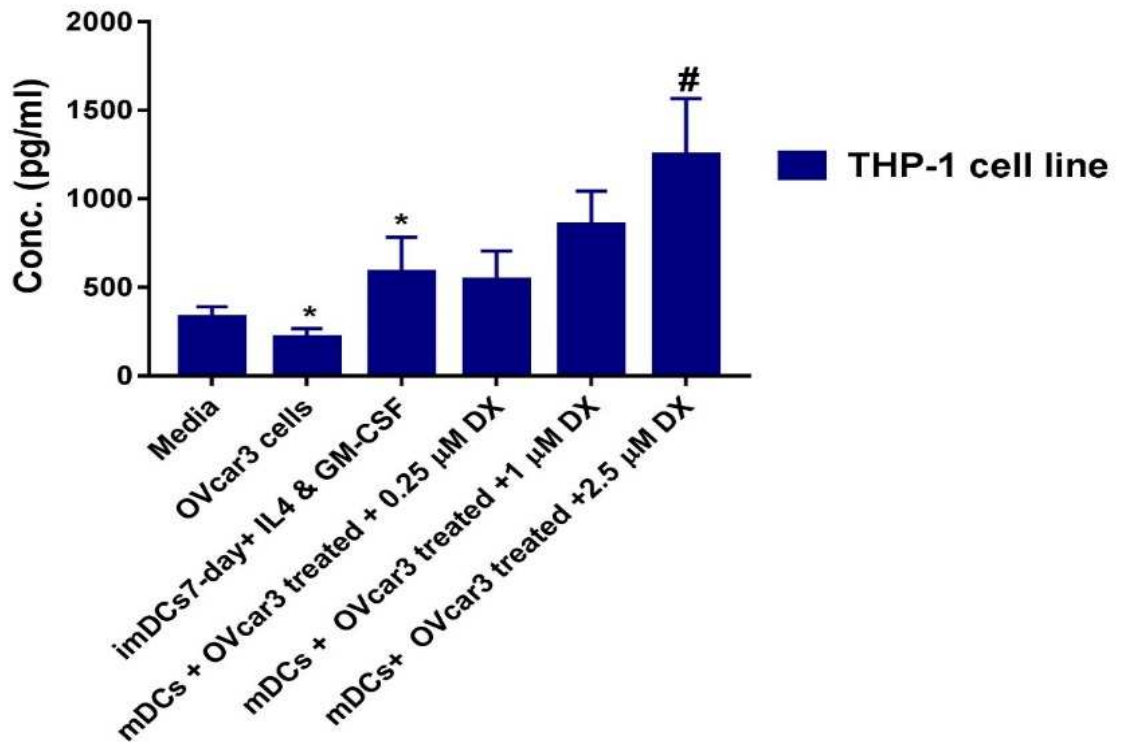


**Figure 5.27. OVcar3 cells pre-treated with high concentrations of doxorubicin induce secretion of IL12/IL23 from THP-1 derived DCs during DC maturation.**

imDCs derived from THP-1 cells were co-incubated with OVcar3 ovarian cancer cells pre-treated with increasing concentrations of doxorubicin (0.25,1, 2.5 μM) to induce DC maturation. After 4 days cell culture supernatants were collected and assessed for the content of IL-12/IL-23 using a commercially available ELISA kit. Data are mean ± SD, from three individual experiments with each determination performed in triplicate. \*p<0.05 basal media vs. untreated cells at day 0. #<0.05 treatments vs untreated cells at day 0.

#### **5.4.13. The effect of mDCs on T-cell proliferation**

The results presented so far in this chapter indicate that imDCs can be derived *in vitro* and that these cells can then be induced to undergo maturation to mDCs as assessed by cell surface markers and secretion of co-stimulatory cytokines IL12 and IL23. As described in the introduction to this chapter mDCs are the interface between foreign and tissue-specific antigens and T lymphocytes. *In vivo* maturation of DCs, presentation of antigens and secretion of IL12 is associated with activation and thus proliferation of naïve T lymphocytes, ultimately leading to ICD. Since both exogenous and endogenous CRT were able to induce DC maturation the next set of experiments were carried out to examine whether CRT alone or these mature DCs could activate T cells.

T lymphocytes were isolated from peripheral blood mononuclear cells from healthy donors by MACS® Technology using a CD8+ T Cell Isolation Kit (Miltenyi Biotec). Successful enrichment of the isolated cells with T- cells was determined by flow cytometry after dual labelling with fluorescently antibodies against T cell markers i.e. CD3-APC and CD8-FITC (Figure 5.28). These data indicate a cell population highly enriched for naïve T cells.

Isolated T lymphocytes were stained with CFSE and then incubated with mediators to induce activation/proliferation for 5 days. Flow cytometry was then carried out (gating for CD-3 expressing cells i.e. mature T cells) to examine CFSE fluorescence in the proliferated cells. CFSE covalently labels intracellular molecules and thus when a CFSE-labelled cell divides the daughter cells each take half the CFSE. This allows each cell division to be assessed by measuring the corresponding decrease in CFSE fluorescence (Quah, 2010) i.e. each peak of fluorescence approximately corresponds to a cell division (see Figure 5.29 below)

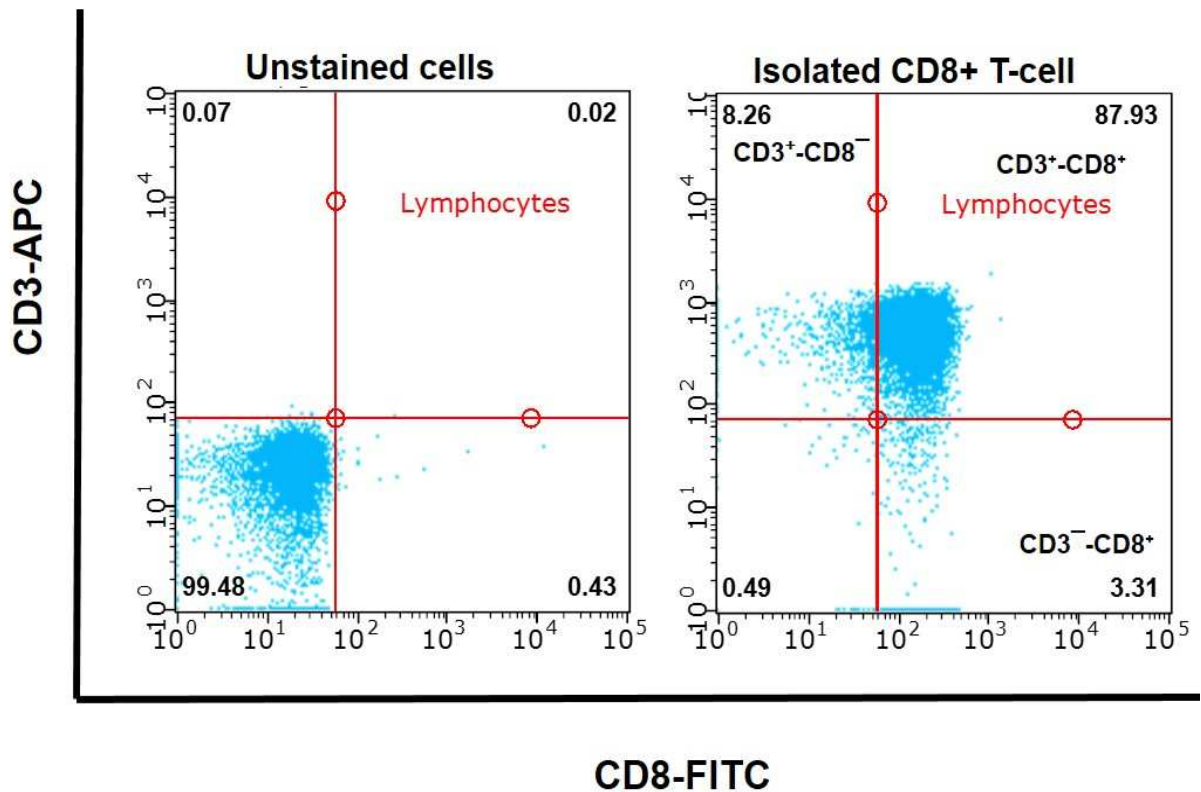


**Figure 5.28. Flow cytometry analysis of a typical CD8 T-cell purification using negative selection magnetic bead technology.** Isolated lymphocytes were fluorescently stained with anti-human CD8-FITC antibody and anti-human CD3-APC antibody. The live cell population was gated on an FSC-A vs SSC-A plot and cell debris excluded from the analysis. Fluorescently stained cells were identified by gating out unstained cells. The experiment was repeated 10 times.

#### **5.4.14. Activation of human T cells by Human T-Activator CD3/CD28 Dynabeads®.**

Initial experiments were carried out using a positive control i.e. isolated T cells were incubated with magnetic beads bound to antibodies to the T-cell co-stimulatory molecules CD3/CD28 in the presence of the additional stimulator IL2. It can be seen from Figure 5.29 that the combination of the anti-CD3/CD28 Dynabeads and IL2 induced T-cell proliferation and that proliferation over 5 days could be effectively measured by CFSE staining and flow cytometry. The number of stained daughter cells increased at each cell division until day 5 (Figure 5.29 c). As expected fluorescent intensity steadily decreased in the cell populations as each daughter cell only took half of the fluorescence in the parent cell (Figure 5.29 a). Unstimulated cells did not divide. These results indicate that CFSE labelling and flow cytometry is an effective method of examining T-cell proliferation *in vitro*.

#### **5.4.15. Activation of human T cells by mDCs induced to mature by various treatments (see Figure 5.30)**

Experiments were then carried out to examine whether mDCs induced to mature by (i) LPS (positive control), (Nagata et al., 2016) exogenous CRT or (iii) OVCa3 cells pre-treated with doxorubicin to expose endogenous CRT, could subsequently stimulate naïve T-cell activation and proliferation. After maturation by these methods DCs were incubated with T-cells stained with CFSE staining and after 5 days T-cell proliferation was analysed by flow cytometry.

The results are summarised in Figure 5.31. It can be seen that DCs matured by all treatments induced T-cell proliferation. For example T-cells incubated with DCs matured by 0.5 µg/ml CRT increased in number by approximately 1-fold at division 1, 1.2 fold at division 2, 1.7 fold at division 3 and 2.2 fold at division 4 (Figure 5.31.,b,c). DCs matured by 1 and 2.5 µg/ml also induced T-cell proliferation, with an apparent dose response i.e. the ability of DCs to induce T-cell proliferation appeared to be dependent on the concentration of CRT that the DCs were previously exposed to. For instance after 4 days numbers of T-cells were  $395.6 \pm 5$ ,  $632.3 \pm 57$  and  $702.8 \pm 6$  after co-culture of T-cells with DCs matured with 0.5, 1 and 2.5 µg/ml CRT respectively. Interestingly, DCs treated with 2.5 µg/ml CRT

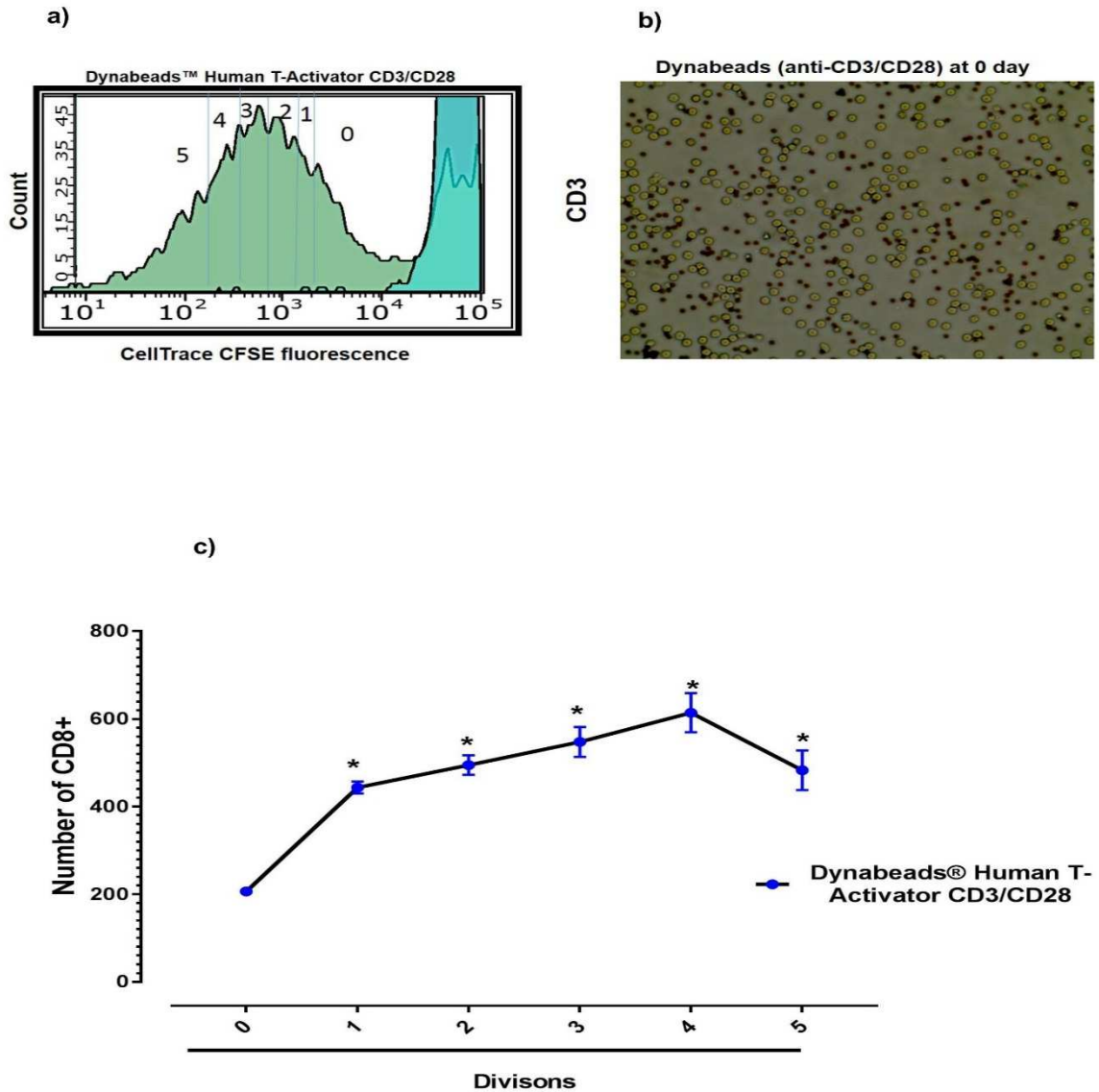


**Figure 5.29. T lymphocyte proliferation induced by human T-activator anti-CD3/CD28 Dynabeads™ and assessed by CFSE fluorescence** (a) Human T lymphocytes were stained with the CellTrace™ CFSE cell proliferation kit and cultured for 5 days with CD3/CD28 Dynabeads and IL-2. Cells were then analysed using flow cytometry with 488 nm excitation and a 530/30 nm emission filter. Successive generations of live cells are represented by the discrete green peaks. The blue colour indicates the unstimulated parent generation. (b) Microscopic image of T lymphocytes bound to anti CD3/CD28 microbeads at (day 0). (c) Graph showing numbers of daughter cells at each division (from a). Results are mean  $\pm$  SD, \* $p < 0.05$  vs control,  $n = 10$ .

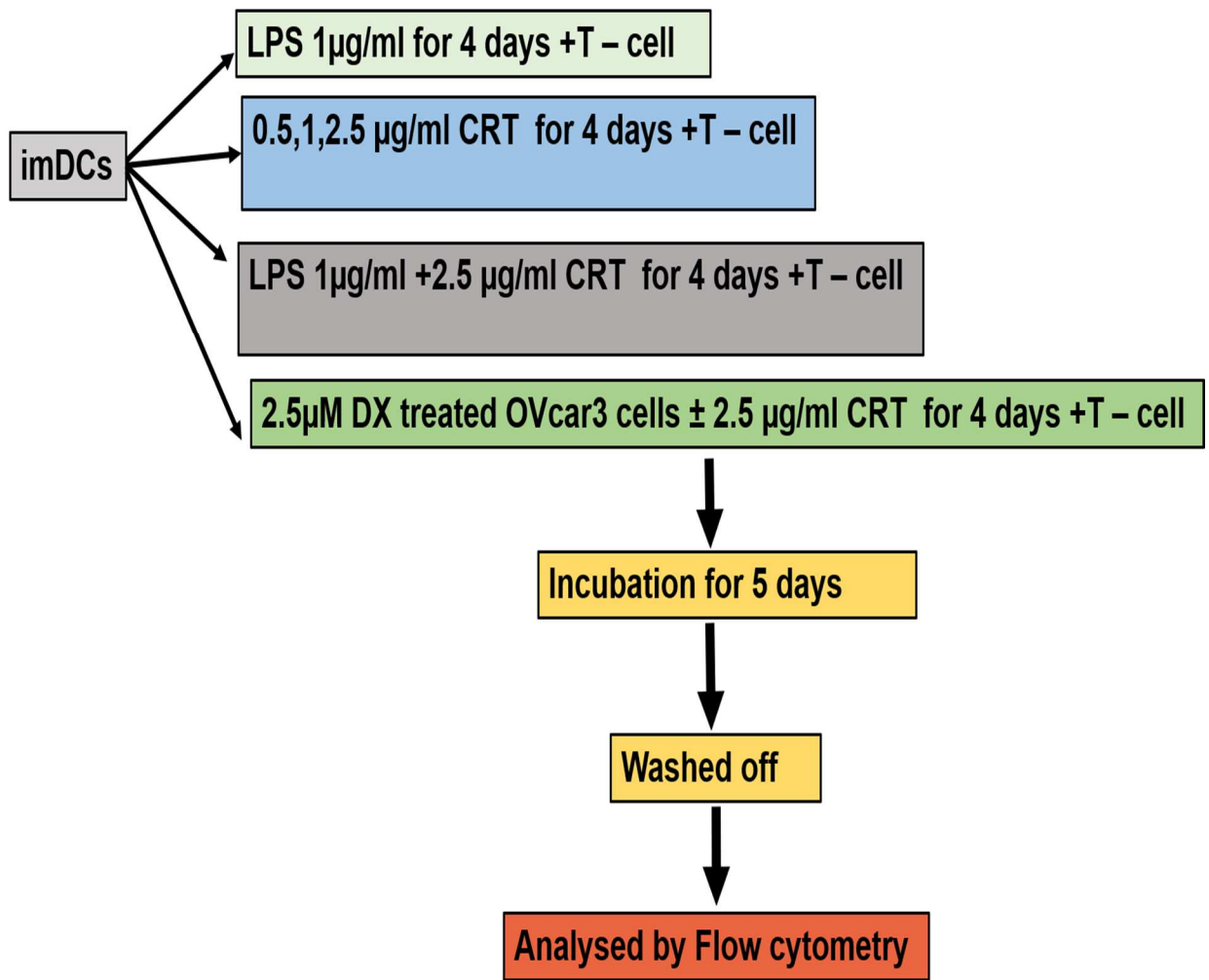
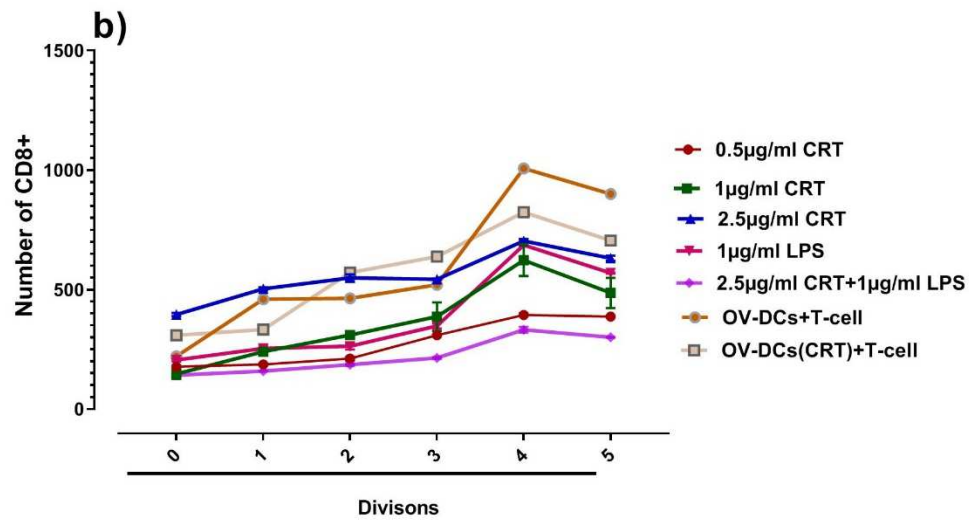
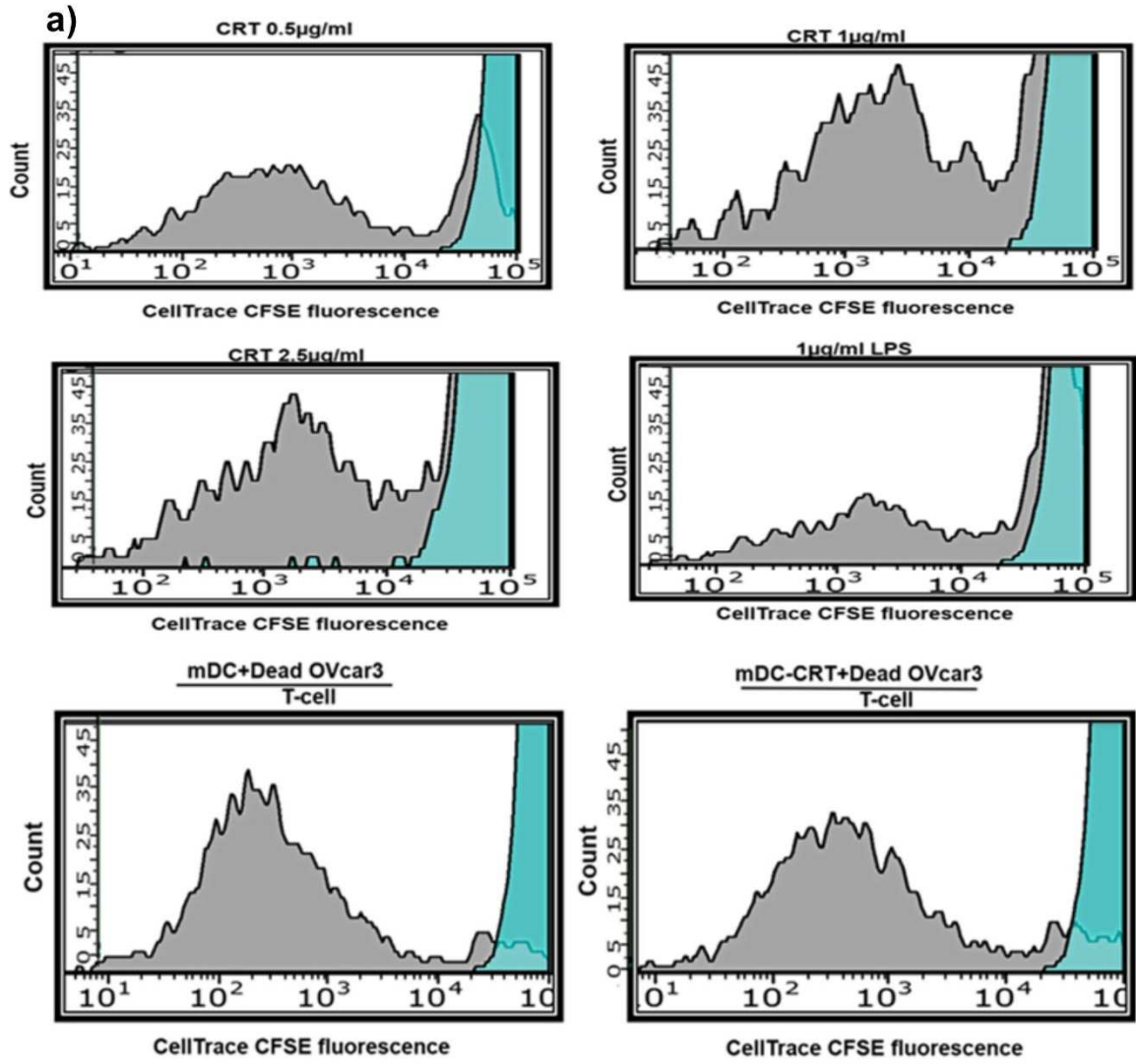


**Figure 5.30. Schematic diagram showing the experimental plan of studies carried out to examine whether DCs induced to mature by various treatments could subsequently stimulate T-cell proliferation.** Immature DCs (imDCs) were incubated with 0.5, 1, or 2.5µg/ml of CRT; 1µg/ml LPS ± 2.5µg/ml of CRT; OVCAR3 pre-treated with 2.5µg/ml doxorubicin (DX) or OVCAR3 pre-treated with 2.5µg/ml CRT to induce maturation. The mDCs were then co-cultured with carboxyfluorescein succinimidyl ester (CFSE)-labelled T-cells and T-cell proliferation was assessed after 5 days by flow cytometry.



c)

Dose	0	1	2	3	4	5	Significant
0.5 µg/ml CRT	177.3 ± 2.217	187.5 ± 3.317	213.5 ± 7.895	309.5 ± 4.123	395.5 ± 5.447	387.3 ± 2.986	*
1µg/ml CRT	151.8 ± 19.36	242.8 ± 9.142	311.5 ± 8.021	399.8 ± 55.63	632.3 ± 57.52	500 ± 58.69	*
2.5µg/ml CRT	396.8 ± 5.852	504.8 ± 6.076	552 ± 12.88	544 ± 2.708	702.8 ± 6.185	634.3 ± 10.4	*
1µg/ml LPS	204.3 ± 5.058	253 ± 10.39	265 ± 11.34	351 ± 10.52	682.5 ± 9.609	569.5 ± 1.732	*
2.5µg/ml CRT+1µg/ml LPS	142.8 ± 1.893	159.5 ± 0.5774	184.5 ± 5.26	215.3 ± 3.775	334 ± 10.23	301 ± 1.414	*
OV-DCs+T-cell	221.3 ± 2.062	459.3 ± 4.272	464.8 ± 3.686	522.8 ± 9.142	1005 ± 10.68	900.3 ± 2.062	*
OV-DCs(CRT)+T-cell	306.8 ± 7.89	332 ± 5.416	573.5 ± 5.066	638.5 ± 5.972	827.8 ± 19.16	704 ± 8.679	*

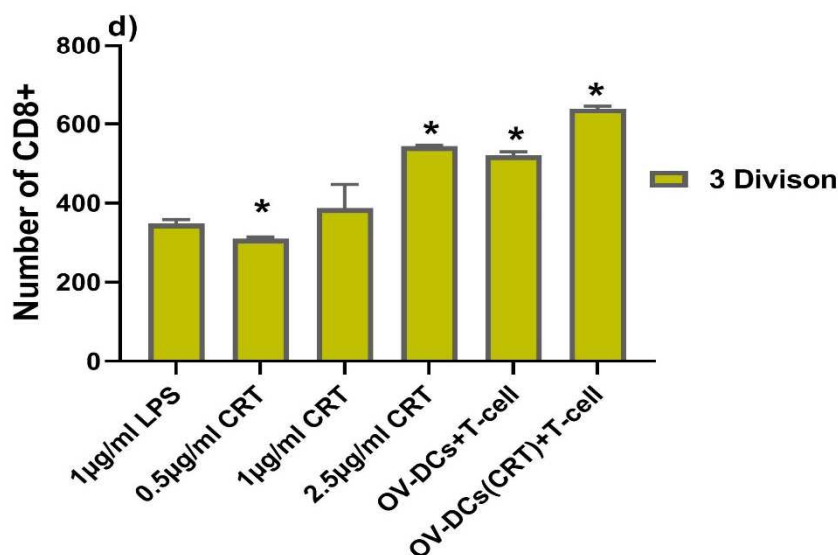


**Figure 5.31. DCs induced to mature by either exogenous or cancer cell surface bound CRT subsequently induce T-cell activation as assessed by proliferation.** imDCs were incubated with 0.5, 1, or 2.5µg/ml of CRT; 1µg/ml LPS; OVCAR3 pre-treated with 2.5µg/ml doxorubicin; pre-treated OVCAR3 + 2.5µg/ml CRT, to induce maturation. The mDCs ( $1 \times 10^6$ ), were then co-cultured with CFSE-labelled T cells ( $1 \times 10^5$ ) in 24-well plates in the presence of IL-2 (30µg/ml) and proliferation was assessed after 5 days by flow cytometry (a) Flow cytometry histograms showing proliferation of CFSE labelled T-cells (b) Mean number of cells at each division with the different treatments, (c) Table displaying results presented in (b), \*p=0.05 day 5 vs day 0. (d) Comparison of T-cell numbers at the 3<sup>rd</sup> generation with the different mDC populations \*p = 0.05 vs LPS, b, c,d show mean ±SD from 10 separate experiments.



were more effective at inducing T-cell proliferation than the positive control, LPS ( $351 \pm 10.52$  T-cells after 3 days).

Importantly, it was found that T- cells co-cultured with DCs that had been matured by co-incubation with  $2.5\mu\text{g/ml}$  doxorubicin-treated OVcar3 showed the greatest levels of proliferation. After 4 days T-cell numbers were  $1005 \pm 10$  compared with the LPS ( $682.5 \pm 9$  T-cells after 4 days) i.e. OVcar3 with exposed CRT were approximately 30% more effective at inducing T-cell proliferation than LPS. Interestingly, T-cell proliferation induced by DCs matured in the presence of both doxorubicin-treated OVcar3 and CRT did not show enhanced proliferation over maturation induced by OVcar3 alone  $827.8 \pm 19$  vs  $1005 \pm 10$ , perhaps suggesting that DCs matured by surface expressed endogenous CRT are most efficient at inducing T-cell proliferation. Surprisingly, DCs matured by both LPS and exogenous CRT ( $2.5\mu\text{g/ml}$ ) were the least effective at stimulating T-cell proliferation.

## **5.5. Discussion**

Options for effective ovarian cancer chemotherapy remain limited and therefore interest in alternative therapeutics such as immunotherapy and induction of ICD and immune-mediated eradication has increased (Drakes and Stiff, 2016, Mantia-Smaldone et al., 2012). However, this remains a challenge due to the poor immunogenicity of cancer cells (Kandalaf et al., 2011). ICD requires recognition and uptake of cancer cells by professional phagocytes and APCs such as DCs and then activation of a T-cell mediated response to generate T cells that can recognise and destroy the cancer cells. Indeed, enhanced DC activation is linked to increased survival in a number of cancers (Fu and Jiang, 2018). Recently, it has been reported that CRT at the cell surface enhances DC maturation and MHC-I based antigen presentation to promote activation of T- cytotoxic responses in non-small-cell lung cancer (Vansteenkiste et al., 2013). The work in this chapter aimed to examine whether similar responses could be observed in EOC. Since levels of surface bound CRT could be increased either by addition of exogenous CRT or by induction of the translocation of endogenous CRT to the cell surface, both approaches were investigated (see Figure 5.23).

Thus, the overall aim of this chapter was to investigate whether exogenous CRT or translocated (and cell bound) endogenous CRT could promote maturation of imDCs and T cell activation responses i.e. T-cell proliferation. imDCs were derived from both the THP-1 cell line and peripheral blood monocytes and both the differentiation of imDCs from monocytes and the maturation of DCs were fully characterised.

The main findings of this chapter were:

1. imDCs derived from both THP-1 and peripheral blood monocytes could be matured to cells displaying the phenotypic and secretory characteristics of mDCs by both exogenously added CRT and cancer cells with cell surface bound CRT.
2. The mDCs induced by these treatments and exogenous CRT alone were able to stimulate T-cell activation as assessed by T-cell proliferation.

#### **Effect of exogenous CRT on maturation of imDCs.**

Previously published data reported that the THP-1 cell line can be differentiated into highly pure monotypic DCs presenting with the morphologic and functional properties of imDCs, including co-stimulatory (maturation marker) molecule expression on the cell surface (Berges et al., 2005).

In this study imDCs were generated from the THP-1 cell line by incubation for 7 days with GM-CSF and IL-4 and a significant increase was observed in levels of the DC surface markers CD11c, CD86 and HLA-DR, although the increase in levels of CD80 and CD83 did not reach significance. These data agree with similar reports in the literature. For instance, it has been reported that THP-1 cells and the CD34+ (KG-1) leukaemia cell line incubated with varying concentrations of rhGM-CSF and rhIL-4 for 5 days showed upregulated levels of CD11c, CD80 and CD86 and of the cell-surface receptors CD40, CD209 (DC-SIGN) but failed to express CD83 (Monti et al., 2003).

THP-1 imDCs stimulated with the positive control, LPS, for 4 days to generate mDCs showed upregulation of CD11c, CD80, CD83, HLA-DR and CD86 but lower expression of CD14. All of these changes in marker expression have been observed on the cell surface of mature dendritic cells (Tokunaga et al., 2005, Halin et al., 2005) confirming that DC maturation could be induced in the *in vitro* system used here.

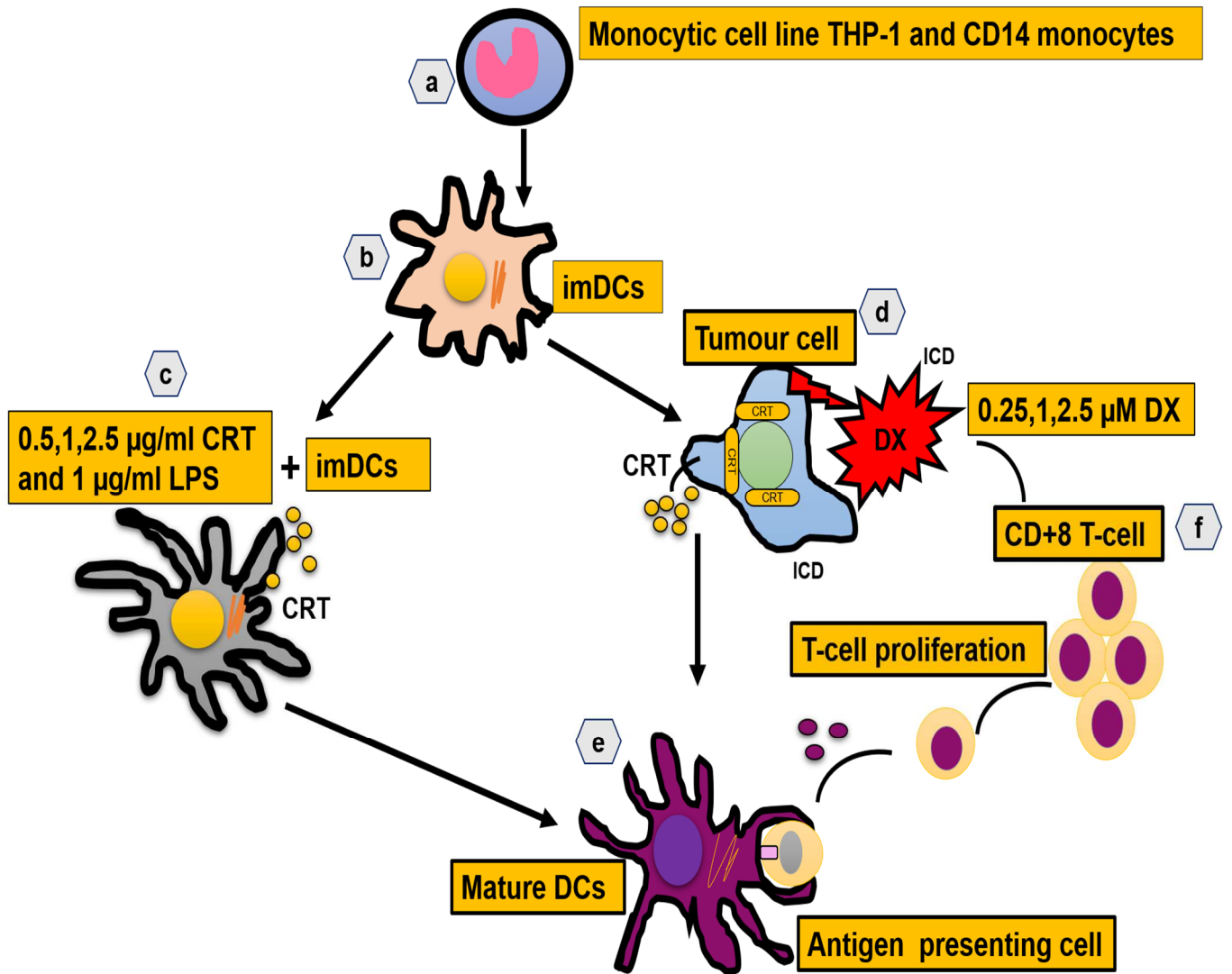


**Figure 5.32. Schematic representation of the experimental procedures used in this chapter.** The human monocytic cell line THP-1 or CD14+ monocytes collected from peripheral blood **(a)** were differentiated to immature dendritic cells (imDCs) **(b)**. These imDCs were exposed to 1µg/ml LPS as a positive control, CRT (0.5, 1, 2.5 µg/ml) **(c)** or OVcar3 ovarian cancer cells pre-treated with doxorubicin (DX to induce surface CRT expression **(d)**. DC maturation was assessed by expression of surface markers and cytokine secretion **(e)**. The ability of these mature DCs or CRT to stimulate T-cell responses **(f)** i.e. proliferation was examined.

Exogenous CRT triggered a response to enhance maturation of THP-1 imDCs. Interestingly 0.5 µg/ml CRT was not sufficient to enhance expression of all maturation markers whereas expression of CD11C, HLA-DR, CD80 and CD83 were all increased by treatment with 1 and 2.5 µg/ml CRT for 4 days. This observation was supported by the ELISA for IL-12 /IL-23 which only showed increased secretion at 1 µg/ml in the THP-1 cell line.

These results were supported by ELISA measurement of IL12/IL23 secretion (Reinhardt et al., 2006). Upregulated secretion of these cytokines has been reported in mDCs and this was also observed here. Maturation of THP-1 derived imDCs induced by exogenous CRT at increasing concentrations was accompanied by increased secretion of IL12/IL23 cytokines. These results demonstrate for the first time that CRT is able to induce maturation of human THP-1 derived DCs as assessed by increased secretion of cytokines IL12/IL23. These data are supported by studies on animal cells. For instance, maturation of imDCs derived from BALB/c mouse bone marrow cells by rCRT/39-272 (30 µg/ml) purified from *Escherichia coli*, was accompanied by increased expression of IL-12/IL-23 (p40) and IL-1β (Li et al., 2015).

The DC responses studied in THP-1 cells were also examined in DCs derived from freshly isolated CD14+ monocytes collected from a healthy donors and enriched using a magnetic separation method similar to that previously described (Neu et al., 2013). Similar to THP-1 cells, the stimulating factors GM-CSF and IL-4 efficiently differentiated imDCs from the isolated monocytes, inducing cells with high expression of HLA-DR, CD80, CD83, and CD86. These data are similar to reports in the literature, for instance Thurner et al. (Thurner et al., 1999) showed significant upregulation of CD14, CD86 and CD83 in monocyte derived DCs induced by treatment with 500 U/ml IL-4 and 800 U/ml GM-CSF for 5 days.

DC maturation was also studied in monocyte-derived imDCs by changes in surface expression of key maturation markers. 0.5 µg/ml CRT significantly increased expression of CD83 and HLA-DR only, but similarly to the THP-1 cells higher CRT concentrations (1, 2.5 µg/ml) were more efficient at inducing maturation of DCs. Treatment of imDCs with 2.5 µg/ml CRT led to significant changes in surface expression of all markers studied (CD80, CD11c, HLA-DR, and CD83, CD 86 and

CD14) and secretion of the pro-inflammatory cytokines IL12/IL23. This confirms that CRT is a potent stimulator of DC maturation. This has also been observed in other recent studies. For example Bajor et al. (Bajor et al., 2011) reported that imDCs derived from peripheral blood monocytes and stimulated by 10 µg/ml CRT showed increased expression of CD80 and CD86 on the surface of mDCs, and decreased expression of CD14.

The observation that in both THP-1 and monocyte derived DCs expression of maturation markers was greater following exposure to higher concentrations of CRT suggests that there is a threshold level of CRT required to induce efficient maturation. Additionally, the highest concentration used i.e. 2.5. µg/ml was as effective as inducing DC maturation as the positive control, LPS, suggesting that the levels used in previous studies were unnecessarily high e.g. 10 µg/ml. (Bajor et al., 2011).

In classical immune responses damaged or stressed cells display pathogen-associated molecular pattern molecules (PAMPs), derived from microorganisms and/or damage-associated molecular pattern molecules (DAMPs) which are cell derived and can initiate immune responses to trauma in the absence of infection. Both can be recognised by corresponding pattern recognition receptors (PPRs) on the surface of imDCs, triggering phagocytosis. The DCs engulf these signposted target cells and then enter a maturation process during which the phagocytosed cellular antigens are presented on the cell surface in association with MHC class I and II complexes. These antigen complexes are then recognised by T cell receptors on both CD4<sup>+</sup> and CD8<sup>+</sup> T cells which triggers initial activation of naïve CD8<sup>+</sup> T cells into activated cytotoxic CD8<sup>+</sup> T cells. The process of DC maturation is accompanied by expression of surface molecules and secretion of cytokines which act as co-stimulatory molecules for the T cell activation.

Cell surface CRT is a recognised DAMP translocated to the cell surface in response to ER stress and has been reported to contribute to uptake by dendritic cells (Gold et al., 2015, Obeid et al., 2007, Bajor et al., 2011). Importantly CRT has been shown to be a C1q receptor on the cell surface of early apoptotic cells and the two proteins associate to form an “eat me” that interacts with the globular region of CD91 on phagocytes to enhance phagocytosis, (Wiersma et al., 2015). Thus, integration of

changes on the surface of dying cells signal to DCs. However, intriguingly in the data presented here CRT alone added exogenously very efficiently induced DC maturation in the absence of antigen processing or other dying cell surface molecules, suggesting that CRT is able to induce DC maturation in the absence of any other associated cell surface molecules or antigens.

It is not fully understood how CRT induces maturation of DCs. However, recently, it has been shown that CRT has a very strong attraction for LPS which is a potent PAMP and that all preparations of recombinant CRT and CRT isolated from human tissue contain bound LPS, including the *Pichia pastoris* rCRT used here (Pandya et al., 2019).

This suggests that this is a physiologically relevant finding and that CRT-LPS act in concert to enhance immune responses, raising the possibility that the direct effects of CRT observed here are due to the combination of the two immune activators acting together to induce DC maturation, by an as yet unknown mechanism.

### **The effect of surface exposed endogenous CRT on DC maturation.**

Translocation of intracellular CRT in cancer cells has been observed in response to chemotherapeutic agents such as the anthracycline, doxorubicin (Zitvogel et al., 2010) and as discussed in Chapter 1 (Introduction) CRT has been reported to activate APCs and regulate innate and adaptive immune responses. The results presented in Chapter 4b indicate that doxorubicin induced CRT exposure and secretion in various cancer cell lines. Therefore, since exogenous CRT very effectively induced DC maturation in both types of imDCs studied, experiments were carried out to examine whether surface exposed endogenous CRT could have the same effect.

One of the key findings of this study was that OVcar3 ovarian cancer cells pre-treated with doxorubicin (to induce CRT translocation to the cell surface) did induce iDC maturation in both DC models studied. This effect appeared to be dependent on the original concentration of doxorubicin used to treat the OVcar3 cells. OVcar3 treated with both 1 and 2.5  $\mu$ M induced increased expression of CD11c, CD80, CD83, CD86 and HLA-DR compared with untreated imDCs derived from both THP-1 cells and blood

monocytes, although this did not reach significance for CD80. OVcar3 treated with all concentrations of doxorubicin significantly reduced CD14 expression on both types of DCs. It is possible that these differences could be attributed to increased levels of translocated CRT on the surface of the dying cancer cells in response to the greater doses of doxorubicin (Michaud et al., 2011). These results indicate that cancer cells treated with a chemotherapy primarily used as a toxic agent may also play an important role in activating DCs and thus the adaptive immune system in EOC. Chapter 4 indicated that doxorubicin also induced secretion of CRT and it is possible that the secreted CRT induced DC maturation, since exogenous CRT was a very effective activator. However, the doxorubicin treated cancer cells used here were treated and then washed, to remove the doxorubicin, before co-incubation with the iDCs. This suggests that it is more likely that CRT already translocated to the surface was activating the DCs, but does not fully rule out a role for secreted CRT.

Additionally, *in vivo*, increased expression of CRT on tumour cells induced by photodynamic therapy in a mouse model correlated with increased maturation of dendritic cells, with enhanced expression of markers such as CD80 and CD86 (Wang et al., 2015).

OVcar3 treated with 2.5  $\mu$ M doxorubicin also induced significant secretion of the cytokines IL12/23 from maturing DCs, which play a critical role in T cell proliferation. Previously, reports indicated that treatment of tumour cells (MCF-7 breast cancer and A2780 ovarian cancer cells) with doxorubicin for 72 hours at different concentrations was sufficient to stimulate the activation of cell-mediated immunity by release of cytokines TNF- $\alpha$ , CXCL8, and CXCL1 (Edwardson et al., 2017). This supports the possibility that doxorubicin-treated tumour cells could enhance cell-mediated immunity.

DC maturation by CRT has been reported in other systems. Treatment with a recombinant calreticulin fragment, rCRT/39-27 treatment induced phenotypic maturation of imDCs derived from BALB/c mouse bone marrow cells (Li et al., 2015).

## **Effects of exogenous and surface exposed endogenous CRT on T- cell proliferation**

It is now widely accepted that CD8+ T cell proliferation can be studied *in vitro* e.g. an early study by (Hodge et al., 2000) measured relative T-cell proliferation (cell number) of murine tumour cells after exposure to either rF- or rV-TRICOM vectors to enhance proliferation. Since exogenous and endogenous surface-exposed CRT induced DC maturation, the next step was to examine whether the mDCs produced could activate the T cell responses normally observed in the development of an adaptive immune response i.e. clonal expansion or proliferation. Thus, pre-treated matured DCs were co-incubated with freshly isolated T-cells labelled with CFSE which allowed proliferative cycles to be followed (BJ, 2010). It has been reported that T-cells collected from human peripheral blood and incubated with antiCD3/CD28 showed increased proliferation at day 3 of treatment which then gradually declined to baseline levels after ~10 days (Quah et al., 2007). Therefore, initial studies using magnetic beads coated with anti-CD3/CD28 were carried out to validate the technique. The results showed a robust stimulation of T cell proliferation with anti-CD3/CD28 coated beads which could be followed by flow cytometry to detect the CFSE labelled daughter cell populations.

DCs matured by exogenous CRT alone, at all concentrations tested, induced T-cell proliferation. However, as for the other immune responses studied, this was dose dependent, with cells matured by 2.5µg/ml CRT inducing the greatest proliferative effect. It is not known whether this maturation was induced by the levels of LPS in the CRT preparation. However, the reported LPS levels in *Pichia pastoris* CRT are very low (Pandya et al., 2019), so again it is possible that the effects seen are a response to the combination of the two activating agents. This is supported by the observation that the highest level of CRT used (2.5µg/ml) was considerably more effective at inducing T cell proliferation than the LPS alone used as the positive control. In contrast to these findings a conjugate of CRT and ovalbumin-derived peptide did not show enhanced T cell activation *in vitro* or in a mouse model (Del Cid et al., 2012).

Importantly, the results showed, for the first time, that DCs matured by pre-incubation with OVcar3 cancer cells (with exposed surface CRT) also induced robust proliferation of T-cells and this response was greater than that observed with DCs matured with either CRT (at any dose) or LPS, the positive control. These results suggest that cell



surface CRT acts in concert with other cell surface changes on treated cancer cells to induce an integrated response in DCs as they mature, resulting in DCs presenting enhanced co-stimulatory molecules to T cells compared with CRT or LPS alone. Previously published data also reported that an increase in DC CRT (induced by infection with recombinant Ad-CALR) enhanced the maturation of DCs which subsequently induced T cell proliferation. Specifically the authors reported that the mDCs induced MAGE-A3-specific CD8+ cytotoxic T lymphocyte responses to non-small-cell lung carcinoma cells *in vitro* (Wang et al., 2012) (Liu et al., 2016b).

## **5.6. Conclusions**

In summary, this chapter has established that exogenous and endogenous CRT are potent stimulators of DC maturation and that DCs matured by exposure to both exogenous CRT and ovarian cancer cells previously treated with doxorubicin were subsequently able to induce DC8+ T cell activation and expansion. These data confirm that CRT is a key molecule in the development of ICD of tumour cells, and understanding the specific mechanisms that drive CRT to activate immune responses could highlight exciting new therapies for the treatment of ovarian cancer. Clearly, strategies that enhance CRT on the surface of targeted tumour cells or increase levels of exogenous CRT could theoretically be exploited as treatments. However, although these findings highlight an important regulatory role of CRT that may be exploitable for cancer immunotherapy, the precise mechanisms by which CRT evokes such anti-cancer immunity are still not fully understood.

## Chapter6 : Final discussion

CRT is a  $\text{Ca}^{2+}$  binding protein chaperone primarily located in the ER of all eukaryotic nucleated cells. In recent years, knowledge of the functional complexity of CRT both within and outside the ER has expanded exponentially. As a result CRT has been implicated in almost every aspect of normal physiological and pathological cell function, including important roles in health, disease, and the regulation of ICD i.e. immunogenically active apoptosis induced by some cancer therapies such as doxorubicin and types of radiotherapy (Eggleton and Michalak, 2013). In particular translocation of CRT from the ER to the cell surface is thought to mediate cancer cell engulfment by phagocytes and DC maturation and the subsequent activation of adaptive immune responses which can lead to cancer cell killing i.e. T cell expansion.

Activation of ICD is now recognised as a potential therapeutic tool for the elimination of cancer cells and EOC is becoming a focus for this therapy. EOC is the most lethal of all gynaecological cancers due to non-specific initial symptoms and the advanced stage of the disease at diagnosis in around 75% of patients. Together with the low 5 year survival rate of ovarian cancer patients in the UK (<50%) and only modestly improved treatment over the last decades, it is clear that research into strategies to induce ICD in ovarian cancer could be of great benefit, contributing to development of new and more efficient treatments and diagnosis.

The mechanism(s) by which CRT may be involved in ICD responses against ovarian cancer have been examined in this thesis using *in vitro* methodologies. This chapter will summarise the findings presented in this thesis, it will outline the gaps in the field which have been explored and those that require further work to develop a novel therapeutic strategy that exploits the immunogenic activity of CRT to selectively activate innate and adaptive immune responses to ovarian cancer cells.

The first step of this research (Chapter 3) was to establish a purification step for recombinant human CRT expressed in *E. coli* and *Pichia pastoris*. Briefly, expressed CRT was purified by FPLC affinity and size exclusion chromatography and characterised for future use. This provided monomeric CRT that was used in further experiments as an *in vitro* model for investigating the immune roles of extracellular CRT. As mentioned in Chapter 5, since this work was completed it has been reported

that physiologically CRT appears to be bound to LPS and that the two proteins may induce integrated cellular responses (Pandya et al., 2019). The *Pichia pastoris* CRT used here did contain low levels of CRT (Pandya et al., 2019) raising the possibility that some of the cellular responses seen may result from the effects of the two agents combined.

In the second step (Chapter 4) strategies to enhance cell surface levels of EOC CRT were investigated since this is thought to be a critical requirement for ICD of cancer cells. EOC binding of endogenous and exogenous CRT under ER stress and non-stress conditions were investigated in a panel of ovarian cancer cell lines (SKov3, OVcar3, and A2780). Initially, exogenous CRT was labelled with FITC to allow direct analysis of bound CRT by microscopy and flow cytometry. Ovarian cancer cells bound exogenous CRT under resting conditions and this binding increased dramatically in cells under stress conditions e.g. doxorubicin or the ER stressor thapsigargin. This increased binding was accompanied by apoptotic cell death and bound CRT levels were significantly greater on dying cells compared with living cells. Pre-treatment of cells with TUDCA, which has been reported to relieve ER stress, partially but significantly, protected cells against doxorubicin and thapsigargin induced cell death and simultaneously had similar effects on CRT binding.

The externalisation of endogenous CRT was also studied in cells treated with doxorubicin or thapsigargin. The resulting cell death was accompanied by an increase in surface exposure of CRT which again was greater in cells undergoing apoptosis and necrosis. This enhanced externalisation was accompanied by increased expression and secretion of CRT. Pre-treatment of cells with TUDCA again, partially but significantly, reduced doxorubicin and thapsigargin induced cell death and also reduced CRT expression, externalisation, and secretion.

It has been previously shown that CRT binds directly to PS (Tarr et al., 2010b) and since both early and late apoptotic cells have increased external membrane exposed PS as assessed by annexin V binding, it is assumed that surface bound CRT from both exogenous and endogenous sources bound to the cell surface via interaction with PS. These data suggest that in ovarian cancer cells agents such as doxorubicin induce apoptotic cell death by an ER stress mediated mechanism. This cell death is accompanied by increased expression and translocation of CRT to the cell membrane,

some of which remains associated with the cell surface and some of which is secreted and may subsequently also bind to the cell surface, increasing total levels. This CRT may act as an 'eat-me' signal that promotes the uptake of CRT-coated tumour cells, presentation of the resulting antigens by dendritic cells and T cell activation (Obeid et al., 2007, Chaput et al., 2007)

To investigate this possibility further the last stage of the study (Chapter 5), involved an *in vitro* investigation of the ability of exogenous and externalised cell surface CRT to enhance maturation of DCs and subsequent activation of a T cell response. Methodologies were established to: isolate peripheral blood monocytes and T cells; generate imDCs from both THP-1 cells and peripheral blood monocytes; characterise imDCs and mDCs and assess T cell proliferation. Flow cytometric analysis of surface markers of maturation indicated that both exogenous CRT and EOC previously treated with doxorubicin (to induce enhanced surface CRT levels) were able to stimulate maturation of DCs. Further studies indicated that DCs matured with both sources of CRT were able to activate T- expansion. Importantly the DCs matured by exposure to doxorubicin were most effective in inducing T cell activation.

These results suggest that CRT, either cell bound or in solution, can initiate DC maturation. CRT acts as a DAMP and, when cell associated, allows for the uptake of tumour cells by DCs, ultimately resulting in a T-cell mediated tumouricidal response (Hanke et al., 2013). Importantly, the results presented here suggest that this mechanism could be harnessed as a therapeutic strategy for ovarian cancer since EOC cells treated with doxorubicin initiated maturation of DCs and these mDCs were then able to activate robust T cell responses. Intriguingly, CRT alone i.e. not cell bound, induced DC maturation and these mDCs were also able to induce T cell expansion in the absence of presentation of tumour cell antigens. It is not possible to deduce a mechanism for these responses from the data presented. However, a recent study showed that the release of CRT from dying cells, prior to PS cell surface appearance, binds to macrophages thereby inducing numerous immune activities including pro-inflammatory cytokines, cell polarization and migration (Osman et al., 2017). It is possible that the exogenous CRT may act as a 'sponge' for even trace levels of LPS found in the solutions or media used e.g. trace levels of LPS have been found in foetal bovine serum (Kirikae et al., 1997) and that these two molecules may act in

concert to enhance DC maturation. Indeed, it has been demonstrated that CRT and other chaperones elicited immune functions against tumours *in vivo* possibly due to LPS binding and that following removal of associated LPS, numerous immune responses were lost except ERK phosphorylation (Reed et al., 2003). The study in this thesis is the first to demonstrate a role for ovarian cancer cell associated CRT and exogenous CRT in maturation of DCs and that the DCs matured by both of these routes induce proliferation of T-cells. These data confirm that exogenous CRT is a powerful activator of immune responses and could potentially have therapeutic potential for ovarian cancer cells therapies. Figure 6.1 summarises the key findings from this study.

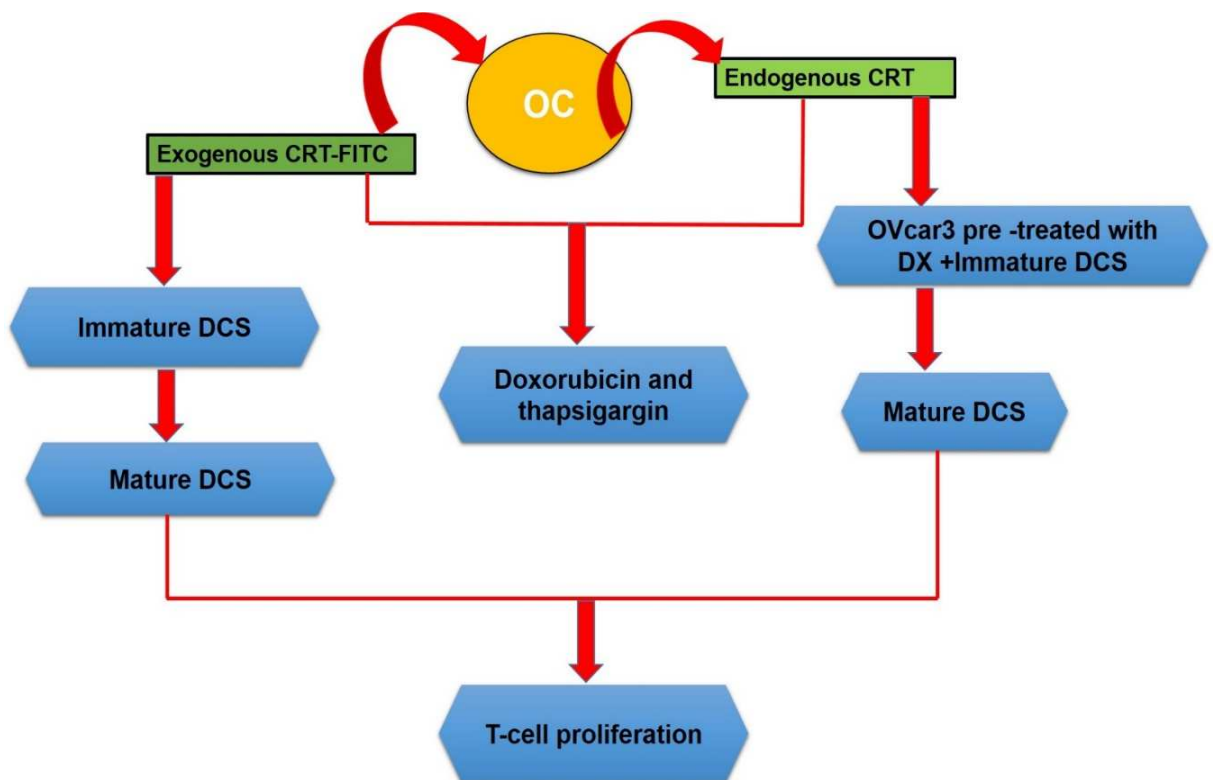


**Figure 6.1. Flowchart representing the key finding of this study.** Specifically, surface levels of CRT on EOC cells can be enhanced by treating cells with ER stressors such as doxorubicin and thapsigargin to externalise endogenous CRT or by adding exogenous CRT. EOC cells displaying surface CRT and exogenous CRT can induce DC maturation and DCs matured by both approaches can stimulate T-cell proliferation.

## **Limitations**

There are some limitations to this work that could be improved in future studies. For instance it was noted that the TUDCA was not 100% effective at reducing CRT translocation or cell death. This may have occurred because the TUDCA treatment conditions needed optimisation and this could be addressed by preliminary optimisation studies. Additionally, an alternative agent known to reduce ER stress could be used, for instance N-acetylcysteine (NAC). NAC reduces oxidative stress and, by inhibiting ROS-mediated ER stress, has been reported to prevent the ER-stress-related apoptosis pathway (Aggarwal et al., 2010). For instance, NAC exerts protective effects against iopromide-induced epithelial cell apoptosis by suppressing ROS overproduction and subsequent ER stress (Yang et al., 2014).

Secondly, *in vivo*, CD4+ T lymphocytes or T-helper cells play a major role in the development of immune responses by interacting with other cells including CD8+ killer cells and are essential in the formation of protective memory CD8+ T cells. Time did not allow an in depth investigation on the effects of CRT on CD4+ lymphocytes, but further studies in this area could have enhanced the data obtained.

## **Further work and potential projects**

**Manipulating CD 47 and CRT interactions.** A potential study that could be carried would be to manipulate surface levels of CD47 and CRT to determine the optimum ratio between “eat me” and “don’t eat me” signals that control the phagocytic fate of EOC cells. CD47 is a ubiquitously expressed surface glycoprotein that plays a critical role in immune self-recognition i.e. acts as a ('don't-eat-me' signal) mediating immune evasion of self-cells. To achieve this it is recognised by signal regulatory protein- $\alpha$  expressed on macrophages, neurons, dendritic cells and neutrophils. Some cancers take advantage of this mechanism and express CD47 to avoid cell death. Blockade of CD47 e.g. with antibodies that prevent CD47-SIRP $\alpha$  interaction ultimately inhibits the "don't eat me" signal (Jiang et al., 1999). Since CRT is known to act as an “eat me” signal (de Bruyn et al., 2015) (Wiersma et al., 2015) then an examination of optimum blockade of CD47 and the mechanism of achieving optimum CRT levels to achieve pro-phagocytic signals could be investigated.

**Expression and evaluation of a bi-specific antibody to bind to ovarian cancer cells.** The results found here clearly demonstrate that EOC with enhanced levels of cell surface CRT could induce DC maturation and subsequent T cell expansion. Thus, one novel therapeutic strategy could be to exploit this pro-immunogenic activity of CRT to ovarian cancer cells by developing a bi-specific human antibody which carries CRT and recognises EpCAM on the surface of the EOC cells. Administration of such an antibody therapeutically could potentially enhance CRT associated with the cell surface of the ovarian cancer cells, triggering an adaptive immune response and leading to cancer cell death. If used in combination with conventional chemotherapy such a strategy could reduce dosages and thus alleviate toxic side effects. The technology to produce a CRT/EpCAM antibody is being developed by one of the co-supervisors on this project and initial experiments could evaluate the specific binding of this antibody to EpCAM expressing and non-expressing cells using an anti-CRT antibody (Figure 6.2).

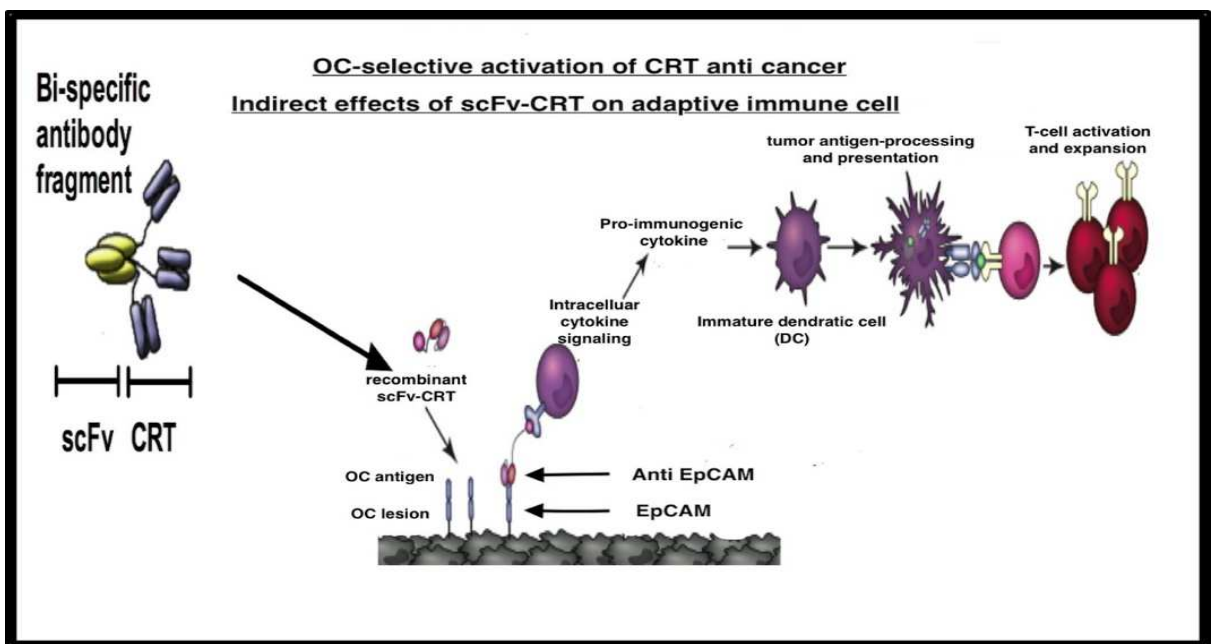


**Figure 6.2. Possible use of EpCAM / CRT bi-specific antibody fragments that directly target CRT to tumour cells.** Preliminary work has developed a bi-specific antibody fragment that carries CRT and recognises EpCAM (epithelial cell adhesion molecule). Since EpCAM is overexpressed on carcinoma cells, including ovarian cancer cells, administration of this antibody would facilitate enhanced surface levels of CRT on these cells. This could encourage both innate and adaptive immune responses directed against ovarian cancers.

**Animal models.** Future work could also involve the use of animal models using similar approaches to those described *in vitro*. For instance administering rCRT, an expression plasmid encoding CRT or CRT bound to the bi-specific antibody described above to improve the effective role of CRT to reduce tumour growth (Figure 6.3) (Eggleton et al., 2016).

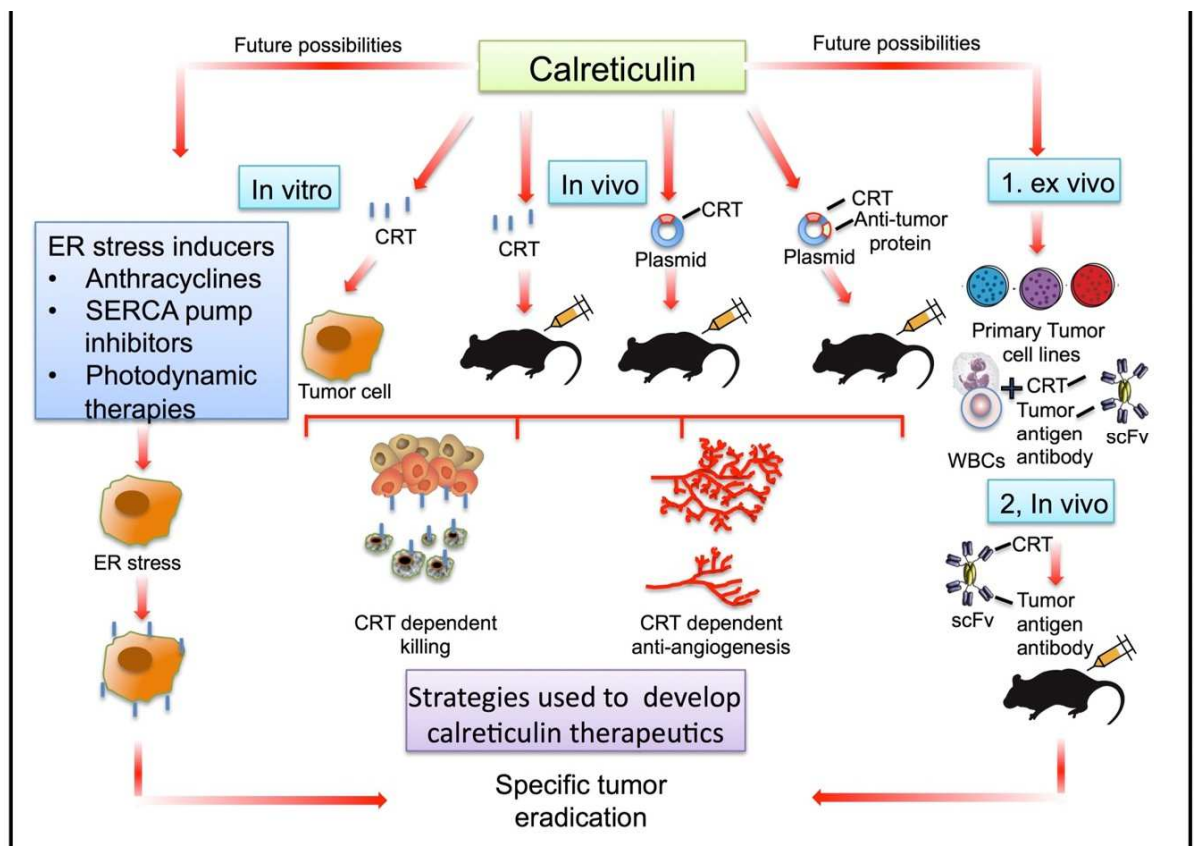


**Figure 6.3. Possible future *in vivo* strategies to test whether enhancing surface levels of CRT could be an anti-cancer therapeutic strategy.** *In vitro* studies have indicated that extracellular cell surface associated CRT promotes the immunogenicity of early apoptotic cancer cells, leading to their immunogenic cell death. Thus, strategies to enhance tumour associated extracellular CRT could have therapeutic potential CRT e.g. inoculation of exogenous CRT or plasmids encoding CRT alone or CRT with anti-tumour DNA.



## **Chapter 7. Critique of the experimental approaches used in this thesis.**

A number of additional experimental controls and experimental approaches could have been included in the data and studies described in this thesis. Suggested approaches for additional data will be presented according to the original results chapter they relate to.

### **7.1. Chapter 3. Purification of calreticulin and preparation of monomeric CRT.**

This chapter describes the purification of purified full length human rCRT from the bacterium *E. coli* and the yeast *Pichia pastoris* using anion exchange chromatography followed by size exclusion chromatography. Additionally, the CRT preparation from *E. coli* was treated using the antibiotic polymyxin B to neutralise any LPS activity as in the studies by (Bak et al., 2008).

**Suggested additional experiment: to confirm the neutralisation of LPS complexed to the *E. coli* CRT preparation by polymyxin B treatment and to assess whether any LPS was present on the *Pichia pastoris* CRT preparation.**

**Rationale:** LPS is the most predominant lipid on the outer layer of gram negative bacteria and is capable of triggering cellular responses (Kelley et al., 2013). Although, (Bak et al., 2008 showed extracellular immune function of CRT in a bacterial preparation which was reported to have no endotoxin contamination following polymyxin B treatment, it was still was important to assess the levels of LPS in the CRT preparations purified. Since LPS is a bacterial protein it was assumed that it would not be present on the CRT protein expressed in the *Pichia pastoris* expression system. However, additional experiments could have been carried out to confirm both this and the effectiveness of the polymyxin B treatment to neutralise LPS in the *E. coli* preparation.

**Suggested methodology:** Detected LPS levels could have been quantified using the Limulus Amebocyte Lysate (LAL) Endotoxin Detection Assay as described in (Pandya et al., 2019). This assay is commercially available and measures endotoxin levels

using a colourimetric endpoint that can be measured by reading the absorbance. Samples would be run in triplicate and a standard curve constructed with absorbance of standards on the x-axis and corresponding endotoxin concentration on the y-axis to allow quantification of endotoxin (EU/ $\mu$ g) in each sample.

## **7.2. Chapter 4a. Examination of the conditions required for binding of exogenous calreticulin to EOC cells.**

In Chapter 4a a series of studies were carried out to examine the effect of the ER stressors doxorubicin and thapsigargin on the binding of exogenous, fluorescently labelled CRT (FITC-CRT) to the surface of EOC cells. Since TUDCA has been reported to reduce ER stress (Vang et al., 2014) the CRT binding induced by doxorubicin and TUDCA was also examined in the presence of TUDCA to assess whether reversing ER stress could reduce CRT binding. Exogenous FITC-CRT binding was examined by flow cytometry and immunocytochemistry. A number of additional experimental controls and experimental approaches could have been either shown or included in these studies to reinforce the results.

***Suggested additional control: to investigate whether the observed FITC binding to the surface of EOC cells could be the result of free FITC in the experimental system.***

***Rationale:*** The CRT-FITC preparation used in these studies was prepared as described in chapter 4a by conjugation of free FITC with CRT and subsequent purification of the conjugated protein by FPLC. It was assumed that the binding of this highly purified FITC-CRT to the surface of ovarian cancer cells reflected direct binding of CRT-FITC to the cells. During the manufacture of the FITC-CRT all free FITC should have removed by gel filtration. However, to confirm that any remaining free FITC does not bind non-specifically to cells directly under experimental conditions, FITC without protein could be added to cells. This experiment was actually performed, but not included in Chapter 4a. The data are now shown in (Figure 7.1).

***Methodology:*** OVcar3 cells were incubated with 2 $\mu$ g/ml free FITC as the control or 2 $\mu$ g/ml FITC-CRT for 30 minutes in the dark at room temperature and the fluorescence

intensity of FITC and FITC-CRT bound to the cells was determined by flow cytometry. Unstained cells were examined for comparison.

*Results:* It can be seen from figure 7.1 that binding of free FITC to OVcar3 cells was negligible. Although, there is a very slight shift in the fluorescence intensity of the FITC stained cells compared with unstained cells the FITC-CRT bound cells show a clear and distinct peak of fluorescence. The fact that the x-axis is a log scale and that the levels of free FITC used should be far in excess of any free FITC remaining after purification of the conjugated FITC-CRT suggest that the cell association of free FITC in these studies is negligible.

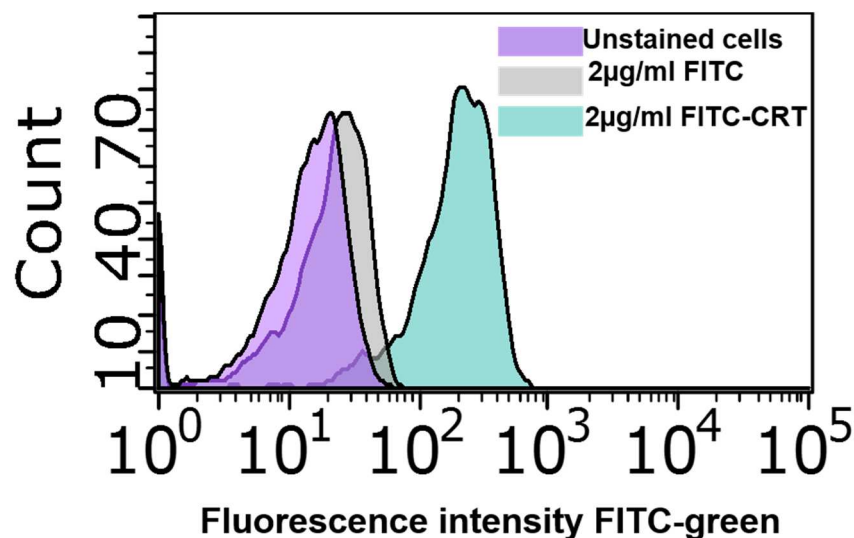


**Figure 7.1. Free FITC does not bind to the surface of OVcar3 ovarian cancer cells.** OVcar3 cells were incubated with 2µg/ml free FITC or 2µg/ml FITC-CRT and fluorescence intensity of FITC and FITC-CRT bound to the cells was determined by flow cytometry. Unstained cells were examined for comparison. A representative graph (of three with similar data) is shown.

**Suggested additional control: Evaluation of any data from negative or positive controls in each individual experiment contributing to the averaged data set for each study; thus ensuring reliability of the averaged data.**

Rationale: In a negative control cells are not exposed to the experimental treatment but are exposed to the medium plus levels of the solvent in which any treatment is dissolved (vehicle) at equivalent levels to that present in the treatments. Ideally, no effect should be seen. A positive control, where included, should produce the expected effect. Both inform about the reliability of the data obtained and allow anomalous results to be identified.

It was noted that in the representative graph shown in (Figure 4a.7 (c)) cells exposed to the negative control i.e. 0 µg/ml FITC-HAS, did demonstrate fluorescence and that inclusion of these data in the averaged graphs in Figure 4a.8 could influence the results obtained. It was therefore important to re-examine all of the relevant primary data and controls to examine this possibility.

Methodology: All of the negative controls in the individual repeats that contributed to the graphs in Figure 4a.8 were re-examined to investigate whether the data in (Figure 4a.7 (c)) were anomalous or if there was a consistent fluorescent shift which could indicate an experimental error or artefact. The graphs in (Figure 4a.8) were then redrawn with re-analysed data from experiments where the negative control did not show fluorescence.

Results: 5 out of the 6 repeats for this experiment did not show a fluorescent shift in the negative control and a representative graph showing the flow cytometry data is shown in (Figure 7.2).

The data shown originally in Figure 4a.8 have been recalculated excluding the data set where the 0µg/ml controls showed fluorescence and the results are shown in (Figure 7.3).

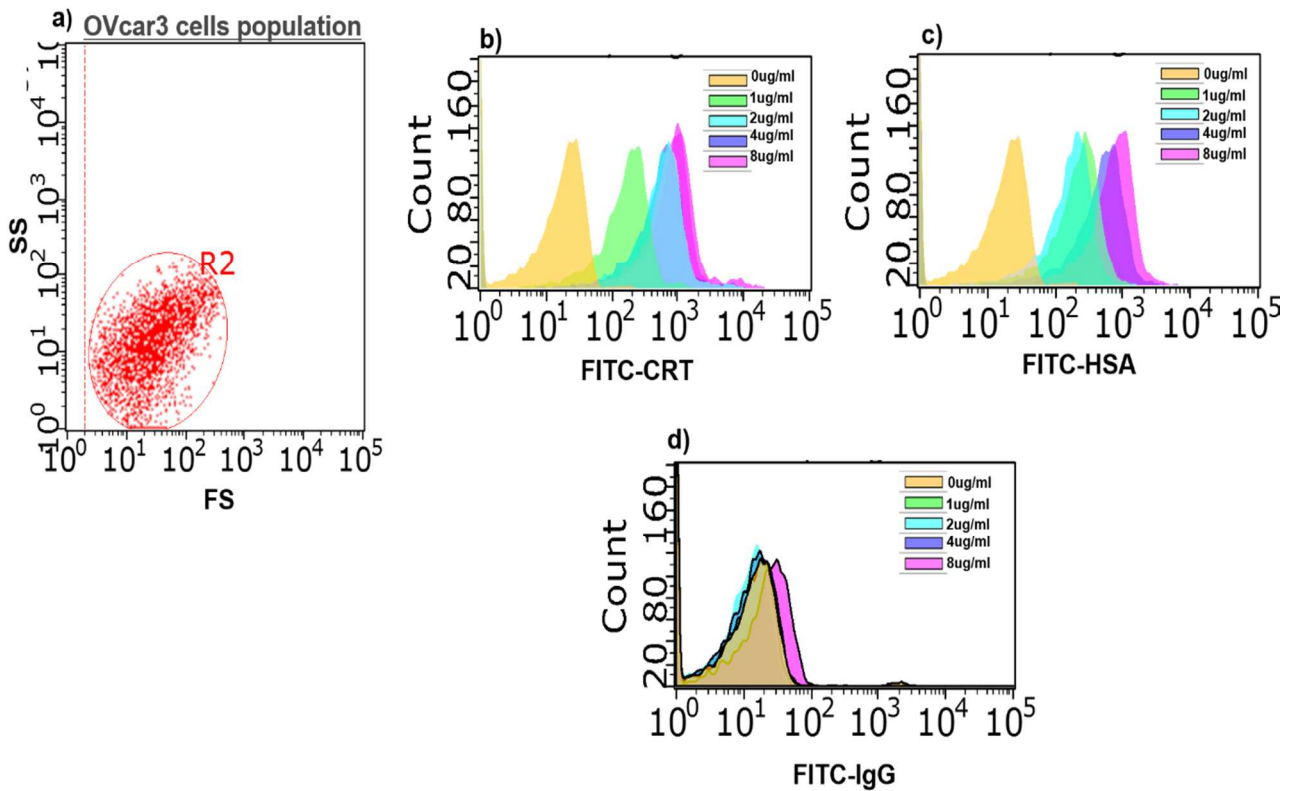


**Figure 7.2. Demonstration of FITC-CRT, FITC-HSA and FITC-IgG binding to OVcar3 cancer cells by flow cytometry.** OVcar3 cells were treated with different concentrations (1- $\mu$ g - 8 $\mu$ g/ml) of FITC protein or untreated (0, auto-fluorescence control) and analysed by flow cytometry (a) Typical dot plot of the cells showing their size (forward scatter-FSC) and granularity (side scatter-SS). (b)-(d) Flow cytometry histograms of cells labelled with (b) CRT-FITC (c) HSA-FITC (positive control) (d) IgG-FITC (negative control). Representative graphs from at least three independent experiments are shown.

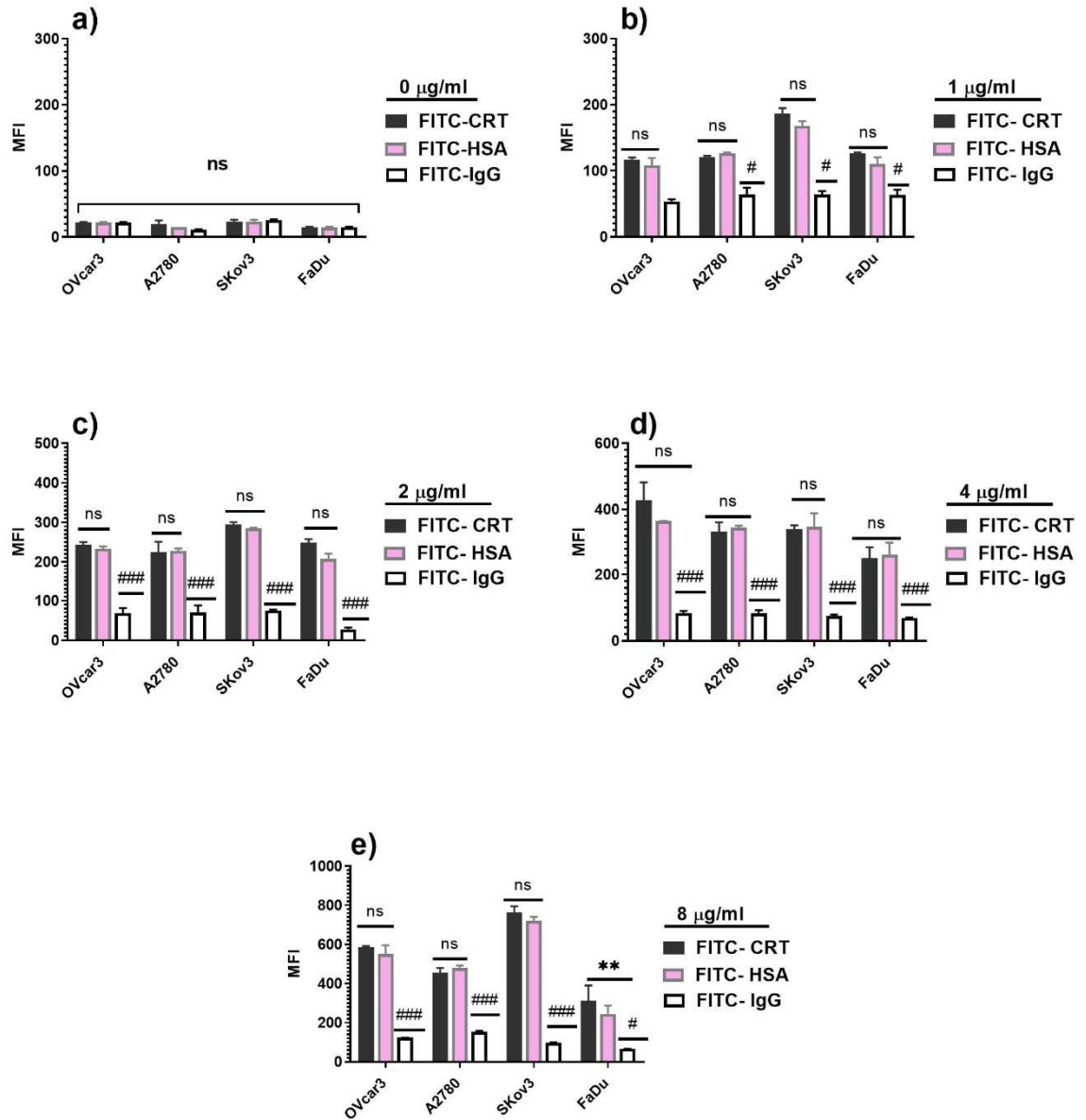


**Figure 7.3. Exogenous FITC-CRT binds to four cancer cell lines at all concentrations tested.** Cancer cells were incubated with increasing concentrations (0-8 µg/ml) of FITC-CRT, FITC-HSA (positive control) or FITC-IgG (negative control) for 30 min at 37°C in the dark. After incubation the amount of FITC-conjugated protein bound to cells was assessed by flow cytometry. (a), (b), (c), (d) and (e) cells treated with 0 (buffer alone, control), 1, 2, 4, 8 µg/ml FITC-CRT, HSA-FITC and IgG-FITC, respectively. Data are mean ± SD and analysed by one-way ANOVA and Tukey's multiple comparison test ### p<0.001, n=5. Significance is between HSA and IgG where indicated and between CRT and IgG where not specified.

**Suggested additional experiment: to confirm that treatment of EOC cells with increasing concentrations of doxorubicin does induce enhanced surface exposure of phosphatidylserine (PS).**

Rationale: CRT has been reported to bind to PS exposed on the outer leaflet of the plasma membrane. Therefore, it was assumed that the increased exogenous CRT binding induced by doxorubicin was the result of increased PS exposure. This hypothesis could have been confirmed by assessing changes in externalised PS in response to doxorubicin treatment using annexin V which is known to bind to PS.

Methodology: EOC would be treated with increasing concentrations of doxorubicin (0, 2.5 $\mu$ M, 6.3 $\mu$ M, 12.5 $\mu$ M, 25 $\mu$ M) for 16 hours prior to incubation with fluorescently labelled annexin and analysis by flow cytometry.

Results: these experiments were actually performed as part of the studies described in this thesis and a representative graph is shown in (Figure 7.4). It can be seen that treatment of cancer cells with increasing concentrations of doxorubicin induces a corresponding increase in cell surface PS as detected by flow cytometry.

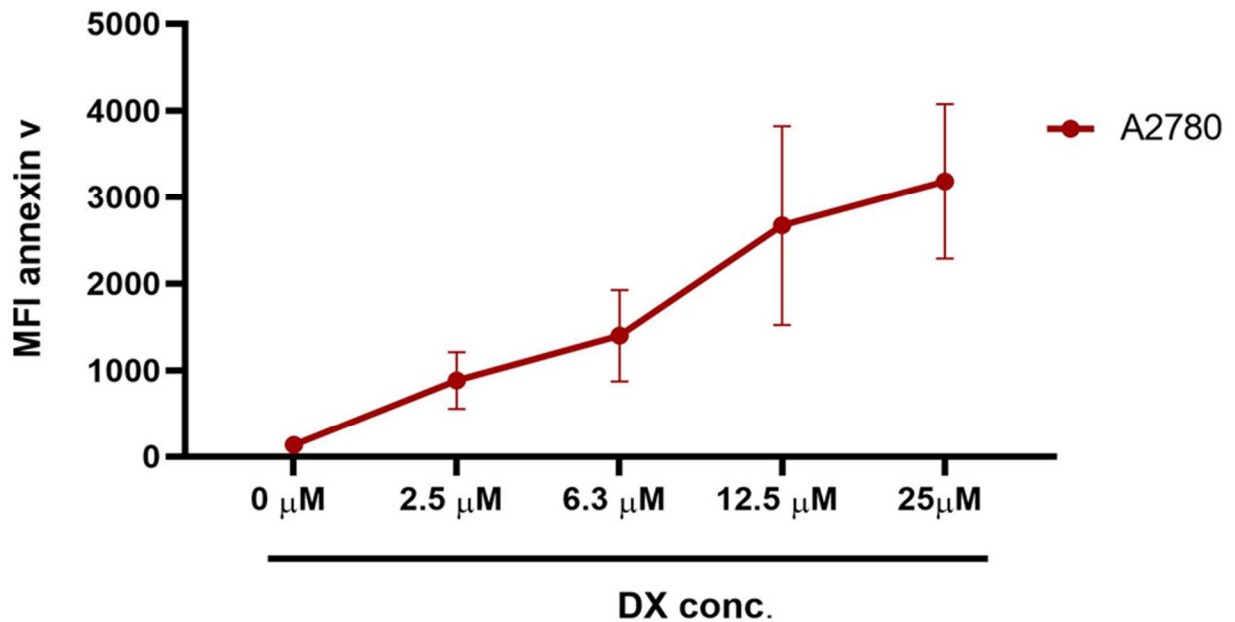


**Figure 7.4. Doxorubicin (DX) induces externalisation of phosphatidylserine in A2780 ovarian cancer cells as assessed by annexin V binding.** A2780 cells were treated with increasing concentrations of doxorubicin (0, 2.5 $\mu\text{M}$ , 6.3 $\mu\text{M}$ , 12.5 $\mu\text{M}$ , 25 $\mu\text{M}$ ) for 16 hours. Cell were then exposed to fluorescently labelled annexin V (5 $\mu\text{l}$  in 100  $\mu\text{l}$  of calcium binding buffer for 15min at 37 °C in the dark) and analysed by flow cytometry. Data are mean  $\pm$  SD from three independent experiments.

**Note:** DMSO or ethanol was included in all experiments at appropriate concentrations as a vehicle control. Doxorubicin was dissolved in dH<sub>2</sub>O and the stock was so highly diluted in the final concentrations that a vehicle equivalent was not added.



**Suggested additional experiment: to confirm that the ER stressors used in these studies i.e. doxorubicin and thapsigargin, do induce ER stress in the EOC cells studied.**

Rationale: both doxorubicin and thapsigargin have been reported in the literature to induce ER stress and thus it was assumed in this thesis that the process led to PS externalisation and enhanced CRT binding. However, in the studies described here ER stress was not confirmed in the cells used and therefore experiments could have been designed to study this.

Methodology: ER stress could be examined in EOC cells treated  $\pm$  doxorubicin or thapsigargin by assessment of activation of eukaryotic initiation factor 2 (eIF2 $\alpha$ ) and caspase 8 which are both activated downstream of ER stress and have been studied as ER stress markers (Osowski and Urano, 2011) (Glab et al., 2017). Briefly, levels of activated i.e. phosphorylated, eIF2 $\alpha$  could be assessed by western blotting with an appropriate anti-phospho antibody and levels of activated caspase 8 could be assessed by commercially available kit (e.g. Abcam, Cambridge, UK)

**Suggested additional experiment: to examine whether enhanced exogenous CRT binding in response to the ER stressors doxorubicin and thapsigargin is specific to cancer cells.**

Rationale: ICD, mediated by enhanced surface levels of CRT, has been reported to occur in cancer cells in response to chemotherapy such as doxorubicin via induction of ER stress. The results presented in chapter 4a indicate that both doxorubicin and the ER stressor thapsigargin do induce cellular changes in EOC cells that result in enhanced surface binding of exogenous CRT. The specificity of these results to cancer cells could have been tested by repeating these experiments in human non-cancer cells, preferably primary cells, which better reflect normal *in vivo* cell physiology. For instance, primary human endothelial cells from several sources are routinely cultured in the laboratories in Exeter. The data presented in Figure 4b.2 suggest that doxorubicin does not induce cell death in non-cancer cells such as

endothelial cells, but an investigation into whether doxorubicin treatment could lead to enhanced binding of exogenous CRT to these cells was not carried out.

Methodology: Endothelial cells pre-treated  $\pm$  doxorubicin or thapsigargin at concentrations indicated in Chapter 4 would be incubated with 2 $\mu$ g/ml CRT-FITC and the binding of the fluorescent protein to the endothelial cell surface assessed by immunocytochemistry and flow cytometry.

**Suggested additional experiment: to examine whether the observed effect of doxorubicin on exogenous CRT binding is specific to anthracyclines that induce ICD.**

Rationale: as previously mentioned doxorubicin is a member of the anthracycline class of anti-proliferative therapeutics and it has been reported to additionally induce ICD. Other anthracyclines such as idarubicin have also been reported to induce ICD (Garg et al., 2017). Additional control experiments could therefore be carried out to examine not only whether the enhanced CRT binding observed occurs with other ICD inducing agents, but also whether an established chemotherapeutic that does not stimulate ICD induces the same effect e.g. mitomycin C.

Methodology: EOC cells would be treated with increasing concentrations of idarubicin or mitomycin C, as indicated by the available literature and the known pharmacological levels, and binding of exogenous fluorescently labelled CRT would be investigated using flow cytometry and immunocytochemistry as previously described in Chapter 4a. Additionally, exposure of PS on the outer plasma membrane would be assessed as above using flow cytometry.

These latter two additional studies could also additionally be carried out for the studies described in Chapter 4b which examined surface exposure of endogenous CRT in response to doxorubicin.

### **7.3. Chapter 4b. Examination of the conditions required for surface exposure of translocated endogenous calreticulin in ovarian cancer cells**

In Chapter 4b studies were carried out to examine the effect of the ER stressors doxorubicin and thapsigargin on translocation of endogenous CRT to the cell surface of EOC cells. Again, since TUDCA has been reported to reduce ER stress (Vang et al., 2014), CRT translocation induced by doxorubicin and TUDCA was also examined in the presence of TUDCA to assess whether reversing ER stress could reduce CRT exposure. Levels of surface CRT were examined by flow cytometry and immunocytochemistry.

***Suggested additional control: inclusion of negative controls in the immunocytochemistry studies.***

***Rationale:*** It is important to confirm that CRT labelling examined by immunocytochemistry is specific. Therefore, controls should include cells treated with the fluorescent secondary antibody and the nuclear counterstain DAPI, but no primary antibody (but include vehicle or isotype control antibody only) to examine non-specific binding of the secondary antibody. Additional controls could include staining cells with DAPI only to confirm that this staining was successful. Cells could also be visualised by phase contrast microscopy before and after staining to confirm no loss of cells during the fixation and staining procedure.

***Methodology:*** Cells treated with doxorubicin or thapsigargin  $\pm$  TUDCA should be fixed with 4% (w/v) paraformaldehyde and then sequentially incubated with primary antibody (anti-CRT) or vehicle (PBS) or isotype control antibody; fluorescently labelled secondary antibody alone or vehicle (PBS); DAPI, as required, before examining using fluorescence microscopy. These vehicle only controls were carried out for the immunocytochemistry performed in this thesis, but not included in the data shown (e.g. Figures 4b.1, 4b.5 and 4b.8).

***Results:*** The data in (Figure 7.5) confirm that negative control cells which received vehicle alone and no primary antibody, in this case anti-CRT, did not show any non-specific binding of the secondary antibody.

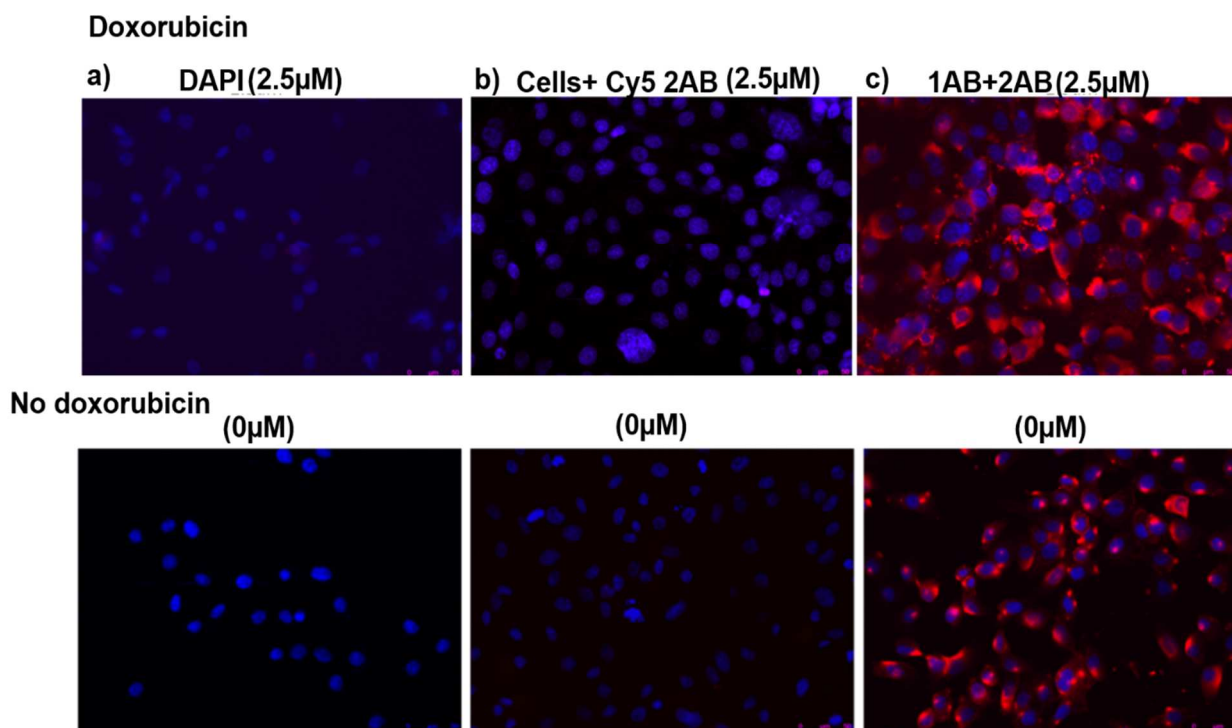


**Figure 7.5. No non-specific binding of secondary antibody is observed in cells treated with vehicle in place of primary antibody prior to staining with Cy5 secondary antibody.** SKov3 cells were treated  $\pm$  2.5  $\mu$ M doxorubicin for 16 hours and then stained for exogenous CRT by immunocytochemistry. Cells were fixed with 4% (w/v) paraformaldehyde and then incubated firstly with either primary antibody (anti-CRT) or PBS, followed by Cy5-labelled secondary antibody (or PBS) and then with DAPI. Fluorescence microscopy images were taken at 20 x magnification. Upper panels, cells treated with doxorubicin 2.5  $\mu$ M; lower panels, untreated cells. Column A, cells received only vehicle plus DAPI; column B, cells received vehicle instead of primary antibody plus DAPI; column C, cells received primary and secondary antibody, plus DAPI.

It should also be noted that to ensure consistency in the collection of images of fluorescently labelled cells all cells were examined on a LEICA microscope and captured with LEICA software. Images were collected from randomly selected areas within each well and within each experiment microscope settings and image analysis settings were kept the same.

#### **7.4. Chapter 5. Investigation into whether exogenous CRT or cancer cells expressing surface CRT can induce maturation of DCs and subsequent activation of T-cells.**

This chapter described a series of studies that investigated whether exogenous CRT or CRT expressed on the surface of EOC cells could induce maturation of iDCs to mDCs and whether the mDCs induced by these treatments could stimulate T-cell activation as assessed by T-cell proliferation.

**Suggested additional control: to include imDCs in the studies examining mDC activation of T-cell proliferation (Figure 5.1).**

**Rationale:** The studies described in this thesis examined the ability of mDCs (which had been stimulated to mature by various treatments) to induce T-cell proliferation. This experiment could have been improved by additionally including imDCs in the T-cell proliferation assay. This would have controlled for non-specific activation of T-cells by cell types other than mature mDCs and also confirmed a differential effect of immature and mature DCs.

**Methodology:** The experiments described in section 5.4.15 could be repeated, but additionally include imDCs as a control. Additionally, values for unstained cells should be included as a negative control for the CFSE staining.

These experiments were carried out, but not previously included in this thesis.

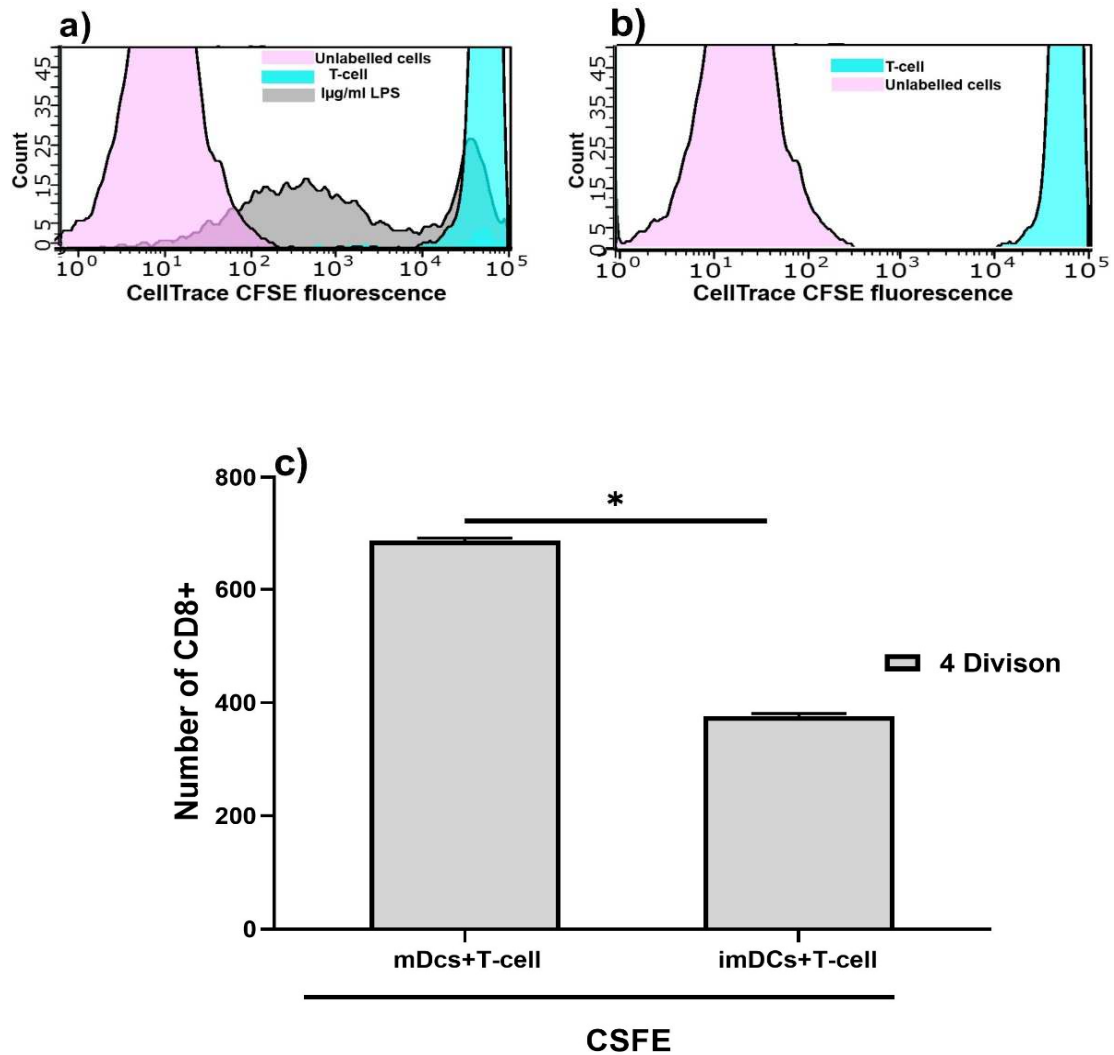


**Figure 7.6. Mature DCs induce significantly more T-cell proliferation than imDCs.** Immature DCs were incubated +  $1\mu\text{g/ml}$  LPS to induce maturation. Either mDCs or the untreated iDCs were then co-cultured with CSFE -labelled T-cells in a 24-well plate in the presence of IL-2 ( $30\mu\text{g/ml}$ ) and T-cell proliferation was assessed after 5 days by flow cytometry. Data are mean + SD from 10 independent experiments,  $*p<0.05$  mDCs+ T-cell vs imDCs +T-cells. Data from 4<sup>th</sup> cell division is shown as an example.

**Suggested additional control: to examine the secretion of IL12/IL23 from iDCs incubated with untreated OVcar3 cells.**

**Rationale:** the data presented in Figure 5.27 show that imDCs incubated with OVcar3 cells previously treated with increasing concentrations of doxorubicin secrete IL12/IL23 which is indicative of DC maturation (Khayrullina et al., 2008). An additional control that should have been included in this experiment would have been incubation of iDCs with OVcar3 cells which received no pre-treatment with doxorubicin. This would allow the specific effect of pre-treatment of OVcar3 cells with doxorubicin to be assessed. This additional control was actually carried out, but not included in the data presented.

**Methodology:** imDCs derived from THP-1 cells were co-incubated with OVcar3 ovarian cancer cells which had received no pre-treatment with doxorubicin for 4 days. Cell culture supernatants were collected and assessed for the content of IL-12/IL-23 using a commercially available ELISA kit.

**Results:** incubation of iDCs with OVcar3 cells for 4 days did not significantly increase secretion of IL12/IL23 compared with iDCs alone. iDCs incubated with OVcar3 cells pre-treated with 2.5  $\mu$ M doxorubicin secreted significantly more IL12/IL23 than iDCs incubated with untreated OVcar3.

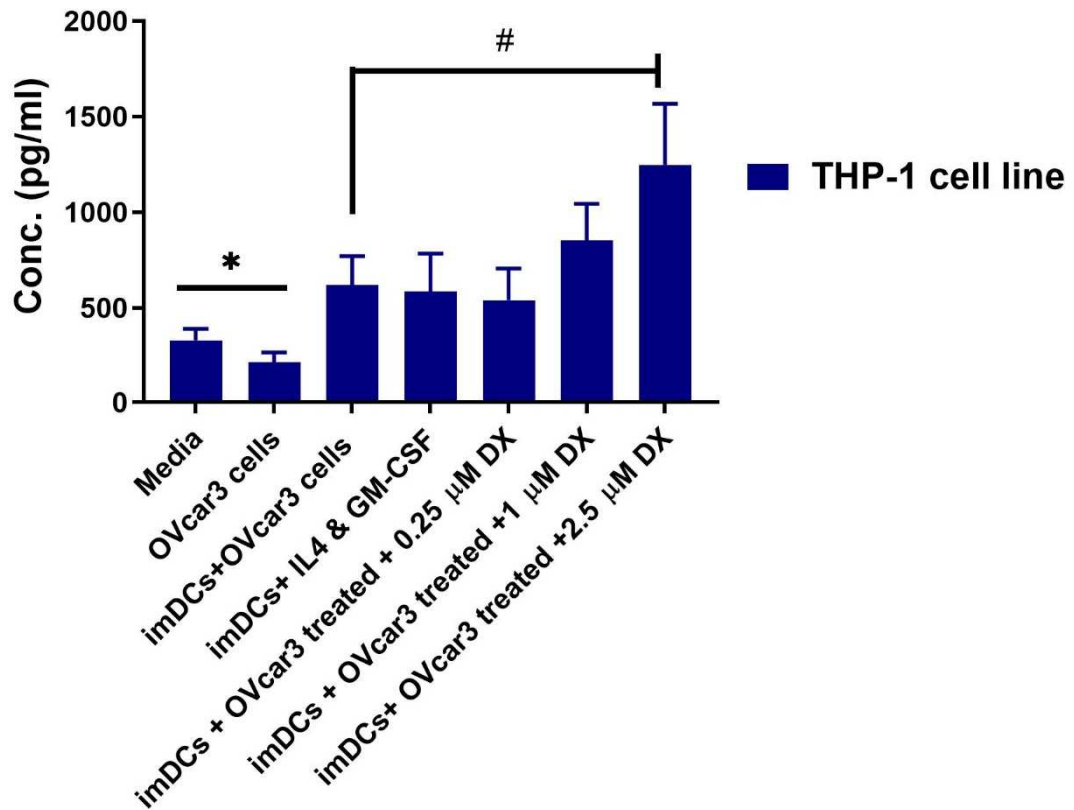


**Figure 7.7. OVcar3 ovarian cancer cells pre-treated with high concentrations of doxorubicin induce secretion of IL12/IL23 from THP-1 derived imDCs during DC maturation.** imDCs derived from THP-1 cells were co-incubated with IL4&GM-CSF (positive control for DC maturation), OVCar3 cells alone or OVcar3 cells pre-treated with increasing concentrations of doxorubicin (DX, 0.25,1, 2.5 μM). After 4 days cell culture supernatants were collected and assessed for the content of IL-12/IL-23 using a commercially available ELISA kit. Data are mean + SD from three individual experiments with each determination performed in triplicate. \* $p < 0.05$  basal media vs.OVcar3 cells at day 0. # $< 0.05$  imDCs +OVcar3 vs imDCs +OVcar3 pre-treated with 2.5μM.



**Suggested additional experiment: to examine whether the observed ability of rCRT to induce imDC maturation could be due to the presence of LPS in the rCRT preparation.**

Rationale: Although it was assumed that the CRT expressed in *Pichia pastoris* was free of LPS because the expression system was a yeast, (Pandya et al., 2019) indicate that low levels of LPS are present in this preparation. Since maturation of imDCs was induced by exogenous LPS, control experiments could be carried out to investigate whether the maturation of imDCs induced by rCRT could be due to the associated LPS.

Methodology: the studies examining maturation of iDCs by CRT could be repeated in the presence or absence of polymyxin B at 10 µg/ml (plus polymyxin B alone as a control) as described by (Li et al., 2015). As discussed above polymyxin B neutralises LPS and this study would indicate whether the maturation of imDCs is due to LPS or genuinely due to CRT. However, polymyxin B is toxic to cells so results using polymyxin B must be interpreted with caution (Ahmed et al., 2017).

**Suggested additional experiment: to examine the secretion of interferon gamma (IFN-gamma) during maturation of DCs.**

Rationale: The experiments previously described in chapter 5 examined maturation of DCs by assessing expression of relevant surface markers and secretion of the cytokines IL12/23. IFN-gamma has also been reported to be secreted during DC maturation (Pan et al., 2004); therefore, measurement of secreted IFN-gamma levels in the cell culture medium also be could carried out as an additional assessment to confirm maturation of DCs in the conditions studied.

Methodology: Cell culture media would be collected from DCs matured for 4 days as described in section 5.4.11 and IFN-gamma levels would be measured by commercially available ELISA (R&D Systems, Abingdon, UK).

## References

- @CR\_UK. 2016. <https://www.cancerresearchuk.org/about-cancer/ovarian-cancer> [Online]. [Accessed].
- ©KISSPNG.COM 2019. Major Histocompatibility
- ABBOTT, K. L., LIM, J. M., WELLS, L., BENIGNO, B. B., MCDONALD, J. F. & PIERCE, M. 2010. Identification of candidate biomarkers with cancer-specific glycosylation in the tissue and serum of endometrioid ovarian cancer patients by glycoproteomic analysis. *Proteomics*, 10, 470-81.
- ADIGUN, R. & BHIMJI, S. S. 2018. Necrosis, Cell (Liquefactive, Coagulative, Caseous, Fat, Fibrinoid, and Gangrenous). *StatPearls*. Treasure Island (FL).
- AGGARWAL, A., MISRO, M. M., MAHESHWARI, A., SEHGAL, N. & NANDAN, D. 2010. N-acetylcysteine counteracts oxidative stress and prevents hCG-induced apoptosis in rat Leydig cells through down regulation of caspase-8 and JNK. *Mol Reprod Dev*, 77, 900-9.
- AGOSTINI, M., TUCCI, P. & MELINO, G. 2011. Cell death pathology: perspective for human diseases. *Biochem Biophys Res Commun*, 414, 451-5.
- AHMED, M. U., VELKOV, T., LIN, Y. W., YUN, B., NOWELL, C. J., ZHOU, F., ZHOU, Q. T., CHAN, K., AZAD, M. A. K. & LI, J. 2017. Potential Toxicity of Polymyxins in Human Lung Epithelial Cells. *Antimicrob Agents Chemother*, 61.
- ALAIYA, A., ROBLICK, U., EGEVAD, L., CARLSSON, A., FRANZEN, B., VOLZ, D., HUWENDIEK, S., LINDER, S. & AUER, G. 2000. Polypeptide expression in prostate hyperplasia and prostate adenocarcinoma. *Anal Cell Pathol*, 21, 1-9.
- ALBERTS, B. 2002. Molecular Biology of the Cell.
- ALICIA ALGECIRAS-SCHIMNICH 2013. Ovarian Cancer. AACC.
- ALPINI, G., UENO, Y., GLASER, S. S., MARZIONI, M., PHINIZY, J. L., FRANCIS, H. & LESAGE, G. 2001. Bile acid feeding increased proliferative activity and apical bile acid transporter expression in both small and large rat cholangiocytes. *Hepatology*, 34, 868-76.
- AMJADI, F., SALEHI, E., MEHDIZADEH, M. & AFLATOONIAN, R. 2014. Role of the innate immunity in female reproductive tract. *Adv Biomed Res*, 3, 1.
- ANDRIN, C., CORBETT, E. F., JOHNSON, S., DABROWSKA, M., CAMPBELL, I. D., EGGLETON, P., OPAS, M. & MICHALAK, M. 2000. Expression and purification of mammalian calreticulin in *Pichia pastoris*. *Protein Expr Purif*, 20, 207-15.
- APETOH, L., GHIRINGHELLI, F., TESNIERE, A., OBEID, M., ORTIZ, C., CRIOLLO, A., MIGNOT, G., MAIURI, M. C., ULLRICH, E., SAULNIER, P., YANG, H., AMIGORENA, S., RYFFEL, B., BARRAT, F. J., SAFTIG, P., LEVI, F., LIDEREAU, R., NOGUES, C., MIRA, J. P., CHOMPRET, A., JOULIN, V., CLAVEL-CHAPELON, F., BOURHIS, J., ANDRE, F., DELALOGUE, S., TURSZ, T., KROEMER, G. & ZITVOGEL, L. 2007. Toll-like receptor 4-dependent contribution of the immune system to anticancer chemotherapy and radiotherapy. *Nat Med*, 13, 1050-9.
- ARAKI, K. & NAGATA, K. 2011. Protein folding and quality control in the ER. *Cold Spring Harb Perspect Biol*, 3, a007526.
- ARMSTRONG, D. K., BUNDY, B., WENZEL, L., HUANG, H. Q., BAERGEN, R., LELE, S., COPELAND, L. J., WALKER, J. L., BURGER, R. A. & GYNECOLOGIC ONCOLOGY, G. 2006. Intraperitoneal cisplatin and paclitaxel in ovarian cancer. *N Engl J Med*, 354, 34-43.
- AROSA, F. A., DE JESUS, O., PORTO, G., CARMO, A. M. & DE SOUSA, M. 1999. Calreticulin is expressed on the cell surface of activated human peripheral blood T lymphocytes in association with major histocompatibility complex class I molecules. *J Biol Chem*, 274, 16917-22.
- ARRUDA, A. P. & HOTAMISLIGIL, G. S. 2015. Calcium Homeostasis and Organelle Function in the Pathogenesis of Obesity and Diabetes. *Cell Metab*, 22, 381-97.
- ATALE, N., GUPTA, S., YADAV, U. C. & RANI, V. 2014. Cell-death assessment by fluorescent and nonfluorescent cytosolic and nuclear staining techniques. *J Microsc*, 255, 7-19.

- BAJOR, A., TISCHER, S., FIGUEIREDO, C., WITTMANN, M., IMMENSCHUH, S., BLASCZYK, R. & EIZ-  
VESPER, B. 2011. Modulatory role of calreticulin as chaperokine for dendritic cell-based  
immunotherapy. *Clin Exp Immunol*, 165, 220-34.
- BAK, S. P., AMIEL, E., WALTERS, J. J. & BERWIN, B. 2008. Calreticulin requires an ancillary adjuvant for  
the induction of efficient cytotoxic T cell responses. *Mol Immunol*, 45, 1414-23.
- BAKSH, S., BURNS, K., BUSAAN, J. & MICHALAK, M. 1992. Expression and purification of recombinant  
and native calreticulin. *Protein Expr Purif*, 3, 322-31.
- BAKSH, S. & MICHALAK, M. 1991. Expression of calreticulin in Escherichia coli and identification of its  
Ca<sup>2+</sup> binding domains. *J Biol Chem*, 266, 21458-65.
- BELKAID, Y. & HAND, T. W. 2014. Role of the microbiota in immunity and inflammation. *Cell*, 157,  
121-41.
- BENGTSSON, S., KROGH, M., SZIGYARTO, C. A., UHLEN, M., SCHEDVINS, K., SILFVERSWARD, C.,  
LINDER, S., AUER, G., ALAIYA, A. & JAMES, P. 2007. Large-scale proteomics analysis of human  
ovarian cancer for biomarkers. *J Proteome Res*, 6, 1440-50.
- BENHAM, A. M. 2012. Protein secretion and the endoplasmic reticulum. *Cold Spring Harb Perspect  
Biol*, 4, a012872.
- BEREK, J. S. 2003. Epithelial Ovarian Cancer.
- BERGES, C., NAUJOKAT, C., TINAPP, S., WIECZOREK, H., HOH, A., SADEGHI, M., OPELZ, G. & DANIEL,  
V. 2005. A cell line model for the differentiation of human dendritic cells. *Biochem Biophys  
Res Commun*, 333, 896-907.
- BERNSTEIN, M. B., GARNETT, C. T., ZHANG, H., VELCICH, A., WATTENBERG, M. M., GAMEIRO, S. R.,  
KALNICKI, S., HODGE, J. W. & GUHA, C. 2014. Radiation-induced modulation of costimulatory  
and coinhibitory T-cell signaling molecules on human prostate carcinoma cells promotes  
productive antitumor immune interactions. *Cancer Biother Radiopharm*, 29, 153-61.
- BINJU, M., PADILLA, M. A., SINGOMAT, T., KAUR, P., RAHMANTO, Y. S., COHEN, P. & YU, Y. 2018.  
Mechanisms underlying acquired platinum resistance in high grade serous ovarian cancer - a  
mini review. *Biochim Biophys Acta Gen Subj*.
- BJ, Q. 2010. The use of carboxyfluorescein diacetate succinimidyl ester (CFSE) to monitor  
lymphocyte proliferation. *J Vis Exp*.
- BOEHM, I. 2006. Apoptosis in physiological and pathological skin: implications for therapy. *Curr Mol  
Med*, 6, 375-94.
- BONILLA, F. A. & OETTGEN, H. C. 2010. Adaptive immunity. *J Allergy Clin Immunol*, 125, S33-40.
- BORASCHI, D. & ITALIANI, P. 2018. Innate Immune Memory: Time for Adopting a Correct  
Terminology. *Front Immunol*, 9, 799.
- BOSSHART, H. & HEINZELMANN, M. 2016. THP-1 cells as a model for human monocytes. *Ann Transl  
Med*, 4, 438.
- BOUSSIOS, S., MOSCHETTA, M., TATSI, K., TSIOURIS, A. K. & PAVLIDIS, N. 2018. A review on  
pregnancy complicated by ovarian epithelial and non-epithelial malignant tumors:  
Diagnostic and therapeutic perspectives. *J Adv Res*, 12, 1-9.
- BOYER, J. L. 2013. Bile formation and secretion. *Compr Physiol*, 3, 1035-78.
- BRAUCHLE, E., THUDE, S., BRUCKER, S. Y. & SCHENKE-LAYLAND, K. 2014. Cell death stages in single  
apoptotic and necrotic cells monitored by Raman microspectroscopy. *Sci Rep*, 4, 4698.
- BRINTON, L. A., TRABERT, B., SHALEV, V., LUNENFELD, E., SELLA, T. & CHODICK, G. 2013. In vitro  
fertilization and risk of breast and gynecologic cancers: a retrospective cohort study within  
the Israeli Maccabi Healthcare Services. *Fertil Steril*, 99, 1189-96.
- BROHET, R. M., GOLDGAR, D. E., EASTON, D. F., ANTONIOU, A. C., ANDRIEU, N., CHANG-CLAUDE, J.,  
PEOCK, S., EELES, R. A., COOK, M., CHU, C., NOGUES, C., LASSET, C., BERTHET, P., MEIJERS-  
HEIJBOER, H., GERDES, A. M., OLSSON, H., CALDES, T., VAN LEEUWEN, F. E. & ROOKUS, M. A.  
2007. Oral contraceptives and breast cancer risk in the international BRCA1/2 carrier cohort  
study: a report from EMBRACE, GENEPSO, GEO-HEBON, and the IBCCS Collaborating Group. *J  
Clin Oncol*, 25, 3831-6.

- BRYNHILDSEN, J. 2014. Combined hormonal contraceptives: prescribing patterns, compliance, and benefits versus risks. *Ther Adv Drug Saf*, 5, 201-13.
- BUONCERVELLO, M., BORGHINI, P., ROMAGNOLI, G., SPADARO, F., BELARDELLI, F., TOSCHI, E. & GABRIELE, L. 2012. Apicidin and docetaxel combination treatment drives CTCFL expression and HMGB1 release acting as potential antitumor immune response inducers in metastatic breast cancer cells. *Neoplasia*, 14, 855-67.
- BURIKHANOV, R., ZHAO, Y., GOSWAMI, A., QIU, S., SCHWARZE, S. R. & RANGNEKAR, V. M. 2009. The tumor suppressor Par-4 activates an extrinsic pathway for apoptosis. *Cell*, 138, 377-88.
- BURNETTE, W. N. 1981. "Western blotting": electrophoretic transfer of proteins from sodium dodecyl sulfate--polyacrylamide gels to unmodified nitrocellulose and radiographic detection with antibody and radioiodinated protein A. *Anal Biochem*, 112, 195-203.
- BUSTAMANTE-MARIN, X. M. & OSTROWSKI, L. E. 2017. Cilia and Mucociliary Clearance. *Cold Spring Harb Perspect Biol*, 9.
- CAROLINA VERA CASTILLO 2016. The Nerve Growth Factor alters calreticulin translocation from the endoplasmic reticulum to the cell surface and its signaling pathway in epithelial ovarian cancer cells.
- CARTER, B. Z., MILELLA, M., ALTIERI, D. C. & ANDREEFF, M. 2001. Cytokine-regulated expression of survivin in myeloid leukemia. *Blood*, 97, 2784-90.
- CHAO, M. P., JAISWAL, S., WEISSMAN-TSUKAMOTO, R., ALIZADEH, A. A., GENTLES, A. J., VOLKMER, J., WEISKOPF, K., WILLINGHAM, S. B., RAVEH, T., PARK, C. Y., MAJETI, R. & WEISSMAN, I. L. 2010. Calreticulin is the dominant pro-phagocytic signal on multiple human cancers and is counterbalanced by CD47. *Sci Transl Med*, 2, 63ra94.
- CHAPLIN, D. D. 2010. Overview of the immune response. *J Allergy Clin Immunol*, 125, S3-23.
- CHAPUT, N., DE BOTTON, S., OBEID, M., APETOH, L., GHIRINGHELLI, F., PANARETAKIS, T., FLAMENT, C., ZITVOGEL, L. & KROEMER, G. 2007. Molecular determinants of immunogenic cell death: surface exposure of calreticulin makes the difference. *J Mol Med (Berl)*, 85, 1069-76.
- CHAUX, P., LUITEN, R., DEMOTTE, N., VANTOMME, V., STROOBANT, V., TRAVERSARI, C., RUSSO, V., SCHULTZ, E., CORNELIS, G. R., BOON, T. & VAN DER BRUGGEN, P. 1999. Identification of five MAGE-A1 epitopes recognized by cytolytic T lymphocytes obtained by in vitro stimulation with dendritic cells transduced with MAGE-A1. *J Immunol*, 163, 2928-36.
- CHEN, C. N., CHANG, C. C., SU, T. E., HSU, W. M., JENG, Y. M., HO, M. C., HSIEH, F. J., LEE, P. H., KUO, M. L., LEE, H. & CHANG, K. J. 2009. Identification of calreticulin as a prognosis marker and angiogenic regulator in human gastric cancer. *Ann Surg Oncol*, 16, 524-33.
- CHIANG, W. F., HWANG, T. Z., HOUR, T. C., WANG, L. H., CHIU, C. C., CHEN, H. R., WU, Y. J., WANG, C. C., WANG, L. F., CHIEN, C. Y., CHEN, J. H., HSU, C. T. & CHEN, J. Y. 2013. Calreticulin, an endoplasmic reticulum-resident protein, is highly expressed and essential for cell proliferation and migration in oral squamous cell carcinoma. *Oral Oncol*, 49, 534-41.
- CHOUQUET, A., PAIDASSI, H., LING, W. L., FRACHET, P., HOUEN, G., ARLAUD, G. J. & GABORIAUD, C. 2011. X-ray structure of the human calreticulin globular domain reveals a peptide-binding area and suggests a multi-molecular mechanism. *PLoS One*, 6, e17886.
- CIPLY, E., ZITKUS, E., GOLD, L. I., DAUBRIAC, J., PAVLIDES, S. C., HOJRUP, P., HOUEN, G., WANG, W. A., MICHALAK, M. & SLIBINSKAS, R. 2015. High-level secretion of native recombinant human calreticulin in yeast. *Microb Cell Fact*, 14, 165.
- COLEMAN, M. L., SAHAI, E. A., YEO, M., BOSCH, M., DEWAR, A. & OLSON, M. F. 2001. Membrane blebbing during apoptosis results from caspase-mediated activation of ROCK I. *Nat Cell Biol*, 3, 339-45.

- COOSEMANS, A., DECOENE, J., BAERT, T., LAENEN, A., KASRAN, A., VERSCHUERE, T., SEYS, S. & VERGOTE, I. 2016. Immunosuppressive parameters in serum of ovarian cancer patients change during the disease course. *Oncoimmunology*, 5, e1111505.
- CORNELISSEN, M., PHILIPPE, J., DE SITTER, S. & DE RIDDER, L. 2002. Annexin V expression in apoptotic peripheral blood lymphocytes: an electron microscopic evaluation. *Apoptosis*, 7, 41-7.
- CRISTEA, M., HAN, E., SALMON, L. & MORGAN, R. J. 2010. Practical considerations in ovarian cancer chemotherapy. *Ther Adv Med Oncol*, 2, 175-87.
- DAIGNEAULT, M., PRESTON, J. A., MARRIOTT, H. M., WHYTE, M. K. & DOCKRELL, D. H. 2010. The identification of markers of macrophage differentiation in PMA-stimulated THP-1 cells and monocyte-derived macrophages. *PLoS One*, 5, e8668.
- DE BRUYN, M., WIERSMA, V. R., HELFRICH, W., EGGLETON, P. & BREMER, E. 2015. The ever-expanding immunomodulatory role of calreticulin in cancer immunity. *Front Oncol*, 5, 35.
- DE KOKER, S., LAMBRECHT, B. N., WILLART, M. A., VAN KOOYK, Y., GROOTEN, J., VERVAET, C., REMON, J. P. & DE GEEST, B. G. 2011. Designing polymeric particles for antigen delivery. *Chem Soc Rev*, 40, 320-39.
- DEL CID, N., SHEN, L., BELLEISLE, J. & RAGHAVAN, M. 2012. Assessment of roles for calreticulin in the cross-presentation of soluble and bead-associated antigens. *PLoS One*, 7, e41727.
- DEMCHENKO, A. P. 2013. Beyond annexin V: fluorescence response of cellular membranes to apoptosis. *Cytotechnology*, 65, 157-72.
- DIERGAARDE, B. & KURTA, M. L. 2014. Use of fertility drugs and risk of ovarian cancer. *Curr Opin Obstet Gynecol*, 26, 125-9.
- DOMINGUES, M. M., INACIO, R. G., RAIMUNDO, J. M., MARTINS, M., CASTANHO, M. A. & SANTOS, N. C. 2012. Biophysical characterization of polymyxin B interaction with LPS aggregates and membrane model systems. *Biopolymers*, 98, 338-44.
- DONNELLY, S., ROAKE, W., BROWN, S., YOUNG, P., NAIK, H., WORDSWORTH, P., ISENBERG, D. A., REID, K. B. & EGGLETON, P. 2006. Impaired recognition of apoptotic neutrophils by the C1q/calreticulin and CD91 pathway in systemic lupus erythematosus. *Arthritis Rheum*, 54, 1543-56.
- DOUFEKAS, K. & OLAITAN, A. 2014. Clinical epidemiology of epithelial ovarian cancer in the UK. *Int J Womens Health*, 6, 537-45.
- DRAKES, M. L. & STIFF, P. J. 2016. Understanding dendritic cell immunotherapy in ovarian cancer. *Expert Rev Anticancer Ther*, 16, 643-52.
- DU, X. L., HU, H., LIN, D. C., XIA, S. H., SHEN, X. M., ZHANG, Y., LUO, M. L., FENG, Y. B., CAI, Y., XU, X., HAN, Y. L., ZHAN, Q. M. & WANG, M. R. 2007. Proteomic profiling of proteins dysregulated in Chinese esophageal squamous cell carcinoma. *J Mol Med (Berl)*, 85, 863-75.
- DUDEK, A. M., MARTIN, S., GARG, A. D. & AGOSTINIS, P. 2013. Immature, Semi-Mature, and Fully Mature Dendritic Cells: Toward a DC-Cancer Cells Interface That Augments Anticancer Immunity. *Front Immunol*, 4, 438.
- DUMITRIU, I. E., BARUAH, P., VALENTINIS, B., VOLL, R. E., HERRMANN, M., NAWROTH, P. P., ARNOLD, B., BIANCHI, M. E., MANFREDI, A. A. & ROVERE-QUERINI, P. 2005. Release of high mobility group box 1 by dendritic cells controls T cell activation via the receptor for advanced glycation end products. *J Immunol*, 174, 7506-15.
- DUNN, G. P., BRUCE, A. T., IKEDA, H., OLD, L. J. & SCHREIBER, R. D. 2002. Cancer immunoediting: from immunosurveillance to tumor escape. *Nat Immunol*, 3, 991-8.
- ECCLES, S. A. & WELCH, D. R. 2007. Metastasis: recent discoveries and novel treatment strategies. *Lancet*, 369, 1742-57.
- EDWARDSON, D. W., BOUDREAU, J., MAPLETOFT, J., LANNER, C., KOVALA, A. T. & PARISENTI, A. M. 2017. Inflammatory cytokine production in tumor cells upon chemotherapy drug exposure or upon selection for drug resistance. *PLoS One*, 12, e0183662.

- EGGLETON, P., BREMER, E., DUDEK, E. & MICHALAK, M. 2016. Calreticulin, a therapeutic target? *Expert Opin Ther Targets*, 20, 1137-47.
- EGGLETON, P. & MICHALAK, M. 2013. Calreticulin for better or for worse, in sickness and in health, until death do us part. *Cell Calcium*, 54, 126-31.
- ELMORE, S. 2007. Apoptosis: a review of programmed cell death. *Toxicol Pathol*, 35, 495-516.
- ENGELS, E. A., PFEIFFER, R. M., FRAUMENI, J. F., JR., KASISKE, B. L., ISRANI, A. K., SNYDER, J. J., WOLFE, R. A., GOODRICH, N. P., BAYAKLY, A. R., CLARKE, C. A., COPELAND, G., FINCH, J. L., FLEISSNER, M. L., GOODMAN, M. T., KAHN, A., KOCH, L., LYNCH, C. F., MADELEINE, M. M., PAWLISH, K., RAO, C., WILLIAMS, M. A., CASTENSON, D., CURRY, M., PARSONS, R., FANT, G. & LIN, M. 2011. Spectrum of cancer risk among US solid organ transplant recipients. *JAMA*, 306, 1891-901.
- EOH, K. J., LEE, J. Y., NAM, E. J., KIM, S., KIM, Y. T. & KIM, S. W. 2017. Long-Term Survival Analysis of Intraperitoneal versus Intravenous Chemotherapy for Primary Ovarian Cancer and Comparison between Carboplatin- and Cisplatin-based Intraperitoneal Chemotherapy. *J Korean Med Sci*, 32, 2021-2028.
- FADEEL, B. & XUE, D. 2009. The ins and outs of phospholipid asymmetry in the plasma membrane: roles in health and disease. *Crit Rev Biochem Mol Biol*, 44, 264-77.
- FENG, M., MARJON, K. D., ZHU, F., WEISSMAN-TSUKAMOTO, R., LEVETT, A., SULLIVAN, K., KAO, K. S., MARKOVIC, M., BUMP, P. A., JACKSON, H. M., CHOI, T. S., CHEN, J., BANUELOS, A. M., LIU, J., GIP, P., CHENG, L., WANG, D. & WEISSMAN, I. L. 2018. Programmed cell removal by calreticulin in tissue homeostasis and cancer. *Nat Commun*, 9, 3194.
- FERRIS, S. P., KODALI, V. K. & KAUFMAN, R. J. 2014. Glycoprotein folding and quality-control mechanisms in protein-folding diseases. *Dis Model Mech*, 7, 331-41.
- FU, C. & JIANG, A. 2018. Dendritic Cells and CD8 T Cell Immunity in Tumor Microenvironment. *Front Immunol*, 9, 3059.
- FU, H. Y., SANADA, S., MATSUZAKI, T., LIAO, Y., OKUDA, K., YAMATO, M., TSUCHIDA, S., ARAKI, R., ASANO, Y., ASANUMA, H., ASAKURA, M., FRENCH, B. A., SAKATA, Y., KITAKAZE, M. & MINAMINO, T. 2016. Chemical Endoplasmic Reticulum Chaperone Alleviates Doxorubicin-Induced Cardiac Dysfunction. *Circ Res*, 118, 798-809.
- FULDA, S. & DEBATIN, K. M. 2006. Extrinsic versus intrinsic apoptosis pathways in anticancer chemotherapy. *Oncogene*, 25, 4798-811.
- GALAZIS, N., OLALEYE, O., HAOULA, Z., LAYFIELD, R. & ATIOMO, W. 2012. Proteomic biomarkers for ovarian cancer risk in women with polycystic ovary syndrome: a systematic review and biomarker database integration. *Fertil Steril*, 98, 1590-601 e1.
- GALLUZZI, L., BUQUE, A., KEPP, O., ZITVOGEL, L. & KROEMER, G. 2017. Immunogenic cell death in cancer and infectious disease. *Nat Rev Immunol*, 17, 97-111.
- GALLUZZI, L., VITALE, I., AARONSON, S. A., ABRAMS, J. M., ADAM, D., AGOSTINIS, P., ALNEMRI, E. S., ALTUCCI, L., AMELIO, I., ANDREWS, D. W., ANNICCHIARICO-PETRUZZELLI, M., ANTONOV, A. V., ARAMA, E., BAEHRECKE, E. H., BARLEV, N. A., BAZAN, N. G., BERNASSOLA, F., BERTRAND, M. J. M., BIANCHI, K., BLAGOSKLONNY, M. V., BLOMGREN, K., BORNER, C., BOYA, P., BRENNER, C., CAMPANELLA, M., CANDI, E., CARMONA-GUTIERREZ, D., CECCONI, F., CHAN, F. K., CHANDEL, N. S., CHENG, E. H., CHIPUK, J. E., CIDLOWSKI, J. A., CIECHANOVER, A., COHEN, G. M., CONRAD, M., CUBILLOS-RUIZ, J. R., CZABOTAR, P. E., D'ANGIOLELLA, V., DAWSON, T. M., DAWSON, V. L., DE LAURENZI, V., DE MARIA, R., DEBATIN, K. M., DEBERARDINIS, R. J., DESHMUKH, M., DI DANIELE, N., DI VIRGILIO, F., DIXIT, V. M., DIXON, S. J., DUCKETT, C. S., DYNLACHT, B. D., EL-DEIRY, W. S., ELROD, J. W., FIMIA, G. M., FULDA, S., GARCIA-SAEZ, A. J., GARG, A. D., GARRIDO, C., GAVATHIOTIS, E., GOLSTEIN, P., GOTTLIEB, E., GREEN, D. R., GREENE, L. A., GRONEMEYER, H., GROSS, A., HAJNOCZKY, G., HARDWICK, J. M., HARRIS, I. S., HENGARTNER, M. O., HETZ, C., ICHIJO, H., JAATTELA, M., JOSEPH, B., JOST, P. J., JUIN, P. P., KAISER, W. J., KARIN, M., KAUFMANN, T., KEPP, O., KIMCHI, A., KITSIS, R. N., KLIONSKY, D. J., KNIGHT, R. A., KUMAR, S., LEE, S. W., LEMASTERS, J. J., LEVINE, B., LINKERMANN, A., LIPTON,

- S. A., LOCKSHIN, R. A., LOPEZ-OTIN, C., LOWE, S. W., LUEDDE, T., LUGLI, E., MACFARLANE, M., MADEO, F., MALEWICZ, M., MALORNI, W., MANIC, G., et al. 2018. Molecular mechanisms of cell death: recommendations of the Nomenclature Committee on Cell Death 2018. *Cell Death Differ*, 25, 486-541.
- GANLEY, I. G., WONG, P. M., GAMMOH, N. & JIANG, X. 2011. Distinct autophagosomal-lysosomal fusion mechanism revealed by thapsigargin-induced autophagy arrest. *Mol Cell*, 42, 731-43.
- GAO, C. & WANG, A. Y. 2009. Significance of increased apoptosis and Bax expression in human small intestinal adenocarcinoma. *J Histochem Cytochem*, 57, 1139-48.
- GARDAI, S. J., MCPHILLIPS, K. A., FRASCH, S. C., JANSSEN, W. J., STAREFELDT, A., MURPHY-ULLRICH, J. E., BRATTON, D. L., OLDENBORG, P. A., MICHALAK, M. & HENSON, P. M. 2005. Cell-surface calreticulin initiates clearance of viable or apoptotic cells through trans-activation of LRP on the phagocyte. *Cell*, 123, 321-34.
- GARG, A. D., KRYSKO, D. V., VERFAILLIE, T., KACZMAREK, A., FERREIRA, G. B., MARYSAEL, T., RUBIO, N., FIRCUZUK, M., MATHIEU, C., ROEBROEK, A. J., ANNAERT, W., GOLAB, J., DE WITTE, P., VANDENABEELE, P. & AGOSTINIS, P. 2012. A novel pathway combining calreticulin exposure and ATP secretion in immunogenic cancer cell death. *EMBO J*, 31, 1062-79.
- GARG, A. D., MORE, S., RUFO, N., MECE, O., SASSANO, M. L., AGOSTINIS, P., ZITVOGEL, L., KROEMER, G. & GALLUZZI, L. 2017. Trial watch: Immunogenic cell death induction by anticancer chemotherapeutics. *Oncoimmunology*, 6, e1386829.
- GARG, A. D., NOWIS, D., GOLAB, J., VANDENABEELE, P., KRYSKO, D. V. & AGOSTINIS, P. 2010. Immunogenic cell death, DAMPs and anticancer therapeutics: an emerging amalgamation. *Biochim Biophys Acta*, 1805, 53-71.
- GARRIDO, C., PACO, L., ROMERO, I., BERRUGUILLA, E., STEFANSKY, J., COLLADO, A., ALGARRA, I., GARRIDO, F. & GARCIA-LORA, A. M. 2012. MHC class I molecules act as tumor suppressor genes regulating the cell cycle gene expression, invasion and intrinsic tumorigenicity of melanoma cells. *Carcinogenesis*, 33, 687-93.
- EGINAT, J., NIZZOLI, G., PARONI, M., MAGLIE, S., LARGHI, P., PASCOLO, S. & ABRIGNANI, S. 2015. Immunity to Pathogens Taught by Specialized Human Dendritic Cell Subsets. *Front Immunol*, 6, 527.
- GELEBART, P., OPAS, M. & MICHALAK, M. 2005. Calreticulin, a Ca<sup>2+</sup>-binding chaperone of the endoplasmic reticulum. *Int J Biochem Cell Biol*, 37, 260-6.
- GENTILE, C. L., FRYE, M. & PAGLIASSOTTI, M. J. 2011. Endoplasmic reticulum stress and the unfolded protein response in nonalcoholic fatty liver disease. *Antioxid Redox Signal*, 15, 505-21.
- GERMAIN, R. N. 2002. T-cell development and the CD4-CD8 lineage decision. *Nat Rev Immunol*, 2, 309-22.
- GHEBREHIWET, B. & PEERSCHKE, E. I. 2004. Role of C1q and C1q receptors in the pathogenesis of systemic lupus erythematosus. *Curr Dir Autoimmun*, 7, 87-97.
- GIGLIO, P., GAGLIARDI, M., BERNARDINI, R., MATTEI, M., COTELLA, D., SANTORO, C., PIACENTINI, M. & CORAZZARI, M. 2018. Ecto-Calreticulin is essential for an efficient immunogenic cell death stimulation in mouse melanoma. *Genes Immun*.
- GLAB, J. A., DOERFLINGER, M., NEDEVA, C., JOSE, I., MBOGO, G. W., PATON, J. C., PATON, A. W., KUEH, A. J., HEROLD, M. J., HUANG, D. C., SEGAL, D., BRUMATTI, G. & PUTHALAKATH, H. 2017. DR5 and caspase-8 are dispensable in ER stress-induced apoptosis. *Cell Death Differ*, 24, 944-950.
- GOICOECHEA, S., ORR, A. W., PALLERO, M. A., EGGLETON, P. & MURPHY-ULLRICH, J. E. 2000. Thrombospondin mediates focal adhesion disassembly through interactions with cell surface calreticulin. *J Biol Chem*, 275, 36358-68.
- GOLD, L., WILLIAMS, D., GROENENDYK, J., MICHALAK, M. & EGGLETON, P. 2015. Unfolding the complexities of ER chaperones in health and disease: report on the 11th international calreticulin workshop. *Cell Stress Chaperones*, 20, 875-83.

- GOLD, L. I., EGGLETON, P., SWEETWYNE, M. T., VAN DUYN, L. B., GREIVES, M. R., NAYLOR, S. M., MICHALAK, M. & MURPHY-ULLRICH, J. E. 2010. Calreticulin: non-endoplasmic reticulum functions in physiology and disease. *FASEB J*, 24, 665-83.
- GOLD, L. I., RAHMAN, M., BLECHMAN, K. M., GREIVES, M. R., CHURGIN, S., MICHAELS, J., CALLAGHAN, M. J., CARDWELL, N. L., POLLINS, A. C., MICHALAK, M., SIEBERT, J. W., LEVINE, J. P., GURTNER, G. C., NANNEY, L. B., GALIANO, R. D. & CADACIO, C. L. 2006. Overview of the role for calreticulin in the enhancement of wound healing through multiple biological effects. *J Invest Dermatol Symp Proc*, 11, 57-65.
- GREPPI, M., TABELLINI, G., PATRIZI, O., CANDIANI, S., DECENSI, A., PAROLINI, S., SIVORI, S., PESCE, S., PALEARI, L. & MARCENARO, E. 2019. Strengthening the AntiTumor NK Cell Function for the Treatment of Ovarian Cancer. *Int J Mol Sci*, 20.
- HACKER, N. F. 1989. Controversial aspects of cytoreductive surgery in epithelial ovarian cancer. *Baillieres Clin Obstet Gynaecol*, 3, 49-57.
- HALIN, C., MORA, J. R., SUMEN, C. & VON ANDRIAN, U. H. 2005. In vivo imaging of lymphocyte trafficking. *Annu Rev Cell Dev Biol*, 21, 581-603.
- HAN, T. H., JIN, P., REN, J., SLEZAK, S., MARINCOLA, F. M. & STRONCEK, D. F. 2009. Evaluation of 3 clinical dendritic cell maturation protocols containing lipopolysaccharide and interferon-gamma. *J Immunother*, 32, 399-407.
- HANKE, N., ALIZADEH, D., KATSANIS, E. & LARMONIER, N. 2013. Dendritic cell tumor killing activity and its potential applications in cancer immunotherapy. *Crit Rev Immunol*, 33, 1-21.
- HANSEN, M. & ANDERSEN, M. H. 2017. The role of dendritic cells in cancer. *Semin Immunopathol*, 39, 307-316.
- HARRIES, M. & GORE, M. 2002. Part I: chemotherapy for epithelial ovarian cancer-treatment at first diagnosis. *Lancet Oncol*, 3, 529-36.
- HART, D. N. 1997. Dendritic cells: unique leukocyte populations which control the primary immune response. *Blood*, 90, 3245-87.
- HASSAN, M., WATARI, H., ABUALMAATY, A., OHBA, Y. & SAKURAGI, N. 2014. Apoptosis and molecular targeting therapy in cancer. *Biomed Res Int*, 2014, 150845.
- HEALEY, G. D., ELVIN, S. J., MORTON, M. & WILLIAMSON, E. D. 2005. Humoral and cell-mediated adaptive immune responses are required for protection against *Burkholderia pseudomallei* challenge and bacterial clearance postinfection. *Infect Immun*, 73, 5945-51.
- HELLMAN, K., ALAIYA, A. A., SCHEDVINS, K., STEINBERG, W., HELLSTROM, A. C. & AUER, G. 2004. Protein expression patterns in primary carcinoma of the vagina. *Br J Cancer*, 91, 319-26.
- HENSON, P. M. & HUME, D. A. 2006. Apoptotic cell removal in development and tissue homeostasis. *Trends Immunol*, 27, 244-50.
- HERSPERGER, A. R., PEREYRA, F., NASON, M., DEMERS, K., SHETH, P., SHIN, L. Y., KOVACS, C. M., RODRIGUEZ, B., SIEG, S. F., TEIXEIRA-JOHNSON, L., GUDONIS, D., GOEPFERT, P. A., LEDERMAN, M. M., FRANK, I., MAKEDONAS, G., KAUL, R., WALKER, B. D. & BETTS, M. R. 2010. Perforin expression directly ex vivo by HIV-specific CD8 T-cells is a correlate of HIV elite control. *PLoS Pathog*, 6, e1000917.
- HETZ, C., CHEVET, E. & HARDING, H. P. 2013. Targeting the unfolded protein response in disease. *Nat Rev Drug Discov*, 12, 703-19.
- HODGE, J. W., GARNETT, C. T., FARSACI, B., PALENA, C., TSANG, K. Y., FERRONE, S. & GAMEIRO, S. R. 2013. Chemotherapy-induced immunogenic modulation of tumor cells enhances killing by cytotoxic T lymphocytes and is distinct from immunogenic cell death. *Int J Cancer*, 133, 624-36.
- HODGE, J. W., RAD, A. N., GROSENBACH, D. W., SABZEVARI, H., YAFAL, A. G., GRITZ, L. & SCHLOM, J. 2000. Enhanced activation of T cells by dendritic cells engineered to hyperexpress a triad of costimulatory molecules. *J Natl Cancer Inst*, 92, 1228-39.
- HOESEL, B. & SCHMID, J. A. 2013. The complexity of NF-kappaB signaling in inflammation and cancer. *Mol Cancer*, 12, 86.



- HOLMGREN, G., SYNNERGREN, J., BOGESTAL, Y., AMEEN, C., AKESSON, K., HOLMGREN, S., LINDAHL, A. & SARTIPY, P. 2015. Identification of novel biomarkers for doxorubicin-induced toxicity in human cardiomyocytes derived from pluripotent stem cells. *Toxicology*, 328, 102-11.
- HOLSCHNEIDER, C. H. & BEREK, J. S. 2000. Ovarian cancer: epidemiology, biology, and prognostic factors. *Semin Surg Oncol*, 19, 3-10.
- HORNE, F. M. 2018. Focus on Ovarian Cancer.
- HOUGHTON, A. N. & GUEVARA-PATINO, J. A. 2004. Immune recognition of self in immunity against cancer. *J Clin Invest*, 114, 468-71.
- [HTTP://WWW.BIOLOGY.LIFEEASY.ORG/742/WHAT-IS-PROGRAMMED-CELL-DEATH-PCD](http://www.biology.lifesci.dundee.ac.uk/2017/cell-death-and-apoptosis/) What is Programmed Cell Death (PCD)?
- [HTTPS://WWW.LIFESCI.DUNDEE.AC.UK/](https://www.lifesci.dundee.ac.uk/2017/cell-death-and-apoptosis/) 2017. Cell Death and Apoptosis.
- [HTTPS://WWW.NCBI.NLM.NIH.GOV/BOOKS/NBK27156/](https://www.ncbi.nlm.nih.gov/books/nbk27156/) 2001. Immunobiology: The Immune System in Health and Disease.
- [HTTPS://WWW.THERMOFISHER.COM/UK/EN/HOME/LIFE-SCIENCE/PROTEIN-BIOLOGY/PROTEIN-ASSAYS-ANALYSIS/IMMUNOPRECIPITATION/MAGNETS-IMMUNOPRECIPITATION-CO-IP-PULL-DOWN.HTML](https://www.thermofisher.com/uk/en/home/life-science/protein-biology/protein-assays-analysis/immunoprecipitation/magnets-immunoprecipitation-co-ip-pull-down.html) 2011. Dynabeads® Human T-Activator CD3/CD28.
- IGNEY, F. H. & KRAMMER, P. H. 2002. Death and anti-death: tumour resistance to apoptosis. *Nat Rev Cancer*, 2, 277-88.
- INFO.EMEA@BIO-TECHNE.COM 2108. UPR and ER Stress FAQs
- INOUE, S., BROWNE, G., MELINO, G. & COHEN, G. M. 2009. Ordering of caspases in cells undergoing apoptosis by the intrinsic pathway. *Cell Death Differ*, 16, 1053-61.
- INOUE, S., SETOYAMA, Y. & ODAKA, A. 2014. Doxorubicin treatment induces tumor cell death followed by immunomodulation in a murine neuroblastoma model. *Exp Ther Med*, 7, 703-708.
- JAMES, E. 2016. Awakening the force: T cells enter the battle against cancer.
- JANSSEN, S., ROSEN, D. M., RICKLIS, R. M., DIONNE, C. A., LILJA, H., CHRISTENSEN, S. B., ISAACS, J. T. & DENMEADE, S. R. 2006. Pharmacokinetics, biodistribution, and antitumor efficacy of a human glandular kallikrein 2 (hK2)-activated thapsigargin prodrug. *Prostate*, 66, 358-68.
- JIANG, P., LAGENAUR, C. F. & NARAYANAN, V. 1999. Integrin-associated protein is a ligand for the P84 neural adhesion molecule. *J Biol Chem*, 274, 559-62.
- JOHANSSON, S. M., ADMYRE, C., SCHEYNIUS, A. & GABRIELSSON, S. 2008. Different types of in vitro generated human monocyte-derived dendritic cells release exosomes with distinct phenotypes. *Immunology*, 123, 491-9.
- JUNGBLUTH, A. A., CHEN, Y. T., STOCKERT, E., BUSAM, K. J., KOLB, D., IVERSEN, K., COPLAN, K., WILLIAMSON, B., ALTORKI, N. & OLD, L. J. 2001. Immunohistochemical analysis of NY-ESO-1 antigen expression in normal and malignant human tissues. *Int J Cancer*, 92, 856-60.
- KACZMAREK, A., VANDENABEELE, P. & KRYSKO, D. V. 2013. Necroptosis: the release of damage-associated molecular patterns and its physiological relevance. *Immunity*, 38, 209-23.
- KAGEYAMA, S., ISONO, T., IWAKI, H., WAKABAYASHI, Y., OKADA, Y., KONTANI, K., YOSHIMURA, K., TERAJ, A., ARAI, Y. & YOSHIKI, T. 2004. Identification by proteomic analysis of calreticulin as a marker for bladder cancer and evaluation of the diagnostic accuracy of its detection in urine. *Clin Chem*, 50, 857-66.
- KAMINSKY, V. & ZHIVOTOVSKY, B. 2010. To kill or be killed: how viruses interact with the cell death machinery. *J Intern Med*, 267, 473-82.
- KANDALAFT, L. E., POWELL, D. J., JR., SINGH, N. & COUKOS, G. 2011. Immunotherapy for ovarian cancer: what's next? *J Clin Oncol*, 29, 925-33.
- KANTOFF, P. W., HIGANO, C. S., SHORE, N. D., BERGER, E. R., SMALL, E. J., PENSON, D. F., REDFERN, C. H., FERRARI, A. C., DREICER, R., SIMS, R. B., XU, Y., FROHLICH, M. W., SCHELLHAMMER, P.

- F. & INVESTIGATORS, I. S. 2010. Sipuleucel-T immunotherapy for castration-resistant prostate cancer. *N Engl J Med*, 363, 411-22.
- KELLEY, S. L., LUKK, T., NAIR, S. K. & TAPPING, R. I. 2013. The crystal structure of human soluble CD14 reveals a bent solenoid with a hydrophobic amino-terminal pocket. *J Immunol*, 190, 1304-11.
- KEPP, O., SENOVILLA, L., VITALE, I., VACCHELLI, E., ADJEMIAN, S., AGOSTINIS, P., APETOH, L., ARANDA, F., BARNABA, V., BLOY, N., BRACCI, L., BRECKPOT, K., BROUGH, D., BUQUE, A., CASTRO, M. G., CIRONE, M., COLOMBO, M. I., CREMER, I., DEMARIA, S., DINI, L., ELIOPOULOS, A. G., FAGGIONI, A., FORMENTI, S. C., FUCIKOVA, J., GABRIELE, L., GAIPL, U. S., GALON, J., GARG, A., GHIRINGHELLI, F., GIESE, N. A., GUO, Z. S., HEMMINKI, A., HERRMANN, M., HODGE, J. W., HOLDENRIEDER, S., HONEYCHURCH, J., HU, H. M., HUANG, X., ILLIDGE, T. M., KONO, K., KORBELIK, M., KRYSKO, D. V., LOI, S., LOWENSTEIN, P. R., LUGLI, E., MA, Y., MADEO, F., MANFREDI, A. A., MARTINS, I., MAVILIO, D., MENDER, L., MERENDINO, N., MICHAUD, M., MIGNOT, G., MOSSMAN, K. L., MULTHOFF, G., OEHLER, R., PALOMBO, F., PANARETAKIS, T., POL, J., PROIETTI, E., RICCI, J. E., RIGANTI, C., ROVERE-QUERINI, P., RUBARTELLI, A., SISTIGU, A., SMYTH, M. J., SONNEMANN, J., SPISEK, R., STAGG, J., SUKKURWALA, A. Q., TARTOUR, E., THORBURN, A., THORNE, S. H., VANDENABEELE, P., VELOTTI, F., WORKENHE, S. T., YANG, H., ZONG, W. X., ZITVOGEL, L., KROEMER, G. & GALLUZZI, L. 2014. Consensus guidelines for the detection of immunogenic cell death. *Oncoimmunology*, 3, e955691.
- KERR, J. F., WYLLIE, A. H. & CURRIE, A. R. 1972. Apoptosis: a basic biological phenomenon with wide-ranging implications in tissue kinetics. *Br J Cancer*, 26, 239-57.
- KHAYRULLINA, T., YEN, J. H., JING, H. & GANEA, D. 2008. In vitro differentiation of dendritic cells in the presence of prostaglandin E2 alters the IL-12/IL-23 balance and promotes differentiation of Th17 cells. *J Immunol*, 181, 721-35.
- KIERTSCHER, S. M. & ROTH, M. D. 1996. Human CD14+ leukocytes acquire the phenotype and function of antigen-presenting dendritic cells when cultured in GM-CSF and IL-4. *J Leukoc Biol*, 59, 208-18.
- KIM, S. J., PARK, K. M., KIM, N. & YEOM, Y. I. 2006. Doxorubicin prevents endoplasmic reticulum stress-induced apoptosis. *Biochem Biophys Res Commun*, 339, 463-8.
- KIRIKAE, T., TAMURA, H., HASHIZUME, M., KIRIKAE, F., UEMURA, Y., TANAKA, S., YOKOCHI, T. & NAKANO, M. 1997. Endotoxin contamination in fetal bovine serum and its influence on tumor necrosis factor production by macrophage-like cells J774.1 cultured in the presence of the serum. *Int J Immunopharmacol*, 19, 255-62.
- KIRKIN, V., JOOS, S. & ZORNIG, M. 2004. The role of Bcl-2 family members in tumorigenesis. *Biochim Biophys Acta*, 1644, 229-49.
- KLION, A. D. & NUTMAN, T. B. 2004. The role of eosinophils in host defense against helminth parasites. *J Allergy Clin Immunol*, 113, 30-7.
- KORBELIK, M., BANATH, J., SAW, K. M., ZHANG, W. & CIPLYS, E. 2015. Calreticulin as cancer treatment adjuvant: combination with photodynamic therapy and photodynamic therapy-generated vaccines. *Front Oncol*, 5, 15.
- KRAUSE, K. H. & MICHALAK, M. 1997. Calreticulin. *Cell*, 88, 439-43.
- KROEMER, G., GALLUZZI, L., KEPP, O. & ZITVOGEL, L. 2013. Immunogenic cell death in cancer therapy. *Annu Rev Immunol*, 31, 51-72.
- KRYSKO, D. V., AGOSTINIS, P., KRYSKO, O., GARG, A. D., BACHERT, C., LAMBRECHT, B. N. & VANDENABEELE, P. 2011. Emerging role of damage-associated molecular patterns derived from mitochondria in inflammation. *Trends Immunol*, 32, 157-64.
- KRYSKO, D. V., GARG, A. D., KACZMAREK, A., KRYSKO, O., AGOSTINIS, P. & VANDENABEELE, P. 2012. Immunogenic cell death and DAMPs in cancer therapy. *Nat Rev Cancer*, 12, 860-75.
- KRYSKO, D. V., RAVICHANDRAN, K. S. & VANDENABEELE, P. 2018. Macrophages regulate the clearance of living cells by calreticulin. *Nat Commun*, 9, 4644.

- KRYSTEL-WHITTEMORE, M., DILEEPAN, K. N. & WOOD, J. G. 2015. Mast Cell: A Multi-Functional Master Cell. *Front Immunol*, 6, 620.
- KUMAR, H., KAWAI, T. & AKIRA, S. 2011. Pathogen recognition by the innate immune system. *Int Rev Immunol*, 30, 16-34.
- KUPPNER, M. C., GASTPAR, R., GELWER, S., NOSSNER, E., OCHMANN, O., SCHARNER, A. & ISSELS, R. D. 2001. The role of heat shock protein (hsp70) in dendritic cell maturation: hsp70 induces the maturation of immature dendritic cells but reduces DC differentiation from monocyte precursors. *Eur J Immunol*, 31, 1602-9.
- LABRIOLA, C. A., CONTE, I. L., LOPEZ MEDUS, M., PARODI, A. J. & CAMELO, J. J. 2010. Endoplasmic reticulum calcium regulates the retrotranslocation of Trypanosoma cruzi calreticulin to the cytosol. *PLoS One*, 5.
- LI, S., ZHAO, Y., HE, X., KIM, T. H., KUHARSKY, D. K., RABINOWICH, H., CHEN, J., DU, C. & YIN, X. M. 2002. Relief of extrinsic pathway inhibition by the Bid-dependent mitochondrial release of Smac in Fas-mediated hepatocyte apoptosis. *J Biol Chem*, 277, 26912-20.
- LI, Y. & KURLANDER, R. J. 2010. Comparison of anti-CD3 and anti-CD28-coated beads with soluble anti-CD3 for expanding human T cells: differing impact on CD8 T cell phenotype and responsiveness to restimulation. *J Transl Med*, 8, 104.
- LI, Y., ZENG, X., HE, L. & YUAN, H. 2015. Dendritic cell activation and maturation induced by recombinant calreticulin fragment 39-272. *Int J Clin Exp Med*, 8, 7288-96.
- LIN, H. W., TU, Y. Y., LIN, S. Y., SU, W. J., LIN, W. L., LIN, W. Z., WU, S. C. & LAI, Y. L. 2011. Risk of ovarian cancer in women with pelvic inflammatory disease: a population-based study. *Lancet Oncol*, 12, 900-4.
- LIU, C. C., LECLAIR, P., MONAJEMI, M., SLY, L. M., REID, G. S. & LIM, C. J. 2016a. alpha-Integrin expression and function modulates presentation of cell surface calreticulin. *Cell Death Dis*, 7, e2268.
- LIU, X., LI, J., LIU, Y., DING, J., TONG, Z., LIU, Y., ZHOU, Y. & LIU, Y. 2016b. Calreticulin acts as an adjuvant to promote dendritic cell maturation and enhances antigen-specific cytotoxic T lymphocyte responses against non-small cell lung cancer cells. *Cell Immunol*, 300, 46-53.
- LLC, N. B. 2018. How to count cells using a hemacytometer.
- LU, Y. C., WENG, W. C. & LEE, H. 2015. Functional roles of calreticulin in cancer biology. *Biomed Res Int*, 2015, 526524.
- LV, Z., BIAN, Z., SHI, L., NIU, S., HA, B., TREMBLAY, A., LI, L., ZHANG, X., PALUSZYNSKI, J., LIU, M., ZEN, K. & LIU, Y. 2015. Loss of Cell Surface CD47 Clustering Formation and Binding Avidity to SIRPalpha Facilitate Apoptotic Cell Clearance by Macrophages. *J Immunol*, 195, 661-71.
- LWIN, Z. M., GUO, C., SALIM, A., YIP, G. W., CHEW, F. T., NAN, J., THIKE, A. A., TAN, P. H. & BAY, B. H. 2010. Clinicopathological significance of calreticulin in breast invasive ductal carcinoma. *Mod Pathol*, 23, 1559-66.
- MAHER, J. & DAVIES, E. T. 2004. Targeting cytotoxic T lymphocytes for cancer immunotherapy. *Br J Cancer*, 91, 817-21.
- MAK, T. W. 2006. T Cell Activation.
- MALLA, S., NIRLAULA, N. P., LIOU, K. & SOHNG, J. K. 2009. Enhancement of doxorubicin production by expression of structural sugar biosynthesis and glycosyltransferase genes in Streptomyces peucetius. *J Biosci Bioeng*, 108, 92-8.
- MALO, A., KRUGER, B., SEYHUN, E., SCHAFFER, C., HOFFMANN, R. T., GOKE, B. & KUBISCH, C. H. 2010. Tauroursodeoxycholic acid reduces endoplasmic reticulum stress, trypsin activation, and acinar cell apoptosis while increasing secretion in rat pancreatic acini. *Am J Physiol Gastrointest Liver Physiol*, 299, G877-86.
- MANDL, M., SCHMITZ, S., WEBER, C. & HRISTOV, M. 2014. Characterization of the CD14<sup>++</sup>CD16<sup>+</sup> monocyte population in human bone marrow. *PLoS One*, 9, e112140.
- MANTIA-SMALDONE, G. M., CORR, B. & CHU, C. S. 2012. Immunotherapy in ovarian cancer. *Hum Vaccin Immunother*, 8, 1179-91.

- MARTIN, S. J., REUTELINGSPERGER, C. P., MCGAHON, A. J., RADER, J. A., VAN SCHIE, R. C., LAFACE, D. M. & GREEN, D. R. 1995. Early redistribution of plasma membrane phosphatidylserine is a general feature of apoptosis regardless of the initiating stimulus: inhibition by overexpression of Bcl-2 and Abl. *J Exp Med*, 182, 1545-56.
- MARTIN, V., GROENENDYK, J., STEINER, S. S., GUO, L., DABROWSKA, M., PARKER, J. M., MULLER-ESTERL, W., OPAS, M. & MICHALAK, M. 2006. Identification by mutational analysis of amino acid residues essential in the chaperone function of calreticulin. *J Biol Chem*, 281, 2338-46.
- MARTINS, I., KEPP, O., GALLUZZI, L., SENOVILLA, L., SCHLEMMER, F., ADJEMIAN, S., MENGER, L., MICHAUD, M., ZITVOGEL, L. & KROEMER, G. 2010. Surface-exposed calreticulin in the interaction between dying cells and phagocytes. *Ann N Y Acad Sci*, 1209, 77-82.
- MARTINS, I., KEPP, O., SCHLEMMER, F., ADJEMIAN, S., TAILLER, M., SHEN, S., MICHAUD, M., MENGER, L., GDOURA, A., TAJEDDINE, N., TESNIERE, A., ZITVOGEL, L. & KROEMER, G. 2011. Restoration of the immunogenicity of cisplatin-induced cancer cell death by endoplasmic reticulum stress. *Oncogene*, 30, 1147-58.
- MASUD, A., MOHAPATRA, A., LAKHANI, S. A., FERRANDINO, A., HAKEM, R. & FLAVELL, R. A. 2007. Endoplasmic reticulum stress-induced death of mouse embryonic fibroblasts requires the intrinsic pathway of apoptosis. *J Biol Chem*, 282, 14132-9.
- MATZINGER, P. 2002. The danger model: a renewed sense of self. *Science*, 296, 301-5.
- MAYORDOMO, A. C., SILVA, J. E., GORLINO, C. V., ARIAS, J. L., BERON, W. & DI GENARO, M. S. 2018. IL-12/23p40 overproduction by dendritic cells leads to an increased Th1 and Th17 polarization in a model of Yersinia enterocolitica-induced reactive arthritis in TNFRp55<sup>-/-</sup> mice. *PLoS One*, 13, e0193573.
- MCDERMOTT, A. M. 2013. Antimicrobial compounds in tears. *Exp Eye Res*, 117, 53-61.
- MELLMAN, I., COUKOS, G. & DRANOFF, G. 2011. Cancer immunotherapy comes of age. *Nature*, 480, 480-9.
- MENCK, K., BEHME, D., PANTKE, M., REILING, N., BINDER, C., PUKROP, T. & KLEMM, F. 2014. Isolation of human monocytes by double gradient centrifugation and their differentiation to macrophages in teflon-coated cell culture bags. *J Vis Exp*, e51554.
- MESAELI, N., NAKAMURA, K., ZVARITCH, E., DICKIE, P., DZIAK, E., KRAUSE, K. H., OPAS, M., MACLENNAN, D. H. & MICHALAK, M. 1999. Calreticulin is essential for cardiac development. *J Cell Biol*, 144, 857-68.
- MICHALAK, M., CORBETT, E. F., MESAELI, N., NAKAMURA, K. & OPAS, M. 1999. Calreticulin: one protein, one gene, many functions. *Biochem J*, 344 Pt 2, 281-92.
- MICHALAK, M., GROENENDYK, J., SZABO, E., GOLD, L. I. & OPAS, M. 2009. Calreticulin, a multi-process calcium-buffering chaperone of the endoplasmic reticulum. *Biochem J*, 417, 651-66.
- MICHALAK, M., ROBERT PARKER, J. M. & OPAS, M. 2002. Ca<sup>2+</sup> signaling and calcium binding chaperones of the endoplasmic reticulum. *Cell Calcium*, 32, 269-78.
- MICHAUD, M., MARTINS, I., SUKKURWALA, A. Q., ADJEMIAN, S., MA, Y., PELLEGATTI, P., SHEN, S., KEPP, O., SCOAZEC, M., MIGNOT, G., RELLO-VARONA, S., TAILLER, M., MENGER, L., VACCHELLI, E., GALLUZZI, L., GHIRINGHELLI, F., DI VIRGILIO, F., ZITVOGEL, L. & KROEMER, G. 2011. Autophagy-dependent anticancer immune responses induced by chemotherapeutic agents in mice. *Science*, 334, 1573-7.
- MLYNARCZYK, C. & FAHRAEUS, R. 2014. Endoplasmic reticulum stress sensitizes cells to DNA damage-induced apoptosis through p53-dependent suppression of p21(CDKN1A). *Nat Commun*, 5, 5067.
- MOAZAMI-GOUDARZI, M., FARSHDOUSTI-HAGH, M., HOSEINPOUR-FEIZI, A., TALEBI, M., MOVASSAGHPUR-AKBARI, A. A., SHAMS-ASANJAN, K., EYVAZI-ZIYAAEE, J. & SEIFI, M. 2016. The acute lymphoblastic leukemia prognostic scoring whether it is possible by BCL-2, BAX gene promoter genotyping. *Caspian J Intern Med*, 7, 105-13.
- MOLINARI, R., D'ELISEO, D., MANZI, L., ZOLLA, L., VELOTTI, F. & MERENDINO, N. 2011. The n<sup>3</sup>-polyunsaturated fatty acid docosahexaenoic acid induces immunogenic cell death in human

- cancer cell lines via pre-apoptotic calreticulin exposure. *Cancer Immunol Immunother*, 60, 1503-7.
- MOMPARLER, R. L., KARON, M., SIEGEL, S. E. & AVILA, F. 1976. Effect of adriamycin on DNA, RNA, and protein synthesis in cell-free systems and intact cells. *Cancer Res*, 36, 2891-5.
- MONTI, P., MERCALLI, A., LEONE, B. E., VALERIO, D. C., ALLAVENA, P. & PIEMONTI, L. 2003. Rapamycin impairs antigen uptake of human dendritic cells. *Transplantation*, 75, 137-45.
- MONTICO, B., NIGRO, A., CASOLARO, V. & DAL COL, J. 2018. Immunogenic Apoptosis as a Novel Tool for Anticancer Vaccine Development. *Int J Mol Sci*, 19.
- MORELLI, A. E., ZAHORCHAK, A. F., LARREGINA, A. T., COLVIN, B. L., LOGAR, A. J., TAKAYAMA, T., FALO, L. D. & THOMSON, A. W. 2001. Cytokine production by mouse myeloid dendritic cells in relation to differentiation and terminal maturation induced by lipopolysaccharide or CD40 ligation. *Blood*, 98, 1512-23.
- NAGATA, S., SUZUKI, J., SEGAWA, K. & FUJII, T. 2016. Exposure of phosphatidylserine on the cell surface. *Cell Death Differ*, 23, 952-61.
- NAKAMURA, K., ZUPPINI, A., ARNAUDEAU, S., LYNCH, J., AHSAN, I., KRAUSE, R., PAPP, S., DE SMEDT, H., PARYS, J. B., MULLER-ESTERL, W., LEW, D. P., KRAUSE, K. H., DEMAUREX, N., OPAS, M. & MICHALAK, M. 2001. Functional specialization of calreticulin domains. *J Cell Biol*, 154, 961-72.
- NEU, C., SEDLAG, A., BAYER, C., FORSTER, S., CRAUWELS, P., NIESS, J. H., VAN ZANDBERGEN, G., FRASCAROLI, G. & RIEDEL, C. U. 2013. CD14-dependent monocyte isolation enhances phagocytosis of listeria monocytogenes by proinflammatory, GM-CSF-derived macrophages. *PLoS One*, 8, e66898.
- NICHOLSON, L. B. 2016. The immune system. *Essays Biochem*, 60, 275-301.
- NIX, R. N., ALTSCHULER, S. E., HENSON, P. M. & DETWEILER, C. S. 2007. Hemophagocytic macrophages harbor Salmonella enterica during persistent infection. *PLoS Pathog*, 3, e193.
- NORDIN, D. A. 2012. *Profile of Ovarian Cancer in England*, [Online]. [Accessed].
- NUNNA, S., REINHARDT, R., RAGOZIN, S. & JELTSCH, A. 2014. Targeted methylation of the epithelial cell adhesion molecule (EpcAM) promoter to silence its expression in ovarian cancer cells. *PLoS One*, 9, e87703.
- OBEID, M., TESNIERE, A., GHIRINGHELLI, F., FIMIA, G. M., APETOH, L., PERFETTINI, J. L., CASTEDO, M., MIGNOT, G., PANARETAKIS, T., CASARES, N., METIVIER, D., LAROCLETTE, N., VAN ENDERT, P., CICCOSANTI, F., PIACENTINI, M., ZITVOGEL, L. & KROEMER, G. 2007. Calreticulin exposure dictates the immunogenicity of cancer cell death. *Nat Med*, 13, 54-61.
- OGDEN, C. A., DECATHELINIEAU, A., HOFFMANN, P. R., BRATTON, D., GHEBREHIWET, B., FADOK, V. A. & HENSON, P. M. 2001. C1q and mannose binding lectin engagement of cell surface calreticulin and CD91 initiates macropinocytosis and uptake of apoptotic cells. *J Exp Med*, 194, 781-95.
- OLIVEIRA, B. L. D. 2016. A Biophysical Systems Approach to Identifying the Pathways of Acute and Chronic Doxorubicin Mitochondrial Cardiotoxicity.
- OSLOWSKI, C. M. & URANO, F. 2011. Measuring ER stress and the unfolded protein response using mammalian tissue culture system. *Methods Enzymol*, 490, 71-92.
- OSMAN, R., TACNET-DELORME, P., KLEMAN, J. P., MILLET, A. & FRACHET, P. 2017. Calreticulin Release at an Early Stage of Death Modulates the Clearance by Macrophages of Apoptotic Cells. *Front Immunol*, 8, 1034.
- OSTWALD, T. J. & MACLENNAN, D. H. 1974. Isolation of a high affinity calcium-binding protein from sarcoplasmic reticulum. *J Biol Chem*, 249, 974-9.
- OZCAN, U., YILMAZ, E., OZCAN, L., FURUHASHI, M., VAILLANCOURT, E., SMITH, R. O., GORGUN, C. Z. & HOTAMISLIGIL, G. S. 2006. Chemical chaperones reduce ER stress and restore glucose homeostasis in a mouse model of type 2 diabetes. *Science*, 313, 1137-40.

- OZOLS, R. F., BOOKMAN, M. A., DU BOIS, A., PFISTERER, J., REUSS, A. & YOUNG, R. C. 2006. Intraperitoneal cisplatin therapy in ovarian cancer: comparison with standard intravenous carboplatin and paclitaxel. *Gynecol Oncol*, 103, 1-6.
- PALUCKA, K., UENO, H., FAY, J. & BANCHEREAU, J. 2011. Dendritic cells and immunity against cancer. *J Intern Med*, 269, 64-73.
- PAN, J., ZHANG, M., WANG, J., WANG, Q., XIA, D., SUN, W., ZHANG, L., YU, H., LIU, Y. & CAO, X. 2004. Interferon-gamma is an autocrine mediator for dendritic cell maturation. *Immunol Lett*, 94, 141-51.
- PANARETAKIS, T., KEPP, O., BROCKMEIER, U., TESNIERE, A., BJORKLUND, A. C., CHAPMAN, D. C., DURCHSCHLAG, M., JOZA, N., PIERRON, G., VAN ENDERT, P., YUAN, J., ZITVOGEL, L., MADEO, F., WILLIAMS, D. B. & KROEMER, G. 2009. Mechanisms of pre-apoptotic calreticulin exposure in immunogenic cell death. *EMBO J*, 28, 578-90.
- PANDEY, M. K., PRASAD, S., TYAGI, A. K., DEB, L., HUANG, J., KARELIA, D. N., AMIN, S. G. & AGGARWAL, B. B. 2016. Targeting Cell Survival Proteins for Cancer Cell Death. *Pharmaceuticals (Basel)*, 9.
- PANDYA, U. M., EGBUTA, C., ABDULLAH NORMAN, T. M., CHIANG, C. E., WIERSMA, V. R., PANCHAL, R. G., BREMER, E., EGGLETON, P. & GOLD, L. I. 2019. The Biophysical Interaction of the Danger-Associated Molecular Pattern (DAMP) Calreticulin with the Pattern-Associated Molecular Pattern (PAMP) Lipopolysaccharide. *Int J Mol Sci*, 20.
- PARK, S. Y. & KIM, I. S. 2017. Engulfment signals and the phagocytic machinery for apoptotic cell clearance. *Exp Mol Med*, 49, e331.
- PATENTE, T. A., PINHO, M. P., OLIVEIRA, A. A., EVANGELISTA, G. C. M., BERGAMI-SANTOS, P. C. & BARBUTO, J. A. M. 2018. Human Dendritic Cells: Their Heterogeneity and Clinical Application Potential in Cancer Immunotherapy. *Front Immunol*, 9, 3176.
- PEAPER, D. R. & CRESSWELL, P. 2008. Regulation of MHC class I assembly and peptide binding. *Annu Rev Cell Dev Biol*, 24, 343-68.
- PENG, W., WANG, H. Y., MIYAHARA, Y., PENG, G. & WANG, R. F. 2008. Tumor-associated galectin-3 modulates the function of tumor-reactive T cells. *Cancer Res*, 68, 7228-36.
- PENNOCK, N. D., WHITE, J. T., CROSS, E. W., CHENEY, E. E., TAMBURINI, B. A. & KEDL, R. M. 2013. T cell responses: naive to memory and everything in between. *Adv Physiol Educ*, 37, 273-83.
- PEREIRA, A., PEREZ-MEDINA, T., MAGRINA, J. F., MAGTIBAY, P. M., RODRIGUEZ-TAPIA, A., PEREGRIN, I., MENDIZABAL, E. & ORTIZ-QUINTANA, L. 2015. International Federation of gynecology and obstetrics staging classification for cancer of the ovary, fallopian tube, and peritoneum: estimation of survival in patients with node-positive epithelial ovarian cancer. *Int J Gynecol Cancer*, 25, 49-54.
- PETERS, L. R. & RAGHAVAN, M. 2011. Endoplasmic reticulum calcium depletion impacts chaperone secretion, innate immunity, and phagocytic uptake of cells. *J Immunol*, 187, 919-31.
- PICCININI, A. M. & MIDWOOD, K. S. 2010. DAMPening inflammation by modulating TLR signalling. *Mediators Inflamm*, 2010.
- POBER, J. S. & SESSA, W. C. 2014. Inflammation and the blood microvascular system. *Cold Spring Harb Perspect Biol*, 7, a016345.
- POCKLEY, A. G., MUTHANA, M. & CALDERWOOD, S. K. 2008. The dual immunoregulatory roles of stress proteins. *Trends Biochem Sci*, 33, 71-9.
- PROSKURYAKOV, S. Y. & GABAI, V. L. 2010. Mechanisms of tumor cell necrosis. *Curr Pharm Des*, 16, 56-68.
- PROSKURYAKOV, S. Y., KONOPLYANNIKOV, A. G. & GABAI, V. L. 2003. Necrosis: a specific form of programmed cell death? *Exp Cell Res*, 283, 1-16.
- PRZYSTAL, J. M., WARAMIT, S., PRANJOL, M. Z. I., YAN, W., CHU, G., CHONGCHAI, A., SAMARTH, G., OLACIREGUI, N. G., TABATABAI, G., CARCABOSO, A. M., ABOAGYE, E. O., SUWAN, K. & HAJITOU, A. 2019. Efficacy of systemic temozolomide-activated phage-targeted gene therapy in human glioblastoma. *EMBO Mol Med*, 11.

- PUTCHA, G. V., HARRIS, C. A., MOULDER, K. L., EASTON, R. M., THOMPSON, C. B. & JOHNSON, E. M., JR. 2002. Intrinsic and extrinsic pathway signaling during neuronal apoptosis: lessons from the analysis of mutant mice. *J Cell Biol*, 157, 441-53.
- QUAH, B. J., WARREN, H. S. & PARISH, C. R. 2007. Monitoring lymphocyte proliferation in vitro and in vivo with the intracellular fluorescent dye carboxyfluorescein diacetate succinimidyl ester. *Nat Protoc*, 2, 2049-56.
- QUAH, B. J. C. 2010. The Use of Carboxyfluorescein Diacetate Succinimidyl Ester (CFSE) to Monitor Lymphocyte Proliferation. *JoVE*.
- RABB, H. 2002. The T cell as a bridge between innate and adaptive immune systems: implications for the kidney. *Kidney Int*, 61, 1935-46.
- RADOGNA, F., PATERNOSTER, L., ALBERTINI, M. C., CERELLA, C., ACCORSI, A., BUCCHINI, A., SPADONI, G., DIAMANTINI, G., TARZIA, G., DE NICOLA, M., D'ALESSIO, M. & GHIBELLI, L. 2007. Melatonin antagonizes apoptosis via receptor interaction in U937 monocytic cells. *J Pineal Res*, 43, 154-62.
- RAGHAVAN, M. 2010. Calreticulin's functions in the adaptive immune response
- RAGHAVAN, M., WIJEYSAKERE, S. J., PETERS, L. R. & DEL CID, N. 2013. Calreticulin in the immune system: ins and outs. *Trends Immunol*, 34, 13-21.
- RAO, R. V. & BREDESEN, D. E. 2004. Misfolded proteins, endoplasmic reticulum stress and neurodegeneration. *Curr Opin Cell Biol*, 16, 653-62.
- RAWSON, P. M., MOLETTE, C., VIDETTA, M., ALTIERI, L., FRANCESCHINI, D., DONATO, T., FINOCCHI, L., PROPATO, A., PAROLI, M., MELONI, F., MASTROIANNI, C. M., D'ETTORRE, G., SIDNEY, J., SETTE, A. & BARNABA, V. 2007. Cross-presentation of caspase-cleaved apoptotic self antigens in HIV infection. *Nat Med*, 13, 1431-9.
- REED, J. C. 2006. Proapoptotic multidomain Bcl-2/Bax-family proteins: mechanisms, physiological roles, and therapeutic opportunities. *Cell Death Differ*, 13, 1378-86.
- REED, R. C., BERWIN, B., BAKER, J. P. & NICCHITTA, C. V. 2003. GRP94/gp96 elicits ERK activation in murine macrophages. A role for endotoxin contamination in NF-kappa B activation and nitric oxide production. *J Biol Chem*, 278, 31853-60.
- REINHARDT, R. L., HONG, S., KANG, S. J., WANG, Z. E. & LOCKSLEY, R. M. 2006. Visualization of IL-12/23p40 in vivo reveals immunostimulatory dendritic cell migrants that promote Th1 differentiation. *J Immunol*, 177, 1618-27.
- RENU, K., V. G. A., P. B. T. & ARUNACHALAM, S. 2018. Molecular mechanism of doxorubicin-induced cardiomyopathy - An update. *Eur J Pharmacol*, 818, 241-253.
- ROCK, K. L. & KONO, H. 2008. The inflammatory response to cell death. *Annu Rev Pathol*, 3, 99-126.
- ROJIANI, M. V., FINLAY, B. B., GRAY, V. & DEDHAR, S. 1991. In vitro interaction of a polypeptide homologous to human Ro/SS-A antigen (calreticulin) with a highly conserved amino acid sequence in the cytoplasmic domain of integrin alpha subunits. *Biochemistry*, 30, 9859-66.
- ROSENBERG, S. A., LOTZE, M. T., MUUL, L. M., LEITMAN, S., CHANG, A. E., ETTINGHAUSEN, S. E., MATORY, Y. L., SKIBBER, J. M., SHILONI, E., VETTO, J. T. & ET AL. 1985. Observations on the systemic administration of autologous lymphokine-activated killer cells and recombinant interleukin-2 to patients with metastatic cancer. *N Engl J Med*, 313, 1485-92.
- SACHET, M., LIANG, Y. Y. & OEHLER, R. 2017. The immune response to secondary necrotic cells. *Apoptosis*, 22, 1189-1204.
- SAELENS, X., FESTJENS, N., VANDE WALLE, L., VAN GURP, M., VAN LOO, G. & VANDENABEELE, P. 2004. Toxic proteins released from mitochondria in cell death. *Oncogene*, 23, 2861-74.
- SAHOO, N., GU, M., ZHANG, X., RAVAL, N., YANG, J., BEKIER, M., CALVO, R., PATNAIK, S., WANG, W., KING, G., SAMIE, M., GAO, Q., SAHOO, S., SUNDARESAN, S., KEELEY, T. M., WANG, Y., MARUGAN, J., FERRER, M., SAMUELSON, L. C., MERCHANT, J. L. & XU, H. 2017. Gastric Acid Secretion from Parietal Cells Is Mediated by a Ca(2+) Efflux Channel in the Tubulovesicle. *Dev Cell*, 41, 262-273 e6.

- SALEH, T. & SHOJAOSADATI, S. A. 2016. Multifunctional nanoparticles for cancer immunotherapy. *Hum Vaccin Immunother*, 12, 1863-75.
- SARASTE, A. & PULKKI, K. 2000. Morphologic and biochemical hallmarks of apoptosis. *Cardiovasc Res*, 45, 528-37.
- SAVINA, A. & AMIGORENA, S. 2007. Phagocytosis and antigen presentation in dendritic cells. *Immunol Rev*, 219, 143-56.
- SAWAI, H. & DOMAE, N. 2011. Discrimination between primary necrosis and apoptosis by necrostatin-1 in Annexin V-positive/propidium iodide-negative cells. *Biochem Biophys Res Commun*, 411, 569-73.
- SCHOCK, H., SURCEL, H. M., ZELENIUCH-JACQUOTTE, A., GRANKVIST, K., LAKSO, H. A., FORTNER, R. T., KAAKS, R., PUKKALA, E., LEHTINEN, M., TONIOLO, P. & LUNDIN, E. 2014. Early pregnancy sex steroids and maternal risk of epithelial ovarian cancer. *Endocr Relat Cancer*, 21, 831-44.
- SCHREIBER, R. D., OLD, L. J. & SMYTH, M. J. 2011. Cancer immunoediting: integrating immunity's roles in cancer suppression and promotion. *Science*, 331, 1565-70.
- SCHUTTE, B., NUYDENS, R., GEERTS, H. & RAMAEKERS, F. 1998. Annexin V binding assay as a tool to measure apoptosis in differentiated neuronal cells. *J Neurosci Methods*, 86, 63-9.
- SELDERS, G. S., FETZ, A. E., RADIC, M. Z. & BOWLIN, G. L. 2017. An overview of the role of neutrophils in innate immunity, inflammation and host-biomaterial integration. *Regen Biomater*, 4, 55-68.
- SHAHSHAHAN, M. A., BECKLEY, M. N. & JAZIREHI, A. R. 2011. Potential usage of proteasome inhibitor bortezomib (Velcade, PS-341) in the treatment of metastatic melanoma: basic and clinical aspects. *Am J Cancer Res*, 1, 913-24.
- SHAO, S., SUN, X., CHEN, Y., ZHAN, B. & ZHU, X. 2019. Complement Evasion: An Effective Strategy That Parasites Utilize to Survive in the Host. *Front Microbiol*, 10, 532.
- SHARMA, P., GNJATIC, S., JUNGBLUTH, A. A., WILLIAMSON, B., HERR, H., STOCKERT, E., DALBAGNI, G., DONAT, S. M., REUTER, V. E., SANTIAGO, D., CHEN, Y. T., BAJORIN, D. F. & OLD, L. J. 2003. Frequency of NY-ESO-1 and LAGE-1 expression in bladder cancer and evidence of a new NY-ESO-1 T-cell epitope in a patient with bladder cancer. *Cancer Immun*, 3, 19.
- SHORTMAN, K. & NAIK, S. H. 2007. Steady-state and inflammatory dendritic-cell development. *Nat Rev Immunol*, 7, 19-30.
- SIEGEL, R. L., MILLER, K. D. & JEMAL, A. 2016. Cancer statistics, 2016. *CA Cancer J Clin*, 66, 7-30.
- SIM, W. J., MALINARICH, F., FAIRHURST, A. M. & CONNOLLY, J. E. 2016. Generation of Immature, Mature and Tolerogenic Dendritic Cells with Differing Metabolic Phenotypes. *J Vis Exp*.
- SINGH, M. S. & BHASKAR, S. 2014. Nanocarrier-based immunotherapy in cancer management and research. *Immunotargets Ther*, 3, 121-34.
- SMITH, M. J. & KOCH, G. L. 1989. Multiple zones in the sequence of calreticulin (CRP55, calregulin, HACBP), a major calcium binding ER/SR protein. *EMBO J*, 8, 3581-6.
- SMITH, P. K., KROHN, R. I., HERMANSON, G. T., MALLIA, A. K., GARTNER, F. H., PROVENZANO, M. D., FUJIMOTO, E. K., GOEKE, N. M., OLSON, B. J. & KLENK, D. C. 1985. Measurement of protein using bicinchoninic acid. *Anal Biochem*, 150, 76-85.
- SON, K. J., CHOI, K. R., RYU, C. K., LEE, S. J., KIM, H. J. & LEE, H. 2017. Induction of immunogenic cell death of tumors by newly synthesized heterocyclic quinone derivative. *PLoS One*, 12, e0173121.
- SONG, M. N., MOON, P. G., LEE, J. E., NA, M., KANG, W., CHAE, Y. S., PARK, J. Y., PARK, H. & BAEK, M. C. 2012. Proteomic analysis of breast cancer tissues to identify biomarker candidates by gel-assisted digestion and label-free quantification methods using LC-MS/MS. *Arch Pharm Res*, 35, 1839-47.
- SONG, X. C., FU, G., YANG, X., JIANG, Z., WANG, Y. & ZHOU, G. W. 2008. Protein expression profiling of breast cancer cells by dissociable antibody microarray (DAMA) staining. *Mol Cell Proteomics*, 7, 163-9.



- SPISEK, R. & DHODAPKAR, M. V. 2007. Towards a better way to die with chemotherapy: role of heat shock protein exposure on dying tumor cells. *Cell Cycle*, 6, 1962-5.
- SRIVASTAVA, P. 2002. Roles of heat-shock proteins in innate and adaptive immunity. *Nat Rev Immunol*, 2, 185-94.
- STOLL, G., IRIBARREN, K., MICHELS, J., LEARY, A., ZITVOGEL, L., CREMER, I. & KROEMER, G. 2016. Calreticulin expression: Interaction with the immune infiltrate and impact on survival in patients with ovarian and non-small cell lung cancer. *Oncoimmunology*, 5, e1177692.
- STUART, G. R., LYNCH, N. J., DAY, A. J., SCHWAEBLE, W. J. & SIM, R. B. 1997. The C1q and collectin binding site within C1q receptor (cell surface calreticulin). *Immunopharmacology*, 38, 73-80.
- SUEYOSHI, T., MCMULLEN, B. A., MARNELL, L. L., DU CLOS, T. W. & KISIEL, W. 1991. A new procedure for the separation of protein Z, prothrombin fragment 1.2 and calreticulin from human plasma. *Thromb Res*, 63, 569-75.
- SULFATE, P. B. 2011. SigmaAldrich Co. LLC.
- TARR, J. M., WINYARD, P. G., RYAN, B., HARRIES, L. W., HAIGH, R., VINER, N. & EGGLETON, P. 2010a. Extracellular calreticulin is present in the joints of patients with rheumatoid arthritis and inhibits FasL (CD95L)-mediated apoptosis of T cells. *Arthritis Rheum*, 62, 2919-29.
- TARR, J. M., YOUNG, P. J., MORSE, R., SHAW, D. J., HAIGH, R., PETROV, P. G., JOHNSON, S. J., WINYARD, P. G. & EGGLETON, P. 2010b. A mechanism of release of calreticulin from cells during apoptosis. *J Mol Biol*, 401, 799-812.
- TAU, G. Z., COWAN, S. N., WEISBURG, J., BRAUNSTEIN, N. S. & ROTHMAN, P. B. 2001. Regulation of IFN-gamma signaling is essential for the cytotoxic activity of CD8(+) T cells. *J Immunol*, 167, 5574-82.
- TESNIERE, A., APETOH, L., GHIRINGHELLI, F., JOZA, N., PANARETAKIS, T., KEPP, O., SCHLEMMER, F., ZITVOGEL, L. & KROEMER, G. 2008. Immunogenic cancer cell death: a key-lock paradigm. *Curr Opin Immunol*, 20, 504-11.
- TEWEY, K. M., ROWE, T. C., YANG, L., HALLIGAN, B. D. & LIU, L. F. 1984. Adriamycin-induced DNA damage mediated by mammalian DNA topoisomerase II. *Science*, 226, 466-8.
- THEOCHARIDES, A. P., LUNDBERG, P., LAKKARAJU, A. K., LYSENKO, V., MYBURGH, R., AGUZZI, A., SKODA, R. C. & MANZ, M. G. 2016. Homozygous calreticulin mutations in patients with myelofibrosis lead to acquired myeloperoxidase deficiency. *Blood*, 127, 3253-9.
- THOMAS, R., AL-KHADAIRI, G., ROELANDS, J., HENDRICKX, W., DERMIME, S., BEDOGNETTI, D. & DECOCK, J. 2018. NY-ESO-1 Based Immunotherapy of Cancer: Current Perspectives. *Front Immunol*, 9, 947.
- THORN, C. F., OSHIRO, C., MARSH, S., HERNANDEZ-BOUSSARD, T., MCLEOD, H., KLEIN, T. E. & ALTMAN, R. B. 2011. Doxorubicin pathways: pharmacodynamics and adverse effects. *Pharmacogenet Genomics*, 21, 440-6.
- THURNER, B., RODER, C., DIECKMANN, D., HEUER, M., KRUSE, M., GLASER, A., KEIKAVOUSSI, P., KAMPGEN, E., BENDER, A. & SCHULER, G. 1999. Generation of large numbers of fully mature and stable dendritic cells from leukapheresis products for clinical application. *J Immunol Methods*, 223, 1-15.
- TJOELKER, L. W., SEYFRIED, C. E., EDDY, R. L., JR., BYERS, M. G., SHOWS, T. B., CALDERON, J., SCHREIBER, R. B. & GRAY, P. W. 1994. Human, mouse, and rat calnexin cDNA cloning: identification of potential calcium binding motifs and gene localization to human chromosome 5. *Biochemistry*, 33, 3229-36.
- TODAR, K. 2018. Todar's Online Textbook of Bacteriology.
- TOKUNAGA, N., MURAKAMI, T., ENDO, Y., NISHIZAKI, M., KAGAWA, S., TANAKA, N. & FUJIWARA, T. 2005. Human monocyte-derived dendritic cells pulsed with wild-type p53 protein efficiently induce CTLs against p53 overexpressing human cancer cells. *Clin Cancer Res*, 11, 1312-8.
- TOPHAM, N. J. & HEWITT, E. W. 2009. Natural killer cell cytotoxicity: how do they pull the trigger? *Immunology*, 128, 7-15.

- TREVINO, L. S., BUCKLES, E. L. & JOHNSON, P. A. 2012. Oral contraceptives decrease the prevalence of ovarian cancer in the hen. *Cancer Prev Res (Phila)*, 5, 343-9.
- TROUW, L. A., BLOM, A. M. & GASQUE, P. 2008. Role of complement and complement regulators in the removal of apoptotic cells. *Mol Immunol*, 45, 1199-207.
- TRUSCOTT, S. M., WANG, X., LYBARGER, L., BIDDISON, W. E., MCBERRY, C., MARTINKO, J. M., CONNOLLY, J. M., LINETTE, G. P., FREMONT, D. H., HANSEN, T. H. & CARRENO, B. M. 2008. Human major histocompatibility complex (MHC) class I molecules with disulfide traps secure disease-related antigenic peptides and exclude competitor peptides. *J Biol Chem*, 283, 7480-90.
- TSENG, D., VOLKMER, J. P., WILLINGHAM, S. B., CONTRERAS-TRUJILLO, H., FATHMAN, J. W., FERNHOFF, N. B., SEITA, J., INLAY, M. A., WEISKOPF, K., MIYANISHI, M. & WEISSMAN, I. L. 2013. Anti-CD47 antibody-mediated phagocytosis of cancer by macrophages primes an effective antitumor T-cell response. *Proc Natl Acad Sci U S A*, 110, 11103-8.
- UPPALA, J. K., GANI, A. R. & RAMAIAH, K. V. A. 2017. Chemical chaperone, TUDCA unlike PBA, mitigates protein aggregation efficiently and resists ER and non-ER stress induced HepG2 cell death. *Sci Rep*, 7, 3831.
- VAN GENDEREN, H. O., KENIS, H., HOFSTRA, L., NARULA, J. & REUTELINGSPERGER, C. P. 2008. Extracellular annexin A5: functions of phosphatidylserine-binding and two-dimensional crystallization. *Biochim Biophys Acta*, 1783, 953-63.
- VANDENBERK, L., BELMANS, J., VAN WOENSEL, M., RIVA, M. & VAN GOOL, S. W. 2015. Exploiting the Immunogenic Potential of Cancer Cells for Improved Dendritic Cell Vaccines. *Front Immunol*, 6, 663.
- VANDIVIER, R. W., OGDEN, C. A., FADOK, V. A., HOFFMANN, P. R., BROWN, K. K., BOTTO, M., WALPORT, M. J., FISHER, J. H., HENSON, P. M. & GREENE, K. E. 2002. Role of surfactant proteins A, D, and C1q in the clearance of apoptotic cells in vivo and in vitro: calreticulin and CD91 as a common collectin receptor complex. *J Immunol*, 169, 3978-86.
- VANG, S., LONGLEY, K., STEER, C. J. & LOW, W. C. 2014. The Unexpected Uses of Urso- and Tauroursodeoxycholic Acid in the Treatment of Non-liver Diseases. *Glob Adv Health Med*, 3, 58-69.
- VANSTEENKISTE, J., ZIELINSKI, M., LINDER, A., DAHABREH, J., GONZALEZ, E. E., MALINOWSKI, W., LOPEZ-BREA, M., VANAKESA, T., JASSEM, J., KALOFONOS, H., PERDEUS, J., BONNET, R., BASKO, J., JANILIONIS, R., PASSLICK, B., TREASURE, T., GILLET, M., LEHMANN, F. F. & BRICHARD, V. G. 2013. Adjuvant MAGE-A3 immunotherapy in resected non-small-cell lung cancer: phase II randomized study results. *J Clin Oncol*, 31, 2396-403.
- VANTOUROUT, P. & HAYDAY, A. 2013. Six-of-the-best: unique contributions of gammadelta T cells to immunology. *Nat Rev Immunol*, 13, 88-100.
- VEGA, H., AGELLON, L. B. & MICHALAK, M. 2016. The rise of proteostasis promoters. *IUBMB Life*, 68, 943-954.
- VERA, C., TAPIA, V., KOHAN, K., GABLER, F., FERREIRA, A., SELMAN, A., VEGA, M. & ROMERO, C. 2012. Nerve growth factor induces the expression of chaperone protein calreticulin in human epithelial ovarian cells. *Horm Metab Res*, 44, 639-43.
- VERA, C. A., OROSTICA, L., GABLER, F., FERREIRA, A., SELMAN, A., VEGA, M. & ROMERO, C. A. 2017. The nerve growth factor alters calreticulin translocation from the endoplasmic reticulum to the cell surface and its signaling pathway in epithelial ovarian cancer cells. *Int J Oncol*, 50, 1261-1270.
- VERNERET, M., TACNET-DELORME, P., OSMAN, R., AWAD, R., GRICHINE, A., KLEMAN, J. P. & FRACHET, P. 2014. Relative contribution of c1q and apoptotic cell-surface calreticulin to macrophage phagocytosis. *J Innate Immun*, 6, 426-34.
- VIGNERON, N., STROOBANT, V., VAN DEN EYNDE, B. J. & VAN DER BRUGGEN, P. 2013. Database of T cell-defined human tumor antigens: the 2013 update. *Cancer Immun*, 13, 15.

- VIVIER, E., RAULET, D. H., MORETTA, A., CALIGIURI, M. A., ZITVOGEL, L., LANIER, L. L., YOKOYAMA, W. M. & UGOLINI, S. 2011. Innate or adaptive immunity? The example of natural killer cells. *Science*, 331, 44-9.
- VIVIER, E., TOMASELLO, E., BARATIN, M., WALZER, T. & UGOLINI, S. 2008. Functions of natural killer cells. *Nat Immunol*, 9, 503-10.
- VIVIER, E., UGOLINI, S., BLAISE, D., CHABANNON, C. & BROSSAY, L. 2012. Targeting natural killer cells and natural killer T cells in cancer. *Nat Rev Immunol*, 12, 239-52.
- WAJANT, H. 2002. The Fas signaling pathway: more than a paradigm. *Science*, 296, 1635-6.
- WALLBERG, F., TENEV, T. & MEIER, P. 2016. Analysis of Apoptosis and Necroptosis by Fluorescence-Activated Cell Sorting. *Cold Spring Harb Protoc*, 2016, pdb prot087387.
- WANG, H. Y. & WANG, R. F. 2007. Regulatory T cells and cancer. *Curr Opin Immunol*, 19, 217-23.
- WANG, H. Y. & WANG, R. F. 2012. Enhancing cancer immunotherapy by intracellular delivery of cell-penetrating peptides and stimulation of pattern-recognition receptor signaling. *Adv Immunol*, 114, 151-76.
- WANG, J., ZOU, Z. H., XIA, H. L., HE, J. X., ZHONG, N. S. & TAO, A. L. 2012. Strengths and weaknesses of immunotherapy for advanced non-small-cell lung cancer: a meta-analysis of 12 randomized controlled trials. *PLoS One*, 7, e32695.
- WANG, M., YIN, B., WANG, H. Y. & WANG, R. F. 2014. Current advances in T-cell-based cancer immunotherapy. *Immunotherapy*, 6, 1265-78.
- WANG, S., KONOREV, E. A., KOTAMRAJU, S., JOSEPH, J., KALIVENDI, S. & KALYANARAMAN, B. 2004. Doxorubicin induces apoptosis in normal and tumor cells via distinctly different mechanisms. Intermediacy of H(2)O(2)- and p53-dependent pathways. *J Biol Chem*, 279, 25535-43.
- WANG, X., JI, J., ZHANG, H., FAN, Z., ZHANG, L., SHI, L., ZHOU, F., CHEN, W. R., WANG, H. & WANG, X. 2015. Stimulation of dendritic cells by DAMPs in ALA-PDT treated SCC tumor cells. *Oncotarget*, 6, 44688-702.
- WANG, Y. J., FLETCHER, R., YU, J. & ZHANG, L. 2018. Immunogenic effects of chemotherapy-induced tumor cell death. *Genes Dis*, 5, 194-203.
- WEST, N. P., PYNE, D. B., RENSHAW, G. & CRIPPS, A. W. 2006. Antimicrobial peptides and proteins, exercise and innate mucosal immunity. *FEMS Immunol Med Microbiol*, 48, 293-304.
- WIECZOREK, M., ABUALROUS, E. T., STICHT, J., ALVARO-BENITO, M., STOLZENBERG, S., NOE, F. & FREUND, C. 2017. Major Histocompatibility Complex (MHC) Class I and MHC Class II Proteins: Conformational Plasticity in Antigen Presentation. *Front Immunol*, 8, 292.
- WIERSMA, V. R., MICHALAK, M., ABDULLAH, T. M., BREMER, E. & EGGLETON, P. 2015. Mechanisms of Translocation of ER Chaperones to the Cell Surface and Immunomodulatory Roles in Cancer and Autoimmunity. *Front Oncol*, 5, 7.
- WIJEYESAKERE, S. J., BEDI, S. K., HUYNH, D. & RAGHAVAN, M. 2016. The C-Terminal Acidic Region of Calreticulin Mediates Phosphatidylserine Binding and Apoptotic Cell Phagocytosis. *J Immunol*, 196, 3896-3909.
- WILSON, K. S., ROBERTS, H., LEEK, R., HARRIS, A. L. & GERADTS, J. 2002. Differential gene expression patterns in HER2/neu-positive and -negative breast cancer cell lines and tissues. *Am J Pathol*, 161, 1171-85.
- WLODKOWIC, D., KHOSHMANESH, K., SHARPE, J. C., DARZYNKIEWICZ, Z. & COOPER, J. M. 2011. Apoptosis goes on a chip: advances in the microfluidic analysis of programmed cell death. *Anal Chem*, 83, 6439-46.
- WONG, R. S. 2011. Apoptosis in cancer: from pathogenesis to treatment. *J Exp Clin Cancer Res*, 30, 87.
- WRIGHT, A. A., BOHLKE, K., ARMSTRONG, D. K., BOOKMAN, M. A., CLIBY, W. A., COLEMAN, R. L., DIZON, D. S., KASH, J. J., MEYER, L. A., MOORE, K. N., OLAWAIYE, A. B., OLDHAM, J., SALANI, R., SPARACIO, D., TEW, W. P., VERGOTE, I. & EDELSON, M. I. 2016. Neoadjuvant chemotherapy for newly diagnosed, advanced ovarian cancer: Society of Gynecologic

- Oncology and American Society of Clinical Oncology Clinical Practice Guideline. *Gynecol Oncol*, 143, 3-15.
- YANG, Y., YANG, D., YANG, D., JIA, R. & DING, G. 2014. Role of reactive oxygen species-mediated endoplasmic reticulum stress in contrast-induced renal tubular cell apoptosis. *Nephron Exp Nephrol*, 128, 30-6.
- YOUNG, P., SZESTAKOWSKA, D., MORSE, R., WINYARD, P., JOHNSON, S. & EGGLETON, P. 2006. Purification of human native and recombinant domains of CRT: structural and functional implications. . *Calcium Binding Proteins*, 1, 160-169.
- YU, J., WANG, C., KONG, Q., WU, X., LU, J. J. & CHEN, X. 2018. Recent progress in doxorubicin-induced cardiotoxicity and protective potential of natural products. *Phytomedicine*, 40, 125-139.
- ZAJAC, P., SCHULTZ-THATER, E., TORNILLO, L., SADOWSKI, C., TRELLA, E., MENGUS, C., IEZZI, G. & SPAGNOLI, G. C. 2017. MAGE-A Antigens and Cancer Immunotherapy. *Front Med (Lausanne)*, 4, 18.
- ZAMANIAN, M., VEERAKUMARASIVAM, A., ABDULLAH, S. & ROSLI, R. 2013. Calreticulin and cancer. *Pathol Oncol Res*, 19, 149-54.
- ZHU, J., YAMANE, H. & PAUL, W. E. 2010. Differentiation of effector CD4 T cell populations (\*). *Annu Rev Immunol*, 28, 445-89.
- ZITVOGEL, L., KEPP, O., SENOVILLA, L., MENGER, L., CHAPUT, N. & KROEMER, G. 2010. Immunogenic tumor cell death for optimal anticancer therapy: the calreticulin exposure pathway. *Clin Cancer Res*, 16, 3100-4.
- ZUNINA, F., GAMBETTA, R. & DI MARCO, A. 1975. The inhibition in vitro of DNA polymerase and RNA polymerases by daunomycin and adriamycin. *Biochem Pharmacol*, 24, 309-11.